

**Insights into the Mechanism and Regulation of EgtD, a
Novel Histidine Methyltransferase from Ergothioneine
Biosynthesis.**

Inauguraldissertation

zur

Erlangung der Würde eines Doktors der Philosophie

vorgelegt der

Philosophisch-Naturwissenschaftlichen Fakultät

der Universität Basel

von

Laëtitia Misson

Aus Thionville, Frankreich

Basel, 2017

Originaldokument gespeichert auf dem Dokumentenserver der
Universität Basel edoc.unibas.ch

Genehmigt von der Philosophisch-Naturwissenschaftlichen Fakultät
auf Antrag von

Prof. Dr. Florian P. Seebeck

Prof. Dr. Wulf Blankenfeldt

Basel, 21. Juni 2016

Prof. Dr. Jörg Schibler

Dekan

Plus l'homme sera éclairé, plus il sera libre.

Voltaire

Table of Contents

| | |
|--|-----------|
| Summary | 1 |
| 1 Introduction: Ubiquity of amino acid betaines..... | 3 |
| 1.1 Glycine betaine..... | 3 |
| 1.1.1 Major functions of an extensively distributed compound | 4 |
| 1.1.2 Glycine betaine transporters..... | 7 |
| 1.1.3 Biosynthetic pathways..... | 8 |
| 1.2 Aromatic amino acid betaines..... | 10 |
| 1.2.1 Hypaphorine | 11 |
| 1.2.2 Trimethyltyrosine..... | 14 |
| 1.2.3 Trimethylhistidine and ergothioneine..... | 15 |
| 1.2.4 First step of ergothioneine biosynthesis: histidine methylation..... | 21 |
| 1.3 Aim of the thesis..... | 22 |
| 2 The methyltransferase EgtD reveals the structural basis of aromatic amino acid betaines biosynthesis..... | 23 |
| 2.1 EgtD activity..... | 24 |
| 2.1.1 Spectrophotometric coupled assay | 24 |
| 2.1.2 EgtD is a specific histidine methyltransferase | 25 |
| 2.2 EgtD crystal structure..... | 26 |
| 2.2.1 Identification of the essential catalytic residues..... | 27 |
| 2.2.2 EgtD is a cooperative enzyme | 31 |
| 2.3 Identification of a tyrosine methyltransferase..... | 35 |
| 2.3.1 Production and characterization of SticA, a tyrosine betaine synthase..... | 36 |
| 2.3.2 Kinetics..... | 38 |
| 2.4 Identification of a fungal tryptophane betaine synthase | 40 |
| 2.4.1 Identification of hypaphorine in wood degrading fungus..... | 40 |
| 2.4.2 Engineered tryptophan methyltransferase..... | 42 |
| 2.4.3 Crystal structure..... | 44 |
| 2.5 Conclusions | 45 |
| 2.6 Experimental | 46 |
| 2.6.1 Kinetics..... | 46 |

| | | |
|----------|--|-----------|
| 2.6.2 | Product identification after methyl transfer..... | 49 |
| 2.6.3 | Extraction and identification of trimethyltryptophan in <i>Dichomitus squalens</i> | 49 |
| 3 | EgtD substrate binding mode provides the basis for inhibitors design | 50 |
| 3.1 | EgtD is product-inhibited..... | 51 |
| 3.1.1 | Kinetics..... | 52 |
| 3.1.2 | Crystal structure of EgtD in complex with its product trimethylhistidine..... | 53 |
| 3.2 | Chlorohistidine is an inhibitor of EgtD | 54 |
| 3.2.1 | Kinetics..... | 55 |
| 3.2.2 | Crystal structure..... | 56 |
| 3.3 | Substrate binding order of EgtD..... | 57 |
| 3.3.1 | Catalytic parameters of EgtD in the presence of different concentrations of histidine | 58 |
| 3.3.2 | Catalytic parameters of EgtD in the presence of different concentrations of SAM..... | 59 |
| 3.3.3 | Substrate binding order | 60 |
| 3.4 | Inhibition mechanisms..... | 61 |
| 3.5 | Design of EgtD inhibitors..... | 63 |
| 3.5.1 | Choice of inhibitors | 63 |
| 3.5.2 | Synthesis..... | 64 |
| 3.5.3 | K_i values | 66 |
| 3.5.4 | Crystal structures..... | 68 |
| 3.6 | Conclusions | 70 |
| 3.7 | Experimental | 71 |
| 3.7.1 | Kinetics..... | 71 |
| 3.7.2 | HPLC traces of the inhibitors | 80 |
| 4 | An active site asparagine catalyzes methyl transfer by stabilizing a near attack conformation | 81 |
| 4.1 | <i>N</i> -methyltransferases | 81 |
| 4.1.1 | Phosphoethanolamine methyltransferase | 81 |
| 4.1.2 | Protein lysine and arginine methyltransferases | 82 |
| 4.1.3 | DNA adenine methyltransferase..... | 84 |
| 4.1.4 | Requirements for methyl transfer | 85 |
| 4.2 | Substrate activation in EgtD..... | 86 |
| 4.3 | EgtD wild type and N166D activities are pH-dependent | 88 |
| 4.3.1 | Theory..... | 88 |

| | | |
|----------|--|------------|
| 4.3.2 | Results | 89 |
| 4.4 | Histidinamide as a substrate of EgtD N166D..... | 92 |
| 4.4.1 | Theory..... | 92 |
| 4.4.2 | Results | 92 |
| 4.5 | Catalytic parameters of EgtD N166D..... | 93 |
| 4.6 | Conclusions and future directions..... | 96 |
| 4.7 | Experimental | 96 |
| 5 | Oxidative regulation of EgtD | 99 |
| 5.1 | EgtD in an oxidative environment: A way to regulate ergothioneine biosynthesis?..... | 99 |
| 5.2 | EgtD wild type activity in the presence of oxidants | 100 |
| 5.2.1 | Suggested mechanisms of regulation | 100 |
| 5.2.2 | EgtD activity in presence of the physiological oxidant hydrogen peroxide..... | 101 |
| 5.2.3 | EgtD activity in presence of HOCl..... | 103 |
| 5.2.4 | Can EgtB protect EgtD from oxidative damage? | 106 |
| 5.2.5 | Reversibility of the oxidative inactivation..... | 107 |
| 5.3 | EgtD Cys139 and Cys285..... | 108 |
| 5.3.1 | Localization of the two cysteine residues..... | 109 |
| 5.3.2 | Activity of the variants..... | 109 |
| 5.4 | Change in quaternary structure induced by oxidative environment..... | 112 |
| 5.4.1 | EgtD wild type | 112 |
| 5.4.2 | EgtD cysteine variants..... | 113 |
| 5.5 | Chemical modifications induced by oxidative environment | 116 |
| 5.5.1 | EgtD wild type | 116 |
| 5.5.2 | EgtD cysteine variants..... | 117 |
| 5.6 | Conclusions and discussion..... | 120 |
| 5.7 | Experimental | 121 |
| 5.7.1 | Kinetics..... | 121 |
| 5.7.2 | Histag cleavage..... | 123 |
| 5.7.3 | FPLC analysis | 124 |
| 6 | Appendix | 125 |
| 6.1 | Cloning and Protein production | 125 |
| 6.2 | Synthesis of the Inhibitors | 129 |

| | |
|------------------------------------|------------|
| List of abbreviations | 137 |
| References | 139 |
| Acknowledgments | 149 |

Summary

Amino acid betaines represent a ubiquitous class of simple natural products. These compounds are increasingly recognized as osmoprotectants, valuable additives in food and cosmetics, therapeutics, or as components of green ionic liquids. The best known representative of this class is trimethylglycine. A large majority of organisms synthesize glycine betaine via a two-step oxidation of choline. Because this pathway is hardly adaptable to producing other betaines, the biosynthetic origin of most amino acid betaines remained unclear. The biosynthetic pathways of ergothioneine, a histidine betaine derivative, were identified in *Mycobacterium smegmatis* and in the fungus *Neurospora crassa*, in 2010 and 2013 respectively. In both pathways, the $N\alpha$ -histidine methyltransferase EgtD catalyzes the first step of the biosynthesis. We characterized EgtD as the first member of an amino acid methyltransferase family (Methyltransf_33) which catalyzes the direct permethylation of its substrate. We demonstrated the cooperativity of EgtD. We suggest that this unique feature among the members of the Methyltransf_33 family enables an upstream substrate control for the following enzyme in the mycobacterial biosynthesis of ergothioneine, EgtB. In addition, by compiling kinetic analysis, X-ray crystallography and bioinformatic searches, we were able to describe the determinants for EgtD substrate specificity and consequently identify new aromatic amino acid betaine synthases which were not reported until now.

Ergothioneine has been recently associated with the virulence of *Mycobacterium tuberculosis*. As this small metabolite is not synthesized by the human body, it emerges as a potential drug target against this pathogen. Interestingly, the Δ egtD deletion mutants of mycobacteria are no longer able to produce this compound. This finding indicated that the presence and the activity of EgtD govern ergothioneine biosynthesis. Based on structural analysis and the identification of the substrate binding mode of EgtD, we designed a series of histidine derivatives that inhibit EgtD activity *in vitro*. Therefore, our findings could direct the development of new inhibitors of ergothioneine biosynthesis in mycobacteria which may be tested *in vivo*.

Furthermore, we propose a mechanism for substrate activation required for the catalysis and two regulation pathways of EgtD activity. Firstly, we identified trimethylhistidine as an inhibitor of the methyltransferase. We suggest that this product inhibition is a means to avoid the accumulation of an unnecessary reaction intermediate, if not used by EgtB. Secondly, we also observed that the presence of a strong oxidant agent such as hypochlorite, down-regulates the activity of EgtD *in vitro* by oxidizing one cysteine residue of the methyltransferase. This finding seems counterintuitive if we consider the antioxidant properties of ergothioneine. However, as

mycobacteria produce both ergothioneine and mycothiol to maintain redox homeostasis, the regulation of the EgtD activity in an oxidative environment *in vivo* might also be associated with mycothiol. Yet, we clearly demonstrated that the rate of histidine methylation is not enhanced in the presence of reactive oxygen species.

1 Introduction: Ubiquity of amino acid betaines

The term betaine refers to a sub-class of zwitterions. The cationic and negative functional groups consist, in most cases, of a positively charged ammonium group and a negatively charged carboxylate. Phosphonium and sulfonium betaines are less common and mainly occur as synthetic intermediates (such as in the Wittig reaction).¹

Betaines are ubiquitous among all six kingdoms of life (Figure 1). Their functions are certainly as diverse as the organisms in which they are found. They serve as osmoprotectants, antioxidants, building blocks and methyl donors, to name only a few. Most of the natural betaines are derived from amino acids. Theoretically, all the amino acids can be converted to their corresponding betaines via the trimethylation of the α -amino group. There are however only a few biosynthetic pathways for amino acid-derived betaines that have been reported in the literature.

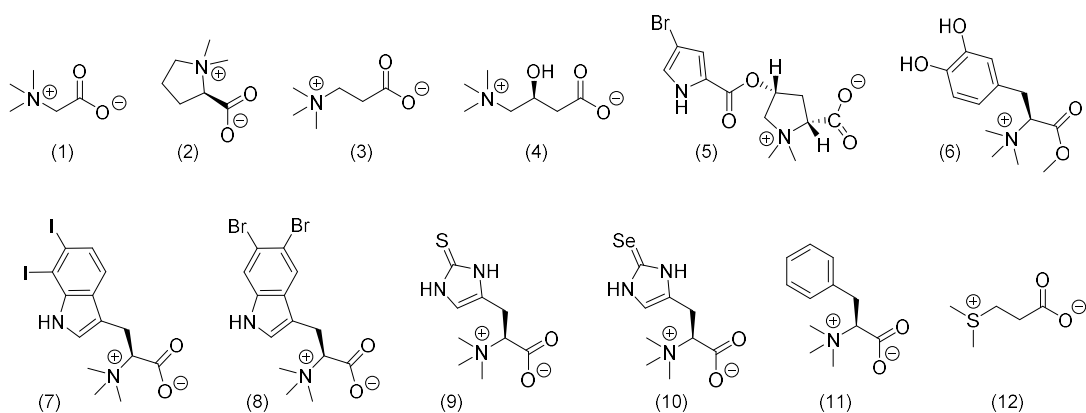


Figure 1 Examples of naturally occurring betaines. Glycine betaine (1), stachydrine (2) and β -alanine betaine (3) are osmoprotectants present in diverse marine algae, flowering plants families, various microorganisms and animals.² Carnitine (4) is an important nutrient involved in fatty acid metabolism of eukaryotes.³ Damituricin (5) was isolated from the Mediterranean sponge *Axinella damicornis*.⁴ Sticticine (6) is a major nitrogenous compound in lichens which might play a role in osmoregulation.⁵ Plakohypaphorine B (7) and 5,6-Dibromo-L-hypaphorine (8) were identified in marine sponges.^{6,7} Ergothioneine (9), synthesized by certain types of bacteria and fungi⁸ and selenoneine (10), found in ocean fish,⁹ have strong antioxidant activity. Phenylalanine betaine (11) was identified from the mushroom *Astraeus pteridis*.¹⁰ Dimethylsulfoniopropionate (12) is produced by phytoplankton and related to the production of organic matter in the ocean.¹¹

1.1 Glycine betaine

Historically, the name betaine referred to trimethylglycine (TMG) which was the first amino acid betaine to be identified.^{12,13} Since its discovery in sugar beet more than 140 years ago, glycine betaine was found in various microorganisms, marine invertebrates, plants and mammals.^{14,15}

This section provides an overview of the chemistry and functions of this ubiquitous and essential compound.

1.1.1 Major functions of an extensively distributed compound

1.1.1.1 Osmoprotectant

A common response to water stresses observed in many organisms such as plants, bacteria or animals, is the accumulation of highly soluble, low molecular weight compounds named osmolytes. These solutes maintain cell volume by absorbing and retaining water. This osmotic adjustment allows the organism to survive a drought or an increase in environment salinity for example. Osmoprotectants include several categories of compounds: betaines such as glycine and proline betaine (Figure 1, 1-2) which are common in bacteria; sugars like sucrose or maltose which are often found in plants and free amino acids such as proline which is accumulated in bacteria or plants under water stress.^{2,16}

Computational studies on glycine betaine microsolvation demonstrated that seven water molecules interact directly with the osmolyte through hydrogen bonding.¹⁷ Moreover, up to twelve water molecules can populate the hydration shell of one TMG molecule.¹⁸ Hence, the increase in TMG concentration leads to an increase in the number of water molecules. Due to its osmoprotective property (and besides its low cost and high availability), TMG is a widely used additive in personal care products.

Glycine betaine is accumulated to assist cell volume regulation in bacteria, plants, marine animals or mammals.^{19,20} The levels of TMG vary significantly among these organisms in response to unfavorable environmental conditions. As an example, the ability of some plants to endure abiotic stress results from the accumulation of this quaternary ammonium.^{21,22} TMG is also found in the human plasma (20 to 70 μM), but at higher concentration in the liver and the kidneys (up to mM). The presence of osmolytes in the kidney is essential to balance the changes in salinity that occur in this organ. In addition to glycine betaine, other osmotically-active compounds such as myo-Inositol, sorbitol and glycerophosphoryl-choline are also found in mammalian and human kidneys.^{23,24} Moreover, TMG protects the cells from the high concentration of urea which causes proteins to unfold.²⁵ Indeed, to counteract the denaturing effect of urea, the presence of TMG induces a more compact protein folding. Due to the positively charged trimethylammonium group, TMG is in fact excluded from the protein immediate

hydration layer. This so-called “osmophobic effect” produces thermodynamic force that leads the protein to adopt a condensed structure.²⁶

1.1.1.2 Glycine betaine in homocysteine recycling

As described above, TMG is also found in the human liver. In this organ, TMG mainly serves as a methyl donor during the synthesis of methionine (Figure 2).²⁷

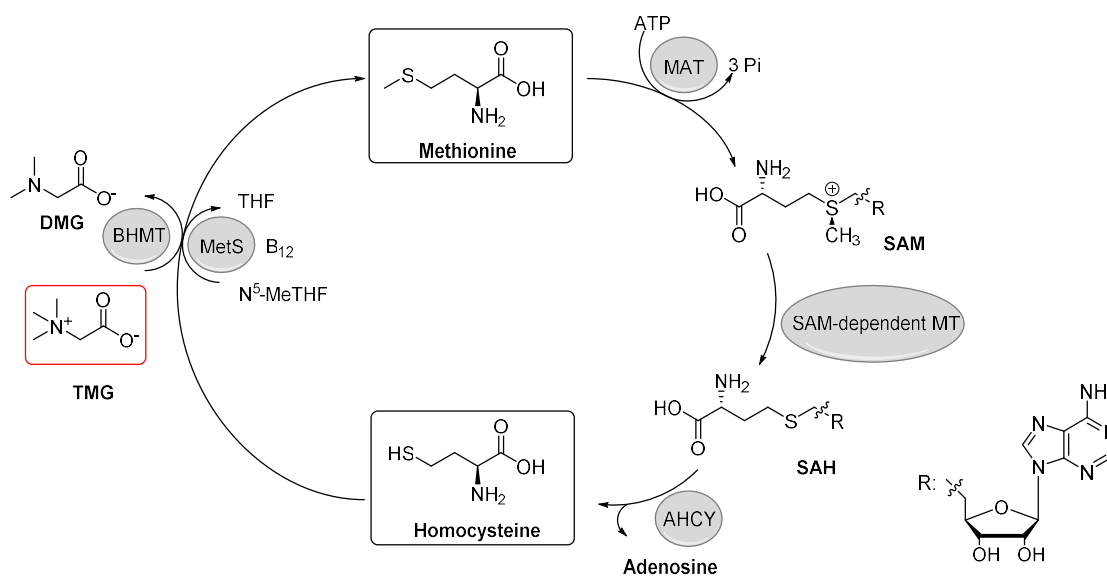


Figure 2 Metabolic pathway of methionine in human liver. BHMT is a betaine homocysteine methyltransferase that catalyzes the transfer of a methyl group from TMG to homocysteine. Methionine is also synthesized from homocysteine in presence of methyl-tetrahydrofolate (N⁵-MeTHF) and the vitamin B₁₂ as the methyl donor and cofactor respectively. This alternative methylation is catalyzed by the methionine synthase (MetS). S-adenosylmethionine (SAM) is synthesized from methionine and ATP by adenosyltransferase, also named SAM synthetase (MAT). SAM is used as a methyl donor by another MT and the resulting S-adenosylhomocysteine (SAH) is then cleaved in two moieties, adenosine and homocysteine by SAH hydrolase (AHCY).²⁸

The recycling of homocysteine and the resulting methionine production in the liver are dependent on two reactions of equal importance: the methyl transfers from glycine betaine catalyzed by BHMT and from methyl-tetrahydrofolate catalyzed by MetS. SAM is also synthesized in the liver from methionine and adenosyltriphosphate (ATP).²⁸ Therefore, glycine betaine plays an important role for the production of both methionine and SAM in the human body. Moreover, TMG supplementation facilitates the reduction of human

hyperhomocysteinemia.²⁹ Elevated homocysteine plasma levels are correlated with various diseases such as insulin resistance, one of the risk factor of non-alcoholic fatty liver disease (NAFLD). In addition, deletion of BHMT in mice was shown to also favor the development of NAFLD.³⁰ For these reasons, the use of glycine betaine to improve human hepatic health was considered. Nevertheless, the first results of TMG administration to humans with NAFLD did not alleviate the symptoms. The importance of BHMT and glycine betaine functions and potential use in the context of this liver disease are still under investigation.¹⁸

1.1.1.3 Protectant against oxidative stress

The previous paragraph gives an example which illustrates the complexity of translating animal studies to potential human curative treatments. Indeed, there is no doubt that the intake, accumulation and synthesis of TMG correlate with several (yet not fully understood) metabolic pathways. For example, studies on genetically modified rice which can synthesize TMG (wild type rice does not accumulate TMG) showed that the transgenic rice is more resistant not only to osmotic stress, but also to oxidative stress compared to the wild type. This stress-tolerant rice produces TMG by expressing the choline oxidase (EC 1.1.3.17) from *Arthrobacter globiformis*. In this bacterium, the oxidase directly converts choline to glycine betaine and H₂O₂.³¹ As H₂O₂ is known to activate stress response pathways,³² the resulting production of H₂O₂ from TMG biosynthesis could subsequently activate stress resistance mechanisms. Another example concerns the decrease in glutathione (GSH) concentration observed after the administration of ethanol to rats. Ethanol is converted by alcohol dehydrogenase to acetaldehyde which can then form an adduct with GSH.³³ This ethanol-induced GSH depletion is reversible in the presence of SAM which concentration can consecutively be increased by TMG administration.³⁴ Therefore, TMG may function as an antioxidant against ethanol induced oxidative injuries.

1.1.1.4 Natural deep eutectic solvent

The glycine betaine market is increasing with the rise of awareness about its functions (such as methyl donor or osmoprotectant) and its nutritional value when used in dietary supplements. As previously mentioned, an industrial application of glycine betaine consists of an additive in personal care products. A less common use of glycine betaine is in the synthesis of green ionic liquids (also named deep eutectic solvents). Ionic liquids (ILs) are considered less toxic than the

usual organic solvents because of their non-volatility. Nevertheless, ILs are, for the most part based on synthetic chemicals (imidazolium cations and fluorinated anions). Their synthetic origin is commonly a source of debate regarding their denomination as “green” solvents. However, a new class of ILs started to emerge. Interestingly, a mixture of choline and urea in 1:2 mole ratio can form a deep eutectic solvent with a melting temperature of 12 °C.³⁵ In addition, ILs synthesized from either glycine betaine itself or its ester derivatives are now under investigation to enhance solvent properties.³⁶ Recently, new glycine betaine-based ILs were demonstrated as effective SO₂ absorbents.³⁷ The development of ILs prepared from naturally occurring small metabolites such as glycine betaine, choline or oxalic acid correspond quite well to green chemistry requirements. It would not be unlikely that other amino acid betaines could provide the cation for new bio-based ILs. Moreover, several combinations of biosynthetic ILs based on amino acids (proline), sugars (glucose) or organic acids (citric or malic acids) were reported. Their ability to solvate enzymes and maintain catalytic activity was tested. It was shown that a laccase could remain active in 50 % water and 50 % of malic acid:choline chloride (1:1). This observation supports the hypothesis that plants could synthesize ionic liquids in case of dehydration. ILs would provide an environment which contains less water but in which enzymatic reactions could still occur.³⁸

1.1.2 Glycine betaine transporters

One of the key issues in understanding glycine betaine metabolism and regulation is to identify how this small metabolite is accumulated in the cells.

The bacterial uptake and efflux of TMG in case of water stress are carried out by both the opposite actions of mechanosensitive channels and betaine transporters.³⁹ In the case of hypoosmotic conditions in *Escherichia coli*, these channels protect the cell from lysis by mediating the efflux of small osmolytes.⁴⁰ In high salinity environments, osmoprotectants will be accumulated through the action of a protein from the family of the Betaine/Carnitine/Choline Transporters, in order to protect the cell against dehydration.⁴¹

Plants also accumulate TMG but little is known about specific glycine betaine transporter in plant cells. However, the cloning of a homologue of proline transporter and a γ -amino butyric acid (GABA) transporter from the plant *Arabidopsis* in yeast indicated that they both had a strong affinity for TMG. The outcome of these experiments suggests a low substrate specificity for these transporters which indicates that the transport of TMG in plants could occur through the action of both proline and GABA transporters.²¹

In mammals and especially in humans, cells in the liver and the kidneys contain specific transport systems needed for the uptake and accumulation of TMG. As previously described, TMG functions as an osmoprotectant to balance the hypertonicity and the elevated urea concentration in this organ where it is accumulated via a betaine-GABA transporter (BGT1). BGT1 is also present in the liver with the highest concentration compared to other organs. It is interesting to mention that the biosynthesis of this transporter is dependent on osmotic stress. Additionally, it is suggested that carnitine and amino acid transport systems support the glycine betaine uptake in the liver. The presence of several means to concentrate glycine betaine in the liver demonstrates its importance for this organ.¹⁸

Although TMG is the most studied amino acid betaine, a better understanding of the mechanism of intake, regulation and effects in the human body is still required. Thus, the efficiency of treatments based on glycine betaine supplements could be improved.

1.1.3 Biosynthetic pathways

TMG can be either accumulated via the transport systems described above or synthesized in the cell. The relative contributions to glycine betaine concentration from either biosynthesis or accumulation are not known yet. Several biosynthetic pathways were identified for the biosynthesis of TMG in bacteria, plants or mammals. The synthesis of the betaine occurs commonly through the oxidation of choline. However the permethylation of glycine was also reported.

1.1.3.1 Choline oxidation

Glycine betaine synthesis in Gram-positive and Gram-negative bacteria, plants or mammals require the oxidation of choline with betaine aldehyde as an intermediate. This two-step oxidation can be catalyzed by two different enzymes (Figure 3, A) or a single one (Figure 3, B).

For Gram-negative bacteria such as *E. coli* or for mammals, the enzyme which catalyzes the oxidation of choline to betaine aldehyde is a membrane-bound choline dehydrogenase (EC 1.1.99.1),^{27,42} whereas for the Gram-positive bacteria *Bacillus subtilis*, this step occurs in the presence of an alcohol dehydrogenase (EC 1.1.1.1).⁴³ In plants, the first step of betaine biosynthesis requires a choline monooxygenase (EC 1.14.15.7).⁴⁴ In all these organisms, a

betaine aldehyde dehydrogenase (EC 1.2.1.8) is then used to catalyze the conversion of betaine aldehyde to glycine betaine.

Certain Gram-positive bacteria, such as *Arthrobacter globiformis*, use yet a single enzyme, a choline oxidase (EC 1.1.3.17), to catalyze the four-electron oxidation of choline to glycine betaine.⁴⁵

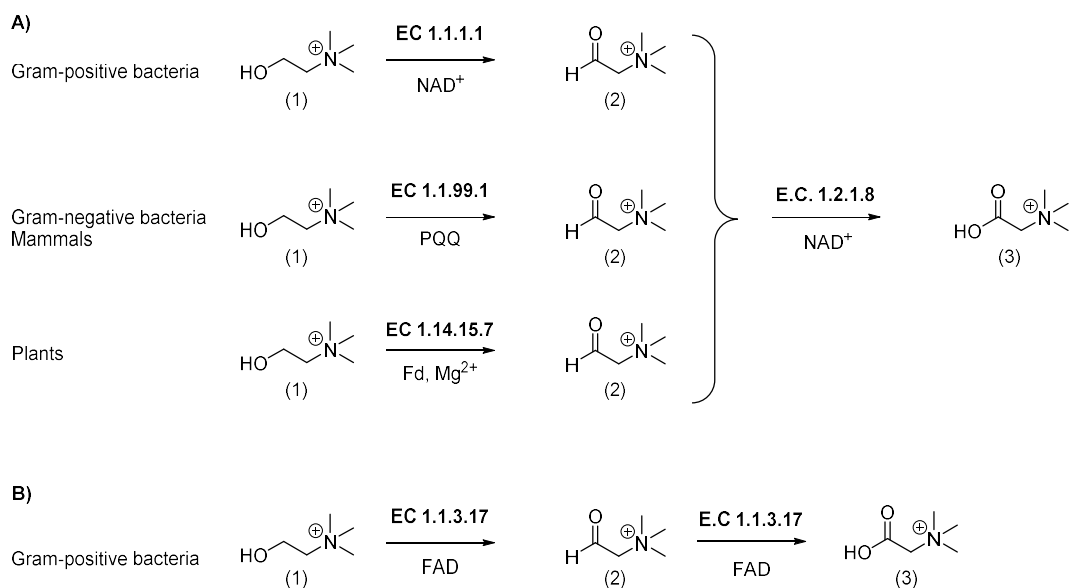


Figure 3 Biosynthetic pathways of glycine betaine (3) from choline (1) through the intermediate betaine aldehyde (2). Different redox co-factors are required: pyrroloquinoline quinone (PQQ), ferredoxin (Fd), flavin adenine dinucleotide (FAD) or nicotinamide adenine dinucleotide (NAD⁺).

1.1.3.2 Glycine methyl transfer

A scarcer biosynthetic pathway of glycine betaine is found in several halotolerant bacteria such as *Actinopolyspora halophila* or *Ectothiorhodospira halochloris*. These organisms synthesize glycine betaine from glycine through a series of methylation reactions that require two SAM-dependent MTs (Figure 4).^{46,47} The regeneration of one methyl group from SAM is an energy consuming process (which costs 12 ATP equivalents to the cell),⁴⁸ which explains why this direct trimethylation of glycine is not as widespread as the oxidation of choline. No enzyme that can catalyze the oxidation of choline to betaine has been identified in *E. halochloris*.⁴⁶ The use of an alternative and energetically expensive pathway by halophilic organisms suggests that they are able to regulate SAM concentration through an efficient balance mechanism.

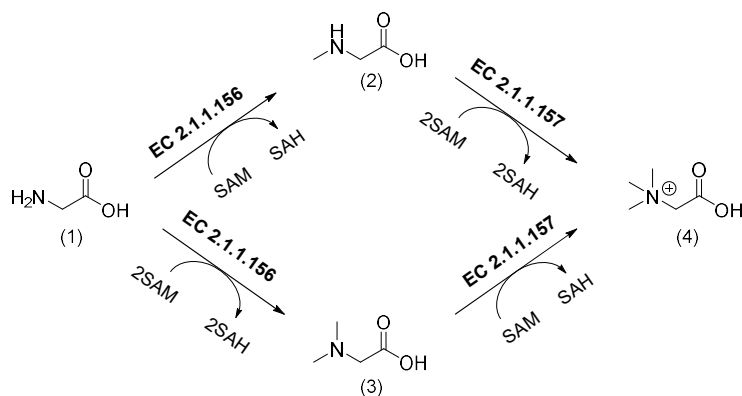


Figure 4 Glycine betaine biosynthesis in halophilic bacteria. The glycine/sarcosine MT (EC 2.1.1.156) catalyzes the formation of either sarcosine (2) or dimethylglycine (3). Sarcosine/dimethylglycine MT (EC 2.1.1.157) methylates both resulting products. Both MTs present an overlap in their substrate specificities which enables them to catalyze the three successive methyl transfers.

To summarize, the different biosynthetic pathways of TMG from either choline or glycine require several enzymes and cofactors. Therefore, they appear barely adaptable to other amino acid betaine synthases. The genes of these enzymes are in fact usually scattered through a whole genome, making the identification of their biosynthetic origins based on the use of genomic data quite challenging. However, the ubiquity of amino acid-based betaines stirs curiosity for the identification of their biosynthetic pathways and functions.

1.2 Aromatic amino acid betaines

Glycine betaine is undeniably defined as an essential osmoprotectant. In addition, quaternary amines such as glycine betaine or choline are important dietary sources of labile methyl groups in mammalian cells. Choline especially represents 60 % of the intake of methyl groups for the human body.⁴⁹ However, the investigation of different betaines, and especially aromatic amino acid betaines, is of great interest as the properties of the side chains might confer additional physiological roles. This section will focus on histidine, tyrosine and tryptophan betaines.

1.2.1 Hypaphorine

1.2.1.1 Occurrence and functions

Hypaphorine or trimethyltryptophan (TMW) was discovered at the end of the 19th century in the seeds of the tropical plant *Erythrina Hypaphorus*. This indole alkaloid was the first naturally occurring tryptophan betaine derivative to be identified.^{50,51} TMW and its halogenated derivatives have since been found in diverse plants, fungi and marine invertebrates and it is clearly established that TMW is an important soil alkaloid.

Hypaphorine is secreted by the ectomycorrhizal fungi of the genus *Pisolithus* (*microcarpus* and *tinctorius*).^{52,53} The symbiotic association between a fungus and a root involves biological interactions and therefore modifications in both organisms. Interestingly, hypaphorine-induced morphogenetic effects on the root hair of *Eucalyptus globulus* were observed. Root hairs are important for water and nutrients intakes,⁵⁴ and act as sensors to detect environmental changes.⁵⁵ The effects of different concentrations of hypaphorine were investigated. The root hair tips present a transitory swelling in presence of 10 to 100 μM of hypaphorine and root hair elongation is fully stopped at higher concentrations (500 μM and more). The *in vivo* concentration in the mycelium is 6 μM ,⁵³ therefore, the reduction of root hair growth is a phenomenon that can occur under physiological conditions. In addition, the contact between the surface of the root host and the mycelium of *P. tinctorius* stimulates hypaphorine accumulation in the mycelium.⁵² These findings suggest that ectomycorrhizal fungi produce hypaphorine to control the root hair elongation of their hosting plants.⁵⁶ The structural similarity between auxin, also named indole-3-acetic acid (IAA) and hypaphorine (Figure 5) suggests a possible effect of hypaphorine on reactions or mechanisms where auxin is involved. As a matter of fact, auxin and hypaphorine have an opposite effect on root hair development. While hypaphorine alters root hair growth, the addition of auxin is able to counteract this effect.⁵⁶ During the establishment of an ectomycorrhiza between the basidiomycete *P. microcarpus* and *E. globulus*, hypaphorine induces an increase in the concentration of calcium ions in root hairs (which plays a key role for their growth),⁵⁷ as well as a reorganization in the actin cytoskeleton of the root hairs.^{58,59} These two reactions are related to each other and provide a reasonable explanation for hypaphorine effect on root hairs growth.

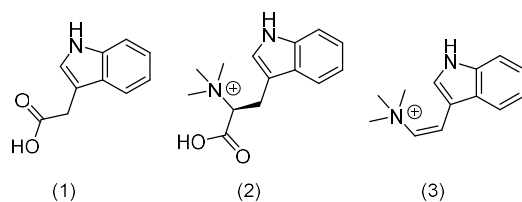


Figure 5 Structural similarity between auxin (1), hypaphorine (2) and conicamin (3).

Hypaphorine was reported to compete with other auxin-binding proteins. The expression of a close homologue (66 % sequence identity) of an auxin-induced glutathione *S*-transferase in *E. globulus* is up-regulated by both auxin and hypaphorine.⁶⁰ This class of enzymes (EC 2.5.1.18) is associated with detoxification reactions or stress responses in plants.⁶¹ However, the exact function of this protein within in plant host is unknown. The fungal indole alkaloid is as well a competitive inhibitor of the auxin binding site in the peroxidase-C found in horseradish.⁶² This outcome strongly supports the role of hypaphorine as an auxin antagonist.

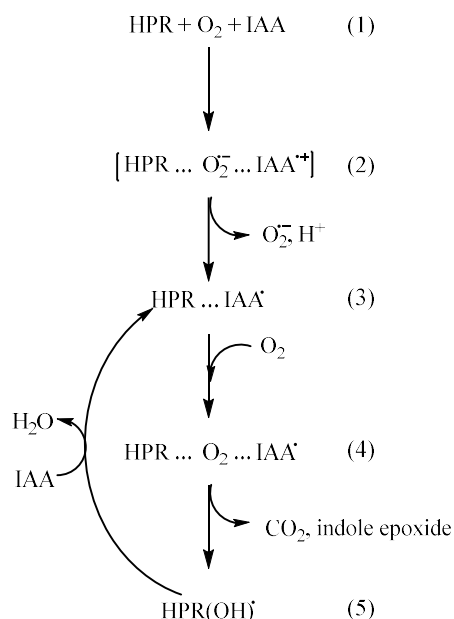


Figure 6 Generation of ROS by the oxidation of IAA catalyzed by horseradish peroxidase HPR. (1) The peroxidase HPR, molecular oxygen and IAA will form a ternary complex (2) where superoxide radical and activated IAA are generated. A binary complex (3) results from the dissociation of the superoxide radical. In the next step, IAA radical is oxidized to indole epoxide (4) and the activated peroxidase (5) can react with a new molecule of IAA to generate a new cycle.

Auxin is an important plant growth regulator that promotes cell elongation. The concentration of this hormone therefore needs to be controlled. The oxidative decarboxylation of IAA by HPR is a major reaction to regulate the level of IAA in this root. During this reaction, molecular oxygen is reduced and oxygen superoxide as well as activated auxin are formed (Figure 6).^{62,63} By competing with auxin, hypaphorine can reduce the formation of reactive oxygen species (ROS), which indicates an indirect antioxidant property. This inhibition might have some medical applications for the regulation of targeted cancer therapy based on the combination of IAA and HRP.⁶⁴

In addition to its function in fungal symbionts, relevant physiological functions in animals were assigned to hypaphorine. However, the indole alkaloid was firstly considered as a poison, but its non-toxicity was afterwards demonstrated.⁶⁵ For example, hypaphorine has a protective effect against seed-eating mammals. Nevertheless it was shown to act more as a feeding deterrent than a toxin.⁶⁶ Recently, its role as an antihyperglycemic agent was reported. Pure hypaphorine from the seeds of *Impatiens niamniamensis* was extracted and isolated then fed to a group of diabetic rats. As a result, a decrease in blood glucose level was observed in this group compared to a control.⁶⁷ Hypaphorine isolated from the leguminous tree *Erythrina velutina*, a Brazilian medicinal plant, was shown to have sleep-promoting effect on mice. Different concentrations of pure extracted compound were administered and led to an enhancement of sleep quality.⁶⁸ This result presents hypaphorine or hypaphorine derivatives as possible candidates for sleeping inducing agents.

Halogenated hypaphorine derivatives widely occur in different species of marine invertebrates^{7,69,70} and are often involved in stress responses or defense mechanisms. Indeed, several halogenated tryptophan and hypaphorine derivatives isolated from marine sources have demonstrated such protective properties.⁶ In particular, compounds containing brominated indole rings, such as 5,6-Dibromo-L-hypaphorine (Figure 1, 8) from the marine sponge *Hyrtios* species, can act as antioxidants.⁶ Moreover, iodine-containing alkaloids (also named plakohypaphorines) from *Plakortis simplex* display relevant medical properties as well. In fact, the antihistamine activity of diiodinated plakohypaphorines (Figure 1, 7) was demonstrated in rats.⁷ In addition, conicamin, an indole derivative isolated from the tunicate *Aplidium conicum* (Figure 5, 3) was shown to also have selective histamine antagonist activity.⁷¹ Thus, these compounds may represent a starting point for the development of drugs with anticancer or anti-inflammatory properties.

Hypaphorine has been also identified in different Leguminosae species such as lentils (100 µg/g), peanuts (70 µg/g) and chickpeas (60 µg/g).⁷²⁻⁷⁴ However, no report is available to provide further information about hypaphorine dietary intake in humans. Nevertheless,

hypaphorine consumed via peanut- and lentil-containing food was found in human milk up to a concentration of 1.24 μM (which is a significant amount as the concentration of free tryptophan in the same sample is 2.23 μM). This demonstrates that hypaphorine is accumulated in the body through the diet.⁷⁴ Therefore, identifying the properties of this indole alkaloid in our body, in view of the interesting properties demonstrated on rodents, is an appealing challenge.

1.2.1.2 Biosynthesis

In order to improve our knowledge regarding hypaphorine properties and possible use as a drug, it is obvious that the determination of the biosynthetic origin of this compound is a prerequisite. We identified two methyltransferases in the wood-degrading fungi *Serpula lacrymans* and *Dichomitus squalens* which permethylate tryptophan. Our findings will be discussed in the following Chapter. The biosynthesis of hypaphorine was unknown up until this point. The discovery of the gene encoding for a hypaphorine synthase is beneficial to identify new derivatives.

1.2.2 Trimethyltyrosine

Hypaphorine illustrates well that the side chain of an aromatic amino acid betaine is the basis for a wide variety of derivatives. In this respect, the tyrosine betaine seems to be a good scaffold for substitutions, even if, unlike hypaphorine, little has been reported about this compound.

1.2.2.1 Occurrence and functions

Trimethyltyrosine and its derivative sticticine (Figure 1, 6) were isolated more than 30 years ago from the lichen *Lobaria laetevinens*.⁷⁵⁻⁷⁷ Tyrosine betaine is also found in the entomopathogen fungus *Metarhizium anisopliae*⁷⁸ as well as in the latex of the South American tree *Moraceae*⁷⁹ and secreted by the beetle *Oreina gloriosa*.⁸⁰ Sticticine was also isolated in Alpine and Ecuadorian Lichens.⁷⁷ Little is known about its function, but the redox active tyrosine side chain indicates a potential role as an antioxidant. In addition, sticticine concentration can exceed 1 M when the thallus of *Lobaria laetevinens* is dehydrated (which corresponds to a water content of 10 to 12 %). Therefore, it might also play a role in efficient osmoregulation.⁵ However, its specific function in the lichen remains still unknown.

1.2.2.2 Biosynthesis

The biosynthetic pathway of sticticine in *Lobaria laetevinens* was proposed in 1981. The first step is the methylation of tyrosine followed by the hydroxylation of the ring and the esterification of the acid moiety.⁵ However, no further research was carried out about the biosynthesis of sticticine or tyrosine betaine.

Recently, we identified the gene encoding for a tyrosine permethylase in the fungus *Aspergillus nidulans* and we tested the activity of this enzyme. Interestingly, the presence of tyrosine betaine in this organism was not reported. Moreover, our results suggest that, in accordance with the proposed pathway of 1981, the biosynthesis of sticticine starts with the methylation of tyrosine. A discussion about this tyrosine methyltransferase ensues in Chapter 2.

1.2.3 Trimethylhistidine and ergothioneine

As hypaphorine, the trimethylhistidine derivative ergothioneine is found in the human body. Yet, a specific transporter which leads to the accumulation of this small metabolite in organs undergoing oxidative stress was identified.⁸¹ In addition, the possible role of ergothioneine for the virulence of *Mycobacterium tuberculosis* was recently reported.⁸² Therefore, the study of both the synthesis of trimethylhistidine and the regulation of ergothioneine biosynthetic pathway is currently of interest.

1.2.3.1 Histidine betaine and its derivatives naturally occur in an extensive range of living organisms

Ergothioneine (Figure 1, 9) was isolated for the first time in 1909 from the ergot fungus *Claviceps purpurea*.⁸³ Trimethylhistidine (TMH) was later identified in mycobacteria as a precursor of ergothioneine.⁸⁴ These two compounds were both recognized as fungal metabolites.⁸⁵ Ergothioneine, TMH and their derivatives are distributed throughout the whole living world. Ergothioneine is not only found in a wide range of microorganisms (such as Ascomycota or Actinobacteria)⁸⁶ but also in plants,^{87,88} animals^{89,90} and in the human body.^{91,92} Recently, new *S*-trimethylhistidine-based alkaloids were identified in the mushroom *Mycena pelianthina*.⁹³ However, in spite of its broad distribution, ergothioneine is known to be only synthesized by certain fungi, such as *Neurospora crassa*,⁸⁵ as well as by bacteria belonging to the

order Actinomycetales and especially the genus *Mycobacterium* (*tuberculosis* and *smegmatis*).⁸⁶ Ergothioneine biosynthesis was also demonstrated to occur in cyanobacteria.^{94,95} To date, there is no evidence of endogenous ergothioneine in higher plants, animals or humans. Plants absorb ergothioneine via associations between soil fungi and their roots.⁹⁶ As ergothioneine is present in common foods such as edible mushrooms (up to 5.5 mg of ergothioneine can be found in 1 g of dried material),⁹⁷ beans or meat products, it is accumulated in animal or human tissues via their respective food chains.^{98,99}

1.2.3.2 Human ergothioneine is accumulated via the specific transporter OCTN1

Ergothioneine is not produced in the human body but it was shown to be accumulated in most human tissues, particularly in red blood cells, bone marrow, seminal fluid, liver, kidneys or eyes, at micromolar to millimolar levels through dietary intake.^{89,100-102} In fact, it was only a few years after its discovery that the presence of this small metabolite in animals was assigned to their consumption of ergothioneine-containing foodstuffs.¹⁰³ In addition, ergothioneine that was fed to rats was shown to be present in their blood and to enter the tissues.¹⁰⁴ This interesting finding at that time already hinted at a mechanism for intake and accumulation of ergothioneine inside the cell. In 2005, Gründemann *et al.* identified a highly specific ergothioneine transporter, named OCTN1, which revealed the mechanism of ergothioneine absorption in the human body. The plasma membrane is not permeable to ergothioneine; therefore, only cells that can express OCTN1 can accumulate and retain ergothioneine. By contrast, cells which lack this transporter do not accumulate ergothioneine.⁸¹

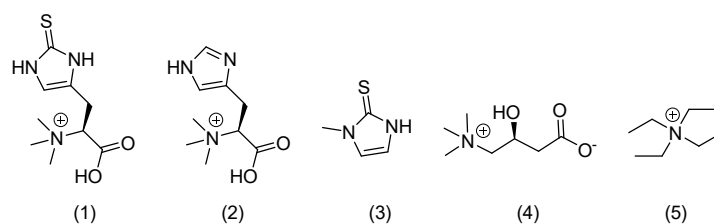


Figure 7 Ergothioneine (1) and structurally similar compounds. OCTN1 substrate specificity was assayed with hercynine (2), methimazole (3), carnitine (4) and TEA (5).

The specificity of this transporter was tested with hercynine, tetraethylammonium (TEA), methimazole and carnitine based on inhibition experiments. The resulting catalytic parameters

of OCTN1 indicate that the affinity for ergothioneine was at least a hundred times stronger than for TEA, methimazole and carnitine, and 25 times better than for hercynine.^{81,105,106} In addition, silencing of the gene encoding for OCTN1 in cell cultures inhibits the uptake of ergothioneine.¹⁰⁷ A similar effect was observed for OCTN1 knockout mice^{108,109} and zebrafish¹¹⁰ in which almost no ergothioneine could be anymore detected. This strongly suggests that no other transporter/mechanism of intake is present. The existence of a specific transporter in human cells suggests an essential function for this histidine betaine derivative.

1.2.3.3 Properties of ergothioneine

Chemically, ergothioneine is a derivative of histidine betaine with a sulfur atom attached to the position 2 of the imidazole ring (Figure 1, 9). The standard redox potentials of naturally occurring thiol such as glutathione (-240 mV at pH 7.0)¹¹¹ or mycothiol (-240 to -260 mV at pH 7.0)^{112,113} usually sit in a range between -200 and -320 mV.⁸ In this aspect, ergothioneine is distinguishable from other biological thiol compounds. Indeed, the standard redox potential of ergothioneine for the thiol-disulfide couple lies outside of this range (-60 mV at pH 7.0).¹¹⁴ In addition, this small metabolite exists as tautomer in solution (Figure 8). This equilibrium tilts in favor of the thione form at physiological pH⁸ and ergothioneine is therefore considered as a thiourea derivative rather than a thiol compound. The prevailing thione tautomer and the unique redox potential of ergothioneine confers a better stability through resistance to auto-oxidation (process that generates superoxide radicals* from H₂O₂ and Fe²⁺) in comparison with other naturally occurring thiols like glutathione.^{106,115,116}

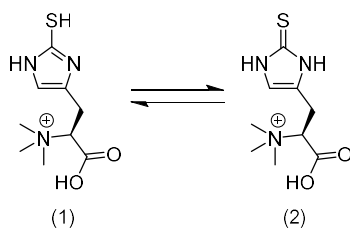


Figure 8 Ergothioneine equilibrium between its two tautomeric forms: thiol (1) and thione (2). At physiological pH, the thione form is predominant.

*Fenton reaction.

1.2.3.4 Physiological properties of ergothioneine

Ergothioneine is a remarkable secondary metabolite with unique properties. It can form complexes with divalent metal cations such as Cu^{2+} , Ni^{2+} , Zn^{2+} or Fe^{2+} , to mention just a few.⁸ Interestingly, the formation of the complex ergothioneine-copper^{II} inactivates the metal cation and then protects DNA from copper-induced DNA damage.¹¹⁷ Ergothioneine can also serve as a nitrogen source for the growth of *Escherichia coli* or the soil bacteria from the *Burkholderia* genus (Figure 9).^{118,119} These organisms express an enzyme called ergothionase which cleaves ergothioneine in two moieties: trimethylammonium and thiolurocanic acid. However the most reported function of ergothioneine in the literature, is as an effective antioxidant and cytoprotectant.^{98,114} Ergothioneine is a powerful scavenger of hydroxyl radicals, hypochlorite or peroxy nitrite and a mild reactant with H_2O_2 .^{114,116,120-122}

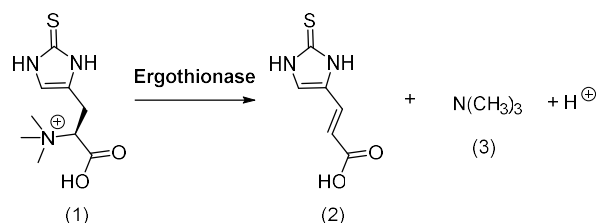


Figure 9 Degradation of ergothioneine (1) catalyzed by the lyase ergothionase. Thiolurocanic acid (2) and trimethylamine (3) are the products of the reaction.

Through deletion of ergothioneine or its transporter OCTN1, the antioxidant effects of the histidine betaine derivative have been reported *in vivo* in bacteria, fungi, nematode and animals. In mycobacteria, two low molecular weight thiol compounds are synthesized: mycothiol and ergothioneine (Figure 10). The mycothiol- and ergothioneine-deficient mutant is more sensitive to peroxide than the wild type. This suggests a protective role of both compounds against oxidative stress.¹²³ $\Delta octn1$ deletion mutant of the nematode *C. elegans* undergoes an increase in the level of oxidative protein damage.¹²⁴ Similarly in mice, OCTN1 knockout decreases the resistance to ROS.¹⁰⁹ Moreover, ergothioneine was found to protect mice against neuronal injuries caused by the two neurotoxic compounds β -amyloid¹²⁵ or D-galactose.¹²⁶ In the fungus *N. crassa*, ergothioneine acts as a protectant against peroxide during germination.¹²⁷

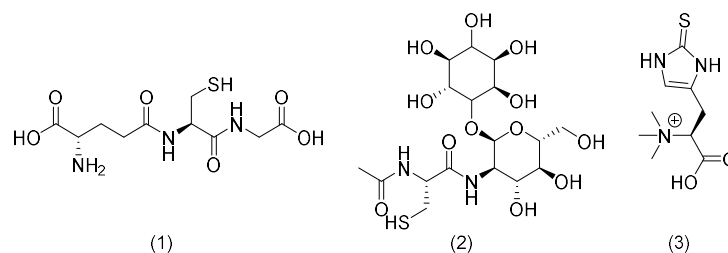


Figure 10 Naturally occurring low molecular weight-thiol compounds: glutathione (1), mycothiol (2) and ergothioneine (3).

During the last decade, significant progress has been made towards understanding the function of ergothioneine not only in fungi and bacteria, but also for higher organisms. If the protective role of ergothioneine is clearly demonstrated *in vitro*, the reactions are often carried out in non-physiological conditions and may therefore not be relevant *in vivo*. Thus, its precise function in the human body remains still unclear. Due to its accumulation in the red blood cells, ergothioneine is proposed as a possible therapeutic treatment for erythrocytes disorders which are predisposed to oxidative damage.¹¹⁶ Moreover, the identification of increased level of ergothioneine in patients suffering of inflammatory pathologies like Crohn's disease^{128,129} indicate this compound as an antioxidant in the human body.¹³⁰ However, despite numerous recent publications about the physiological relevance of ergothioneine, much remains to be discovered.

1.2.3.5 Biosynthesis

The first step in ergothioneine biosynthesis was already suggested in the 1960s by Askari and Melville¹³¹ and Genghof and van Damme.¹³² They proposed hercynine as the first intermediate of the reaction which derives from histidine methylation. More than 40 years after, ergothioneine biosynthetic pathway was identified in *Mycobacterium smegmatis*.¹³³ Ergothioneine synthesis requires five enzymes and is produced from histidine, cysteine, glutamic acid, SAM and molecular oxygen (Figure 11). The discovery of the genes encoding for these five enzymes, namely EgtA, B, C, D and E, provides a considerable contribution to the identification of new organisms producing ergothioneine. In the *M. smegmatis* gene cluster, *egtB* and *egtD* are co-encoded, whereas *egtA*, *egtC* and *egtE* are scattered within the genome.¹³⁴

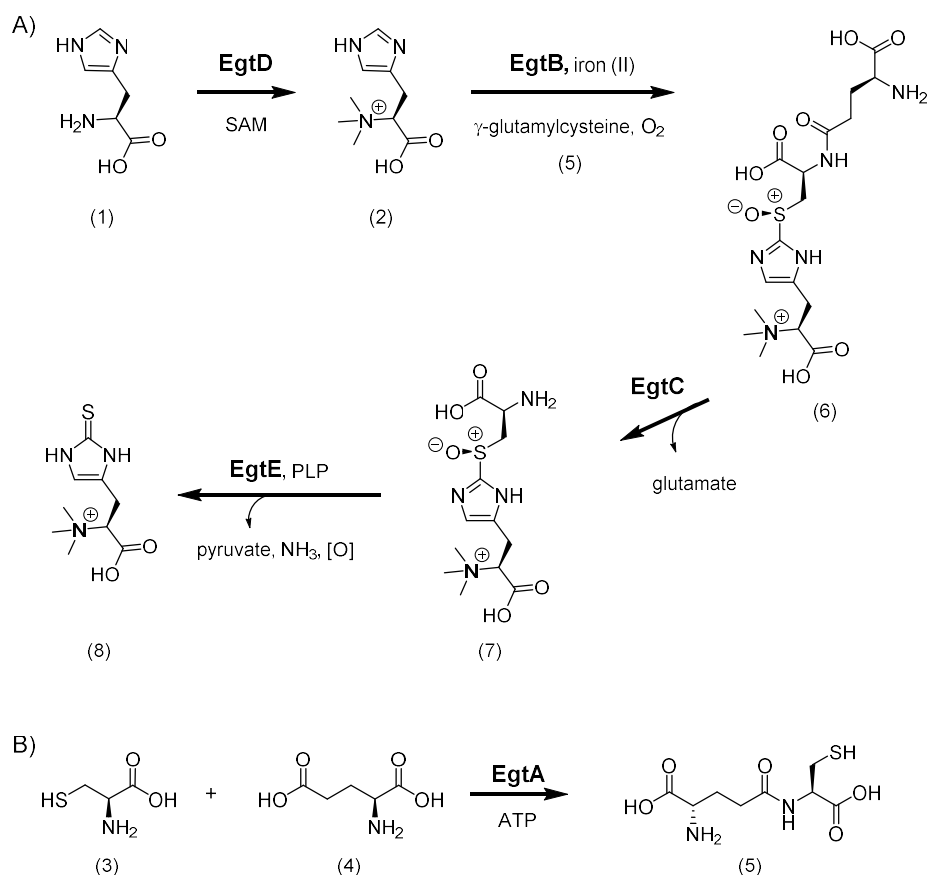


Figure 11 Ergothioneine biosynthetic pathway in *Mycobacterium smegmatis*. **A:** The first step is catalyzed by the SAM-dependent methyltransferase EgtD which trimethylates histidine (1). The resulting hercynine (2) reacts with γ -glutamylcysteine (5) in the presence of oxygen and the non-heme iron enzyme EgtB. The intermediate (6) is then cleaved by EgtC to give hercyncysteine sulfoxide (7). The PLP-binding protein EgtE catalyzes the last step of the biosynthesis and releases ergothioneine (8). **B:** EgtA supplies the dipeptide γ -glutamylcysteine (5) to EgtB from L-cysteine and L-glutamate.¹³⁵

Another pathway was identified in the fungus *Neurospora crassa* (Figure 12).^{127,136,137} In contrast to the mycobacterial synthesis, a single reaction is required to form the intermediate (7) from hercynine. This step is catalyzed by the sulfoxide synthase Egt-1 in the presence of cysteine and molecular oxygen. In contrast to mycobacteria, fungi such as *N.crassa*, synthesize glutathione (Figure 10). GSH results from the condensation of γ -glutamylcysteine and glycine catalyzed by a GSH synthase. Thus the fungal biosynthetic pathways of ergothioneine and GSH do not compete with one another.

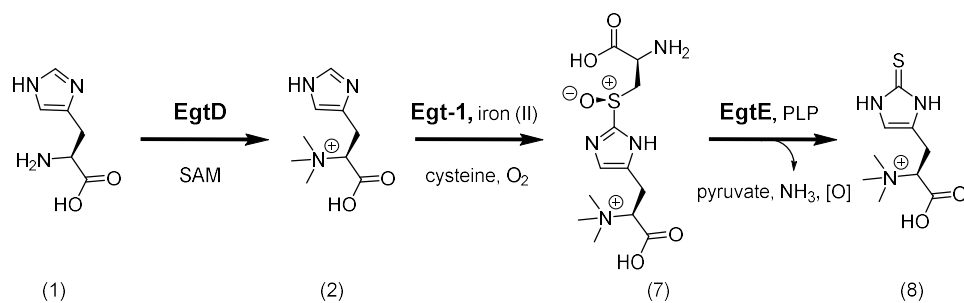


Figure 12 Ergothioneine biosynthetic pathway in *N. crassa*. Like in *M. smegmatis*, the first step is catalyzed by the SAM-dependent methyltransferase EgtD which trimethylates histidine (1). The resulting hercynine (2) reacts with cysteine in the presence of oxygen and the non-heme iron enzyme Egt-1 to give hercyncysteine sulfoxide (7). As its mycobacterial homologue, the fungal C-S lyase EgtE catalyzes the last step of the biosynthesis and releases ergothioneine (8). The numbering was kept identical as Figure 11 for clarity.

In both pathways, EgtD catalyzes the direct permethylation of its substrate histidine.

1.2.4 First step of ergothioneine biosynthesis: histidine methylation

EgtD is the first aromatic amino acid permethylase that has been reported. Up until now, only one enzyme has been identified as an amino acid *N*-trimethylase, the β -alanine betaine (Figure 1, 3) synthase, found in the plant *Limonium latifolium*.^{138,139} This MT was found to be a close homologue of a plant caffeic acid *O*-methyltransferase (67 % sequence identity with *Ziziphus jujuba*).

EgtD is essential for ergothioneine biosynthesis in mycobacteria. The deletion mutants Δ egtD *M. smegmatis* and Δ egtD *M. tuberculosis* no longer produce ergothioneine.^{123,133,140} Moreover, the biosynthesis of ergothioneine in *M. tuberculosis* seems to be altered by the phosphorylation of EgtD¹⁴⁰ and the virulence of *M. tuberculosis* was demonstrated to be dependent of the presence of ergothioneine.¹¹³ In addition, the histidine betaine derivative contributes to the protection of the pathogen against the oxidative stress which results from the defense mechanism of the body.⁸² Therefore, EgtD is an important enzyme for mycobacterial resistance to oxidative environment.

1.3 Aim of the thesis

The aim of this thesis was the characterization of a new family of aromatic amino acid betaine synthases. This project was centered on EgtD, the first member of this newly discovered methyltransferase family.

The residues responsible for the specific binding of histidine in EgtD are described in Chapter 2. Based on this analysis, we identified fungal EgtD homologues with different substrate specificity than EgtD.

The first theme addressed in Chapter 3 is the unique substrate binding mode of EgtD. The second theme concerns the design and analysis of histidine derivatives as inhibitors of the methyltransferase activity.

In Chapter 4, we propose a mechanism for the substrate activation which is required for the methyl transfer to occur in EgtD.

Lastly, the activity of EgtD in an oxidative environment is discussed in Chapter 5.

2 The methyltransferase EgtD reveals the structural basis of aromatic amino acid betaines biosynthesis

EgtD is a histidine methyltransferase (EC 2.1.1.44) that catalyzes the first step of ergothioneine biosynthesis in *Mycobacterium smegmatis*.¹³³ EgtD activity is dependent on the presence of the cofactor S-adenosylmethionine (SAM). SAM is the second most widely used enzyme substrate after adenosine triphosphate (ATP).¹⁴¹ More than 300 enzymatic reactions that are catalyzed by SAM-dependent methyltransferases (MTs) have been described*. These reactions are involved in protein repair, gene silencing, signal transduction or biosynthesis.¹⁴²⁻¹⁴⁵ In this way, SAM-dependent MTs constitute a well characterized and important class of enzymes.

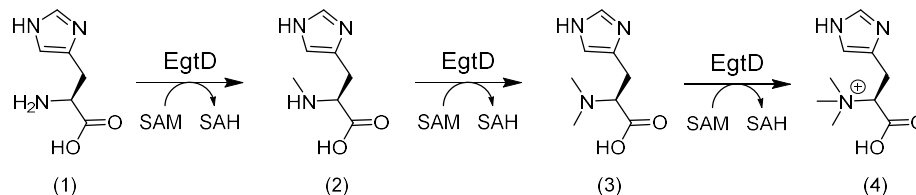


Figure 13 EgtD catalyzes the three consecutive methyl transfers from SAM to the $N\alpha$ of histidine (1). Hercynine (4) is thus the main product of this reaction.

EgtD is the first identified MT that catalyzes direct aromatic amino acid permethylation (Figure 13).¹⁴⁶ In addition to its unique activity, none of the MT structures available in the Protein Data Bank (PDB) is a close homologue to EgtD. The enzyme DOT1L, a human histone lysine MT, is the closest structural homologue of EgtD with 14.53 % identity (PDB: 3QOX). In this Chapter, we investigated the structural basis of EgtD for substrate recognition. The crystal structure of the mycobacterial histidine MT in complex with dimethylhistidine (DMH) and S-adenosylhomocysteine (SAH) revealed the determinants for substrate specificity. From our findings, we were able to convert EgtD into a proficient tryptophan permethylase by enzyme engineering. Moreover, we identified fungal homologs of EgtD that catalyze the methylation of tyrosine and tryptophan.¹⁴⁶

Based on kinetic analysis, X-ray crystallography and bioinformatics searches, we delineated the new Methyltransf_33 protein family as a group of aromatic amino acid methyltransferases.

* Source: enzyme.expasy.org/EC/2.1.1.-

2.1 EgtD activity

2.1.1 Spectrophotometric coupled assay

To characterize the catalytic activity of the MTs, we first implemented a coupled assay for SAM-dependent MTs. The product of the methyl transfer reaction from SAM to histidine is SAH. In 2006, a coupled assay was developed to continuously monitor this conversion (Figure 14).¹⁴⁷

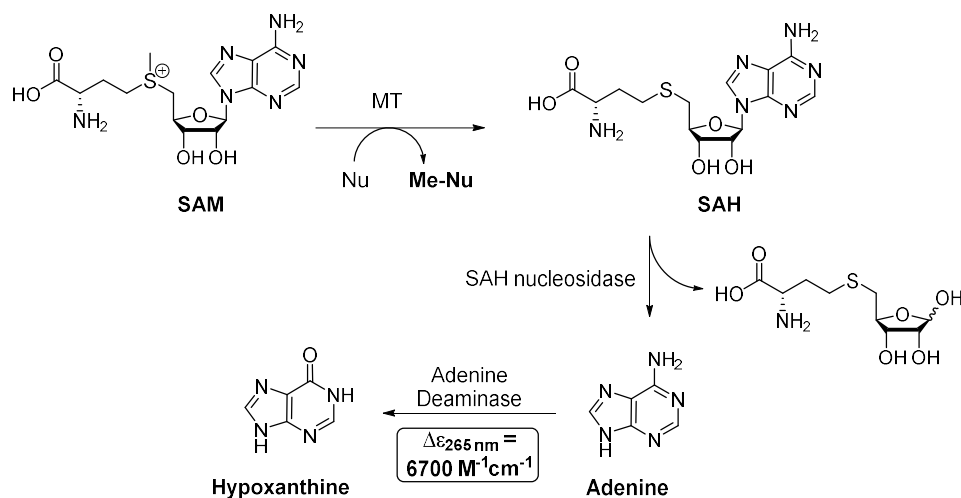


Figure 14 General scheme for the spectrophotometric continuous coupled assay used to characterize the activity of SAM-dependent MTs.

In this assay, the SAM-dependent MT catalyzes the transfer of the methyl group (Me) from SAM to the nucleophile (Nu). The resulting SAH is then cleaved by the nucleosidase into S-ribosylhomocysteine and adenine. Adenine is deaminated to give hypoxanthine. This deamination is accompanied with a decrease in absorbance at 265 nm, which can instantaneously be monitored. Neither the adenine deaminase nor the SAH nucleosidase should be rate limiting. To ensure that the observed rates exclusively correspond to the MT activity, the corresponding concentrations of the coupled enzymes were determined prior to the study of MT kinetics.

The majority of the catalytic parameters determined for the MTs presented in this thesis were determined using this coupled assay. However, some reactions were too slow to be monitored by a change in absorbance at 265 nm (the detection limit being 1.5 $\mu\text{M}/\text{min}$), in these cases, HPLC analysis was used instead.

2.1.2 EgtD is a specific histidine methyltransferase

With this spectrophotometric continuous coupled assay, we first tested the activity of EgtD with the 20 proteinogenic amino acids as potential substrates. The high specificity of EgtD for histidine methylation was already established in 2010.¹³³ This MT is indeed at least 1000 times more active with histidine than with the other 19 amino acids*. We then determined the catalytic parameters of EgtD for the methylation of histidine, methyl- and dimethylhistidine in the presence of 0.5 mM SAM (Table 1).

Table 1 Kinetics parameters of EgtD from *Mycobacterium smegmatis*^a.

| Substrate | k_{cat} (s ⁻¹) | K_M (μM) | k_{cat} / K_M (M ⁻¹ s ⁻¹) |
|--------------------------|-------------------------------------|------------|---|
| Histidine | 0.57 | 107 | 5300 |
| Methylhistidine | 0.23 | 10 | 23000 |
| Dimethylhistidine | 0.40 | 28 | 14500 |

^aReaction conditions: 25 °C, 50 mM Tris/HCl pH 8.0, 50 mM NaCl, 200 μM Mn^{II}, 500 μM SAM, 10-500 μM histidine, MMH or DMH, 5 μM SAH nucleosidase, 10 μM adenine deaminase and 1 to 2 μM of EgtD.

EgtD from *M. smegmatis* (EgtD_{smeg}) catalyzes the methylation of histidine, methylhistidine (MMH) and dimethylhistidine (DMH) with a similar turnover number. As a comparison, another permethylase, the phosphoethanolamine methyltransferase (PfPMT) found in *Plasmodium falciparum* catalyzes the trimethylation of phosphoethanolamine (pEA) to phosphocholine (a precursor of glycine betaine) with a comparable rate (k_{cat} of PfPMT for pEA methylation is 1.8 s⁻¹).¹⁴⁸ The kinetics of histone and peptide methylation performed by protein lysine methyltransferases (PKMTs) is also analogous to the obtained results for EgtD_{smeg} (k_{cat} of SET7/9, a model PKMT, is 0.8 s⁻¹ for histone methylation).¹⁴⁹ Interestingly, EgtD_{smeg} is 40 times faster for histidine methylation than its homolog from *Mycobacterium tuberculosis* (k_{cat} for EgtD_{tub} is 0.013 s⁻¹).¹⁴⁰

With regards to the K_M values, the results differ from one substrate to another. The obtained Michaelis constants of MMH and DMH are lower than the one of histidine; which would suggest that, in order to reach substrate saturation, EgtD requires higher histidine concentration.

* An upper estimate of the catalytic efficiency (5 M⁻¹s⁻¹) was assigned to EgtD with the 19 other amino acids. This estimation was calculated according to the detection limit of the assay and substrate and enzyme concentrations.

However, the steady state kinetics of EgtD with different substrates is not sufficient to distinguish substrate preferences. The different binding affinities between the methyltransferase and the three substrates will be further discussed in section 2.2.2 with the analysis of thermodynamic parameters obtained by isothermal calorimetric titrations (ICT).

Nonetheless, these observations raise the following questions: how does EgtD discriminate against the other 19 amino acids and how do methylated and non-methylated histidine bindings differ from each other?

In order to explore these questions, we investigated the crystal structure of EgtD.

2.2 EgtD crystal structure

EgtD was crystallized and the resulting crystal structures were solved by Allegra Vit at the Helmholtz Center for Infection Research in Braunschweig (DE).

The overall structure of EgtD consists of a typical SAM-dependent MT Rossmann-fold domain combined with an upper domain which is formed by residues 15 to 60 and 196 to 286 (Figure 15).¹⁵⁰ The Rossmann-fold domain of EgtD is comparable to the ones of two other permethylases: a ribosomal *N* α -lysine MT found in bacteria (PrmA) and PfPMT from *Plasmodium falciparum*. It is also interesting to mention that, despite a low sequence similarity of 14 % with EgtD, the SAM/SAH binding sites of EgtD and PfPMT are highly similar.¹⁵¹

As previously mentioned, no structures of any EgtD homologs exist in the PDB. The only structural comparisons that can be made for this enzyme is in the SAM binding sites of PfPMT (PDB: 3UJ7) and PrmA (PDB: 2NXE), as described above. Therefore, EgtD constitutes the first member of a new class of methyltransferase named Methyltransf_33 family.

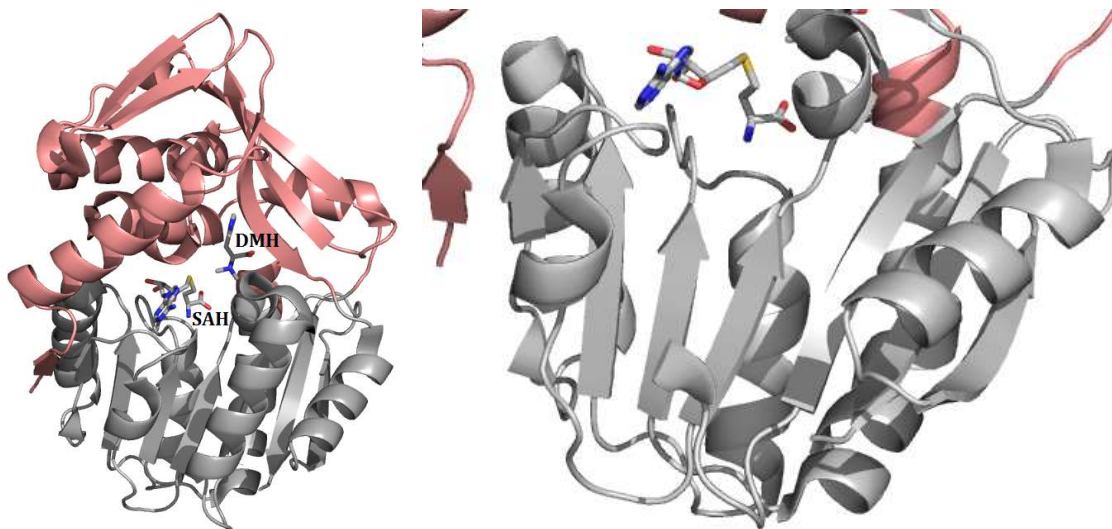


Figure 15 Left: EgtD structure in complex with SAH and DMH (PDB: 4PIO, 1.51 Å). The substrate binding site is located in the gap between the Rossmann-fold domain (grey) and the upper domain (salmon). Right: Enlargement of the Rossmann-fold domain of EgtD.

2.2.1 Identification of the essential catalytic residues

2.2.1.1 Structural basis for ligand binding

EgtD was crystallized in its *apo* form (PDB: 4PIM, 1.75 Å) and in complex with DMH (PDB: 4PIN, 1.9 Å). The positions of the residues that define histidine binding pocket (Phe47, Tyr56, Thr163, Asn166, Thr213, Met252 and Glu282) generally remain unchanged in the presence or absence of substrates. Incidentally, Glu282 is the only residue within the active site that changes conformation consequently to substrate binding (Figure 16).

Overall, the superimposition of the apoenzyme and the ternary complex reveals a pre-organized binding site.¹⁴⁶

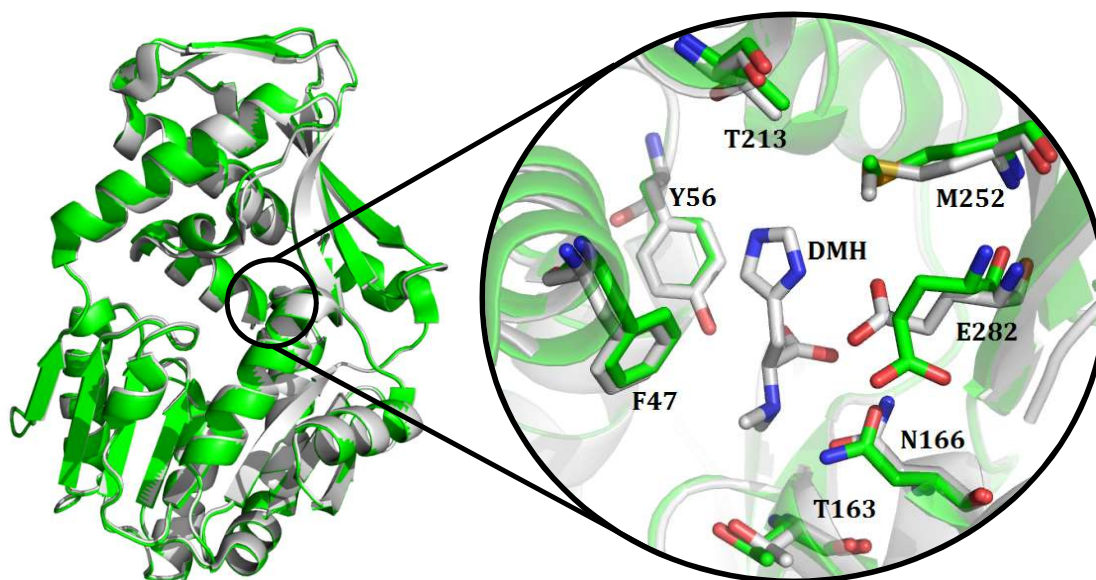


Figure 16 Left: Superimposition of EgtD *apo* (PDB: 4PIM, green) and in a binary complex with dimethylhistidine (PDB: 4PIN, gray). No large scale change is observed upon substrate binding. **Right:** Enlargement of histidine binding site. Only Glu282 moves towards DMH upon binding.

2.2.1.2 Interactions between EgtD and the α -amino and carboxylic groups of histidine within the catalytic site

The catalytic residues within the substrate binding pocket recognize both carboxylic and α -amino groups of DMH through an array of hydrophilic interactions (Figure 17). The negative charge of the carboxylic group of DMH is stabilized by coordination to the side chains of Asn166 ($O\cdots N$ distance: 3.0 Å), as well as Tyr56, Tyr206 and Ser284 ($O\cdots O$ distances: 2.7, 2.9 and 2.8 Å respectively). The latter two form hydrogen bonds to Lys286 ($O\cdots N$ distances: 2.9 and 3.3 Å respectively) which help to stabilize the anionic charge on the substrate. Asn166 also interacts with the α -amino group of DMH ($N\cdots O$ distance 2.8 Å). The orientation of the methyl group suggests that the α -amino group is protonated. Indeed, the tetrahedral geometry of the $N\alpha$ of the substrate indicates that the proton is pointing towards the oxygen of the amide side chain of Asn166. To summarize, all these interactions clearly determine substrate specificity for the α -amino and carboxylic moieties. Yet, they do not provide any evident explanation for the preferential binding of MMH or DMH compared to histidine.

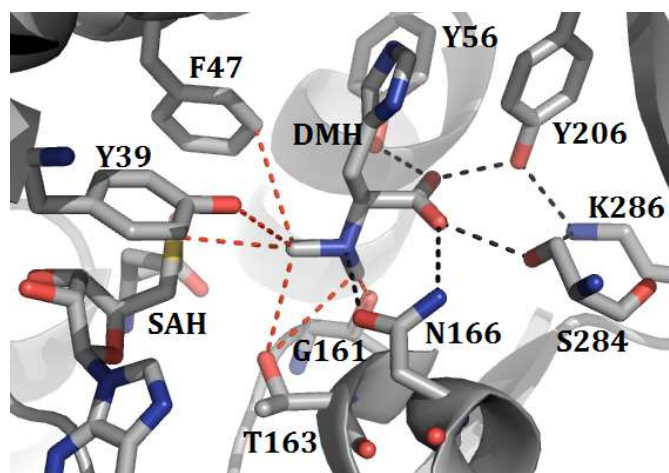


Figure 17 Interactions between dimethylhistidine and the catalytic residues within the binding pocket (PDB: 4PIO). The substrate is recognized by an array of hydrogen bonds (black) and CH...O/C/S interactions (red).

2.2.1.3 Interactions between EgtD and the $N\alpha$ -methyl groups of dimethylhistidine within the catalytic site

We argue that additional interactions, which might be weaker than typical hydrogen bonds (such as van der Waals forces) could occur between the catalytic residues of the enzyme and the two methyl groups of DMH (Figure 17). In fact, one methyl group of DMH points to the sulfur atom of SAH (C...S distance: 3.4 Å, CHS angle: 105.9 °), which represents the spent methyl donor after the methyl transfer. This methyl group is also in van der Waals distance with several residues within the binding site: the oxygen atoms in the side chain of Thr163 and Tyr39 (C...O distances: 3.5 Å for both, CHO angles: 146.8 and 161.3 ° respectively), and the phenyl ring of Phe47 (C...C distance: 3.9 Å, CHC angle: 132.3 °). The second methyl group is in close contact with the backbone carbonyl group of Gly161 (C...O distance: 3.0 Å, CHO angle: 107.3 °) and is also in van der Waals contact with the oxygen atom of Thr163 (C...O distance: 3.6 Å, CHO angle: 141.7 °). According to the distances and angles measured between the different atoms*, most of these interactions could be assigned as CH...O bonds.

The impact of CH...O bonds in biological systems has been increasingly studied over the last 15 years.¹⁵² SAM CH...O hydrogen bonds have already been shown to participate in the coordination of SAM methyl group in the SET domain of PKMT.^{153,154} Moreover, they were also demonstrated to stabilize the binding of the dimethyl ϵ -amine of lysine in the active site of this

*The distance and angular parameters used to define CH...O bonds are described by Horowitz and Trievel.¹⁵² The typical van der Waals distances between the carbon and oxygen atoms as well as between the hydrogen and oxygen atoms are 3.7 and 2.7 Å respectively. The angle defined by the three atoms C, H and O corresponds to the one of a weak conventional hydrogen bond, which is between 90 and 150 °.

MT.¹⁵⁵ In conclusion, even if CH...O hydrogen bonds are weaker than usual hydrogen bonds involving heteroatoms, the accumulation of these minor interactions could end in a significant and stronger binding for DMH compared to histidine.

2.2.1.4 Glu282, an essential residue for histidine binding in EgtD

The residues interacting with both α -carboxylic acid and amino groups of the substrate being identified, we will now focus on the recognition of the side chain of the substrate. Both nitrogen atoms of the imidazole ring of DMH form hydrogen bonds with two residues within the binding pocket: Thr213 and Glu282 (Figure 18).

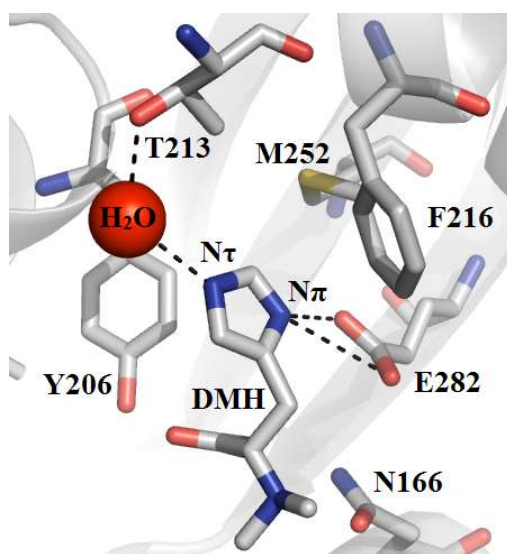


Figure 18 The imidazole side chain of DMH is immobilized through hydrogen bonds to Glu282 and to Thr213 via a water molecule (PDB: 4PI0).

The $N\tau$ of DMH connects to residue Thr213 through a water-mediated bond ($O_{\text{Thr}}\cdots O_{\text{water}}$ distance: 2.7 Å; $O_{\text{water}}\cdots N\tau$ distance: 2.8 Å). A recent study about EgtD activity in *Mycobacterium tuberculosis* shows that this particular residue could be involved, through posttranslational modification, in the regulation of ergothioneine biosynthesis.¹⁴⁰ Moreover, Thr213 is conserved among mycobacterial histidine methyltransferases. The $N\pi$ forms a salt bridge with residue Glu282 ($N\cdots O$ distances: 2.6 and 3.5 Å). Interestingly, this residue is the only one that changes its conformation upon substrate binding (Figure 16). In order to test its importance for substrate recognition, we constructed the E282A variant of EgtD and measured the catalytic parameters of

this mutant for histidine methylation. The substitution for a non-polar residue will suppress the interaction between the N π of the imidazole ring and the catalytic site.

The resulting activity of EgtD E282A toward histidine methylation decreases by a factor of more than a hundred (Table 2) in comparison with the wild type (WT). As the turnover number is only reduced by a factor of five, this loss of catalytic efficiency can be mainly attributed to a drastic increase in the K_M value (25 times higher than for the WT). This indicates that the elimination of the hydrogen bonds between Glu282 and the imidazole side chain significantly alters the affinity of EgtD for its substrate histidine.

Table 2 Kinetics parameters of EgtD E282A compared to EgtD WT^a.

| Enzyme | k_{cat} (s ⁻¹) | K_M (μ M) | k_{cat} / K_M (M ⁻¹ s ⁻¹) |
|-------------------|------------------------------|------------------|--|
| EgtD E282A | 0.10 | 2500 | 40 |
| EgtD WT | 0.57 | 107 | 5300 |

^aReaction conditions: 25 °C, 50 mM Tris/HCl pH 8.0, 50 mM NaCl, 200 μ M Mn^{II}, 500 μ M SAM, 10-7500 μ M histidine, 5 μ M SAH nucleosidase, 10 μ M adenine deaminase and 5 or 1 μ M of EgtD E282A or EgtD WT respectively.

A sequence alignment of EgtD homologues that are encoded in ergothioneine synthetic genes were compared to find that Glu282 is strictly conserved.¹⁴⁶ This strict conservation and the kinetics data obtained for EgtD E282A variant allow us to undoubtedly identify Glu282 as an essential residue responsible for substrate specificity. In addition, we did find distant EgtD homologs in fungi without a glutamate at position 282. As a consequence, these enzymes are characterized by different substrates specificities (see sections 2.3 and 2.4).

2.2.2 EgtD is a cooperative enzyme

2.2.2.1 Affinity enzyme-substrate

EgtD catalyzes three consecutive methyl transfers. A key question is whether EgtD operates as a processive or distributive enzyme. The term processivity refers to the ability of an enzyme to catalyze consecutive reactions steps without releasing the substrate.¹⁵⁶ This feature is

particularly of great importance for DNA polymerases involved in DNA replication as the binding of the template to the enzyme is the rate-limiting step of the process.¹⁵⁷ EgtD would be defined as distributive if, in contrary, the dissociation of the complex enzyme-substrate occurs after each incorporation of a methyl group on histidine. To characterize the processive or distributive feature of EgtD, the distribution of the different products of the reaction (MMH, DMH or hercynine) were analyzed and the dissociation constants K_D of the three substrates of EgtD were measured by isothermal calorimetry titration (ICT).

A reaction containing an equimolar concentration of SAM and histidine catalyzed by EgtD was analyzed by ion-exchange (IE) HPLC to identify the different products. Hercynine is mainly formed ($88 \pm 4 \%$) whereas DMH and MMH are found in much smaller amounts (13 ± 9 and less than 1% respectively). EgtD favors then the formation of the fully methylated substrate. This observation is consistent with the kinetic studies (Table 1) suggesting MMH and DMH as better substrates than histidine for the MT. Nonetheless, the affinity of EgtD for the three substrates can only be accurately compared into knowledge of each of the K_D values (Table 3).

The K_D values were determined by ICT. The ICT experiments were performed by Allegra Vit.

Table 3 Dissociation constants of EgtD substrates established by ICT^a.

| Titrant | His | MMH | DMH | His (SAH)* | MMH (SAH)* | DMH (SAH)* | SAH | SAM |
|--|-----------------|----------------|--------------|-------------------|-------------------|-------------------|-----------------|-----------------|
| K_D (μM) | 290 ± 14 | 70 ± 30 | 4 ± 2 | 37 ± 1 | 14 ± 7 | 2 ± 1 | 210 ± 20 | 270 ± 20 |

^aReaction conditions: 25°C, 20 mM Tris/HCl pH 7.5, 150 mM NaCl, 100 μM EgtD in cell, 5 mM ligand in the syringe.

*: EgtD solution contained 7 mM of SAH.

In the absence of SAH, DMH is a 70- and 17-fold better binder than histidine and MMH respectively. In the presence of SAH, DMH is also preferred compared to histidine and MMH (18- and 2-fold better binder respectively). Therefore, DMH is the favored substrate of the MT, regardless of the presence of SAH. These results demonstrate a preferential substrate binding order which provides an explanation for the almost exclusive formation of hercynine as a product from the methylation of histidine. Through these thermodynamics data, we were able to characterize EgtD as a cooperative MT (the term cooperativity describes the ability of an enzyme to generate underrepresented intermediate products during catalysis).¹⁵⁸ However, this does not necessarily indicate processivity.

2.2.2.2 Probing the determinants for trimethylation

The cooperativity of EgtD arises from the preferential binding of DMH. We were then interested in determining how EgtD favors methylated histidine binding. The structural analysis of the substrate binding pocket reveals interactions between the two methyl groups of DMH and various residues (Figure 17). The accumulation of CH \cdots O hydrogen bonds can drive to a better DMH binding in comparison with histidine.

To probe the structural basis for this unique activity, we first compared the sequences of EgtD and the closest EgtD homolog with known function, EasF¹⁵¹ (24.8 % sequence identity). This enzyme is found in the ergot fungus *Claviceps purpurea* and catalyzes the single methylation of dimethylallyltryptophan into chanoclavine, an intermediate in the biosynthesis of ergotamine and lysergic acid, a precursor of lysergic acid diethylamide.¹⁵⁹ The sequence of an EasF homolog (FgaMT) found in *Aspergillus fumigatus*, which catalyzes the identical reaction but as an intermediate of fumigaclavines biosynthesis,¹⁶⁰ was also compared to EgtD (Figure 19). The idea was to determine if the residues interacting with the methyl groups of DMH in EgtD are conserved in EasF and FgaMT or not. The residues which are in van der Waals contact with the methyl groups of DMH (identified in Figure 17) are indicated in grey in the following alignment. The majority (Tyr39, Gly161, Thr163, Ans166 and Tyr206) are also present in both fungal MTs, with the exception of the two residues Phe47 and Tyr56. Their non-conservation would suggest that these two residues can play a role in the control of the single methylation of the substrate

```
          39      47      56      161 163 166      206
  egtD    F $\mathbf{Y}$ DAVGS $\mathbf{D}$ L $\mathbf{F}$ DQITRLPE $\mathbf{Y}$ YPTR...L $\mathbf{G}$  $\mathbf{S}$  $\mathbf{T}$ I $\mathbf{G}$  $\mathbf{N}$ LTPAP...RAY $\mathbf{D}$ D...
  fgaMT   FYSTKGIQH $\mathbf{W}$ NRHSHAAD $\mathbf{F}$ YPRH...FGLTIGNFSRDN...RAYTA...
  easF    FYSNEGLEH $\mathbf{W}$ NHHSRQPD $\mathbf{F}$ YPRR...LGLTIGNFSRQN...RAYTS...
```

Figure 19 Abbreviated sequence alignment of the 3 methyltransferases (EgtD numbering). The residues highlighted in grey in the sequence of EgtD are in van der Waals contact with the methyl groups of DMH. The corresponding residues indicated in red in the sequences of the two fungal methyltransferases are the only ones, in this respect, which differ from EgtD.

No crystal structure is available for EasF. In order to check the orientation and localization of the residues identified for their participation in methyl group recognition, a homology model of EasF was generated and the resulting structure was superimposed to EgtD (Figure 20). This structural homology model of EasF indicates no major conformational changes for the residues of interest.

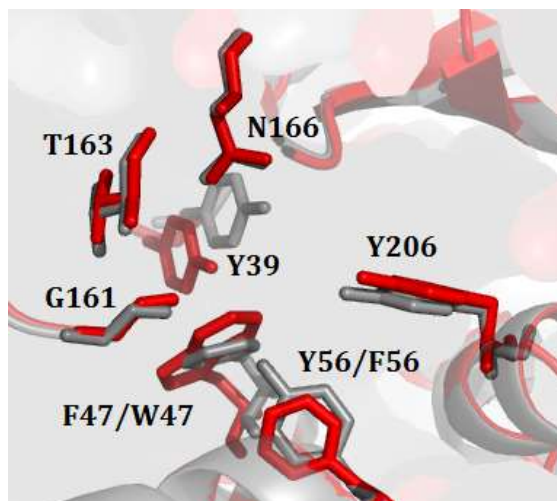


Figure 20 Homology model of EasF binding site (red) superimposed with EgtD (PDB: 4PIN, grey). The residues Asn166, Thr163, Tyr39 and Gly161 are conserved in both MTs and have similar positions within the binding sites. The same observation is made for Phe47 and Trp47, as well as Tyr56 and Phe56 (in EgtD and EasF respectively).

Tryptophan and phenylalanine are found at position 47 and 56 in both mono methyltransferases. We started to investigate their possible role as determinants for trimethylation. The two residues Phe47 and Tyr56 of EgtD were then respectively mutated into a tryptophan and phenylalanine, so to mimic the catalytic site of EasF. We constructed the three following EgtD variants: the single mutants F47W and Y56F and the double mutant F47W Y56F. The qualitative analysis of the products of histidine methylation catalyzed by those three variants determined if the mutated residues have an effect on the consecutive methyl transfers and thus on EgtD cooperativity.

The distribution of the products of histidine methylation catalyzed by either EgtD WT or the three mutants was analyzed by IE HPLC (Figure 21). These experiments were performed in presence of saturated concentrations of histidine and SAM (0.5 mM each).

The mutations inspired by the sequences of both monoMTs EasF and FgaMT did not show the expected repercussion on the enzymatic activity of EgtD. As a matter of fact, both single mutants (EgtD F47W and Y56F) still catalyze three consecutive methyl transfers as hercynine is found as the main product of the reactions catalyzed by these variants (Figure 21C and D). Moreover, no product can be detected even after 10 hours in the presence of the double mutant EgtD F47W Y56F (Figure 21B).

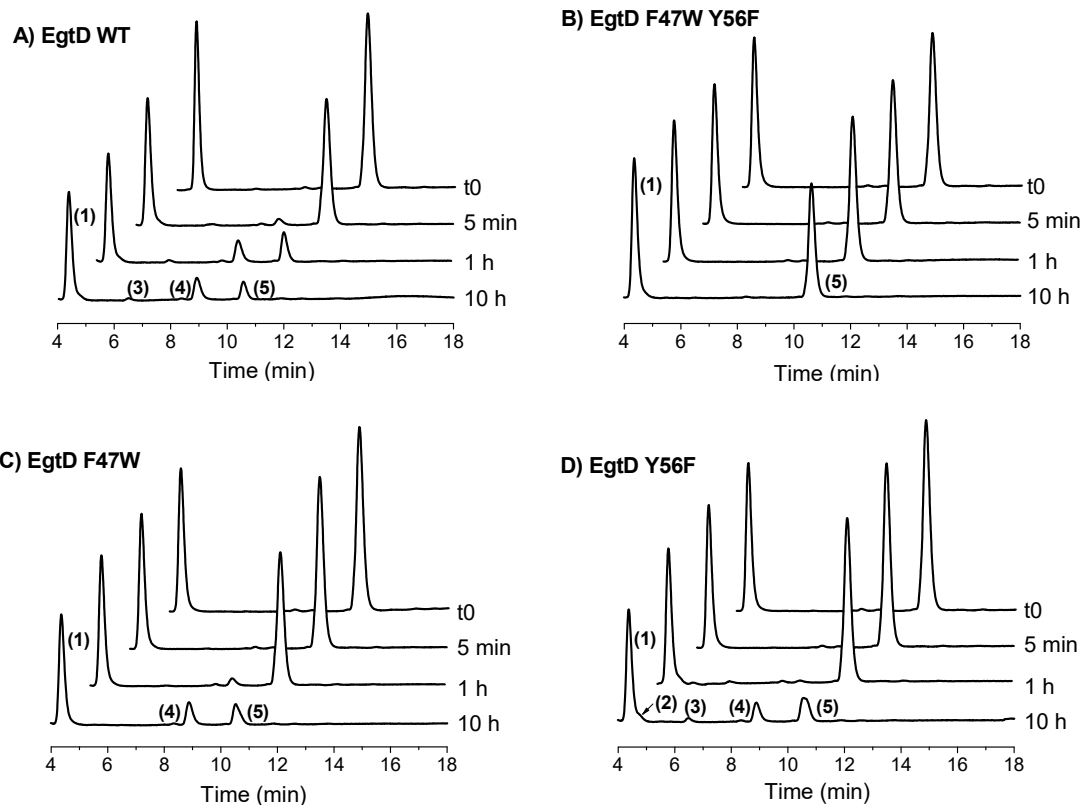


Figure 21 HPLC traces of histidine methylation catalyzed by either EgtD WT or one of the three variants. Reactions conditions: 25 °C, 50 mM Tris/HCl pH 8.0, 50 mM NaCl, 200 μ M Mn^{II}, 0.5 mM SAM, 0.5 mM histidine, 10 μ M SAH nucleosidase, 5 μ M adenine deaminase, 1 μ M MT. The reactions were analyzed at four different time points: 0, 5, 60 and 600 minutes. The numbering corresponds to the following compounds: 1: Histidine (4.4 min), 2: MMH (4.7 min), 3: DMH (6.5 min), 4: TMH (8.9 min) and 5: SAM (10.6 min).

In conclusion, engineering EgtD binding site to imitate a monoMT was not sufficient to limit the catalysis of EgtD to one single methyl transfer. Other interactions, yet unidentified, might then play a critical role in the recognition of the methylated substrate. The cooperativity of EgtD seems to be a complicated and deeply rooted feature of the MT.

2.3 Identification of a tyrosine methyltransferase

We identified Thr213, Met252 and Glu282 as the essential residues for substrate side chain recognition (Figure 18). In particular, kinetics data show that Glu282 is crucial for histidine binding through the formation of hydrogen bonds with the imidazole ring (Table 3). Therefore, we argued that a MT which has a different residue at this precise position has different substrate specificity. In order to pinpoint EgtD homologues which might accept substrates other than

histidine, a bioinformatics search for *egtD*-like genes was performed. The resulting sequences were compared to EgtD in order to determine which residues are present in the substrate binding site of these homologues.

| | 213 | 252 | 282 |
|--------------------------------|---|-----|-----|
| <i>egtD</i> | ...DAAGV T AAFNRN...RIE M WLRARTA...ML T EVSCKFRP... | | |
| <i>Dichomitus squalens</i> | ...DTNGVSRRFVMN...RKRAYYKSGSD...IRVAFSHKFSE... | | |
| <i>Aspergillus nidulans</i> | ...DPDGINHRFVKN...AHNQYYITRAD...LLAVRSXKYDA... | | |
| <i>Talaromyces stipitatus</i> | ...DPEGANQRFVKN...RHSQYYLDAD...LLAIQSHKYDS... | | |
| <i>Exophiala dermatitidis</i> | ...DSENRNNEEFIRN...RHEQYLVPHKD...IFVVSSHKYDT... | | |
| <i>Baudoinia compniacensis</i> | ...DKAGCNKRFILN...RHSQYVVPLTD...VYVVSSYKYDK... | | |
| <i>Serpula lacrymans</i> | ...DREGFAERFCLN...RHEVYYRCTHD...ILLAHSYKYAA... | | |
| <i>Saprolegnia diclina</i> | ...DPSGLHREFVLN...RHEAHLQSLEA...IHVAYSHKYSE... | | |
| <i>Glomus intraradices</i> | ...DPKGINAKFIMN...RHEAYCKVKND...INIGYSHKYNK... | | |

Figure 22 Abbreviated sequence alignment of a selection of fungal EgtD homologues. Thr213, Met252 and Glu282 (highlighted in grey) recognize the imidazole side chain of histidine in EgtD.

Interestingly, the identified fungal sequences lack the essential Glu282 residue, which indicates that histidine is not a substrate for these enzymes. It is principally replaced by non-polar residues like alanine or valine. Overall, the essential residues responsible for histidine binding at positions 213, 252 and 282 significantly vary among the fungal putative methyltransferases (Figure 22). This hints that these putative MTs may have different substrate specificities.

2.3.1 Production and characterization of *SticA*, a tyrosine betaine synthase

An *egtD*-like gene (28.15 % sequence identity with *egtD*) was found in the genome of the fungus *Aspergillus nidulans*. The residues at position 213, 252 and 282 differ from the ones found in EgtD sequence and are respectively replaced by Asn, Gln and Val (Figure 22). A homology model with EgtD shows that the substrate binding pocket is consequently widened (Figure 23), enabling a bigger aromatic amino acid to fit inside. Intuitively, this fungal MT was proposed to be specific for tyrosine, as both Asn and Gln residues could form a hydrogen bond with the hydroxyl group of the side chain.

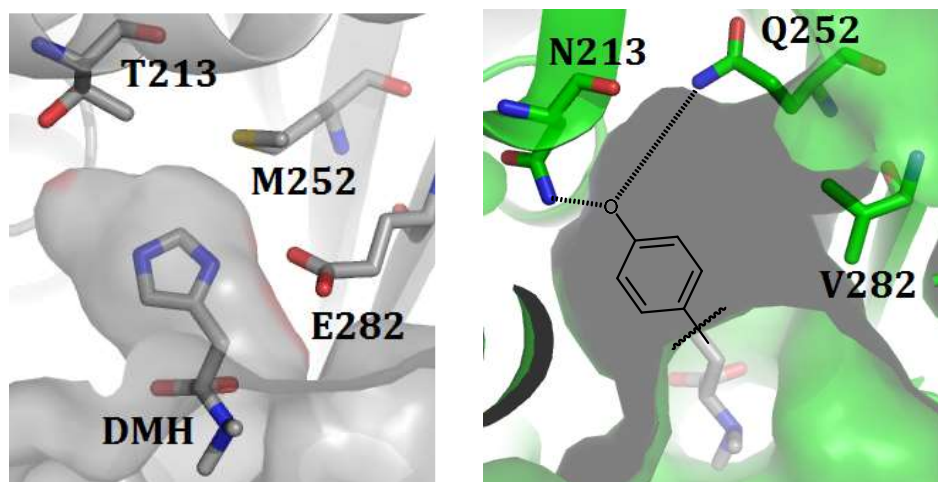


Figure 23 Substrate binding pockets in EgtD and in the MT from *A. nidulans*. **Left:** EgtD crystal structure co-crystallized with DMH (PDB: 4PIN). **Right:** Homology model of the fungal MT. The three residues which define the size of the hydrophobic pocket in EgtD are Thr213, Met252 and Glu282. Their corresponding homologues in the fungal MT are Asn213, Gln252 and Val282 (EgtD numbering).

In the genome of *A. nidulans*, this putative tyrosine MT is co-encoded with a taurine dioxygenase (gene locus XP_681863). This observation allows us to suggest a pathway for the biosynthesis of the tyrosine betaine derivative sticticine in the fungus (Figure 24).

Sticticine is a tyrosine betaine derivative which is thought to play a role in osmoregulation in lichen species such as *Lobaria laetevirens*.^{75,77} The biosynthetic pathway of sticticine in this organism was proposed in 1981 and involves the methylation and hydroxylation of tyrosine, with the methyl transfer taking place first.⁵ Considering that the two fungal enzymes are encoded together, our assumption was that a similar biosynthesis would take place in *A. nidulans* and the putative MT and dioxygenase were thereby named SticA and SticB respectively.

In order to determine which step would be first in *A. nidulans*, the activity of SticA was measured with the 20 proteinogenic amino acids. As dihydroxyphenylalanine (DOPA) appeared as a possible substrate for the MT through the proposed biosynthetic pathway in Figure 24, this compound was also tested as a substrate for the fungal enzyme.

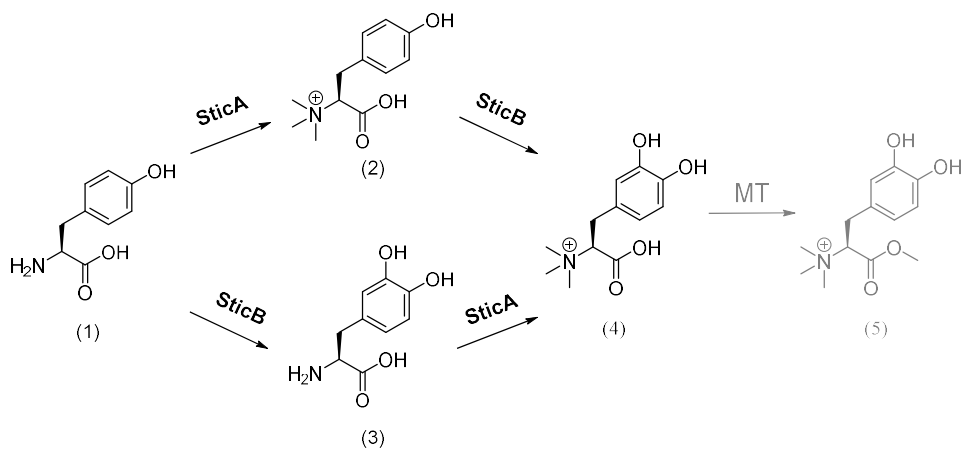


Figure 24 Proposed biosynthesis of sticticine in *A. nidulans*. Two possible pathways were considered. The substrate tyrosine (1) can be either first methylated by SticA, and the resulting tyrosine betaine (2) is then hydroxylated to DOPA betaine (4) and further methylated to sticticine (5), or the first step of sticticine biosynthesis can be the hydroxylation of tyrosine followed by the methylation of the resulting DOPA (3).

2.3.2 Kinetics

As for EgtD, SticA activity was tested *in vitro* and the catalytic parameters of the fungal methyltransferase were determined using the spectrophotometric continuous assay described in section 2.1.1.

Table 4 Kinetics parameters of SticA from *Aspergillus nidulans*^a.

| Substrate | k_{cat} (s ⁻¹) | K_M (μM) | k_{cat} / K_M (M ⁻¹ s ⁻¹) |
|-------------------------|------------------------------|------------|--|
| Tyrosine | 0.11 | 21 | 5240 |
| Dimethyltyrosine | 0.05 | 43 | 1200 |
| Histidine | 0.02 | 33 | 660 |
| Phenylalanine | 0.14 | 5400 | 25 |
| DOPA | 0.10 | 148 | 660 |

^a Reaction conditions: 25 °C, 50 mM Tris/HCl pH 8.0, 50 mM NaCl, 200 μM Mn^{II}, 500 μM SAM, 10 μM to 10 mM nucleophile, 5 μM SAH nucleosidase, 10 μM adenine deaminase and 2 to 5 μM of SticA.

SticA shows significant activity with histidine, phenylalanine, tyrosine, dimethyltyrosine (DMY) and DOPA*. Yet, the catalytic efficiency of the fungal methyltransferase for tyrosine methylation is comparable to histidine methylation catalyzed by EgtD ($5300 \text{ M}^{-1}\text{s}^{-1}$, see Table 1).

The fungal MT also catalyzes the methylation of phenylalanine with a similar turnover number as for tyrosine. However, as indicated by the Michaelis constants, the MT has a greater affinity for tyrosine ($K_{M,\text{Tyr}}$ is 250 times lower than $K_{M,\text{Phe}}$). This observation is coherent with the analysis of the structural homolog of SticA (Figure 23). The binding pocket of SticA is certainly enlarged compared to EgtD; in this way either phenylalanine or tyrosine can fit inside. Nonetheless, Asn213 and Glu252 can form hydrogen bonds with the hydroxyl group of tyrosine providing a reasonable explanation for the preferred binding of tyrosine compared to phenylalanine. The k_{cat} values of SticA with DOPA and tyrosine are also comparable but the $K_{M,\text{DOPA}}$ value is seven times higher than for tyrosine. This difference can be interpreted in the context of the proposed biosynthetic pathway of sticticine (Figure 24). If tyrosine is a better substrate for the MT than DOPA, it suggests that the first step of sticticine biosynthesis is thus the trimethylation of tyrosine. Nevertheless, the similarity in turnover numbers of tyrosine and DOPA also indicates a certain degree of flexibility in the order of the steps involved in sticticine biosynthesis.

Interestingly, the K_M value for histidine is rather similar than the one of tyrosine. In EgtD, the mutation of Glu282 to alanine affects significantly substrate binding through the loss of hydrogen bonds with the imidazole ring. In SticA, the non-polar Val282 cannot form hydrogen bonds with the substrate either. However, Asn213 and Gln252 can provide a polar environment to histidine and compensate the presence of a non-polar residue at the position 282.

In contrast with EgtD which favors histidine trimethylation, the methylated substrate is not preferred by SticA (the catalytic efficiency of the fungal MT is four times higher for tyrosine than for DMY). Moreover, a reaction containing an equimolar concentration of SAM and tyrosine catalyzed by SticA was analyzed by IE HPLC in order to identify the different products. DMY and TMY (trimethyltyrosine) are found in relatively similar amount ($59.7 \pm 5.6 \%$ and $40.3 \pm 2.8 \%$ respectively). This reinforces the idea that the methyl transfers and the hydroxylation of tyrosine may be interchanged with each other during sticticine biosynthesis.

To conclude, by structure analysis and bioinformatics search, we were able to identify SticA as a tyrosine methyltransferase with similar catalytic parameters as EgtD but different substrate specificity.

*As for EgtD, an upper estimate of the catalytic efficiency ($5 \text{ M}^{-1}\text{s}^{-1}$) was assigned to SticA with the 17 other amino acids.

2.4 Identification of a fungal tryptophane betaine synthase

To pursue our structure-guided genome-mining for betaine synthases with alternative activities, we considered EgtD homologs found in two wood degrading fungi.

2.4.1 Identification of hypaphorine in wood degrading fungus

EgtD-like proteins were found in different species of basidiomycetous fungi like *Dichomitus squalens* or *Serpula lacrymans* (26 % and 25 % sequence identity with EgtD respectively). The sequence alignment of the fungal enzymes shows differences at the positions 213, 252 and 282 compared to EgtD sequence (Figure 22). Nevertheless, the other residues responsible for the recognition of both carboxylic and α -amino groups of histidine are identical (Figure 25).

```
          39      56     161  166     206   252   282   286
egtD      ...FYDA...PEYYP...FLGSTIGNLT...RAYDD...IEMWL...TEVSCKFR..
D. squalens ...LYDE...AEYYL...FLGSSLGNFT...MAYND...KRAYY...VAFSHKFS...
S. lacrymans ...LYNE...PDYYL...WLGSSIGNVK...RAYND...HEVYY...LAHSYKYA...
```

Figure 25 Abbreviated sequence alignment of EgtD and EgtD homologs from the two wood degrading fungi *Dichomitus squalens* and *Serpula lacrymans*. The residues highlighted in grey in the sequence of EgtD interact with the substrate DMH in the catalytic pocket. The corresponding residues indicated in red in the sequences of the two fungal methyltransferases are the only ones which differ from EgtD in this respect.

Valine and or alanine are found at positions 252 and 282 in the fungal enzymes. A model of the histidine binding site defined by these non-polar residues describes a bigger substrate binding pocket in which an amino acid larger than histidine or tyrosine could fit (Figure 26). Therefore, we suggest that these organisms could produce tryptophan betaine (also named hypaphorine), either as a simple metabolite or as intermediate in a biosynthetic pathway.

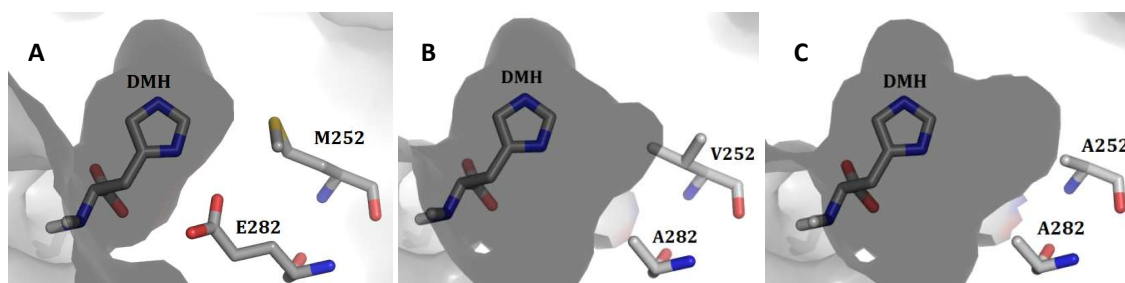


Figure 26 **A:** Histidine binding site within EgtD WT (PDB: 4PIN). The residues Met252 and Glu282 describe a hydrophobic pocket in which the substrate can fit in. **B:** Model of the binding pocket of *Serpula lacrymans*. Met252 and Glu282 are respectively replaced by Val and Ala residues. **C:** Model of the binding pocket of *Dichomitus squalens*. Met252 and Glu282 residues are both changed in Ala residues.

To test this hypothesis, the extracts of both species of wood degrading fungi (*Serpula lacrymans* and *Dichomitus squalens*) were analyzed for the purpose of detecting the presence of trimethyltryptophane (TMW). First, the fungi were grown on malt extract agar for at least two weeks to ensure sufficient matter for analysis. The mycelia were scraped off the plates and extracted with a methanol-containing aqueous solution. Their respective contents were then analyzed by reverse-phase (RP) HPLC (Figure 27).

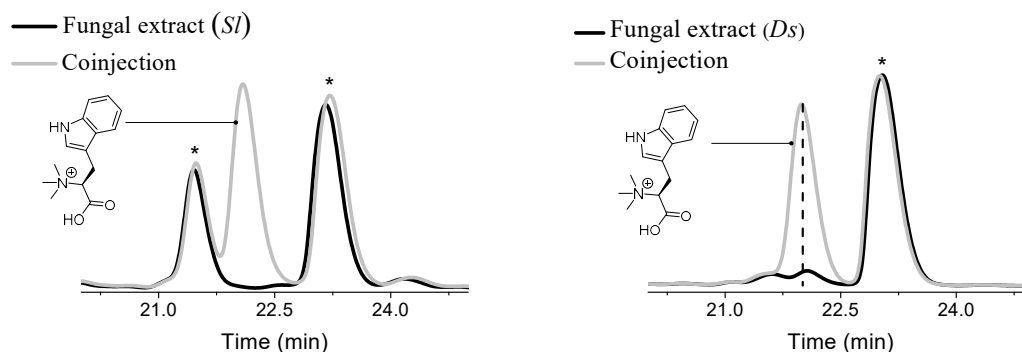


Figure 27 HPLC traces of the crude fungal extracts and co-injected with 1 mM hypaphorine. **Left:** no TMW was detected in *Serpula lacrymans* (*Sl*). **Right:** a compound eluting at the same time as TMW was identified in *Dichomitus squalens* (*Ds*). The compounds indicated with the symbol (*) are present in the crude extracts but were not identified.

In the extract of *Serpula lacrymans*, no compound eluting at the same time as the reference hypaphorine could be identified; while in *Dichomitus squalens*, a compound with a similar retention time was detected. This compound was then isolated. Its elemental composition was determined by HRMS, which confirmed the presence of tryptophan betaine in the fungal extract

(m/z calculated: 247.1441 Da, measured: 247.1441 Da, which is consistent with the elemental composition: $14C19H2N2O^+$). In addition, a second mass of 188.1 Da was also assigned to the presence of isolated hypaphorine. This peak is accounted for the ESI-induced fragmentation of TMW (Figure 28) to trimethylamine and 3-indoleacrylic acid (m/z calculated 188.1 Da, measured 188.1 Da). Betaines of amino acids can easily undergo Hofmann elimination during MS experiments.¹⁶¹ It is thus not unusual to detect the elimination product.

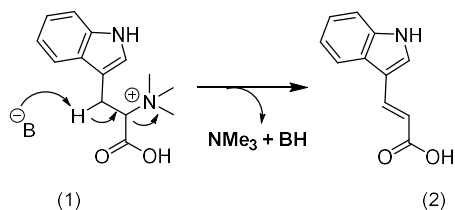


Figure 28 Fragmentation of hypaphorine. The tryptophane betaine (1) is a good candidate to undergo trimethylamine elimination in basic conditions to give 3-indoleacrylic acid (2). In MS/MS experiment, this Hofmann elimination takes place spontaneously.

The identification of hypaphorine in the extract of *Dichomitus squalens* strongly suggests that the *egtD*-like gene found in this wood degrading fungus encodes for a tryptophan methyltransferase. Moreover, it would not be absurd to propose TMW as an intermediate in a biosynthetic pathway for tryptophan betaine-based compounds. Therefore, the absence of TMW in the extract of *Serpula lacrymans* does not demonstrate that this fungal EgtD homologue is not a tryptophan methyltransferase.

2.4.2 Engineered tryptophan methyltransferase

Identifying compounds of interest from an extract constitutes an indirect means to demonstrate enzyme specific activity. Therefore, we attempted to assign the exact function of the protein encoded by the *egtD*-like gene in *Dichomitus squalens* through *in vitro* studies. The fungal enzyme was cloned into a suitable vector for recombinant production (pET28) in *Escherichia Coli*, as done for SticA. Nevertheless, the putative tryptophan MT was not expressed in the bacteria. Therefore, we tried a different approach in order to support the hypothesis that a bigger catalytic pocket in fungal EgtD homologs is a determinant for tryptophan binding. Inspired by the residues identified in the fungal putative MTs (Figures 22 and 26), we constructed variants of EgtD with mutations at the key positions 252 and 282. The following

series of variants was generated: the single mutant M252A, the double mutants E282A M252V and E282A M252A and the triple mutant E282A M252V N217C. These four variants were then tested with the 20 proteinogenic amino acids as potential substrates.

Among the aforementioned constructs, only one variant shows significant tryptophan methyltransferase activity: EgtD E282A M252V. This mutant mimics the binding site of the fungal putative MT from *Serpula lacrymans*. None of the other mutants showed any MT activity that was able to be monitored by the spectrophotometric continuous assay. The engineered tryptophan MT and EgtD WT have similar catalytic efficiencies (5300 and 5500 $M^{-1}s^{-1}$ for the tryptophan and histidine MT respectively). Additionally, a reaction containing an equimolar concentration of SAM and tryptophan catalyzed by EgtD E282A M252V were analyzed by ion exchange HPLC in order to identify the different products. Dimethyltryptophan (DMW) is mainly produced (95 %), while TMW is found in significantly limited amount (less than 5 %).

Table 5 Kinetics parameters of the engineered tryptophan methyltransferase EgtD E282A M252V with tryptophan and dimethyltryptophan^a.

| Substrate | k_{cat} (s^{-1}) | K_M (μM) | k_{cat} / K_M ($M^{-1}s^{-1}$) |
|---------------------------|---|--|---|
| Tryptophan | 0.11 | 20 | 5500 |
| Dimethyltryptophan | 0.01 | 11 | 830 |

^aReaction conditions: 25 °C, 50 mM Tris/HCl pH 8.0, 50 mM NaCl, 200 μM Mn^{II} , 500 μM SAM, 10-500 μM tryptophan or DMW, 5 μM SAH nucleosidase, 10 μM adenine deaminase and 6.6 μM of EgtD E282A M252V.

As shown with the analysis of the products of the reaction, the cooperativity of the MT was not conserved after mutating the catalytic site. We hypothesize that the artificial tryptophan binding pocket is not large enough to favor the last methyl transfer on DMW. However, based on our study of EgtD determinants for histidine recognition, we successfully engineered a proficient MT with different substrate specificity.

2.4.3 Crystal structure

In order to heighten the understanding of this change in specificity arising from two point mutations in the substrate binding site, EgtD E282A M252V was co-crystallized as a ternary complex with tryptophan and SAH (Figure 29).

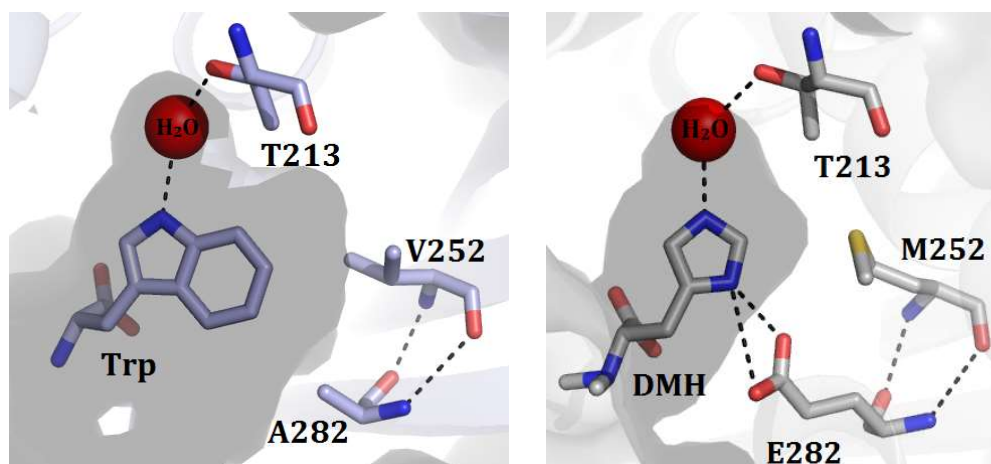


Figure 29 Substrate binding pocket of the engineered tryptophan MT and the native histidine MT. **Left:** EgtD E282A M252V co-crystallized with tryptophan (PDB: 4PIP, 1.8 Å). The resulting binding pocket is larger than in the WT. **Right:** EgtD WT co-crystallized with DMH (PDB: 4PIN).

In EgtD WT, Glu282 recognizes histidine via essential hydrogen bonds and Thr213 interacts with the imidazole ring through a water molecule. In the engineered tryptophan methyltransferase, the nitrogen atom of the indole ring of the substrate coordinates in the same way to Thr213. The two residues Ala282 and Val252 shape a hydrophobic pocket large enough to enable tryptophan to fit inside, however, they do not provide additional interaction with the substrate.

In summary, our model for determining substrate specificity in EgtD homologs based on structural analysis and bioinformatics search has proven to be efficient to identify tryptophan betaine synthases in wood degrading fungi.

2.5 Conclusions

EgtD catalyzes the first step in ergothioneine biosynthesis in *Mycobacterium smegmatis*, namely the trimethylation of histidine. The methyltransferase was recombinantly produced and its catalytic efficiency was determined *in vitro* by a spectrophotometric continuous assay. EgtD is a cooperative enzyme with high specificity for histidine. The crystal structure of EgtD revealed that the mycobacterial MT does not belong to any of the 31 classes of SAM-dependent MT. Instead, EgtD is then the first member of a new family named Methyltransf_33. The residues essential for substrate recognition were delineated. Guided by these structural motifs, fungal tyrosine and tryptophan methyltransferases were identified in unexpected organisms. The catalytic efficiencies of SticA, the tyrosine betaine synthase found in *Aspergillus nidulans*, and EgtD are comparable. We engineered a proficient tryptophan MT which mimics the substrate binding pocket of an EgtD homolog from *Serpula lacrymans*. The drastic change in substrate specificity by only mutating two amino acids in EgtD demonstrates the promiscuity of the members of the Methyltransf_33 family (Table 6).

Table 6 Summary of the kinetics parameters of aromatic amino acid methyltransferases^a. The k_{cat} values are given in s^{-1} and k_{cat}/K_M in $M^{-1}s^{-1}$.

| Substrate | EgtD WT | | EgtD E282A | | SticA | | EgtD E282A M252V | |
|-----------------|-----------|-----------------|------------|-----------------|-----------|-----------------|------------------|-----------------|
| | k_{cat} | k_{cat} / K_M | k_{cat} | k_{cat} / K_M | k_{cat} | k_{cat} / K_M | k_{cat} | k_{cat} / K_M |
| His | 0.58 | 5300 | 0.1 | 40 | 0.002 | 790 | - | 1.9 |
| MMH | 0.23 | 23000 | - | - | - | - | - | - |
| DMH | 0.43 | 17000 | - | - | - | - | - | - |
| Phe | - | 2.4 | - | - | 0.14 | 25 | 0.34 | 100 |
| Tyrosine | - | 1.1 | - | - | 0.11 | 5300 | - | 170 |
| DMY | - | - | - | - | 0.05 | 1200 | - | - |
| DOPA | - | 2.2 | - | - | 0.1 | 660 | - | 4.5 |
| Trp | - | 2 | 0.02 | 125 | - | 7.2 | 0.11 | 5500 |

^aReaction conditions: 25°C, 50 mM Tris/HCl pH 8.0, 50 mM NaCl, 500 μ M SAM, 5 μ M SAH nucleosidase, 10 μ M adenine deaminase, 0.6 to 6.6 μ M MT. Data represents averages from multiple measurements. The standard error is less than 20% of the average value.

Small secondary metabolites have essential functions in cell-to-cell communication. Aromatic amino acid betaines seem to be ubiquitous in the fungal kingdom and are likely to serve more sophisticated roles than glycine betaine due to their functional side chains. Hypaphorine may play a defensive role against oxidative stress during fungal wood degrading. It can also act as a protectant against desiccation stress as *Serpula lacrymans* can live in almost dry wood and betaine derivatives are known to attract water molecules. Furthermore, glycine betaine derivatives are commonly used for ionic liquids (ILs) synthesis.³⁶ A more unusual role that can then be proposed for aromatic amino acid betaines in wood degrading fungi is as the cations of biosynthetic ILs. In addition to the enzymatic processes required for wood degradation, ILs could support the digestion of cellulose and lignin matrices.³⁸ Yet, the prior determination of the biosynthetic origins of amino acid betaines is a prerequisite for a systematic study of their functions. Our structure-based analysis provides then a strong basis to identify aromatic amino acids synthases scattered across whole genomes.

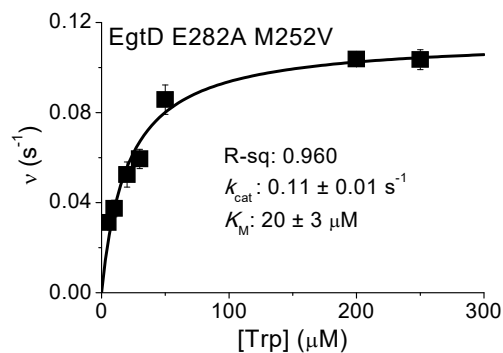
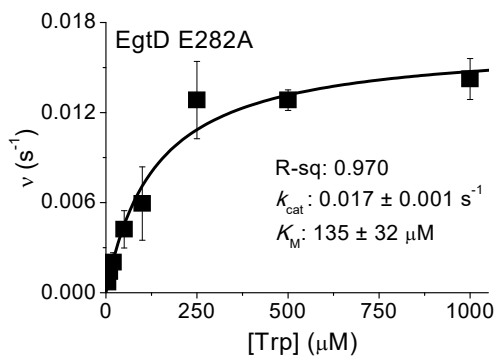
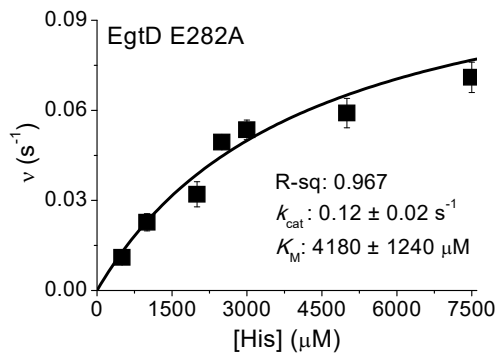
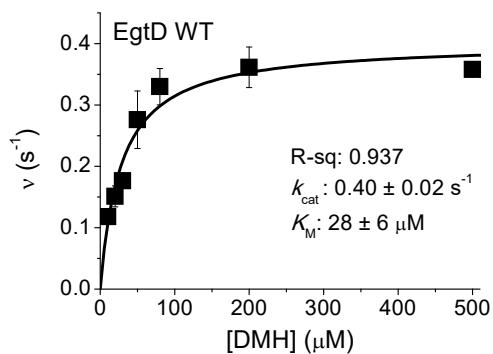
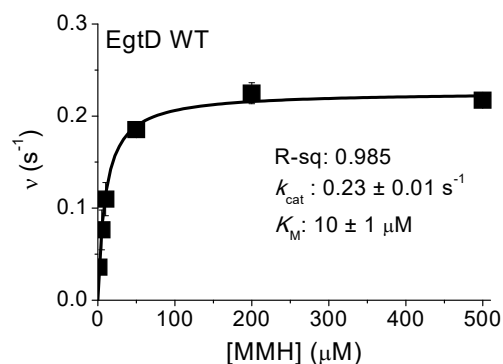
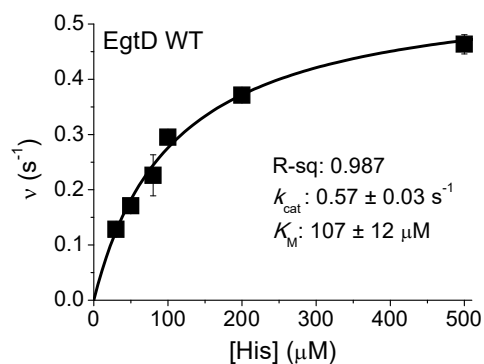
2.6 Experimental

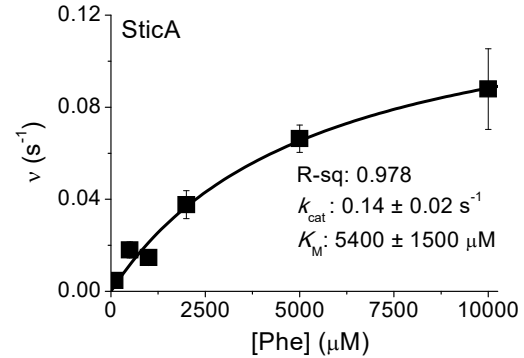
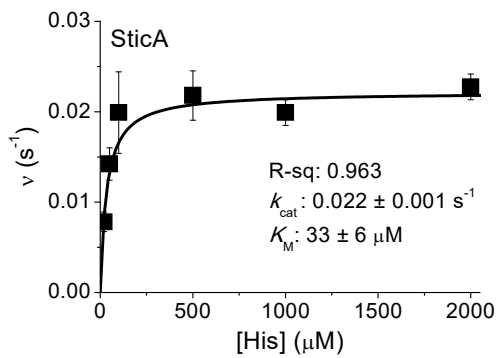
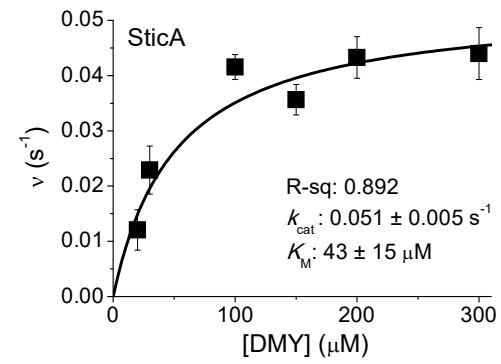
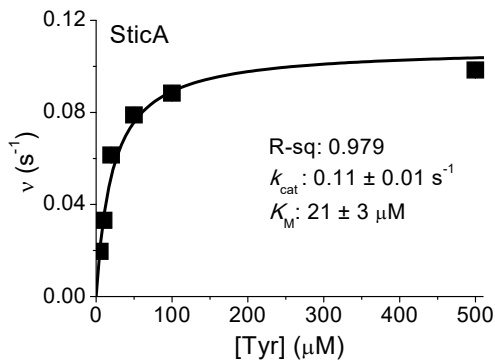
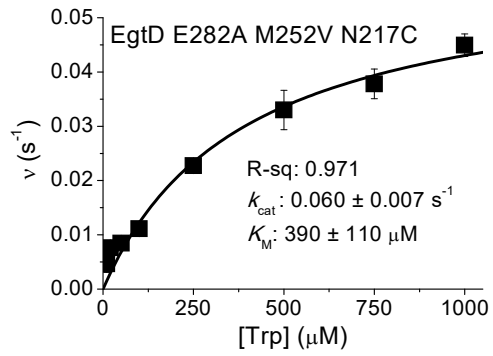
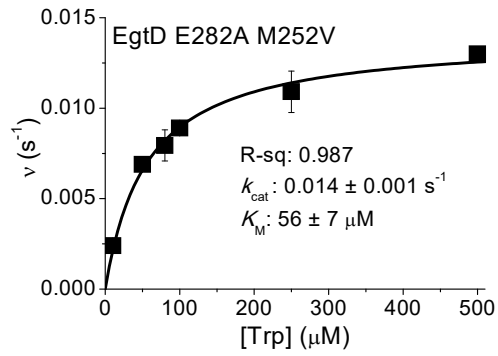
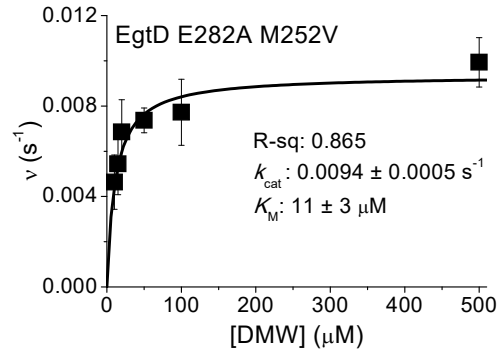
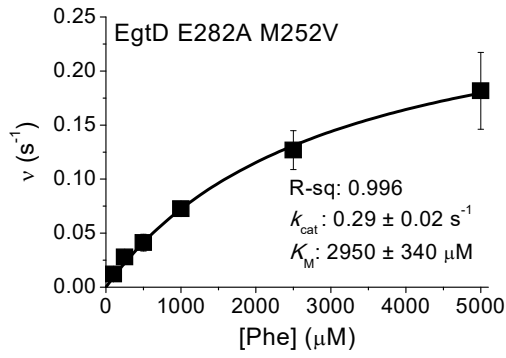
2.6.1 Kinetics

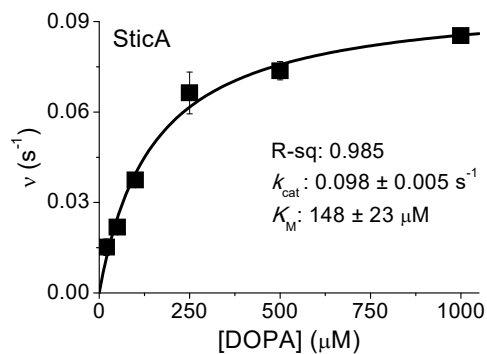
Methyltransferase assay. Methyltransferase activity was determined following published protocols.¹⁴⁷ Reactions were monitored in a 2 mm quartz cuvette at 25°C at 265 nm with a Cary 300 spectrophotometer from Agilent. The 200 μ L reactions contained 50 mM Tris/HCl pH 8.0, 50 mM NaCl, 200 μ M Mn^{II}, 500 μ M SAM, 5 μ M adenine deaminase, 10 μ M SAH nucleosidase, 0.6 to 6.6 μ M methyltransferase and the appropriate amino acid at a concentration of 1 – 10000 μ M. Reactions were started by addition of the methyltransferase.

HPLC assay. Methyltransferase activity was assayed in 50 mM Tris/HCl pH 8.0, 50 mM NaCl, 200 μ M Mn^{II}, 500 μ M SAM, 5 μ M adenine deaminase, 10 μ M SAH nucleosidase, 1 to 10 μ M methyltransferase and the appropriate amino acid at a concentration of 1 – 10000 μ M. Reactions were started by addition of the methyltransferase and incubated at 25°C. 20 μ L aliquots of the reactions were quenched by addition of 10 μ L 1 % TFA and analyzed by either cation exchange HPLC (20 mM phosphoric acid pH 2 as the mobile phase) on a Luna 5u SCX column (100 Å, 150 x 4 mm, Phenomenex), or by reverse phase HPLC (water and 0.1 % TFA as the mobile phase) on a Zorbax Eclipse Plus C₁₈ reverse-phase column (2.1 x 50 mm 1.8-Micron, Agilent). The compounds were eluted in NaCl and acetonitrile gradient respectively. All HPLC chromatograms were recorded at 220 nm.

Michaelis Menten plots. The data obtained by the methods listed above were fitted to the function $v = k_{cat} \cdot [\text{substrate}] / (K_M + [\text{substrate}])$. The corresponding substrates and MTs are indicated on each graph. The k_{cat} and k_{cat}/K_M parameters indicated in Table 6 were determined in the presence of the co-substrate SAM at a concentration at least 3 fold higher than the corresponding $K_{M,SAM}$.







2.6.2 Product identification after methyl transfer

UPLC-MS (1290 Infinity LC System /G6130BA LCMS Single Quad , Agilent) analysis of the products formed during the methylation of tyrosine, tryptophan or histidine was performed on a Zorbax Eclipse Plus C₁₈ reverse-phase column (2.1 x 50 mm 1.8-Micron, Agilent). The compounds were eluted with a gradient mixture of water containing 1% MeCN and 0.1% TFA and MeCN containing 0.1% TFA. The trimethylated products were identified by MS:

m/z calc: 198.12, measured: 198.1 (trimethylhistidine);

m/z calc: 224.13, measured: 224.1 (trimethyltyrosine);

m/z calc: 247.14, measured: 247.1 (trimethyltryptophan);

m/z calc: 240.12, measured: 240.1 (trimethylDOPA).

2.6.3 Extraction and identification of trimethyltryptophan in *Dichomitus squalens*

Dichomitus squalens was purchased from DSMZ (reference DSM 9615) and grown on 1.5% malt extract agar. After three weeks of incubation at 27°C with 70 % humidity, 20 g of fungus were collected. The mycelium was first ground in liquid nitrogen then lysed three times by sonication with 30 mL of MeOH:water (9:1). The lysate was then filtered, frozen and lyophilized overnight. The fungal dry extract was resuspended in 7 mL of ddH₂O. It was then injected on RP HPLC. A coinjection with 1 mM hypaphorine was also performed. The compound eluting at the same time as trimethyltryptophan on RP HPLC was collected in order to perform a MS/MS experiment and to determine its mass by HRMS to get the elemental composition.

3 EgtD substrate binding mode provides the basis for inhibitors design

There are different strategies to regulate metabolic pathways. Often, the final product of the pathway inhibits one of the enzymes needed during the biosynthesis. For instance, this feedback inhibition is of particular importance to balance the production of amino acids.¹⁵⁶ In the context of industrial processes requiring biological catalysts (the degradation of cellulose by hydrolases¹⁶² or the production of lactic acid from biowaste),¹⁶³ product inhibition is an unwanted feature that has to be reduced to improve process efficiency and to limit production costs. However, product inhibition is a physiologically relevant property of enzyme catalysis. Indeed, this control is essential for cell homeostasis to avoid the accumulation of unnecessary metabolites, but also helps to prevent wasting energy, nitrogen or carbon sources for products that will not be used by the cell.¹⁶⁴

By comparing the binding pocket of EgtD in presence of either histidine or DMH (Figure 30), we realized that both methyl groups of DMH provide additional interactions with polar residues in the active site of the MT.

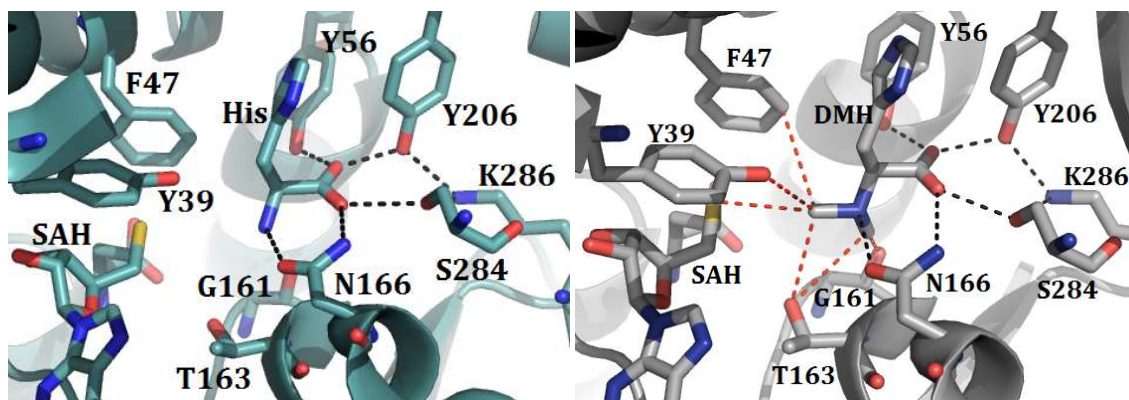


Figure 30 Comparison of the interactions with histidine and DMH within the substrate binding pocket of EgtD. The hydrogen bonds are indicated with black dashes, whereas interactions between the residues that are in van der Waals distance with the methyl groups of DMH are shown with red dashes. **Left:** EgtD co-crystallized with histidine and SAH (PDB: 4UY6, 2.04 Å).¹⁶⁵ **Right:** EgtD co-crystallized with DMH and SAH (PDB: 4PI0).¹⁴⁶

We proposed that this accumulation of weak interactions (CH...O bond energy is commonly estimated as half the energy of a conventional hydrogen bond)¹⁵² contributes to a preferred binding of the methylated substrate which defines EgtD as a cooperative enzyme. This

interesting feature has, so far, not been described for any of the other members of the Methyltrans_33 family. It raises the question whether trimethylhistidine would also bind to the active site, consequently inhibit EgtD activity and thus stop ergothioneine biosynthesis.

In this chapter, we discuss EgtD substrate binding order and the mechanism of product inhibition. These findings provide the basis for the design of histidine derivatives as EgtD inhibitors. The valuable information about the interactions between EgtD and its product and substrates suggest that EgtD is a key enzyme for regulating ergothioneine biosynthesis in *Mycobacterium*.

3.1 EgtD is product-inhibited

While the end product of the reaction SAH is a potent inhibitor of numerous SAM-dependent MTs,¹⁶⁶ the inhibition by the resulting methylated nucleophile is more rare, but has already been reported. For example, the phospholipid *N*-MT PmtA from *Agrobacterium tumefaciens* is inhibited by both SAH and the product of the reaction phosphatidylcholine.¹⁶⁷ Another SAM-dependent MT, the *N*-8-demethyl-8-amino-D-riboflavin dimethyltransferase RosA is also inhibited by both products of the reaction.¹⁶⁸ In our assays, the presence of the coupled enzymes (adenine deaminase and SAH nucleosidase) ensures that the observed inhibitory effects occur due to the interactions with the tested compounds solely, as SAH is not present in the reaction. In this way, if EgtD is product inhibited, it means that TMH competes for the histidine binding site.

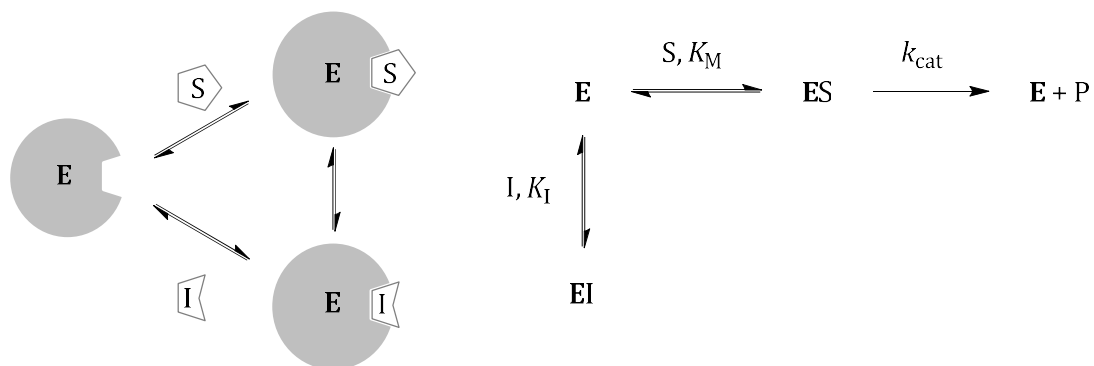


Figure 31 Simplified scheme of a competitive inhibition. If an inhibitor I binds reversibly to the active site of the enzyme E and prevents the binding of the substrate S, I and S compete for the active site and I is said to be a competitive inhibitor.¹⁶⁹

In the absence of an inhibitor, the initial rate of an enzymatic reaction is described by the following equation (Eq.1):

$$v = \frac{[E]_0 \cdot [S] \cdot k_{cat}}{[S] + K_M} \quad (\text{Eq.1})$$

Where $[E]_0$ and $[S]$ represent the concentrations of the enzyme and the substrate respectively.

In the presence of a certain concentration competitive inhibitor $[I]$, this equation becomes:

$$v = \frac{[E]_0 \cdot [S] \cdot k_{cat}}{[S] + K_{M \text{ app}} \cdot \left(1 + \frac{[I]}{K_I}\right)} \quad (\text{Eq.2})$$

Where K_i , the inhibition constant is defined by: $K_i = [E] \cdot [I] / [EI]$. This type of inhibition is thus characterized by an unchanged turnover number in presence of the competitive inhibitor, but an increase in the K_M value by a factor of $(1 + [I]/K_i)$.

3.1.1 Kinetics

In presence of 0.5 mM TMH, the rate of EgtD at saturated substrate concentration (0.5 mM of both histidine and SAM) decreases by more than 80 %. This indicates that EgtD is inhibited by its product. In order to quantify the inhibitory effect of TMH, we determined the K_i value. The rates of histidine methylation catalyzed by EgtD in presence of three concentrations of inhibitor were monitored by the continuous spectrophotometric assay. The resulting catalytic parameters are indicated in the following table.

Table 7 Determination of the K_i value of EgtD in presence of different concentrations of hercynine^a.

| [Hercynine] (μM) | k_{cat} (s^{-1}) | $K_{M \text{ app}}$ (μM) | K_i (μM) |
|-------------------------------|-------------------------------|---------------------------------------|-------------------------|
| 0 | 0.26 ± 0.01 | 51 ± 6 | - |
| 55 | 0.25 ± 0.02 | 109 ± 31 | 48 |
| 140 | 0.22 ± 0.02 | 222 ± 52 | 42 |
| 280 | 0.26 ± 0.02 | 575 ± 90 | 27 |

^aReaction conditions: 25 °C, 50 mM Tris/HCl pH 8.0, 50 mM NaCl, 200 μM Mn^{II} , 500 μM SAM, 10-2000 μM histidine, 5 μM SAH nucleosidase, 10 μM adenine deaminase and 2 μM EgtD.

The average of the three K_i values gives an inhibition constant for L-hercynine* of $39 \pm 11 \mu\text{M}$. Interestingly, this K_i value and the Michaelis constant for the substrate DMH are comparable ($K_M \text{ DMH} = 28 \pm 6 \mu\text{M}$, see Chapter 2).

In the previous chapter, we showed that the major product of histidine methylation catalyzed by EgtD is hercynine. In addition, we now demonstrated that the MT is inhibited by its product. Interestingly, the K_M value of TMH for EgtB ($43 \pm 10 \mu\text{M}$),⁷ the second enzyme involved in ergothioneine biosynthesis (see Chapter 1), is similar to the K_i value of TMH for EgtD. Moreover, EgtB accepts both DMH and TMH as substrates and catalyzes the sulfoxidation with a comparable catalytic efficiency (K. Goncharenko, unpublished results). These interesting findings support the idea that EgtD does not only control the nature of the substrate of EgtB (see Chapter 2), but its activity is also regulated by the substrate intake from the sulfoxide synthase. In other words, the cooperativity of EgtD can be assigned to an upstream control of the substrate of EgtB and in addition, histidine betaine synthesis self-regulates through product inhibition when EgtB is not present to use TMH as a substrate.

To test if product inhibition is a common feature of the Methyltransf_33 family, we also probed the potential inhibitory effect of TMY on SticA activity. In presence of $250 \mu\text{M}$ of TMY, the activity of the fungal tyrosine betaine synthase is not modified. However, at higher concentration of product, SticA is partially inhibited: in presence of 2 mM of TMY, the remaining activity of SticA is $41 \pm 4 \%$. This result indicates that TMY does in fact inhibit MT activity, but with a lower efficiency than the product inhibition of EgtD. We estimated the K_i value of TMY to be 1 mM , that is to say 25 times higher than the K_i value of TMH.

3.1.2 Crystal structure of EgtD in complex with its product trimethylhistidine

In order to identify the interactions accounting for the binding of TMH in the active site and the resulting inhibition, EgtD was co-crystallized in a binary complex with its product (Figure 32, right).

* The chirality of EgtD substrates will be discussed in Section 3.5.2.

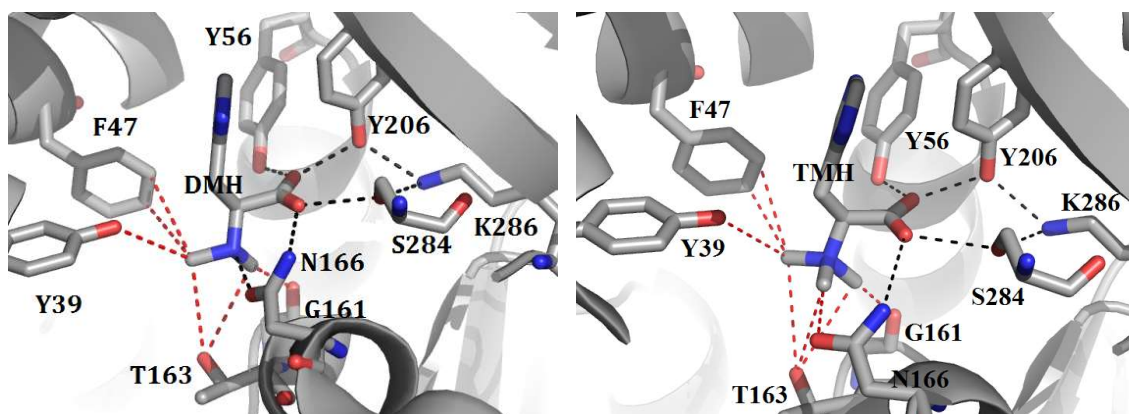


Figure 32 EgtD substrate binding pocket. The hydrogen bonds are indicated with black dashes, whereas interactions between the residues that are in van der Waals distance with the methyl groups are shown with red dashes. **Left:** EgtD co-crystallized with DMH (PDB: 4PIN). **Right:** EgtD co-crystallized with TMH (unpublished results, 1.75 Å).

The hydrogen bond network between the residues Tyr56, Tyr206, Lys286, Ser284 and Asn166 with the carboxylic group of TMH is similar to the one described for DMH (see Chapter 2). Yet, the $N\alpha$ is no more stabilized by hydrogen bonding to Asn166 but is instead replaced by weaker interactions between the carboxylic group of this residue and the additional methyl group ($C\cdots O$ distance: 3.2 Å, CHO angles: 90.2 to 94.3 ° for the 3 hydrogen atoms). Thr163 is in van der Waals distance with the three methyl groups of hercynine ($C\cdots O$ distances between 3.6 and 3.9 Å) and the corresponding angles defined by the three atoms C, H and O are similar (148.9 to 152.8 °). These measurements describe $CH\cdots O$ interactions according to the definition given by Horowitz and Trievel (see Chapter 2).¹⁵² The accumulation of weak interactions between the active site and the methyl groups of TMH provide a reasonable explanation for the binding of the product and the resulting competitive inhibition with the substrate of EgtD.

The dense array of short contacts between the polar residues of the EgtD binding pocket and the three methyl groups of TMH indicates that the trimethyl ammonium moiety is an important recognition motif for EgtD. In order to test if this motif is indeed essential to inhibit the MT, we decided to probe chlorohistidine as a putative inhibitor. The drastic difference between the chemical characteristics of chlorine compared to trimethylammonium (such as size, absence of charge and low polarity) directed the choice for this α -halogenated histidine derivative.

3.2 Chlorohistidine is an inhibitor of EgtD

The α -chloro-substitution of histidine suppresses the hydrogen bond between the oxygen atom of the amide side chain of Asn166 and the substrate/inhibitor. In addition, the whole network of weak interactions established between the methyl groups of DMH or TMH and the polar

residues in the catalytic site is also removed. Therefore, by comparing the inhibitory effect of TMH and chlorohistidine (through the K_i values), the importance of the trimethyl ammonium group regarding EgtD inhibition can be defined.

3.2.1 Kinetics

A racemic mixture of (D,L)-chlorohistidine was used to perform the experiments. The explanation for this choice of stereochemistry is given in section 3.5.2.2.

The rate of EgtD at saturated substrate concentrations was monitored in presence of 0.5 mM chlorohistidine (ClHis). The activity of EgtD was lowered below the detection limit of this assay, suggesting that this histidine derivative is in fact an efficient inhibitor and that, despite the abovementioned loss of interactions resulting from the halogen substitution. Therefore, we determined the K_i value of chlorohistidine with lower concentrations of inhibitor compared to TMH. The rates of histidine methylation in presence of three concentrations of chlorohistidine were monitored by the continuous spectrophotometric assay, as performed for TMH. The resulting catalytic parameters are indicated in the table below.

Table 8 Determination of the K_i value of EgtD in presence of different concentrations of chlorohistidine^a

| [ClHis] (μM) | k_{cat} (s^{-1}) | K_M (μM) | K_i (μM) |
|---------------------------|--------------------------------------|-------------------------|-------------------------|
| 0 | 0.40 ± 0.02 | 101 ± 15 | - |
| 10 | 0.37 ± 0.03 | 230 ± 44 | 7.8 |
| 25 | 0.41 ± 0.04 | 625 ± 139 | 4.8 |
| 50 | 0.36 ± 0.02 | 956 ± 100 | 5.9 |

^aReaction conditions: 25 °C, 50 mM Tris/HCl pH 8.0, 50 mM NaCl, 200 μM Mn^{II} , 500 μM SAM, 50 - 2000 μM histidine, 5 μM SAH nucleosidase, 10 μM adenine deaminase and 2 μM of EgtD.

The K_i value for chlorohistidine is $6.2 \pm 1.5 \mu\text{M}$, which is six times lower than the value of product inhibition. It seems unlikely that the ammonium moiety, which interacts with the catalytic site through an accumulation of van der Waals interactions, is a weaker binder than the relatively inert chlorine atom. We proposed then that the mechanism of inhibition by these two compounds differs. However, prior to mechanistic studies, EgtD was co-crystallized in a binary

complex with chlorohistidine to ensure the absence of interactions between the halogenated histidine derivative and the EgtD active site.

3.2.2 Crystal structure

The substitution of the $N\alpha$ by a hardly polarizable chlorine atom does not, as expected, provide any additional interaction within the catalytic site (Figure 33). On the contrary, the contacts with Tyr39, Phe47, Gly161 and Thr163 are suppressed. Moreover, Asn166 forms solely one hydrogen bond with the carboxylic moiety of chlorohistidine. We also considered an electrostatic interaction between the α -chlorine and Asn166. Indeed, halogen bonds, especially electrostatic interactions involving bromine atoms, have already been shown to contribute to a better binding of inhibitors.¹⁷¹ Nevertheless, the distance between the chlorine and oxygen atoms of the inhibitor and Asn166 indicates that chlorohistidine is not engaged in a halogen bond*.

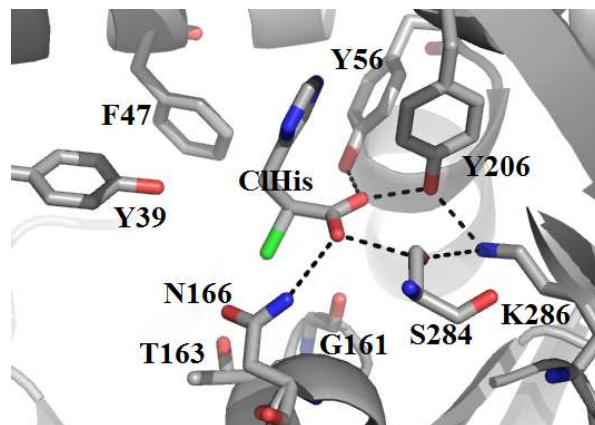


Figure 33 EgtD co-crystallized with chlorohistidine (unpublished results, 1.83 Å).

In the light of the structural differences between TMH and chlorohistidine, we were wondering about the reason for the better inhibitory effect of chlorohistidine compared to hercynine. Either the interactions that were identified from the crystal structure between the trimethyl ammonium moiety and the polar residues within the EgtD binding site are in fact repulsive, or hercynine and chlorohistidine may inhibit EgtD according to different mechanisms. As the ITC measurements showed a better substrate affinity for EgtD with the methylated histidine (see

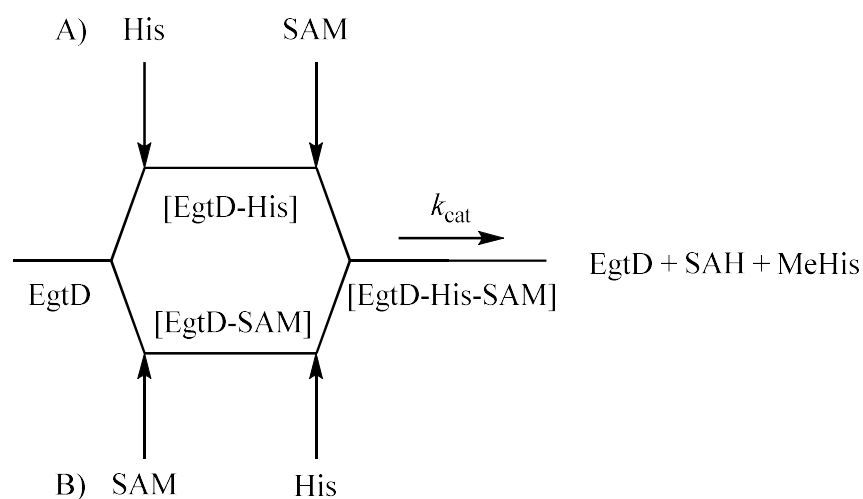
* Auffinger *et al.* define a halogen bond in a biomolecule as a short CX...O interaction where the distance between the halogen X and the oxygen atom is shorter than the sum of their respective van der Waals radii (3.27 Å).¹⁷² We measured a larger distance between the chlorine atom of the inhibitor and the oxygen atom of Asn166 (3.7 Å). Therefore, these two atoms cannot be engaged in such interaction.

Chapter 2), we were skeptical about the repulsion which could have occurred in the catalytic pocket of the MT with the trimethylammonium moiety. Therefore, we argued in favor of a different action of hercynine or chlorohistidine in the binding pocket of EgtD.

3.3 Substrate binding order of EgtD

In order to establish EgtD inhibition mechanism(s) by chlorohistidine and hercynine, it seemed pertinent to firstly understand the substrate binding mechanism which should provide some clarification about the catalysis itself. Moreover it will bring valuable information about the transition state, which, supported by structural analysis, could enable the design of efficient inhibitors.¹⁷³

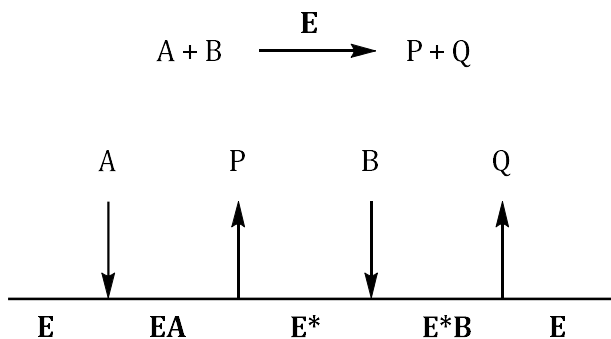
To identify the substrate binding order of EgtD, we considered the simplified scheme of the histidine methylation shown below.



Scheme 1 Sequential mechanism of histidine methylation. Either histidine (A) or SAM (B) can first bind to EgtD. The binding of the second substrate to the binary complex initiates the catalysis. For simplicity, we only considered a single methyl transfer from SAM to histidine.

We were interested in determining in which sequential order (*i.e.* random or ordered) the substrates bind. In a non-sequential mechanism, also called Ping Pong mechanism, the release of one of the products occurs before the binding of all the substrates to the enzyme (Scheme 2). By contrast, in a sequential mechanism, the enzyme binds first all the substrates before product release (Scheme 1).

If we consider SAM-dependent MTs which catalyze the methylation of small molecules (no DNA or protein methyl transfer), only sequential mechanisms are found in the literature to describe substrate binding.¹⁷⁴ Therefore, it is more than likely that SAM and histidine are bound to EgtD in a sequential order. In order to determine if the binding of the substrates occurs according to a random or an ordered sequential mechanism, the kinetics of the methylation were studied in presence of different concentrations of histidine and SAM.



Scheme 2 Ping pong mechanism for a model reaction catalyzed by the enzyme E with A and B as the substrates and P and Q as the products.

3.3.1 Catalytic parameters of EgtD in the presence of different concentrations of histidine

The concentration of SAM was varied in the presence of a fixed concentration of histidine. The rates of the reactions were fitted to a double reciprocal plot (or Lineweaver-Burk plot) which is described by the following formula:

$$\frac{1}{v} = \frac{1}{v_{\max}} + \frac{K_M}{v_{\max} \cdot [S]} \quad (\text{Eq.3})$$

Where $v_{\max} = k_{\text{cat}} \cdot [E]_0$.

This experiment was performed in the presence of six concentrations of histidine (25, 50, 75, 100, 200 and 500 μM). The corresponding fittings are indicated in Figure 34 (left) with the different slopes that represent the ratio K_M/k_{cat} ($\mu\text{M s}$). A secondary plot (or diagnostic plot) ensues and the values of the slopes that can be fitted to a linear regression are represented in Figure 34 (right). This diagnostic plot has no physical meaning but is used to compare two systems. Therefore we performed the same experiment by reversing the roles of both

substrates. The diagnostics plots will then be correlated to determine if it is SAM or histidine which binds first.

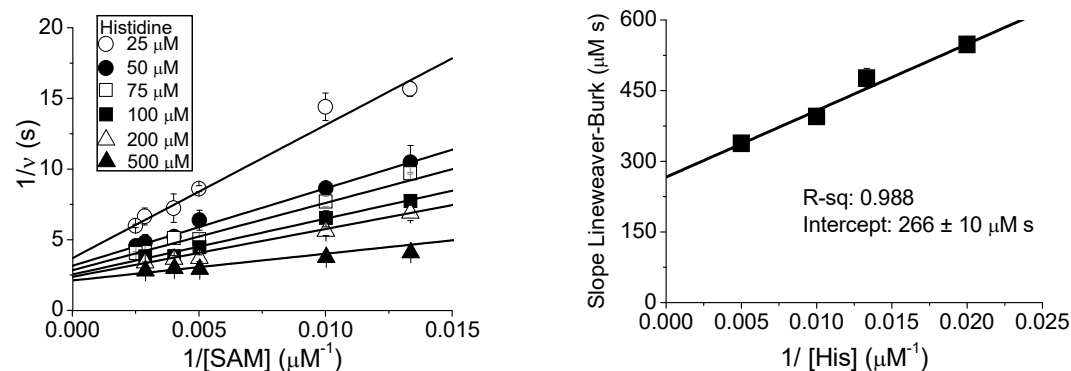


Figure 34 Left: Primary plots with SAM as the varied reactant in presence of different concentrations of histidine (25, 50, 75, 100, 200 or 500 μM). Reaction conditions: 25 $^{\circ}C$, 50 mM Tris/HCl pH 8.0, 50 mM NaCl, 100 μM Mn^{II} , 10 μM AdoNuc, 5 μM adenine deaminase, 2 μM EgtD. **Right:** Secondary plot with SAM as the varied reactant in presence of 4 different concentrations of histidine: 50, 75, 100 and 200 μM .

3.3.2 Catalytic parameters of EgtD in the presence of different concentrations of SAM

The concentration of histidine was varied in presence of a fixed concentration of SAM. As described above, this experiment was performed with five concentrations of SAM (25, 50, 75, 100 and 200 μM). The corresponding primary and secondary plots are respectively indicated in Figure 35.

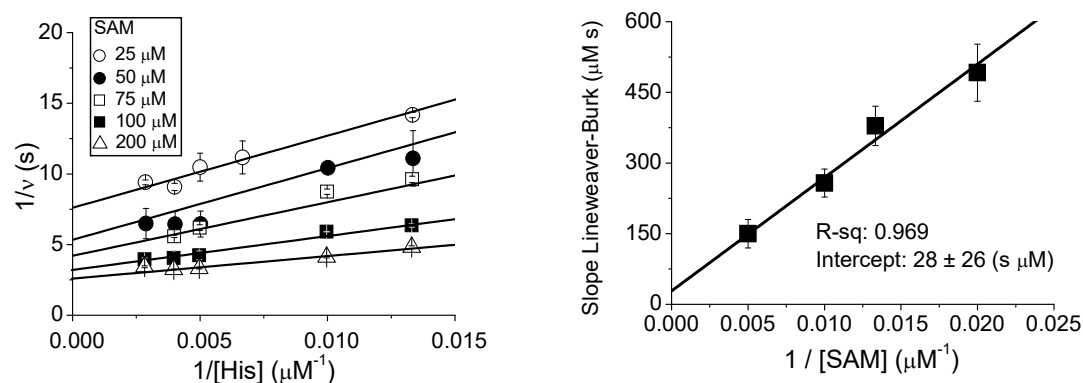
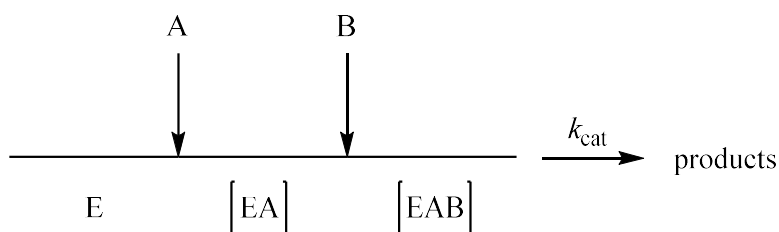


Figure 35 Left: Primary plots with His as the varied reactant in presence of different concentrations of SAM (25, 50, 75, 100 or 200 μM). Reaction conditions: 25 $^{\circ}C$, 50 mM Tris/HCl pH 8.0, 50 mM NaCl, 200 μM Mn^{II} , 10 μM SAH nucleosidase, 5 μM adenine deaminase, 2 μM EgtD. **Right:** Secondary plot with histidine as the varied reactant in presence of 4 different concentrations of SAM: 50, 75, 100 and 200 μM .

3.3.3 Substrate binding order

In order to determine the substrate binding order of EgtD from the two diagnostic plots of SAM and histidine, we consider the simple bi-reactant model in Scheme 3. A is the first substrate to bind to the enzyme E and B binds to the resulting binary EA complex.



Scheme 3 Simplified model of an organized Bi Bi reaction mechanism with A and B the substrates of the enzyme E. The first substrate to bind to the enzyme is A. Then the second substrate B binds to the binary complex EA. The catalysis can then carry on to the formation of products.

For this mechanism, if the concentration of A is varied in order to determine the catalytic parameters of the enzyme ($K_{M,A}$ and $k_{cat,A}$) in presence of different concentrations of B, the $K_{M,A}$ values remain constant regardless of these different concentrations of B. If A is the first substrate to bind, its affinity for the enzyme is not dependent on the concentration of the other substrate. Conversely, if the concentration of the second substrate to bind B is varied in order to determine $K_{M,B}$ and $k_{cat,B}$ in presence of different concentrations of A, the $K_{M,B}$ values differ from each other according to the different concentrations of A.

Inspired by the kinetic analyses in “Enzyme Kinetics and Mechanism” of Cook and Cleland,¹⁷⁵ we used diagnostic plots to graphically represent the binding order depicted in Scheme 3.

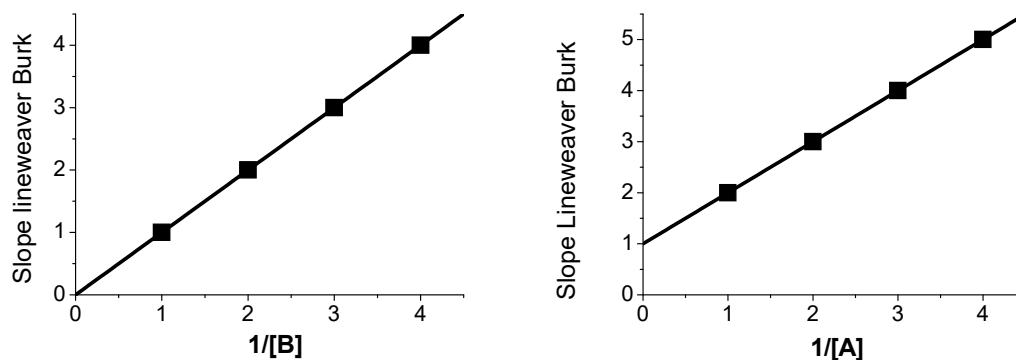
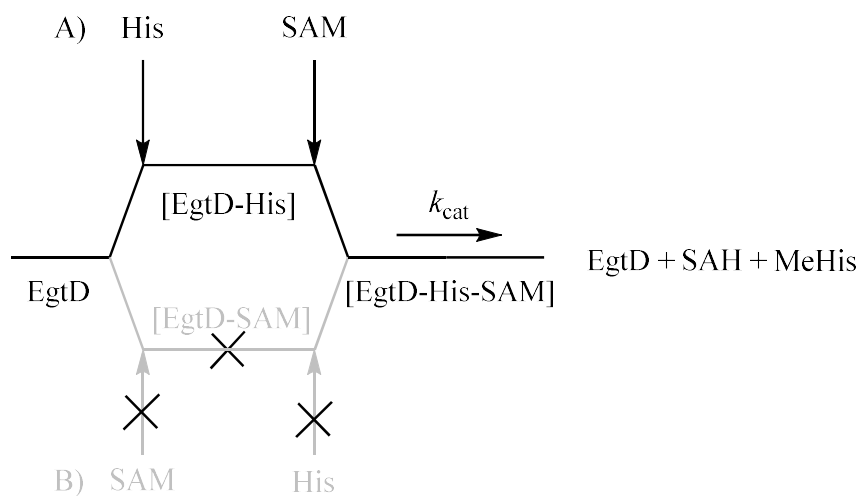


Figure 36 Predicted diagnostic plots for an ordered Bi Bi binding mechanism with A being the first substrate to bind.

The intercepts of these diagnostic plots indicate the binding order of the substrates. If we compare the models in the above figure and the graphs in Figures 34 and 35, we can conclude that EgtD binds its substrates in an ordered sequential mode. In addition, we identified histidine as the first substrate to bind. Therefore we can draw the following scheme which shows the substrate binding order of EgtD.



Scheme 4 Ordered sequential substrate binding mode of EgtD. Histidine is the first substrate to bind and SAM binds to the binary complex EgtD-histidine.

As previously mentioned, SAM-dependent small molecule MTs bind their substrates according to a sequential mechanism (the ordered binding mode being generally preferred).^{167,176-179} Interestingly in these reactions, the nucleophile is always the second substrate to bind. In the following paragraph, we will discuss how the unprecedented substrate binding mode of EgtD can provide an explanation for the stronger inhibition of chlorohistidine compared to hercynine.

3.4 Inhibition mechanisms

In Sections 3.1.1 and 3.2.1, we showed that both chlorohistidine and TMH are competitive inhibitors for the histidine binding site. The K_i value of the chloro derivative is six times lower than for the $K_{i\text{ product}}$. The crystal structure of the binary complex does not show any additional interactions provided by the α -amino to halogen substitution (Figure 33). This seemingly counterintuitive discovery suggests then a different inhibition mechanism for these two compounds. In view of the identification of the substrate binding order of EgtD, we proposed

that the product of the reaction could in fact compete with the substrates histidine and SAM, whereas chlorohistidine only competes with histidine. In order to test this hypothesis, both chlorohistidine and hercynine were tested as potential inhibitors for the SAM binding site. We measured the rate of histidine methylation at saturated concentration of histidine and by varying the concentration of SAM. The experiments were performed in presence of several concentrations of hercynine or chlorohistidine. As depicted in Figure 31, if an inhibitor competes with the SAM binding site, the $k_{cat,SAM}$ remains unchanged but the $K_{M,SAM}$ value increases. On the other hand, if the inhibitor does not compete with the binding site of SAM, it will result in a noncompetitive inhibition characterized by a change in $k_{cat,SAM}$ but not in $K_{M,SAM}$. We used Lineweaver-Burk plots to determine the nature of the inhibition.

The results of these kinetic experiments are shown in the following charts.

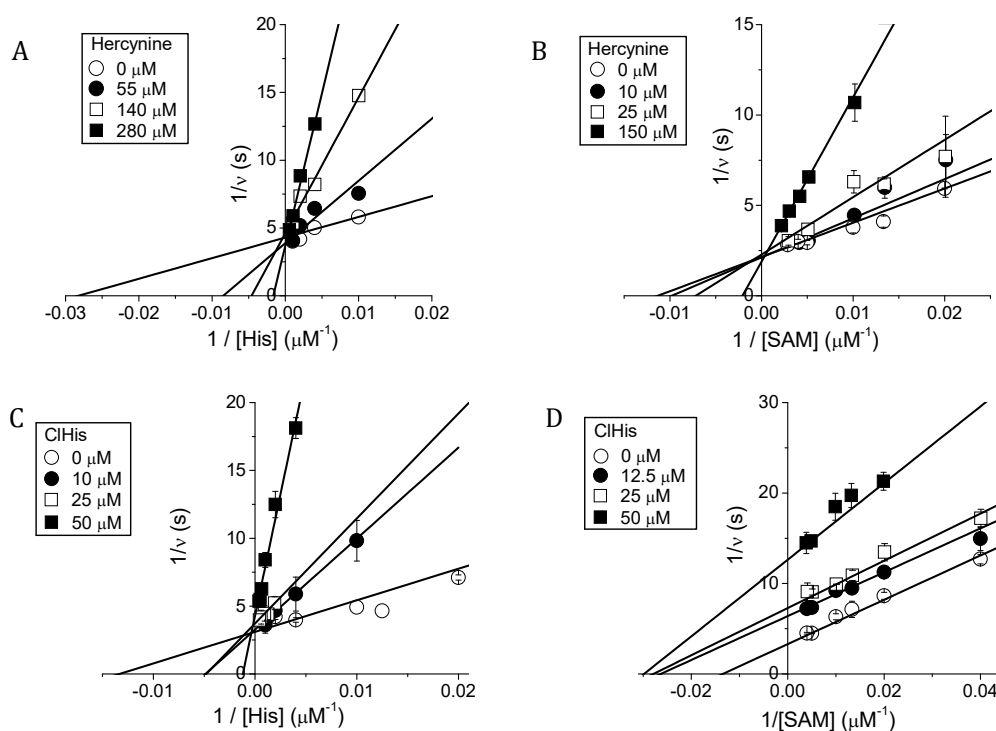


Figure 37 Lineweaver-Burk plots indicating the type of inhibition provided by either chlorohistidine or hercynine. Reaction conditions: 25 °C, 50 mM Tris/HCl pH 8.0, 50 mM NaCl, 200 μM Mn^{II}, 10 μM SAH nucleosidase, 5 μM adenine deaminase and 2 μM EgtD. **A:** The product inhibition tested with histidine is competitive. **B:** The product inhibition tested with SAM is competitive. **C:** Chlorohistidine inhibition tested with histidine is competitive. **D:** Chlorohistidine inhibition tested with SAM is noncompetitive.

Hercynine and chlorohistidine do not compete for the same binding sites. Indeed, product inhibition is competitive for the binding of both substrates SAM and histidine, whereas chlorohistidine only competes for the histidine binding site. Therefore, from these findings, we conclude that their K_i values cannot directly be compared.

Product inhibition patterns are also used to determine the substrate binding order for a multi-substrate enzyme.^{180,181} These results are indeed consistent with the identified sequential substrate binding order of EgtD. Histidine binds first, therefore the effects of hercynine will not only be the competitive inhibition of the histidine binding site, but also a competitive inhibition with the SAM binding site.

In conclusion, TMH is an inhibitor of EgtD, but also a substrate for the sulfoxide synthase EgtB.¹³³ In order to test if the production of ergothioneine could be altered by inhibiting the first step of the biosynthesis, we were then interested in identifying and testing EgtD inhibitors which would not be substrates for EgtB.

3.5 Design of EgtD inhibitors

3.5.1 Choice of inhibitors

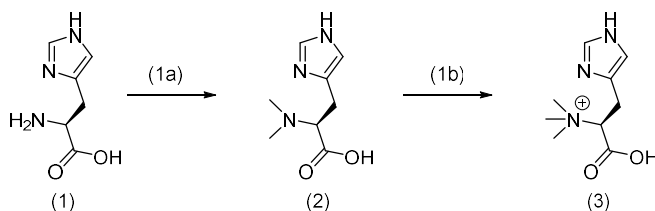
Based on the interactions identified by structural and kinetic analyses, we sought out to rationally design a series of high-affinity inhibitors. EgtD inhibitors should have an essential property: they should be a substrate neither for the MT nor for the sulfoxide synthase. We therefore synthesized and tested two additional α -halogen- (bromo- and fluorohistidine) and the α -methylhistidine derivatives, for which we believed the methylation not to be feasible. We chose the cyclic amine derivatives pyrrolidine and morpholine as substitutes for the α -amino group of histidine. We assumed that the rigidity of the cyclic amines in the catalytic site would prevent any methylation from occurring. In addition, we proposed that the cyclic amine could establish additional CH \cdots O bonds with the polar residues. These supplementary weak interactions could result in a stronger inhibition than hercynine.

All compounds were tested as EgtD substrates and inhibitors. In addition, chlorohistidine and hydroxyhistidine were tested as EgtB substrates.

3.5.2 Synthesis

All the inhibitors were synthesized by Reto Burn. The synthesis routes of EgtD inhibitors are shown in the following Schemes. The MS data and chemical shifts from NMR are given in the Appendix.

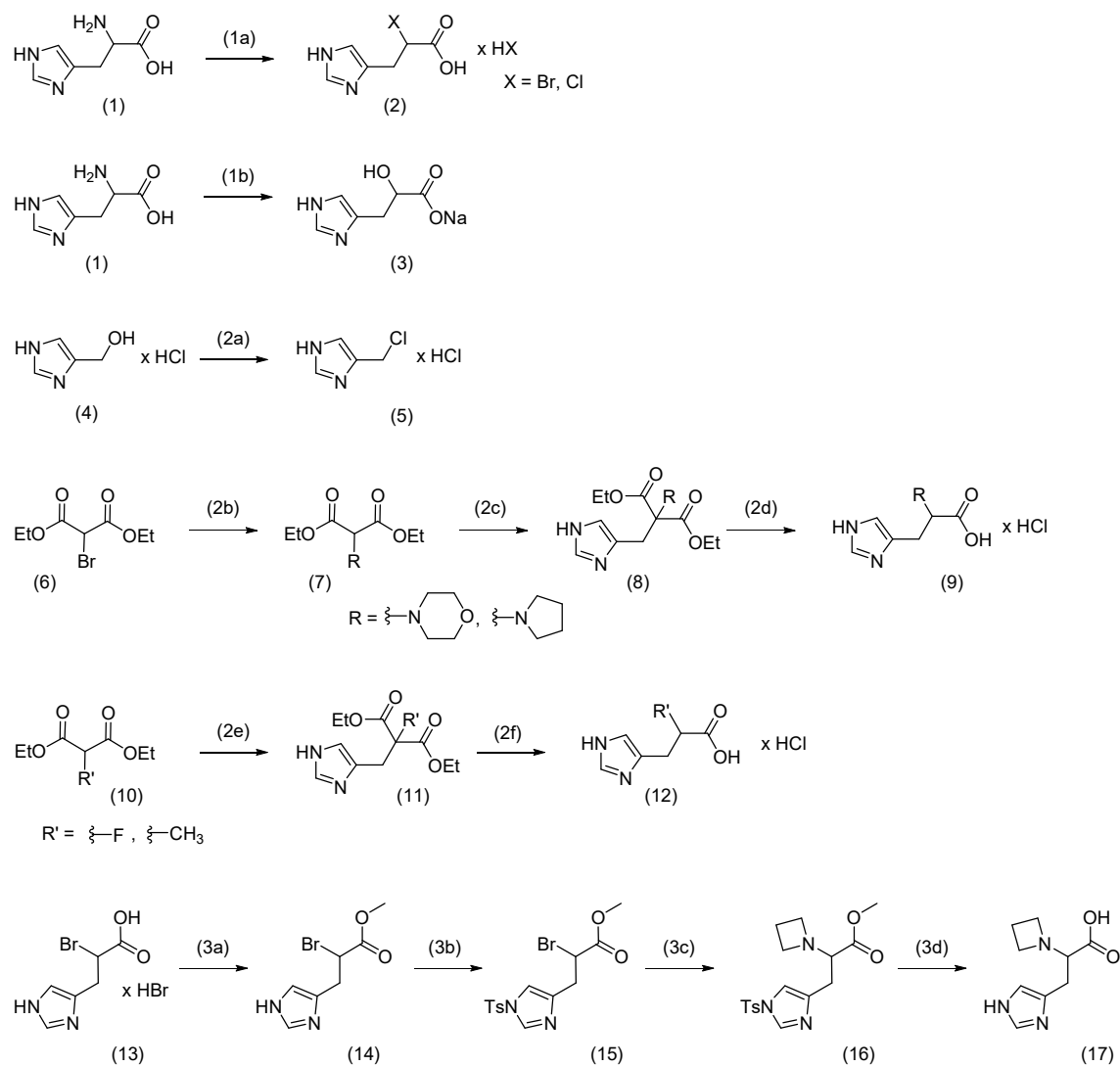
3.5.2.1 Hercynine



Scheme 5 Synthesis of L-hercynine. 1a) CH₂O (37 % aq.), 20 mM HCl in water, Pd/C, 6 bar H₂, overnight, 93 %; 1b) MeOH, NH₄OH (pH 10), MeI, overnight, RT, 42 %.

3.5.2.2 Histidine derivatives

Two different strategies were used to synthesize α -substituted histidine derivatives. The first one consisted of the diazotization of the α -amino group and subsequent nucleophilic substitution by either the halide or water in the absence of an halide (Scheme 6, route 1). The reaction proceeds via a double S_N2 mechanism resulting in retention of the conformation.¹⁸² Another synthesis starting from diethylmalonate derivatives was developed (Scheme 6, route 2), which results in the racemization of the methyl-, fluoro- and amino-histidine derivatives. In order to compare the inhibitory effects of the compounds synthesized with both methods, the first synthesis was performed with an enantiomeric mixture of (D,L)-histidine. Therefore, for both synthesis routes, the products were racemic mixtures.



Scheme 6 Synthesis of α -substituted D,L-histidine derivatives. 1a) Concentrated HX, NaNO_2 , 0 °C to 20 °C, 4 h-20 h, 28-51%; 1b) 4 M sulfuric acid, NaNO_2 , 0 °C to 20 °C, 5 d, 25%; 2a) thionylchloride, 20 °C, 1 d, 99%; 2b) morpholine or pyrrolidine, triethylamine, chloroform, reflux, 2 h - 1 d, 88-95%; 2c) (5), NaH, dimethylformamide, 0 °C to 20 °C, 4 h - 2 d, 40-65%; 2d) 6 M HCl, reflux, 2 d, 80-98%; 2e) (5), NaH, dimethylformamide, 0 °C to 20 °C, 4 h - 2 d, 40-65%; 2f) 6 M HCl, reflux, 2 d, 80-98%; 3a) thionylchloride, methanol, 0 °C to 20 °C, 1.5 h, 76%; 3b) TsCl, trimethylamine, chloroform, 0 °C to 20 °C, 16 h, 60%; 3c) azetidine hydrochloride, Cs_2CO_3 , DMF, 40 °C, 6 h, 8%; 3d) LiOH, water/THF (1:1), 20 °C, 6h, 98%.

3.5.2.3 Chirality of the substrates and inhibitors

EgtD crystal structure and kinetic data showed the specificity of the enzyme for the L-substrates. In principle, enzymes are highly precise both in catalyzing stereospecific reactions and in only binding one stereoisomer of a chiral substrate. Nevertheless, there are also enzymes that can

produce both enantiomers of the product of the reaction in accepting either the L- or the D-substrate. For example, the glutamate racemase (EC 5.1.1.3) catalyzes the interconversion of glutamate enantiomers in most bacterial strains.¹⁸³ Another enzyme was reported to bind both enantiomers at the same time. A protein involved in phenazine biosynthesis in the Gram negative bacteria *Burkholderia cepacia* was shown to simultaneously bind both enantiomers of an inhibitor, as well as each individual enantiomer.¹⁸⁴ Therefore, in order to interpret and compare the inhibitory effects of the tested inhibitors (available as racemic mixtures), we determined the possible effect of D-enantiomers concerning the binding in the catalytic site of EgtD.

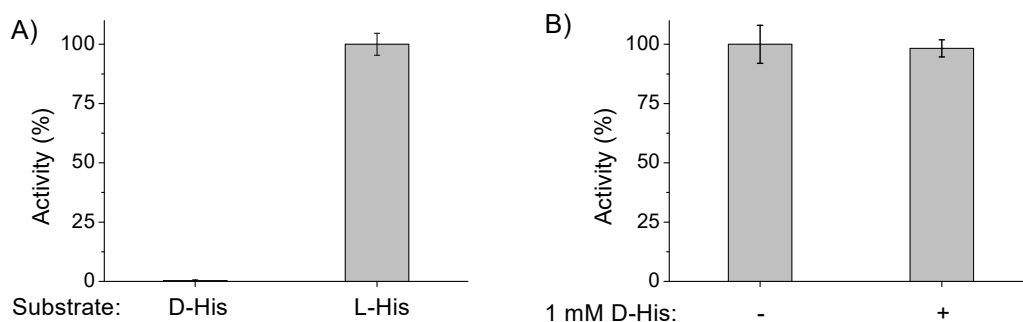


Figure 38 Only L-substrates bind to EgtD. **A:** Comparison of D- and L-histidine as substrates for EgtD. Reaction conditions: 25 °C, 50 mM Tris/HCl pH 8.0, 50 mM NaCl, 200 μ M Mn^{II} , 10 μ M SAH nucleosidase, 5 μ M adenine deaminase, 0.5 mM SAM, 0.5 mM D- or L-histidine and 2 μ M EgtD. **B:** D-histidine is not a potential competitive inhibitor. Reaction conditions: 25 °C, 50 mM Tris/HCl pH 8.0, 50 mM NaCl, 200 μ M Mn^{II} , 10 μ M SAH nucleosidase, 5 μ M adenine deaminase, 0.5 mM SAM, 0.5 mM L-histidine, 0 or 1 mM D-histidine and 2 μ M EgtD.

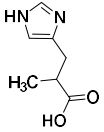
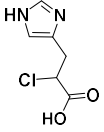
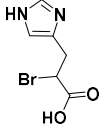
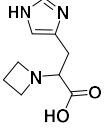
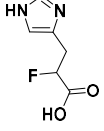
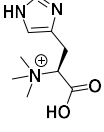
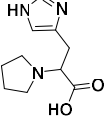
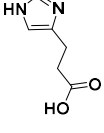
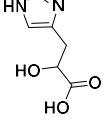
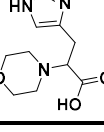
First, we identified L-histidine as the only substrate of the MT (Figure 38A). Then we demonstrated that in the presence of 1 mM of D-histidine, no reduction in activity was observed (Figure 38B). These results suggest that EgtD does not bind D-histidine; thus for a racemic mixture, only the L-enantiomers will interact with the enzyme.

3.5.3 K_i values

To determine the inhibitory effect of the histidine derivatives, the Michaelis-Menten parameters were determined in presence of three concentrations of each inhibitor by the continuous

spectrophotometric assay. The three resulting K_i values were then averaged for each compound and are indicated in Table 9.

Table 9 K_i values for EgtD competitive inhibitors^a.

| Inhibitor | Structure | K_i value (μM) |
|--|---|-------------------------------|
| Methylhistidine |  | 5.4 ± 1.6 |
| Chlorohistidine |  | 6.2 ± 1.5 |
| Bromohistidine |  | 8.2 ± 2.4 |
| Azetidinohistidine |  | 8.5 ± 2.1 |
| Fluorohistidine |  | 25 ± 1 |
| Hercynine product inhibition |  | 39 ± 10 |
| Pyrrolidinohistidine |  | 41 ± 6 |
| 3-(imidazole-4-yl) propionic acid |  | 49 ± 14 |
| Hydroxyhistidine |  | 72 ± 17 |
| Morpholinohistidine |  | 93 ± 11 |

^aReaction conditions: 50 mM Tris/HCl pH 8.0, 50 mM NaCl, 200 μ M Mn^{II}, 5 μ M adenine deaminase, 10 μ M SAH nucleosidase, 0.5 mM SAM, 10-2000 μ M histidine, three different concentrations of each inhibitor and 2 μ M EgtD. The concentrations of inhibitors are indicated on the Michaelis-Menten curves in the Experimental part of this Chapter.

The inhibition constants of each inhibitor (except for hercynine) were calculated for their racemic mixtures. Therefore, we can assume that correct inhibition constants are equal to half of the values displayed in Table 9. We then observed two separate groups: the inhibitors with a significantly better inhibition than the product, at least 10 times stronger, (methyl-,azetidino-, chloro- and bromohistidine) and the others that possess either equivalent or lower inhibition than the product (3-(imidazole-4-yl) propionic acid, fluoro-, pyrrolidino-, hydroxyl- and morpholinohistidine).

Interestingly, the compounds which are the best inhibitors do not provide additional interaction with the polar residues of the catalytic site (Figure 33). We expected the histidine amino derivatives to increase the CH \cdots O bonding network which should have resulted in better inhibition. Thus, to understand why pyrrolidino- and morpholinohistidine do not have a stronger inhibitory effect, the binary complexes of EgtD co-crystallized with both cyclic aminohistidine derivatives were analyzed (Figure 39).

3.5.4 Crystal structures

The kinetic data in Table 9 show that neither morpholinohistidine nor pyrrolidinohistidine are stronger inhibitors compared to hercynine. We were then interested in identifying the interactions between the residues in the catalytic site and the amino moieties.

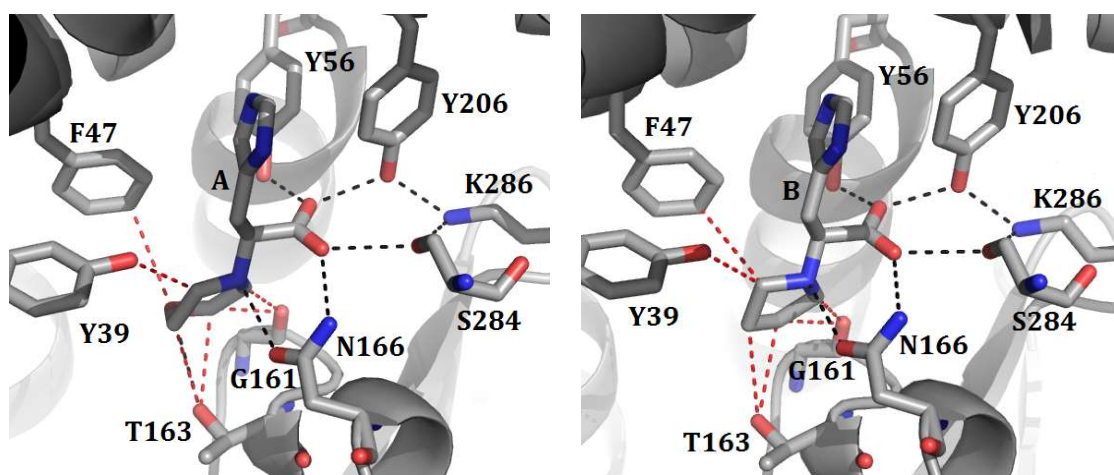


Figure 39 EgtD co-crystallized with either **A** morpholinohistidine (left, unpublished results, 1.85 Å) or **B** pyrrolidinohistidine (right, unpublished results, 1.90 Å). The hydrogen bonds are displayed with black dashes, whereas the possible CH...O with red dashes.

In the above crystal structures, we recognize that the carboxylic groups of both inhibitors form an identical hydrogen-bond network with Tyr56, Tyr206, Ser284 and Lys286 as for DMH or TMH (Figure 32). In addition, Asn166 forms two hydrogen bonds with the carboxylic acid moieties and the $N\alpha$ of the inhibitors. The same interaction was also identified in the presence of DMH (see Chapter 2, Figure 32 left). Tyr39 can also form potential CH...O bonds with morpholinohistidine (C...O distance: 3.2 Å, CHO angle 113.3 °) and pyrrolidinohistidine (3.4 Å, 128.8 °). Gly161 forms a hydrogen bond with the oxygen atom of the morpholino ring, and is in close contact with two carbon atoms of the pyrrolidino derivative (3.2 Å, 96.6 and 98.7 °). While Thr163 can only form a CH...O bond with pyrrolidinohistidine (3.3 Å, 141.3 °), it can either be engaged in a hydrogen bond with the oxygen atom of morpholine or in two CH...O bonds (3.4 and 3.7 Å, 146.8 and 128.7 °). The phenyl ring of Phe47 is also in close contact with the oxygen atom of the morpholine ring (3.7 Å, 112.9 °) and with the pyrrolidino ring (3.9 Å, CHC angle 94.3°).

Overall, both cyclic amino derivatives interact with several residues in the catalytic site of EgtD, which suggests a rather strong binding. However, contrary to our primary hypothesis, their inhibitory effect is not strengthened with respect to product inhibition. It would not be senseless to suggest that these histidine derivatives are, as well as for hercynine, competing for the binding sites of both EgtD substrates, hence the high K_i values compared to chloro- or bromohistidine, which are therefore the best inhibitors of the MT.

3.6 Conclusions

The Alberty-Fromm strategy states that the kinetics of a multi-substrate enzyme in presence of the products of the reaction can provide a certain understanding of the catalysis (in particular concerning substrate binding mode).¹⁷⁴ Our inhibition data combined with the diagnostic plots demonstrate that EgtD binds the two substrates histidine and SAM in a sequential ordered mechanism. In addition, EgtD displays an interesting feature with the nucleophile of the reaction being the first substrate to bind. No other MT has been found to have such a binding order, as SAM is always the first substrate to bind. We did not test the effect of SAH on the kinetics of EgtD, but, unlike hercynine, we only expect competitive inhibition for the SAM binding pocket. As histidine binds before SAM, the K_M value of histidine should not be affected by the presence of SAH.

EgtD is inhibited by its product hercynine. As with EgtD cooperativity (see Chapter 2), product inhibition does not seem to be an inherent property of this enzyme family. We therefore propose that EgtD product inhibition is a rather unique evolved feature which aims to regulate the activity of the MT if EgtB is not available to use hercynine as a substrate.

Saini *et al* showed recently that ergothioneine plays a role for the virulence of *Mycobacterium tuberculosis*.⁸² They demonstrated that ergothioneine is essential for bacterial survival in mice, as well as in macrophages. Moreover, bacterial Δ egtD strains of *M. tuberculosis* and *smegmatis* do not produce ergothioneine.^{123,133,140} This suggests that the first enzyme involved in the biosynthetic pathway can regulate the whole biosynthesis. As ergothioneine is not synthesized by the human body, they propose EgtD as a potential target for anti-tuberculosis treatment. Therefore, there is an increasing interest in inhibiting the activity of the mycobacterial EgtD. We identified a series of histidine derivatives which, in addition to not being substrates of EgtB (apart from pyrrolidino- and morpholinohistidine), demonstrate a 10 times better inhibitory effect on EgtD activity than the product hercynine. It would be interesting to test *in vivo* if either chloro- or methylhistidine could alter ergothioneine biosynthesis.

In order to strongly reduce EgtD activity, the K_I value of the inhibitors should be as low as possible. From our kinetic analyses, we observed that the tested compounds showed competitive inhibition for either one or both substrate binding sites. We propose that more effective inhibitors should in fact compete more actively for both binding sites at the same time. However to provide stronger inhibition of the SAM binding site, we suggest that the substitution on the $N\alpha$ of histidine should mimic the SAM scaffold.¹⁸⁵

3.7 Experimental

Standard conditions for all reactions: 25°C, 50 mM Tris/HCl pH 8.0, 50 mM NaCl, 200 μM Mn^{II} , 10 μM SAH nucleosidase, 5 μM adenine deaminase, 2 μM EgtD WT.

3.7.1 Kinetics

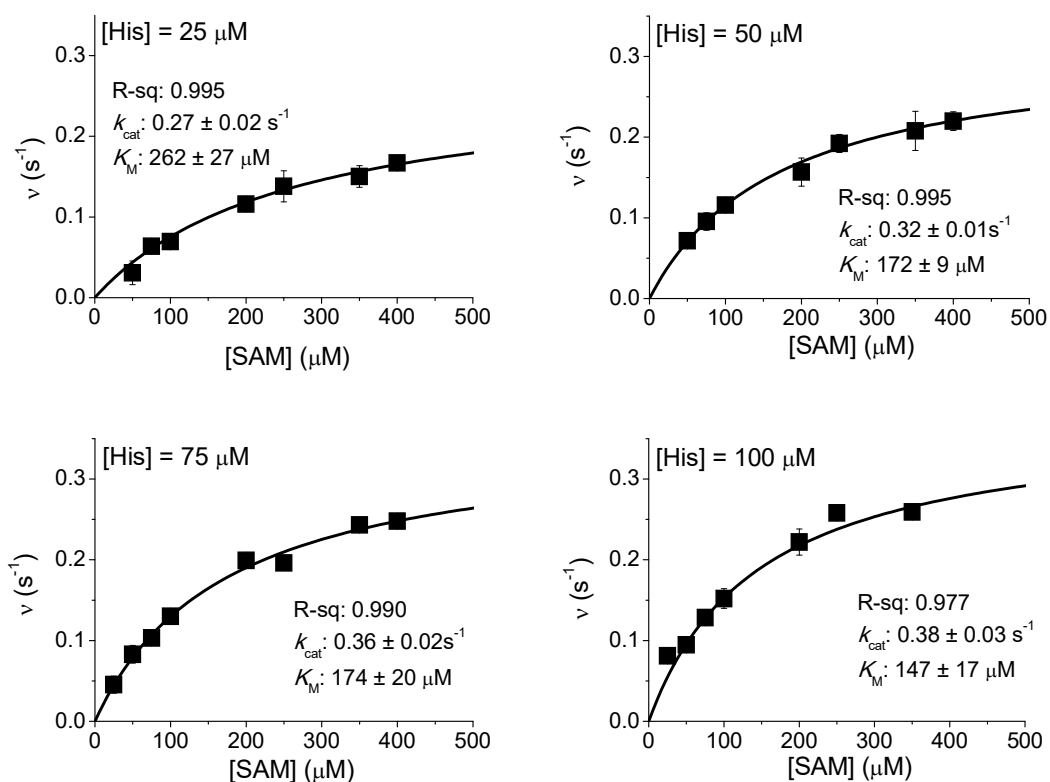
Methyltransferase assay. Methyltransferase activity was determined following published protocols.¹⁴⁷ The 200 μL reactions were monitored in a 2 mm quartz cuvette at 25°C at 265 nm with a Cary 300 spectrophotometer from Agilent. The concentrations of the substrates are indicated on the graphs. Reactions were started by addition of the methyltransferase.

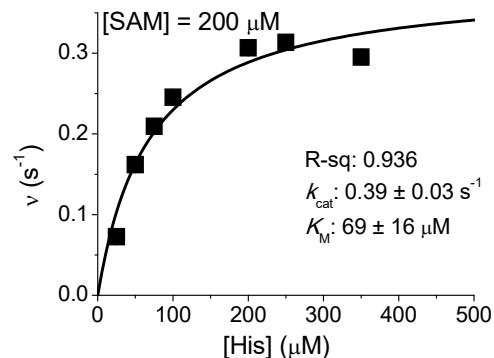
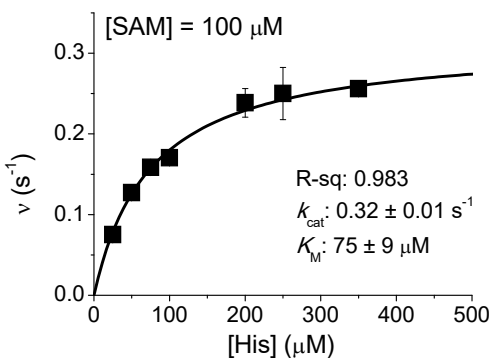
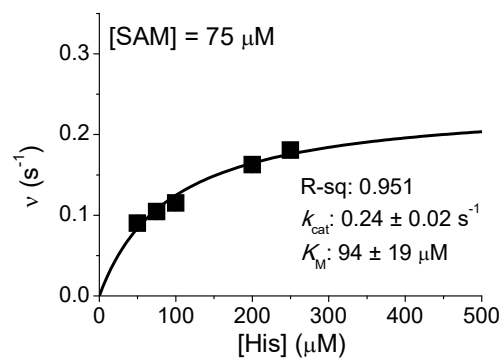
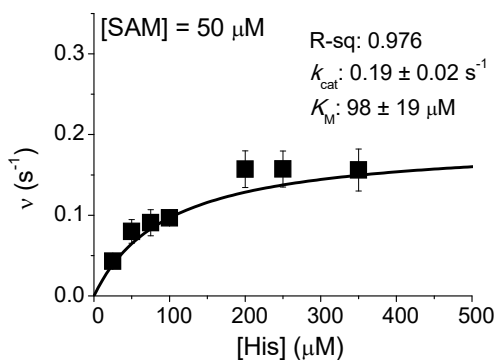
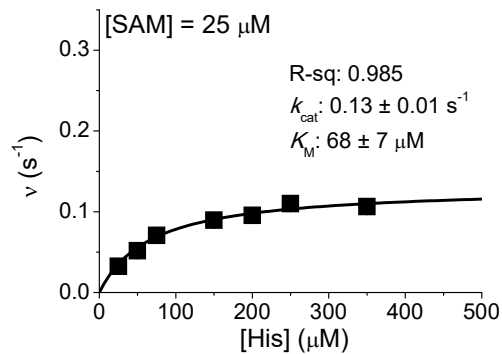
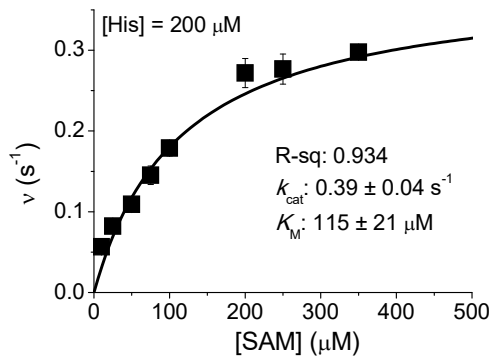
Michaelis Menten plots. The obtained data were fitted to the function:

$v = k_{\text{cat}} \cdot [\text{substrate}] / (K_{\text{M}} + [\text{substrate}])$. The corresponding substrates are indicated in abscissa of each graph.

3.7.1.1 EgtD WT_substrate binding order

The concentrations of histidine and SAM are indicated on the graphs.





3.7.1.2 EgtD inhibition

Determination of K_I values. EgtD was analyzed by UV spectrophotometric continuous coupled assay¹ under the standard conditions in presence of 0.5 mM SAM. The data were fitted to the function $v = k_{\text{cat}} \cdot [\text{His}] / (K_{\text{M app}} + [\text{His}])$.

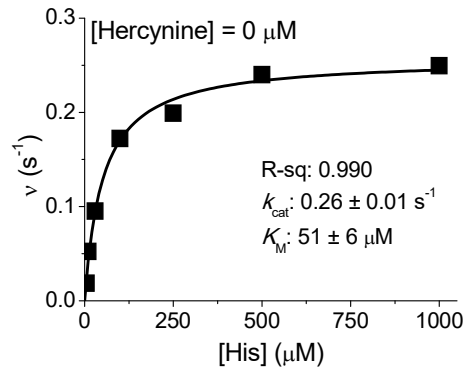
The changes in the apparent K_{M} values (but not in k_{cat}) revealed a competitive mode of inhibition which allowed the determination of the corresponding K_I values (summarized in Table 9) using the following equation derived from (Eq.2):

$$K_I = \frac{K_M \cdot [\text{Inhibitor}]}{K_{M,app} - K_M} \quad (\text{Eq.4})$$

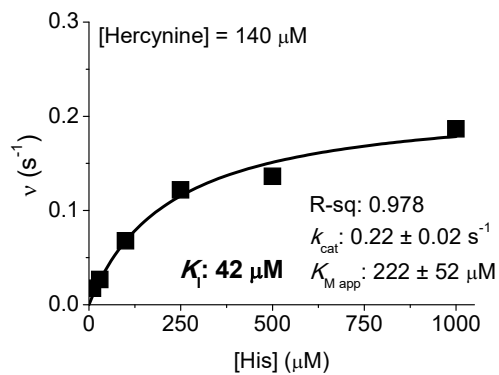
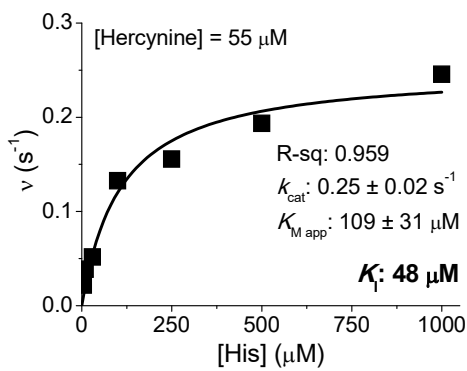
Where K_M and $K_{M,app}$ indicate the Michaelis constants in the absence and the presence of inhibitor respectively. The different concentrations of inhibitor are indicated in each graph.

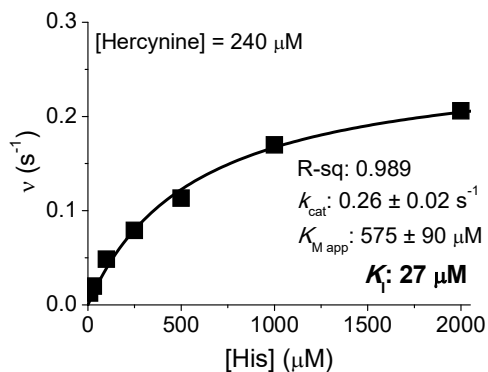
3.7.1.2.1 Product inhibition

➤ K_M value



➤ $K_{M,app}$ values

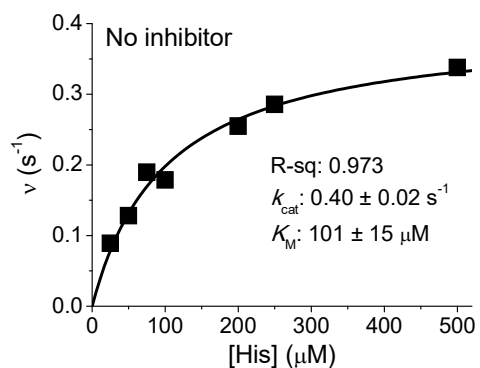




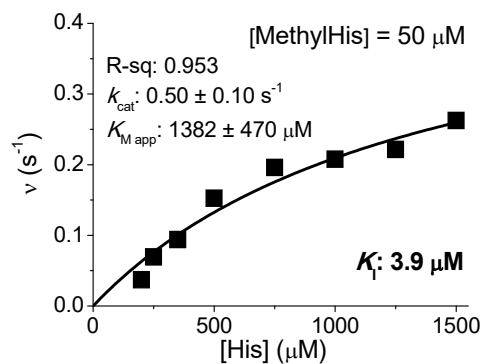
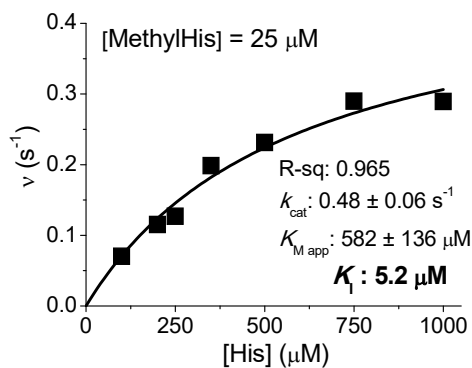
3.7.1.2.2 Histidine derivatives as EgtD inhibitors

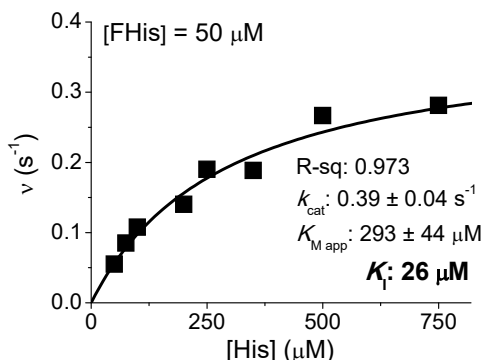
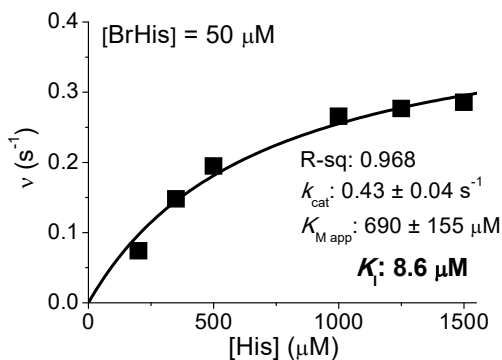
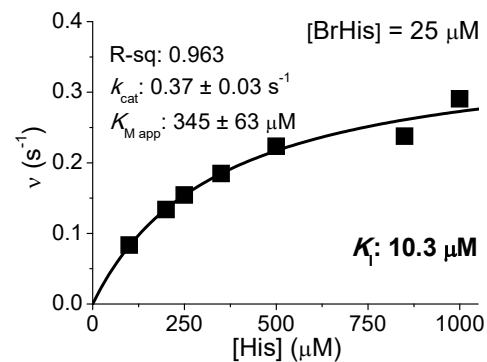
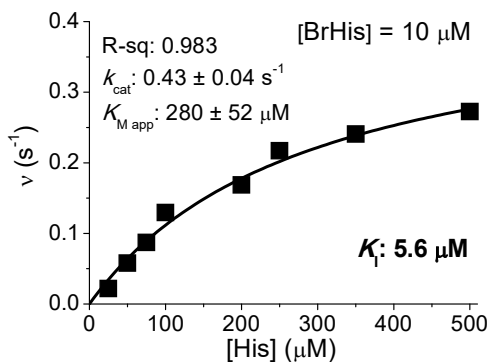
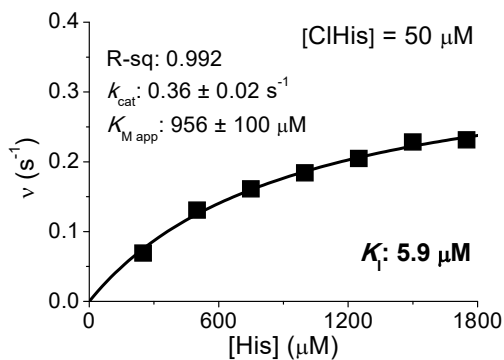
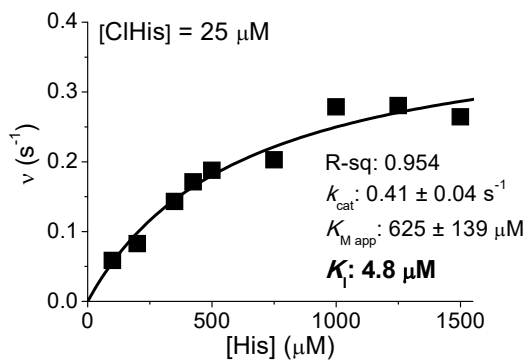
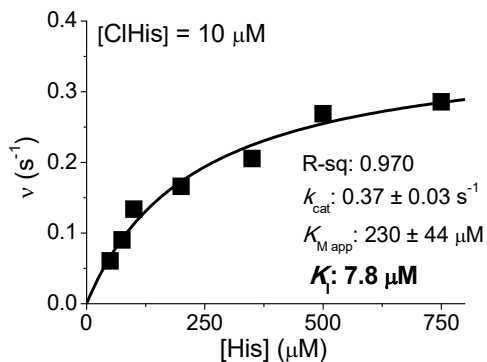
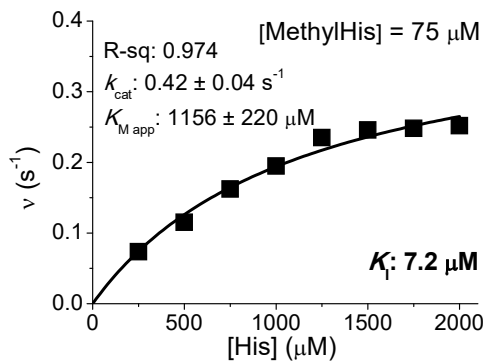
➤ K_M value

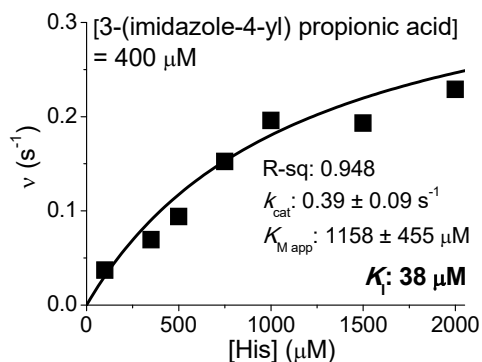
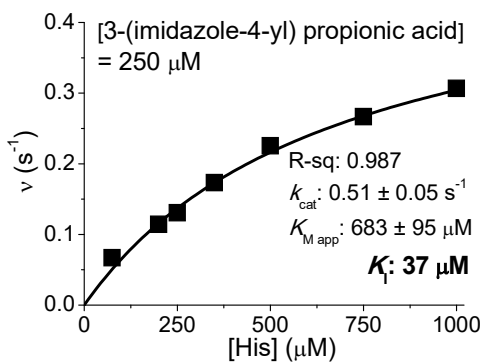
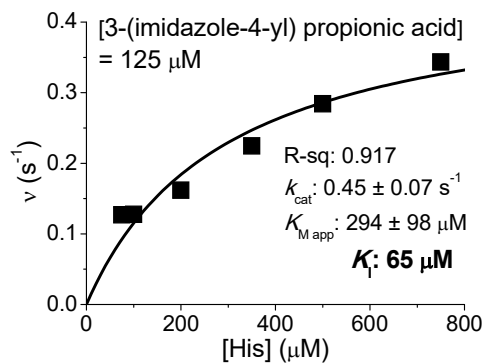
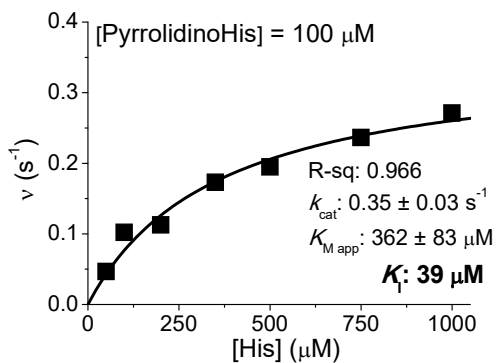
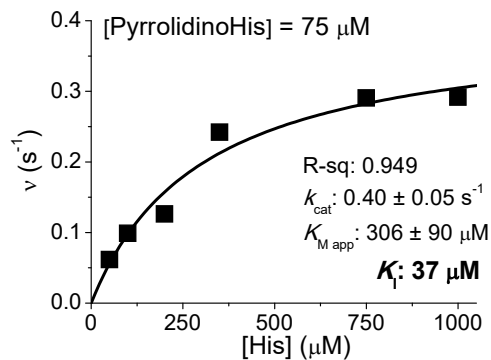
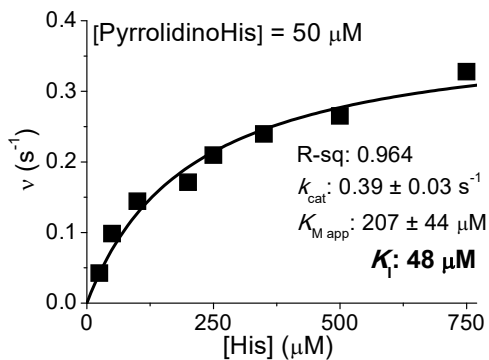
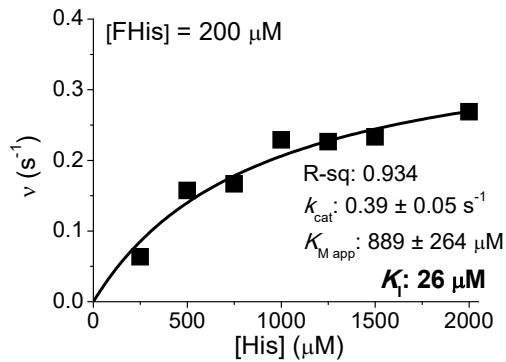
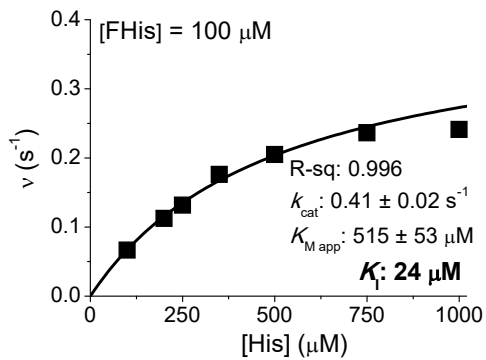
The following Michaelis-Menten curve gives the K_M value (without inhibitor), which was used for all the calculations of the inhibition constants of the tested competitive inhibitors (that is $101 \pm 15 \mu\text{M}$).

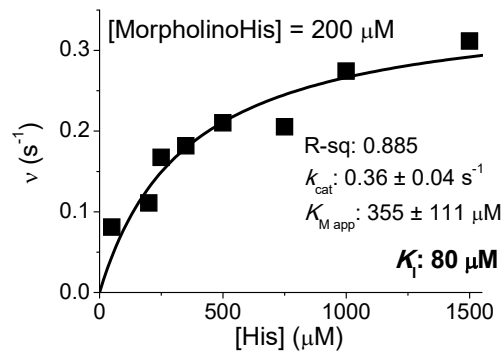
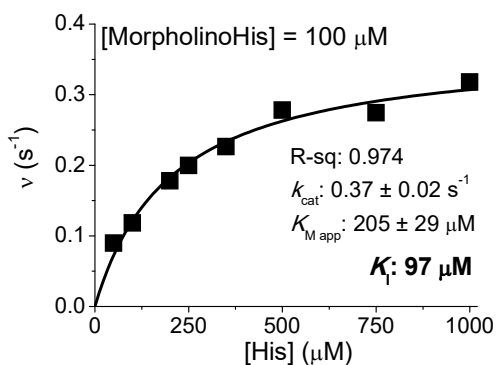
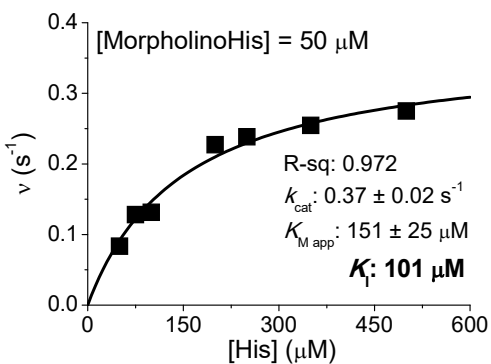
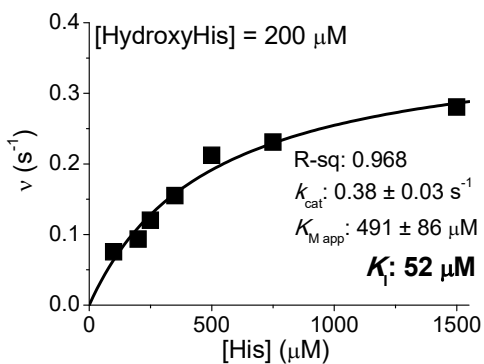
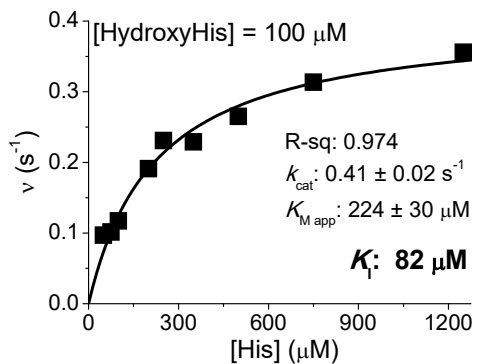
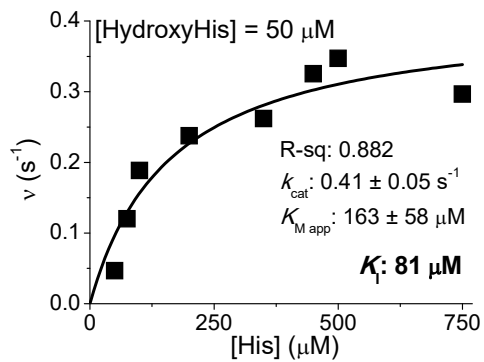


➤ $K_{M \text{ app}}$ values

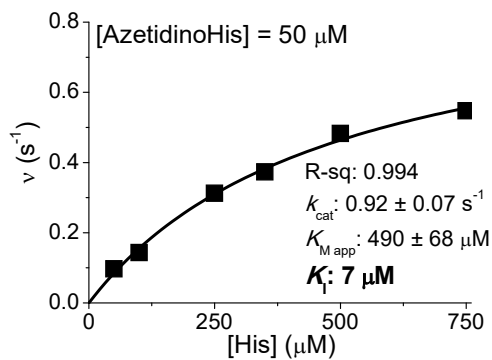
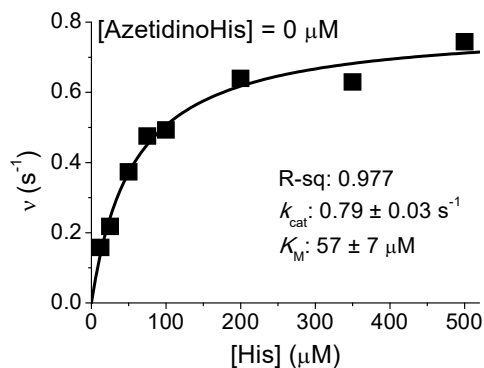


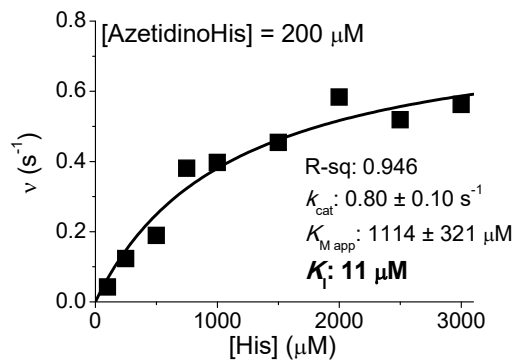
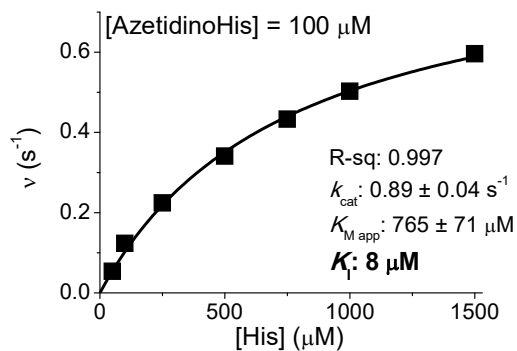




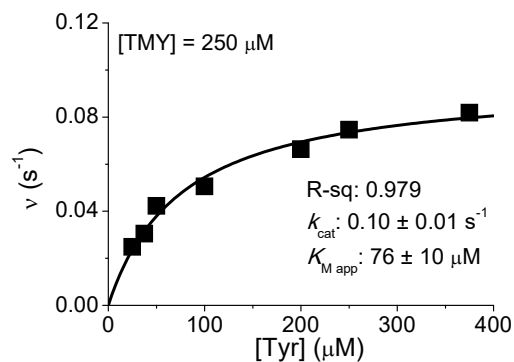
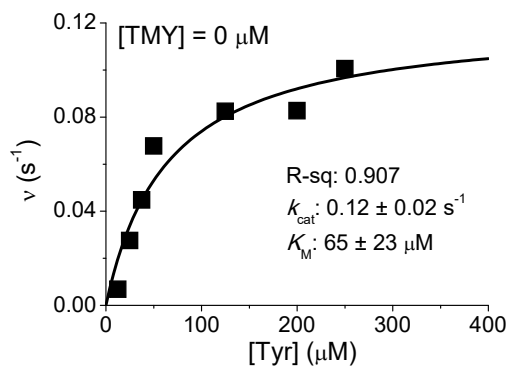


➤ Additional data: Azetidinohistidine





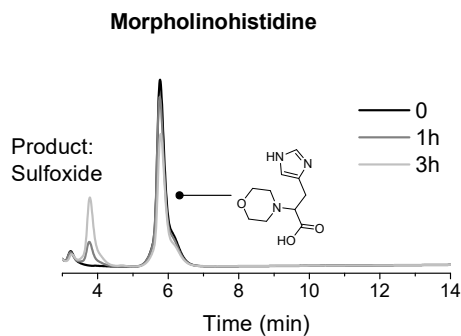
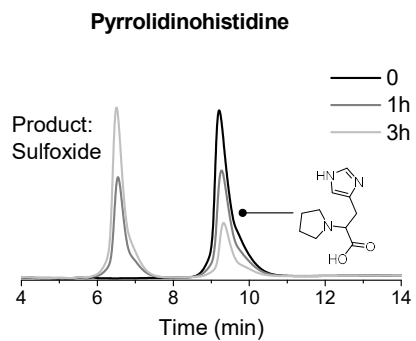
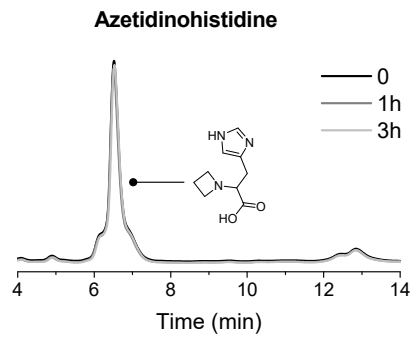
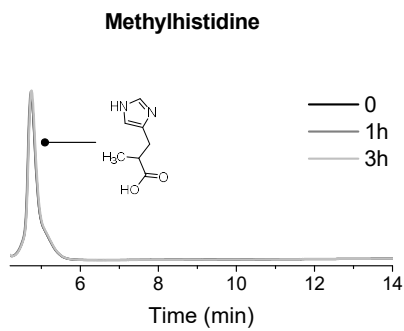
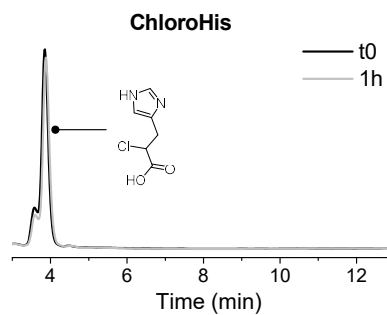
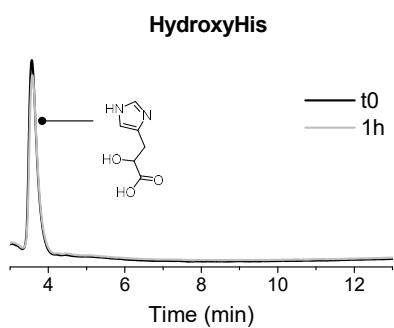
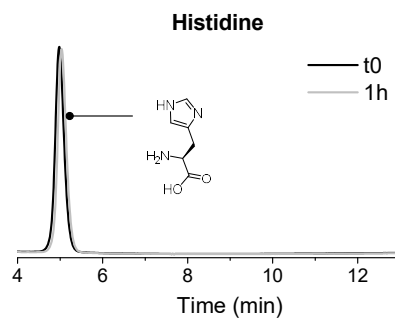
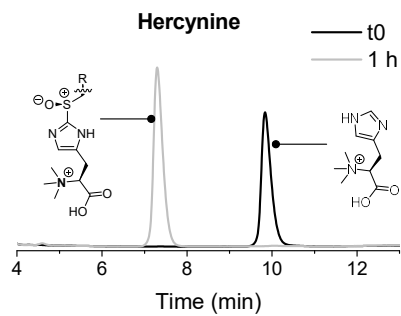
3.7.1.3 *SticA* inhibition



3.7.1.4 *EgtB* substrates

The reactions were carried out at 26°C and followed by IE HPLC at 220 nm. They contained 100 mM HEPES buffer pH 8.0, 100 mM NaCl, 2 mM of TCEP, 2 mM of ascorbate, 40 μM of FeSO_4 , 0.5 mM of γ -glutamylcysteine, 0.5 mM of each histidine derivative and 1 μM of $\text{EgtB}_{\text{smeg}}$.

Hercynine is the substrate of *EgtB* in ergothioneine biosynthetic pathway.¹³³ After one hour, all the substrate is converted into the sulfoxide intermediate (see Chapter I, Figure 11). Chloro-, methyl-, azetidino- and hydroxyhistidine are as bad substrates as histidine.



3.7.2 HPLC traces of the inhibitors

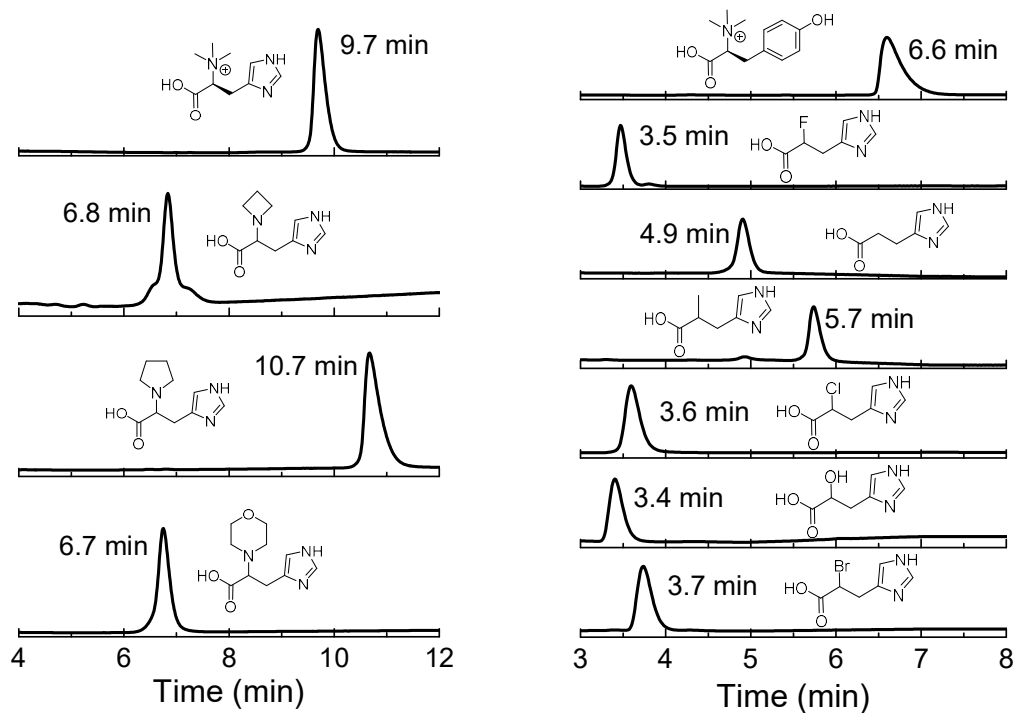


Figure 40 HPLC traces of EgtD competitive inhibitors. The purity and concentration of the compounds were determined by cation-exchange HPLC (20 mM phosphoric acid pH 2 as the mobile phase) on a Luna 5u SCX column (100 Å, 150 x 4 mm, Phenomenex). The compounds were eluted in NaCl gradients. All HPLC chromatograms were recorded at 220 nm.

The concentrations of each inhibitor were determined by IE HPLC using the calibration curve of histidine.

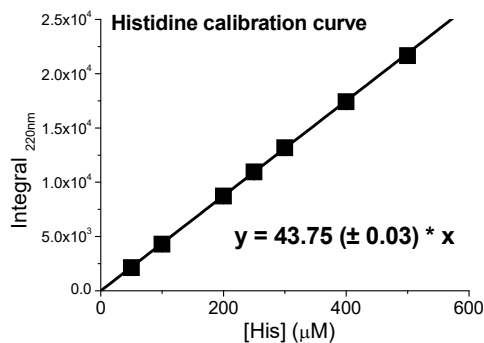


Figure 41 Histidine calibration curve for IE HPLC.

4 An active site asparagine catalyzes methyl transfer by stabilizing a near attack conformation

EgtD catalyzes the SAM-dependent methylation of the α -amino group of histidine, α -methylhistidine and α -dimethylhistidine. The α -amino group of histidine is characterized, with a pKa of 9.2, hence it is 99 % protonated under physiological conditions. The crystal structures of EgtD in complex with DMH (Chapter 2, Figure 17)¹⁴⁶ and several histidine derivatives (Chapter 3, Figures 32 and 39) suggest that the protein binds the ammonium form of the ligand. What is however clear, is that the methyl transfer from SAM can only occur to the amino form of the substrate.

The general mechanism for SAM-dependent methyltransferase is a S_N2 reaction.^{186–188} The substrate needs to be activated for the nucleophilic attack on the methyl group of SAM. Based on structural, kinetic and computational analysis, different catalytic mechanisms have been identified in SAM-dependent MTs that catalyze the trimethylation of amines. Several relevant examples will be presented with particular attention to the nucleophile activation pathways.

4.1 N-methyltransferases

4.1.1 Phosphoethanolamine methyltransferase

Like EgtD, phosphoethanolamine MT (PfPMT) also catalyzes the N α -trimethylation of its substrate.¹⁴⁸ The resulting phosphocholine (Figure 42, 4) is critical in plasmodial membrane biogenesis.

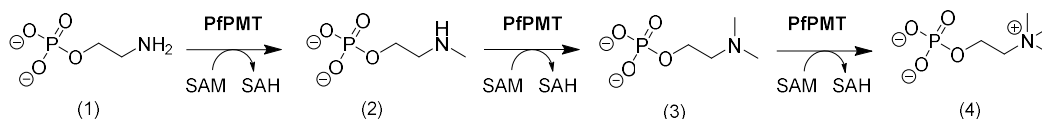


Figure 42 Sequential methylation of phosphoethanolamine (1) to phosphomethylethanolamine (2), phosphodimethylethanolamine (2) and phosphocholine (3) in *P. falciparum* catalyzed by PfPMT.

In most of the S_N2 methyl transfers catalyzed by SAM-dependent MTs, a proton is abstracted from the substrate by a catalytic base. In the reaction catalyzed by PfPMT, phosphoethanolamine (pEA) must first be deprotonated, in order to perform nucleophilic attack on the methyl group of

SAM.¹⁴⁸ Saen-oon *et al.* propose two different mechanisms for $N\alpha$ proton abstraction (Figure 43, left). Based on site-directed mutagenesis analysis, they first suggested that the activation of the $N\alpha$ could occur through the deprotonation catalyzed by the dyad Tyr19-His132 (Figure 43, right A).¹⁴⁸ The histidine residue would act as the base, abstracting the proton from the hydroxyl side chain of the tyrosine residue. Then the resulting negatively charged oxygen atom would interact with the proton of the amine substrate. However, after performing QM/MM calculations, they were able to also identify another residue, Asp128, which seems critical for the methylation of pEA. Thus they could propose an alternative mechanism in which the deprotonation of the substrate would be catalyzed by Asp128, mediated by a water molecule (Figure 43, right B).¹⁸⁹

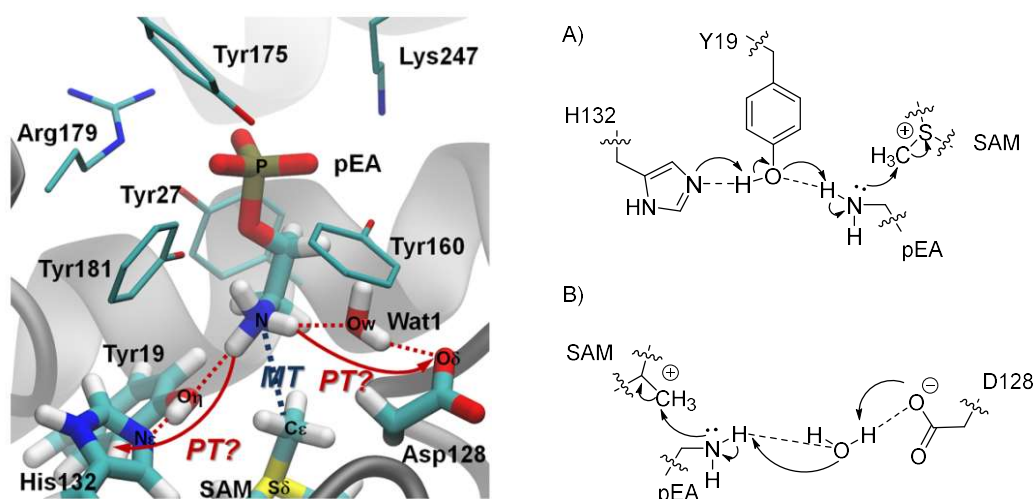


Figure 43 Left: Active site structure illustrating the two proposed pathways for the activation of the $N\alpha$ of pEA through proton transfer (PT) in PfPMT (Saen-oon *et al.* 2014). Right: Mechanistic schemes for $N\alpha$ proton abstraction occurring through (A) the catalytic dyad Tyr19-His132 or (B) Asn128 residue, mediated by a water molecule.

4.1.2 Protein lysine and arginine methyltransferases

Histones consist in the main protein component of chromatin, the scaffold in which eukaryotic DNA is packaged. Histones are subject to post-translational modifications (PTMs), especially on their flexible tails. Seven residues are known to be covalently modified: lysine, arginine, serine, threonine, tyrosine, histidine and glutamate. Most of the PTMs on lysine and arginine proteins correspond to the addition of rather small moieties such as methyl, acetyl or phosphate groups.¹⁹⁰ PTMs of non-histone arginine or lysine protein were not as extensively reviewed as their histone homologues. However, there is an increasing interest in understanding such modifications that occur to RNA or tumor proteins due to their suspected involvement in the cell

cycle, in the regulation of transcription factors or in RNA processing and transcriptional elongation.¹⁹¹

Histone lysine methylation has been correlated with both gene activation and silencing. In particular, this methylation of the *N*-terminal lysine was shown to serve to recruit DNA damage repair proteins that recognize methyl-lysyl residues. These modified lysine residues can be found in *Nε*-monomethylated, dimethylated and trimethylated states.^{155,190} Structural and functional studies of the SET domain of protein lysine MTs (PKMTs) revealed that the general mechanism of substrate activation requires the presence of active site water molecules. During substrate binding, the ϵ -amino group of the lysine forms hydrogen bonds with the hydroxyl group of a tyrosine residue, as well as with two water molecules in the catalytic site. These two latter play a role in both the alignment of the ϵ -amino group of the lysine for the methyl transfers with SAM and in the deprotonation of the ϵ -amine. Indeed, MM calculations showed a decrease of two pH units of the lysine pKa upon the formation of the Michaelis complex. Thus a chain of water molecules was proposed to participate in the deprotonation of the substrate prior to the methyl transfer.¹⁵⁵ Consequently to the successive methyl transfers, the rearrangement or the removal of these solvent molecules provides a larger active site to accommodate the increasing size of the methylated ϵ -amino group. Interestingly in the SET domain of the lysine MT, water molecules (in addition to two tyrosine residues) were also identified to govern the product specificity, that is mono-, di- or trimethylation of the lysine ϵ -amino group.¹⁹²

The histone arginine methylation plays a crucial role in influencing various cellular functions as well, including cellular development and tumorigenesis. The arginine side chain can be either monomethylated or dimethylated (asymmetrically or symmetrically) at the guanidinium η positions.¹⁹⁰ In protein arginine MTs (PRMTs), the higher pKa of the side chain indicates that a different proton transfer mechanism might occur because at physiological pH, solvent molecules are not strong enough to deprotonate the guanidinium group. In addition, the structural analyses of different PRMTs do not suggest the presence of a conserved water molecule which might support the deprotonation of the guanidine moiety.¹⁹³ As for PfPMT, a catalytic dyad (His-Asp) was first proposed to participate in the deprotonation of the arginine nitrogen atom.¹⁹⁴ However, in an alternative mechanism, it is proposed that the deprotonation of the arginine side chain is not essential, even prior to the transfer of the methyl group from SAM to substrate.^{194,195} In that case, the positive charge on the guanidinium group is distributed between the two η -nitrogen atoms. This leaves an electron lone-pair on the nucleophilic $N\eta_2$ which can attack the methyl group of SAM (Figure 44).

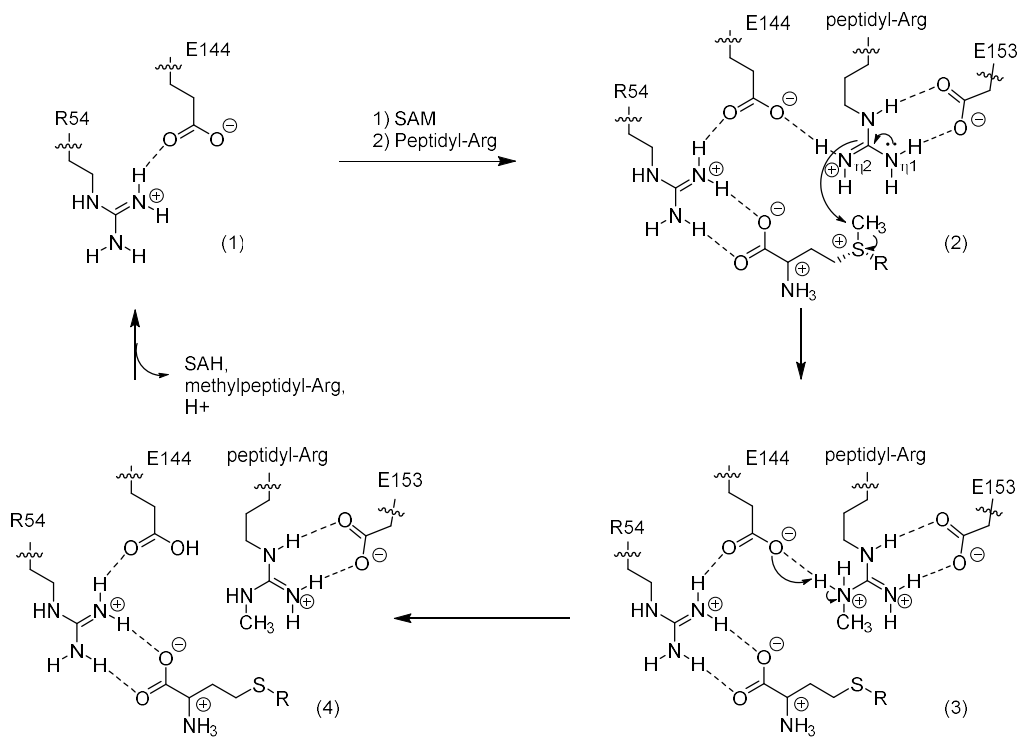


Figure 44 Proposed catalytic mechanism of the human PRMT1. The residues Arg54 and Glu144 (1) help to position the $N_{\eta 2}$ of the substrate for attack on the methyl group of SAM (R represents the adenosyl moiety of SAM). Glu153 plays a role in positioning the arginine substrate as well as initiating an electron rearrangement that leads to the formation of a more nucleophilic guanidinium moiety (2). The methyl transfer results in the formation of a di-cation intermediate (3) that then undergoes the loss of a proton to form the first methylation product (4). A second methylation occurs via the same mechanism to form the final product dimethylpeptidyl-arginine.

4.1.3 DNA adenine methyltransferase

DNA methylation is an epigenetic mechanism involved in various biological functions in prokaryotes and eukaryotes. In the thermophilic bacterium *Thermus aquaticus*, the DNA-(adenine- N^6)-MT is involved in the protection against foreign DNA (restriction-modification systems). The crystal structure indicates that the adenine base of DNA needs to be rotated, in order to bring the nitrogen atom in close proximity to the methyl donor SAM. It was first proposed that the hydrogen bonds established between the amino group of adenine and the backbone oxygen atom of a proline residue and the terminal oxygen of an asparagine residue of the MT could activate the substrate (Figure 45). The nucleophilic attack would then occur due to an increase in the electron density on the nitrogen atom. However, QM calculations indicated that a change in the hybridization from sp^2 to sp^3 of the attacking nitrogen takes place during catalysis (the product of the reaction, the methylated adenine is in sp^3 geometry). This distortion

from the planar adenine to the tetrahedral geometry is not observed in the binary complex [MT:adenine]. Thereby, the hydrogen bonds, shown in Figure 45, do not change the hybridization of the nucleophile nitrogen atom of adenine to activate it for nucleophilic attack. It is in fact the optimal positioning of both substrates in the catalytic site of the enzyme that enhances the rate of the methyl transfer.

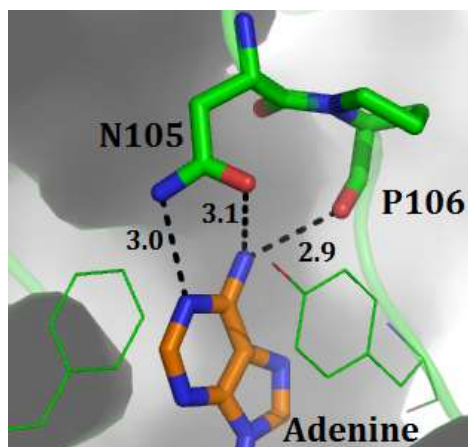


Figure 45 Stabilization of the adenine base in the active site of the DNA-(adenine- N^6)-MT of *T. aquaticus*. (PDB: 1G38, 2.0 Å). Distances are given in Å.

The formation of hydrogen bonds within the catalytic site positions the substrate such that the lone-pair electrons on the nucleophilic nitrogen point towards the incoming methyl group of SAM. When SAM binds, it shifts the nitrogen atom away from a sp^2 geometry, towards sp^3 . This mechanism was then shown to occur in a stepwise manner, with the methyl transfer occurring first, followed by proton abstraction. In the tetrahedral conformation, the N^6 atom is significantly more acidic than in the planar geometry and can be deprotonated by a weak base (such as Asn105) or an active site water molecule, to be transferred to bulk solvent through a water bridge.¹⁹⁶

4.1.4 Requirements for methyl transfer

The examples discussed above all demonstrate that the N -methyl transfers proceeding via a S_N2 reaction require either the activation of the nucleophile by a general acid/base-mediated catalysis (with deprotonation of the nitrogen atom as in PfPMT) or an optimal positioning of the substrates (as for the DNA-(adenine- N^6)-MT). The identification of the residues responsible for

the activation of the $N\alpha$ of histidine is a key point to understanding the S_N2 mechanism of EgtD. Interestingly, inspection of the crystal structure of EgtD in complex with DMH and SAH (Chapter 2, Figure 17) did not reveal a clear candidate for a catalytic base in the proximity of the substrate. This indicates that, as for the DNA-(adenine- N^6)-MT, the orientation of histidine in the catalytic site of EgtD may be more crucial for preparing the $N\alpha$ for nucleophilic attack.

4.2 Substrate activation in EgtD

Analysis of the EgtD crystal structure (s) shows that the recognition of the substrate is made via hydrophilic interactions.¹⁴⁶ In particular, Asn166 forms two hydrogen bonds with the protonated α -amino and carboxylic groups of the substrate (Figure 46). No other residue interacts with the $N\alpha$ of histidine (or MMH or DMH).

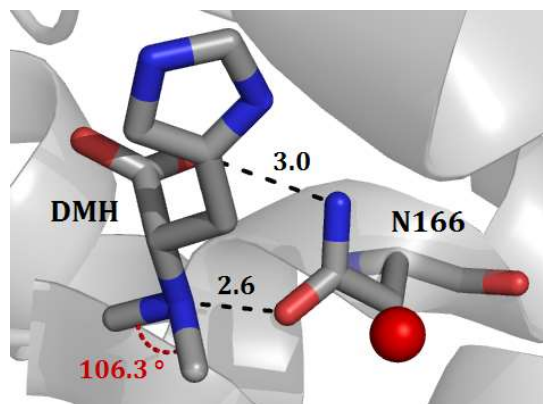


Figure 46 Hydrogen bonds between Asn166 and the substrate DMH. The red sphere represents an active site water in proximity of Asn166 (distance $O\cdots O$: 3.4 Å). Distances are given in Å

The negative charge of the carboxylic group of DMH is stabilized by coordination to the side chains of Asn166 ($O\cdots N$ distance: 3.0 Å). Asn166 also interacts with the α -amino group of DMH ($N\cdots O$ distance 2.6 Å). The orientation of the methyl groups suggests that the α -amino group is protonated. The angle defined by the two methyl groups and the $N\alpha$ of the substrate indicates a tetrahedral geometry with the proton pointing towards the oxygen of the amide side chain of Asn166. Therefore, we propose Asn166 as the catalytic base which abstracts the proton of the $N\alpha$ of the substrate and drives the nucleophilic substitution of the methyl group (Figure 47).

However, asparagine residues are unlikely catalytic bases given the very high acidity of their conjugated acids (the pKa of an amide group is usually above 17). In addition, asparagine and glutamine residues are rarely implicated as catalytic acids or bases during catalysis. Typically, a histidine, aspartate, glutamate, tyrosine or lysine residue are involved in acid/base mechanisms.¹⁹⁷ However, as mentioned for the DNA adenine MT, the formation of the Michaelis complex (with the approaching sulfonium group increasing the acidity of the nitrogen nucleophile) can lower the pKa of the nucleophile, allowing a weak base, such as arginine, to abstract the proton.

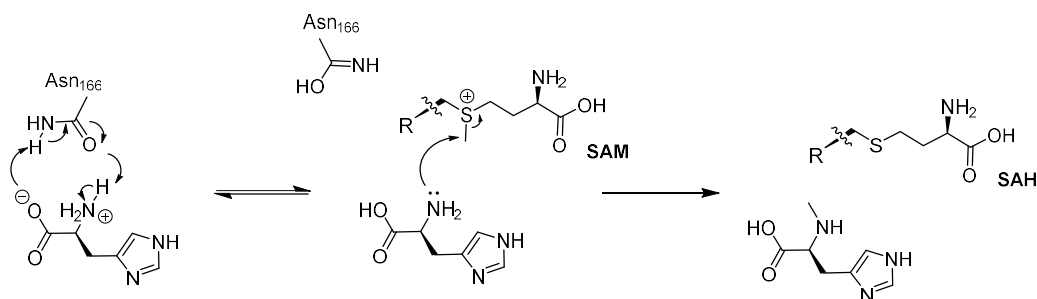


Figure 47 Proposed mechanism for the methylation of histidine catalyzed by EgtD at pH 8. The deprotonated carboxylate of histidine abstracts the proton of the amine group of Asn166, which in turn abstracts a proton from the α -amino group of His, activating it as a nucleophile. The resulting lone pair of $N\alpha$ can then attack the methyl group of SAM. R corresponds to the adenosyl group of SAM.

As already mentioned, it is the ammonium form of the substrate which seems to be bound to EgtD. The proton transfer from the ammonium substrate to Asn166 may be coupled to the binding of SAM, in a similar mechanism as described for the DNA-(adenine- N^6)-MT. The incoming sulfonium ion would certainly lower the pKa of the ammonium group and might therefore mitigate pKa mismatch between the ammonium group and the protonated Asn166 (Figure 47). Therefore, Asn166 would contribute to catalysis by bringing the methyl group donor and acceptor in a near attack conformation and consequently stabilizing the Michaelis complex ([EgtD:DMH:SAM]). During the three successive methyl transfers of histidine, Asn166 requires to be deprotonated after each step. An active water molecule could abstract the proton of Asn166, enabling EgtD to perform another methylation (Figure 46, a water molecule was identified in proximity of Asn166). In addition, based on their crystal structure of EgtD in complex with histidine and SAH (PDB: 4UY6), Jeong *et al.* also suggested that EgtD catalyzes the methyl transfer by a proximity and orientation effect (the lone pair of electrons from the $N\alpha$ of histidine being oriented toward Asn166 by the hydrogen bonds shown in Figure 46).¹⁶⁵

To examine our proposal, we constructed the EgtD variant Asn166Asp. The idea behind this mutation was to compare the results obtained for the EgtD WT and N166D for the experiments listed below, in order to evaluate if Asn166 is indeed the catalytic base in the methyl transfer reaction:

- i. Determination of the MT activity at different pH values;
- ii. Activity of the MT in the presence of histidinamide as a substrate;
- iii. Determination of the catalytic parameters.

4.3 EgtD wild type and N166D activities are pH-dependent

4.3.1 Theory

We proposed Asn166 as the catalytic residue which activates the $N\alpha$ of the nucleophile, driving the methyl transfer in EgtD. Thus we expected a drastic decrease in activity for the aspartate mutant at pH 8 compared to the WT (Figure 48). Although a salt bridge forms between the $N\alpha$ of the substrate and the carboxylate of the side chain of Asp166, the deprotonation of histidine appears to be difficult. Indeed, the repulsion between the carboxylic groups of the substrate and of the Asp166 residue does not favor the stabilization of the substrate within the catalytic site of the variant. However, by lowering the pH value of the reaction, we proposed that the activity of EgtD N166D would be enhanced. Indeed, at lower pH values, two hydrogen bonds could be established between the substrate and the protonated Asp166, as occurring in the WT. Thereby, at low pH, the aspartate residue of the mutant can mimic the role of the asparagine residue in the WT and activate the nucleophile. The pKa of the carboxylic side chain of aspartate is 3.9. However, within the enzyme, the pKa of the aspartate 166 residue might be higher (due to the presence of other nucleophile residues such as Tyr39 or Thr163). Taking this into account, some activity might be detectable at a pH of 5 or 6.

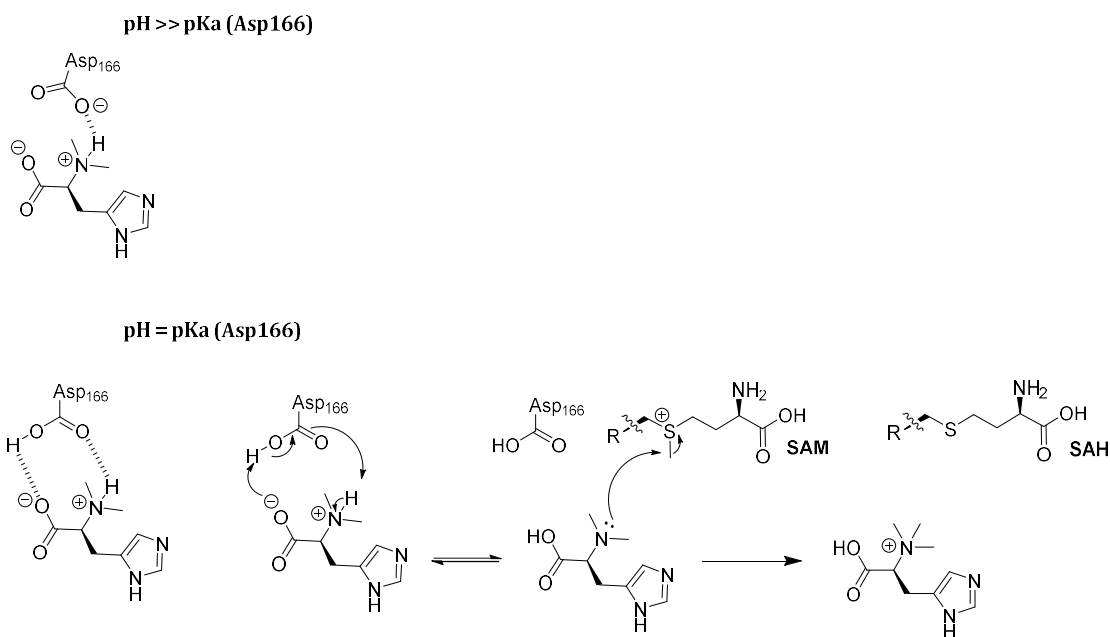


Figure 48 Mechanistic rationale of EgtD N166D activity at different pH values. At high pH ($\text{pH} \gg \text{pKa}$ of Asp166), the side chain of Asp166 is fully deprotonated and carries one negative charge which enables the proton abstraction on the substrate and the consecutive methyl transfer to take place. At pH values close to the pKa of Asp166, half of these residues will be protonated. Therefore the $N\alpha$ can be activated through deprotonation and leads to the similar nucleophilic attack on the methyl group of SAM as described for the WT. R corresponds to the adenosyl group of SAM.

4.3.2 Results

Four reactions were carried out at pH 5, 6, 7 and 8 with saturated concentrations of SAM* and histidine (0.5 mM of both substrates). These reactions were monitored by IE HPLC and analyzed at the following time points: 0, 1, 2, 3 and 24 hours (Figure 49). During the course of the reaction, the methyl group of SAM (3) is transferred to histidine and the resulting SAH is cleaved by the SAH nucleosidase which leads to adenine (1) formation. The nucleosidase is one of the coupled enzymes used to perform the spectrophotometric continuous coupled assay (see Chapter 2, Figure 14). Its presence ensures that no SAH is accumulated during the reaction, as it might inhibit MT activity (see Chapter 3).

EgtD N166D catalyzes the synthesis of TMH (2) at all the tested pH values. In addition, no MMH or DMH was formed in the course of the reaction. Therefore, the mutation does not change MT activity in respect to its cooperativity (see Chapter 2). From this we can conclude that Asn166 does not play the role as determinant for trimethylation.

* See Section 4.5 for the K_M values of SAM and histidine.

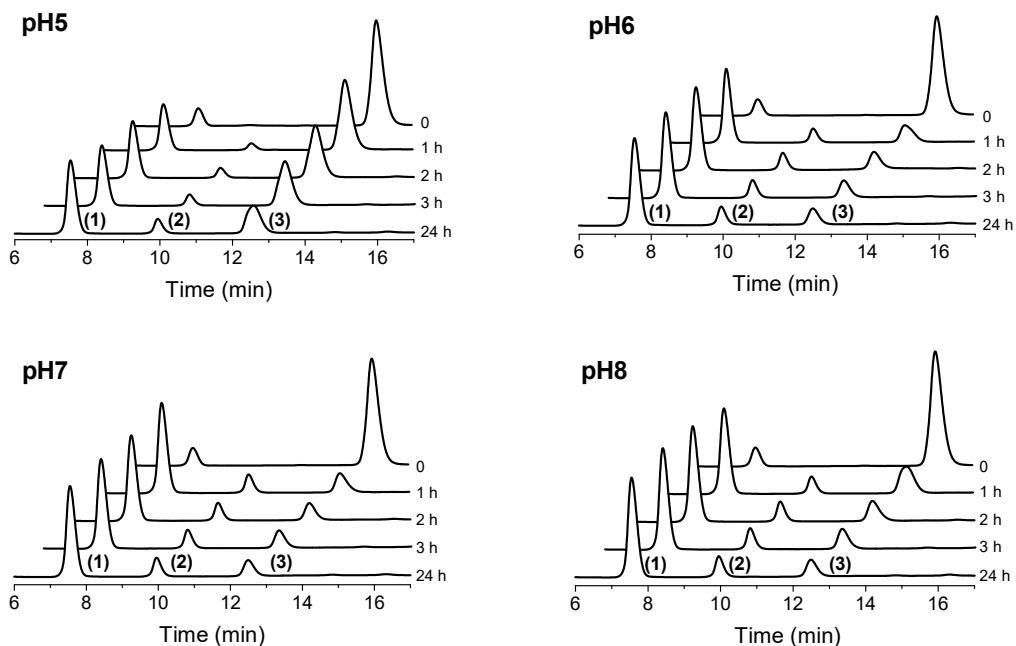


Figure 49 HPLC traces of histidine methylation catalyzed by EgtD N166D at different pH values. The chromatograms were recorded at 220 nm. Reaction conditions: 25 °C, Britton-Robinson buffer pH 5.0 to 8.0, 50 mM NaCl, 10 μ M SAH nucleosidase, 500 μ M SAM, 500 μ M histidine and 50 μ M EgtD N166D. The numbers 1, 2 and 3 correspond to adenine (7.5 min), TMH (9.9 min) and SAM (12.5 min) respectively.

Contrary to our hypothesis, the rate of histidine methylation is not increased by lowering the pH of the reaction. If we compare the consumption of SAM during the course of the reaction, we could determine that after one hour, the reactions at pH 6, 7 and 8 are near to completion; whereas at pH 5, the rate of the reaction is obviously slower. For clarity, the concentration of SAM over time is shown in Figure 50.

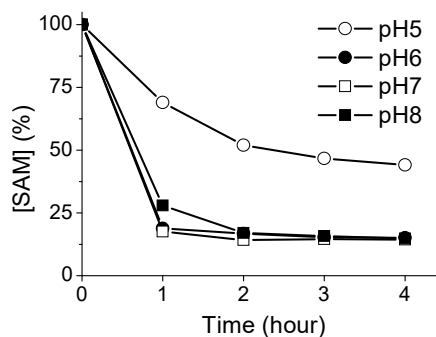


Figure 50 Decrease in relative SAM concentration at different pH values during histidine methylation catalyzed by EgtD N166D.

Therefore, the activity of EgtD N166D is clearly not enhanced at lower pH values. However, the results of this experiment do not necessary imply that the proposed mechanism is incorrect.

The activity of EgtD WT is more than 10 times lower at pH 5 compared to pH 8 (Figure 51). In general, the properties of enzymes are dependent on the external environmental factors of the reaction, such as the temperature or the pH. The external pH influences enzyme stability and can affect the binding of the substrate to the enzyme and the ionization of the catalytic residues or of the substrate. For example, at a pH value below 6, the majority of the substrate histidine will be protonated (the pKa imidazole side chain is 6.0). This can destabilize the formation of the complex [enzyme-substrate]. Therefore, this weakened binding could lead to a decrease of activity at low pH for the wild type, but also for the Asn166Asp variant.

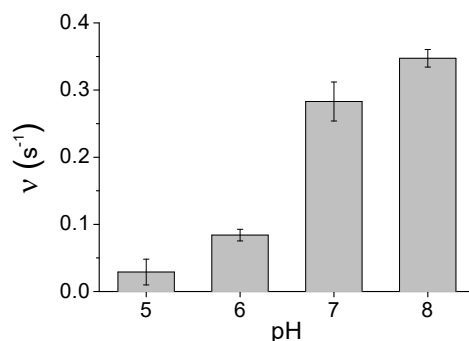


Figure 51 The activity of EgtD WT is dependent on the pH value. Reaction conditions: 25 °C, Britton-Robinson buffer pH 5.0 to 8.0, 50 mM NaCl, 200 μM Mn^{II} , 10 μM SAH nucleosidase, 500 μM SAM, 500 μM histidine and 2 μM EgtD WT.

As previously mentioned, we expected a drastic enhancement of the methylation rates of histidine catalyzed by EgtD N166D at low pH values (especially at pH 5) compared to the reaction taking place at pH 8. Nevertheless, the results of these preliminary pH-dependency experiments were not sufficient to support our hypothesis and the establishment of the pH-activity profile of the variant would be required to do so.

Our next experiment was to assay the possible formation of a different [Enzyme-Substrate] binary complex in the presence of EgtD N166D and a new substrate. We proposed that by inverting the location of the amide and carboxylic groups in the complex [EgtD WT:Histidine], the same type of interactions described in Figure 47 could take place. Therefore, we tested the activity of EgtD N166D with histidinamide (His-NH_2) as a substrate.

4.4 Histidinamide as a substrate of EgtD N166D

4.4.1 Theory

We proposed that His-NH₂ could be a better substrate than histidine for EgtD N166D (Figure 52). The rationale is that a hydrogen bond could form between the side chain carboxylate of Asp166 and the *N*α of histidinamide (as observed in EgtD WT and histidine in Figure 46). The amide moiety is also stabilized by a second hydrogen bond. Thus, the complex [EgtD N166D:His-NH₂] should mimic the configuration in the wild type with histidine. In addition, the Michaelis complex formed upon the following SAM binding would imitate the one of the wild type.

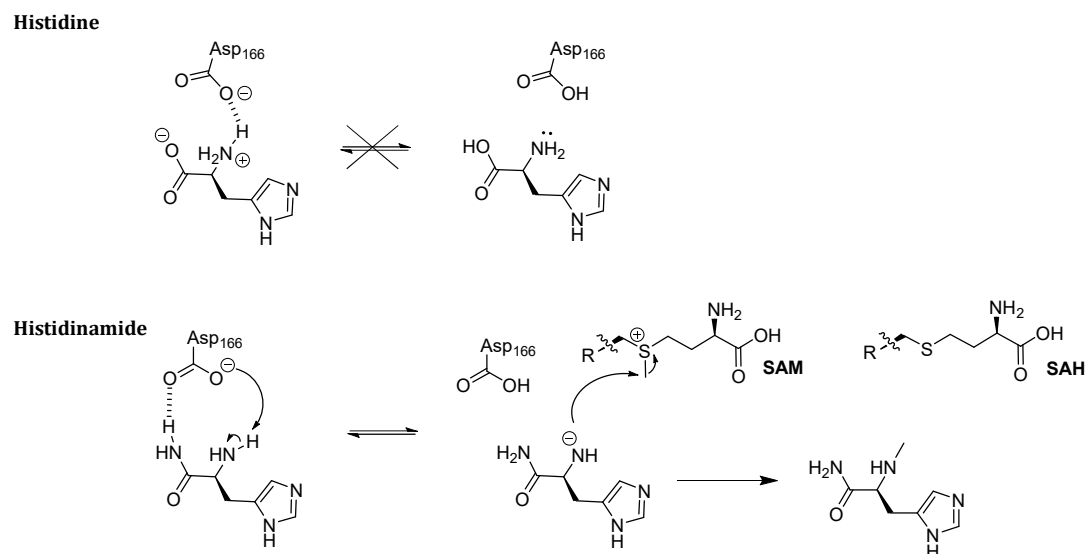


Figure 52 Proposed mechanism for histidinamide methylation catalyzed by EgtD N166D. Histidinamide might be a better substrate for EgtD N166D than histidine at pH 8. R corresponds to the adenosyl group of SAM.

4.4.2 Results

The methylation rates of histidine and histidinamide were determined at saturated concentrations of substrate* (0.5 mM of each nucleophile and SAM) for EgtD WT and EgtD N166D. The comparison of the different rates is shown in the following Table.

* See Section 4.5 for the *K_M* values of SAM and histidine.

Table 10 Rates (s^{-1}) of histidine or histidinamide methylation catalyzed by either EgtD WT or EgtD N166D.^a

| SAM concentration | Substrate | EgtD WT | EgtD N166D |
|-------------------|---------------|----------------------|-----------------------|
| 0.5 mM | Histidine | 4.2×10^{-1} | 5.7×10^{-4} |
| | Histidinamide | 6.1×10^{-4} | 4.3×10^{-4} |
| 1.0 mM | Histidinamide | 7.6×10^{-4} | 7.5×10^{-4} |
| 2.0 mM | Histidinamide | 9.9×10^{-4} | 10.8×10^{-4} |

^aReaction conditions: 25 °C, 50 mM Tris/HCl pH 8.0, 50 mM NaCl, 200 μ M Mn^{II}, 10 μ M SAH nucleosidase, 0.5, 1 or 2 mM SAM, 500 μ M histidine (first line) or His-NH₂, 1 or 25 μ M EgtD WT or EgtD N166D respectively.

As expected, histidine is a significantly better substrate for EgtD WT than His-NH₂. The rate of His-NH₂ methylation is more than 3300 times lower than for histidine methylation in the presence of 0.5 mM SAM. The two amide moieties from the Asn166 side chain and the tested substrate are stabilized by two hydrogen bonds, but as no negative charge is present, the deprotonation of histidinamide seems difficult (Figure 53).

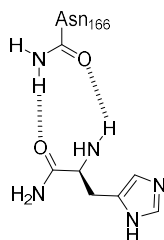


Figure 53 Hydrogen bonds between Asn166 of EgtD WT and histidinamide.

The reaction catalyzed by EgtD N166D with histidine as a substrate is 700 times slower than for EgtD WT. However, histidinamide is not a better substrate for the variant compared to the wild type (independently of the concentration of SAM). This observation disproves the proposed favored formation of the binary complex [EgtD N166D:His-NH₂] compared to [EgtD WT:His-NH₂] in Figure 52.

4.5 Catalytic parameters of EgtD N166D

The k_{cat} and K_M values of histidine, MMH, DMH and SAM were determined for EgtD N166D. The rates of methylation catalyzed by this mutant are significantly slower than for the wild type.

Thus the spectrophotometric continuous coupled assay described in Chapter 2 could not be employed to monitor those reactions. Instead, the rates were analyzed by IE HPLC. Our goal was to compare the catalytic parameters of EgtD N166D and the WT. If the turnover number k_{cat} decreases due to this point mutation, it would mean that Asn166 plays a role in the catalytic mechanism and not in the binding of the substrate. And conversely, if the K_M value increases drastically, it would suggest that this residue's main function is associated with substrate binding.

Table 11 Catalytic parameters of EgtD WT and N166D^a. The k_{cat} and K_M values are given in s^{-1} and μM respectively.

| Co-substrate | Catalytic parameters | WT | N166D |
|--------------|----------------------|-----------------|---------------------|
| His | $k_{cat, SAM}$ | 1.08 ± 0.06 | 0.018 ± 0.004 |
| | $K_{M, SAM}$ | 156 ± 16 | 1690 ± 550 |
| MMH | $k_{cat, SAM}$ | 0.99 ± 0.03 | 0.16 ± 0.01 |
| | $K_{M, SAM}$ | 117 ± 7 | 2174 ± 235 |
| DMH | $k_{cat, SAM}$ | 0.88 ± 0.08 | 0.35 ± 0.03 |
| | $K_{M, SAM}$ | 181 ± 39 | 1760 ± 220 |
| SAM | $k_{cat, His}$ | 0.66 ± 0.03 | 0.0049 ± 0.0004 |
| | $K_{M, His}$ | 79 ± 10 | 512 ± 59 |
| | $k_{cat, MMH}$ | 0.65 ± 0.06 | 0.029 ± 0.002 |
| | $K_{M, MMH}$ | 39 ± 9 | 456 ± 63 |
| | $k_{cat, DMH}$ | 0.43 ± 0.03 | 0.052 ± 0.005 |
| | $K_{M, DMH}$ | 30 ± 7 | 586 ± 186 |

^aReaction conditions: 25 °C, 50 mM Tris/HCl pH 8.0, 50 mM NaCl, 200 μM Mn^{II}, 5 μM SAH nucleosidase, 10 μM adenine deaminase, and either 1 μM of EgtD WT or 10 μM of N166D. The $k_{cat, SAM}$ and $K_{M, SAM}$ values were determined in the presence of saturated concentrations of co-substrate (0.5 mM and 2 mM for EgtD WT and EgtD N166D respectively). The k_{cat} and K_M values of the three substrates histidine, MMH and DMH were determined with a non-saturated SAM concentration of 0.5 mM.

The K_M value of histidine is not drastically affected by the mutation (the $K_{M, His}$ in N166D compared to the WT increases by a factor of six), whereas the affinity of the mutant for DMH

seems to be more altered ($K_{M, DMH}$ increases by a factor of 20). However, the K_M value of SAM increases by a factor of 10 (the k_{cat} and K_M values of SAM were determined in the presence of either 2 mM histidine, MMH or DMH, which is at least 4-fold higher than their respective K_M values). Since SAM does not directly interact with Asn166 (see Chapter 2, Figure 17), this suggests that the mutation destabilizes the EgtD:DMH conformer that can bind SAM with respect to the conformer that cannot bind SAM. Inspection of the crystal structures of EgtD:DMH:SAM (PDB: 4PIO) and EgtD:TMH suggests that the second methyl group should change its position in order to allow SAM to bind (Figure 54). Also, we have previously shown that product inhibition by TMH shows both histidine and SAM-competitive behavior (see Chapter 3). Thus, the high $K_{M, SAM}$ value in EgtD N166D can be explained by the circumstance that SAM binding is dependent on histidine binding.

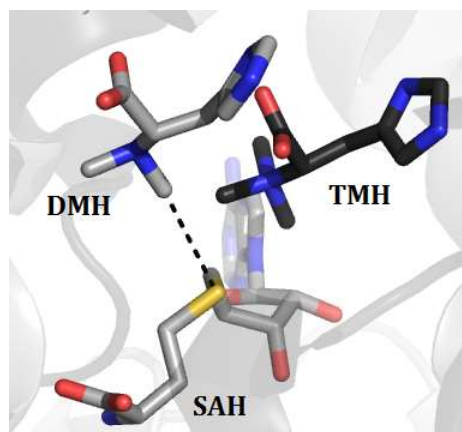


Figure 54 Superimposition of EgtD co crystallized with SAH and DMH (light grey) and with TMH (dark grey). The methylated amino group of DMH should rotate to enable the binding of SAM and the last methyl transfer step to occur.

It is worth mentioning that the kinetic parameters of histidine, MMH and DMH are underestimated. Indeed, they were determined in the presence of 0.5 mM SAM, which is lower than $K_{M, SAM}$. This means that in the reaction assay the mutant could not be saturated with SAM. Nevertheless, we observed a significant difference for the turnover numbers of EgtD N166D when histidine, MMH or DMH are the substrates for the reaction. The k_{cat} value of histidine decreases by 135-fold, in contrast to only 2.5-fold for DMH. This observation for DMH clearly shows that Asn166 is not involved in the transition state stabilization. Moreover, the charge distribution in the N166D mutant compared to the WT could lead to misalignment of methyl acceptor with donor. Therefore, the reduced k_{cat} in the case of histidine compared to DMH could be accounted for a greater conformational flexibility of the ternary complex, due to less steric

bulk. In addition, the turnover number of EgtD N166D for MMH methylation sits between the values determined for histidine and DMH. The monomethylated substrate presents more steric bulk than histidine but less than DMH. This observation supports the hypothesis of conformational flexibility of the substrate in EgtD N166D.

4.6 Conclusions and future directions

In the DNA-(adenine- N^6)-MT, coulomb attraction has been implicated as a factor in aiding substrate orientation to drive the nucleophilic attack. Weak bases such as asparagine or a solvent water molecule were demonstrated to be strong enough to deprotonate the substrate upon the approach of the sulfonium group of SAM.¹⁹⁶

In EgtD, we proposed that the increase in the acidity of the $N\alpha$ proton of histidine, induced by the positioning of substrate in the catalytic site by Asn166 would drive the methyl transfer. Asn166 is conserved in all EgtD type amino acid betaine synthases and was identified as a determinant for the formation of the Michaelis complex. However, more complex studies are required to fully assess the role of residue for the catalysis, such as the determination of the pH-activity profile of EgtD N166D (for this experiment, we must also emphasize that the possible increase in activity at lower pH values for EgtD N166D could be counteracted by a decrease in activity which was observed for EgtD WT). If a shift in the optimum pH value would be observed for the mutant compared to the wild type, this would indicate that our proposed mechanism displayed in Figure 47 is correct.

4.7 Experimental

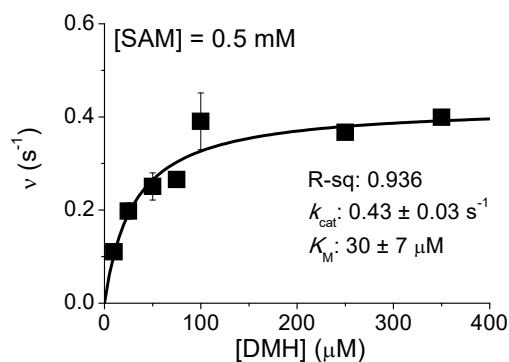
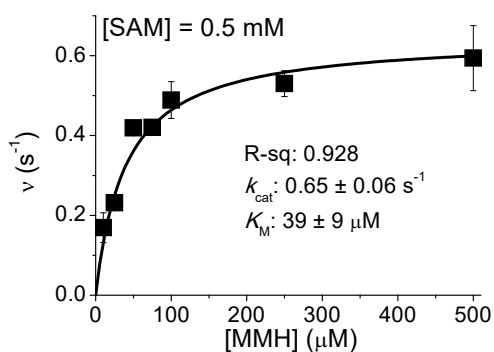
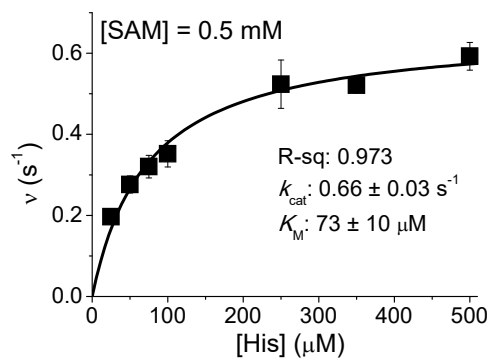
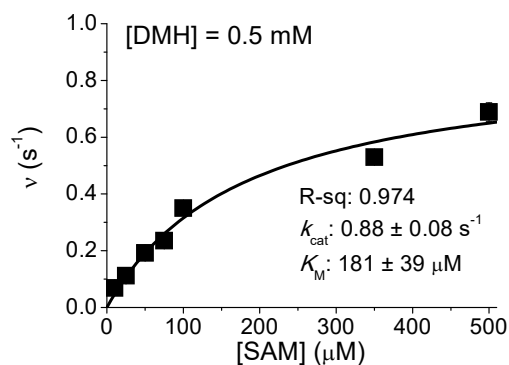
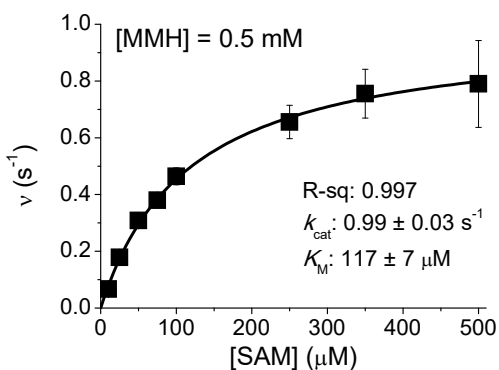
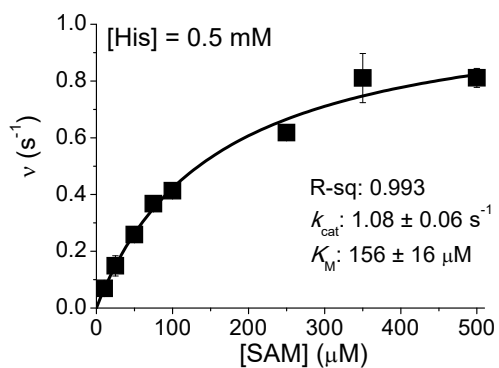
Standard conditions for all the reactions (except the pH-dependency experiments): 25°C, 50 mM Tris/HCl pH 8.0, 50 mM NaCl, 200 μ M Mn^{II} , 10 μ M SAH nucleosidase, 5 μ M adenine deaminase and 2 μ M to 25 μ M methyltransferase (either EgtD WT or N166D). The concentrations of the substrates are indicated on the graphs. For the comparison of the MTs activities at different pH values, Britton-Robinson buffer was used instead of Tris/HCl pH 8.0. The pH values were then adjusted with 10 M NaOH.

HPLC assay. Reactions were started by addition of the methyltransferase and incubated at 25°C. 20 μ L aliquots of the reactions were quenched by addition of 10 μ L 1 % TFA and analyzed by ion-exchange HPLC (20 mM phosphoric acid pH 2 as the mobile phase) on a Luna 5u SCX column

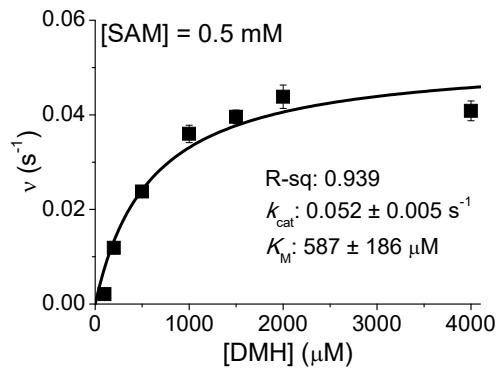
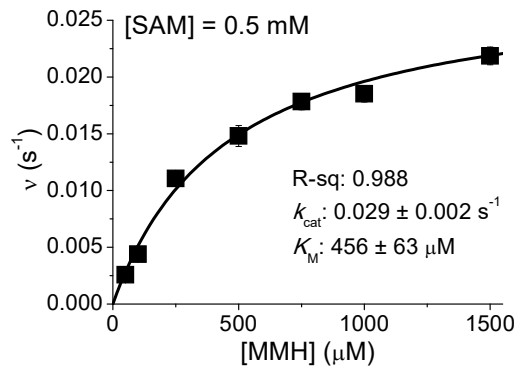
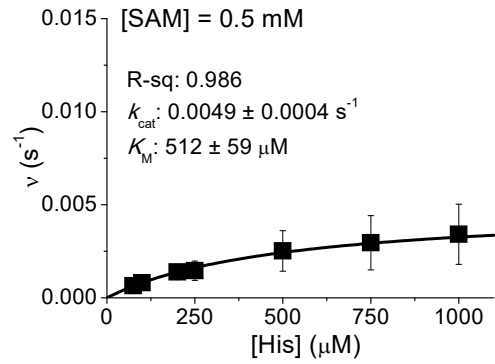
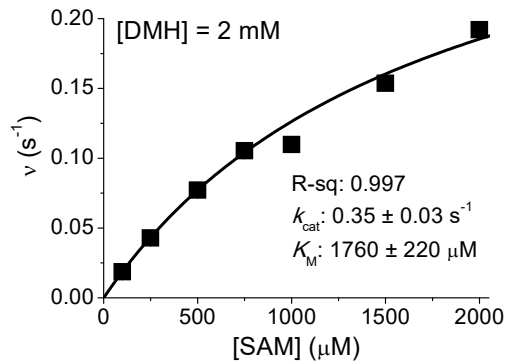
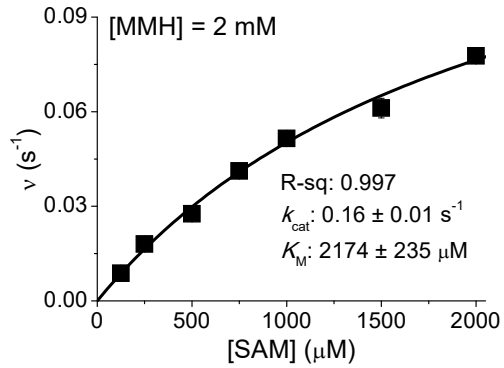
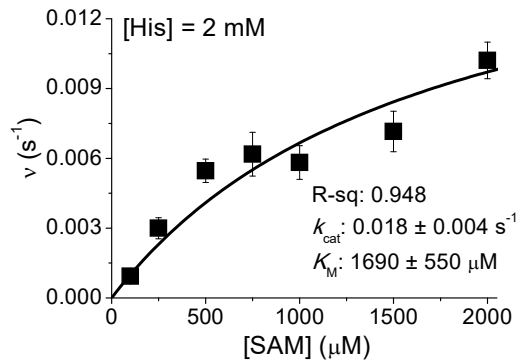
(100 Å, 150 x 4 mm, Phenomenex). The compounds were eluted in an NaCl gradient All HPLC chromatograms were recorded at 220 nm.

Michaelis Menten plots. The reaction rates obtained for EgtD WT and EgtD N166D were fitted to the function $v = k_{cat} \cdot [\text{substrate}] / (K_M + [\text{substrate}])$. The corresponding substrates are indicated in abscissa of each graph.

➤ EgtD WT



➤ EgtD N166D



5 Oxidative regulation of EgtD

5.1 EgtD in an oxidative environment: A way to regulate ergothioneine biosynthesis?

In the structure of EgtD co-crystallized with DMH and SAH (PDB: 4PIO), we observed that Cys285 is present in an oxidized form, as a sulfinic acid (Figure 55). Due to this oxidation two arginine residues (Arg172 and Arg249) are now able to interact with the additional oxygen atoms of Cys285. The resulting sulfinic acid moiety forms two hydrogen bonds (one direct, one water-mediated) with Arg172. Arg249 residue rotates and adopts an alternative conformation to form a new hydrogen bond with the second oxygen atom of the oxidized Cys285.

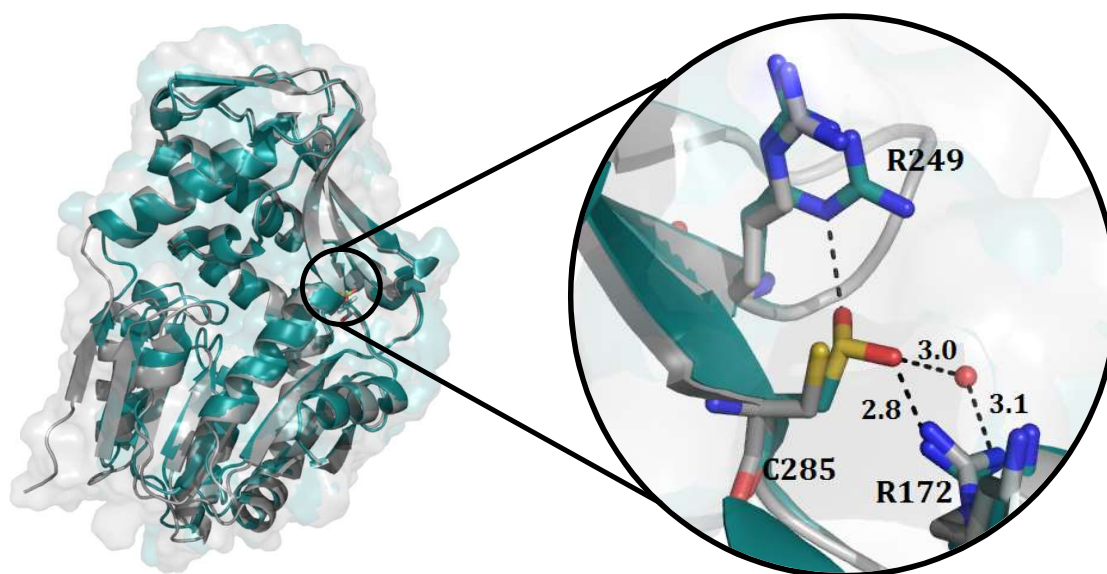


Figure 55 Superimposition of EgtD_{red} (PDB: 4PIN, light grey) and EgtD_{ox} (PDB: 4PIO, deep teal). The oxidative modification of Cys285 leads to the formation of new hydrogen bonds (black dashes) with two arginine residues. The red sphere on the right represents a water molecule. Distances are given in Å.

Aside from this oxidation and formation of three new hydrogen bonds, the oxidized and reduced structures are superimposable, with the oxidation of Cys285 not changing the overall conformation of EgtD.

Given the suggested involvement of ergothioneine as an antioxidant in mycobacteria (see Chapters 2 and 3),^{8,82} the observed modification raises the possibility of oxidation as a regulator of the first step in ergothioneine biosynthesis. We were therefore interested in determining the activity of EgtD in an oxidative environment to evaluate if the production of hercynine can be either up- or down-regulated in the presence of reactive oxygen species (ROS). This could thus consequently influence the biosynthetic pathway of ergothioneine.

5.2 EgtD wild type activity in the presence of oxidants

5.2.1 Suggested mechanisms of regulation

As mentioned in Chapter 3, ergothioneine biosynthesis is likely to be regulated in accordance with a cellular need for redox homeostasis. Recently, a redox sensor protein was demonstrated to modulate the production of ergothioneine in *M. tuberculosis* in response to the catabolism of various carbon sources (mainly fatty acids) in the bacteria.⁸² However, as mycobacterial Δ *egtD* strains of *tuberculosis* and *smegmatis* do not synthesize ergothioneine in contrast to their wild types,^{123,133,140} the regulation of the whole pathway might be dependent on the activity of EgtD.

Several mechanisms are currently proposed to control the ergothioneine biosynthetic pathway through modifications to EgtD. The activity of MT in *M. tuberculosis* is proposed to be regulated via the phosphorylation of Thr163.¹⁴⁰ In EgtD from *M. smegmatis*, this conserved residue is important for substrate recognition as it interacts with the imidazole side chain of histidine through a water-mediated hydrogen bond (see Chapter 2, Figure 18). However, in *smegmatis*, the positioning of this residue in the active site (Figure 56) suggests that Thr163 is not accessible for a kinase. Taking this structural insight into account, this post-translational modification is thus unlikely to occur in *smegmatis*.

We demonstrated that EgtD is inhibited by its product hercynine with an inhibitory constant of 39 μ M. We explored the hypothesis that product inhibition in EgtD may regulate the whole biosynthetic pathway of ergothioneine (see Chapter 3).

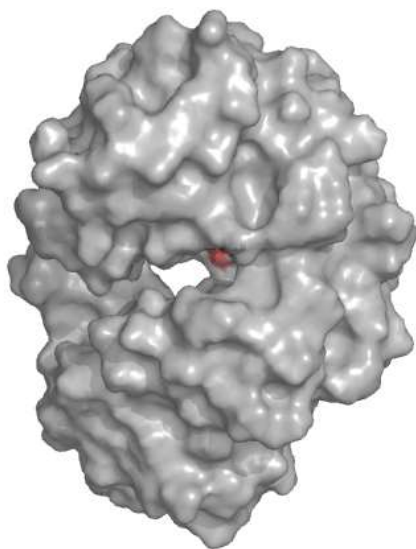


Figure 56 Surface representation of EgtD in its apo form (PDB: 4PIM). Thr163 (red) is buried within the catalytic site of the MT, between the upper and lower domains, hindering kinase access.

In this Chapter, we proposed an alternative mechanism for the regulation of EgtD. In the crystal structure of EgtD in complex with SAM and DMH (Figure 55), the observed oxidized Cys285 suggests that EgtD could also be subject to oxidative (up- or down-) regulation. Therefore, we investigated whether this oxidative modification on Cys285 modulates EgtD activity.

5.2.2 EgtD activity in presence of the physiological oxidant hydrogen peroxide

Hydrogen peroxide (H_2O_2) is the most abundant ROS *in vivo*. In aerobic organisms, it is continuously produced intracellularly (as a byproduct of aerobic metabolism)¹⁹⁸ and extracellularly (as a result of phagocyte activation).¹⁹⁹ H_2O_2 also plays a role in redox signaling and can modulate gene expression through the modification of cysteine residues on transcription factors.²⁰⁰ The activation of these sulfhydryl sensors takes place via the nucleophilic attack of the thiolate on H_2O_2 . Considering this reactivity of H_2O_2 with thiol groups and the observed sulfinic-Cys285 in the crystal structure, we probed the potential oxidant effect of H_2O_2 on EgtD.

In order to determine the effect of H_2O_2 on EgtD, the MT was incubated on ice, for one hour with different concentrations of H_2O_2 (0, 1 or 10 mM). The activity of the H_2O_2 -incubated EgtD was

then measured (Figure 57). To ensure that H_2O_2 does not interfere with the coupled enzymes, $1 \mu\text{M}$ catalase was added in the reaction mixture.

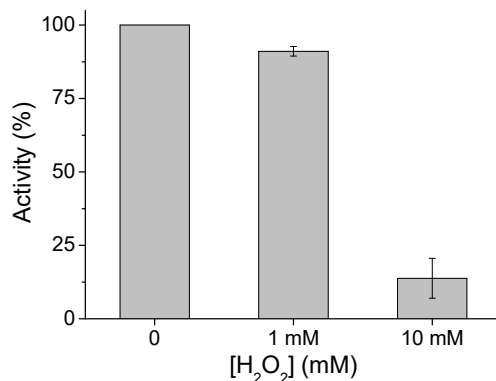


Figure 57 Relative activity of EgtD in presence of H_2O_2 . $100 \mu\text{M}$ of EgtD was incubated with 0, 1 or 10 mM H_2O_2 for 1 hour on ice and the activity of the MT was then determined by spectrophotometric continuous coupled assay in presence of $1 \mu\text{M}$ catalase. Reaction conditions: $25 \text{ }^\circ\text{C}$, 50 mM Tris/HCl pH 8.0, 50 mM NaCl, $200 \mu\text{M}$ Mn^{II} , $5 \mu\text{M}$ adenine deaminase, $10 \mu\text{M}$ SAH nucleosidase, $500 \mu\text{M}$ SAM, $500 \mu\text{M}$ histidine and $2 \mu\text{M}$ pre-treated EgtD.

These kinetic studies showed that the activity of EgtD is not altered by the presence of 1 mM H_2O_2 . This concentration is rather high compared to physiological levels of H_2O_2 measured in different organisms (usually a concentration above $50 \mu\text{M}$ is considered as cytotoxic in a wide range of animal, plant and bacterial cells in culture).²⁰¹ Therefore, we concluded that under physiological conditions, H_2O_2 is not an effector of EgtD. However, the observation that EgtD slowly inactivates over a period of 48 hours in absence of any added oxidant (Figure 58) promotes further investigation into an oxidation-based regulation mechanism.

During protein purification (see Appendix), EgtD is dialyzed for approximately 12 to 16 hours against 50 mM Tris/HCl pH 8.0 and 50 mM NaCl at $4 \text{ }^\circ\text{C}$. If the enzyme is kept in the dialysis buffer at $4 \text{ }^\circ\text{C}$ for two more days, it loses its catalytic activity. Interestingly, this inactivation could be partially reversed upon the addition of a reducing agent such as DTT (Figure 58). This result suggests thus a reversible oxidative modification of EgtD.

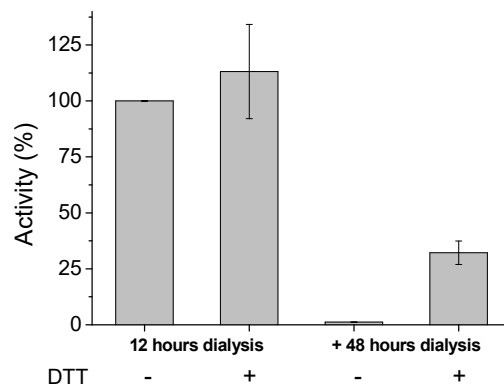


Figure 58 Relative activity of EgtD WT after 12 or 60 hours of dialysis against 50 mM Tris/HCl pH 8.0 and 50 mM NaCl at 4 °C. The activity of the MT was then determined by spectrophotometric continuous coupled assay. Reaction conditions: 25 °C, 50 mM Tris/HCl pH 8.0, 50 mM NaCl, 200 μ M Mn^{II}, 5 μ M adenine deaminase, 10 μ M SAH nucleosidase, 500 μ M SAM, 500 μ M histidine, 2 μ M EgtD WT and 0 (-) or 2 (+) mM DTT.

In order to identify the nature of this modification, we chose to test the activity of EgtD in presence of a stronger oxidant: HOCl, which we expected to oxidize faster the enzyme than H₂O₂.

5.2.3 EgtD activity in presence of HOCl

HOCl is a powerful antimicrobial agent in the immune system it is however present at much lower concentrations than H₂O₂ (the concentration in zebra fish for example do not exceed 0.5 μ M).²⁰² Nevertheless, the purpose on this experiment was not to determine the effect of HOCl at physiological concentration, but to provide information about the possible EgtD modifications occurring under oxidative conditions.

Prior to determining the effect of HOCl on EgtD activity, we first had to establish that this oxidant would not interfere with the activities of the adenine deaminase and the SAH nucleosidase used in the assay. As the tested concentrations of HOCl did not influence the coupled enzymes, a similar experiment as for H₂O₂ was performed. After a one-hour-long incubation on ice of EgtD in the presence of different concentrations of HOCl, the activity of the MT was measured (Figure 59).

In the presence of one equivalent of HOCl, EgtD loses more than 95 % of its activity. We concluded that HOCl oxidizes EgtD with a 1:1 stoichiometry and that this oxidation leads to the inactivation of the MT.

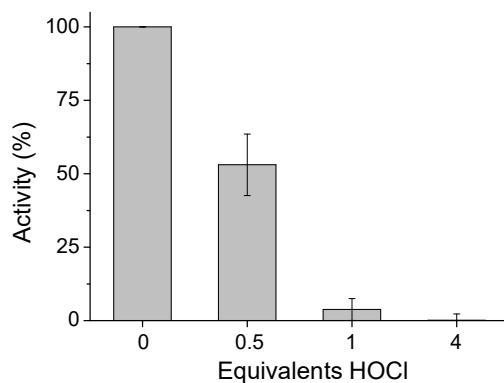


Figure 59 Relative activity of EgtD in presence of HOCl. 50 μ M of EgtD were incubated with 0, 25, 50 or 200 μ M HOCl for 1 hour on ice and the activity was then determined by spectrophotometric continuous coupled assay in the conditions described in Figure 57.

EgtD is recombinantly produced with an N-terminal His-tag which is required for the purification step performed by affinity chromatography (see Appendix). As the presence of a His-tag might influence the activity of the enzyme²⁰³ and to ensure the inactivation is in fact due to a modification on EgtD, the activity of the His-tag free EgtD was also determined. However, the protocol for proteolysis requires a two-day-long dialysis of the MT in presence of a protease at 4 °C. We have previously showed that, under these conditions, EgtD with His-tag undergoes auto-oxidation (Figure 58). Therefore, it was not surprising to observe that after proteolysis, the MT did not show any activity in presence or absence of the oxidant. Yet, the addition of 2 mM DTT could reactivate the enzyme, suggesting, as for the His-tagged EgtD, that this auto-oxidation is indeed a reversible modification (Figure 60). In both the absence and presence of a N-terminal His Tag, EgtD is subjected to auto-oxidation. This reveals that the His-tag does not influence the inactivation process due to the oxidation of EgtD.

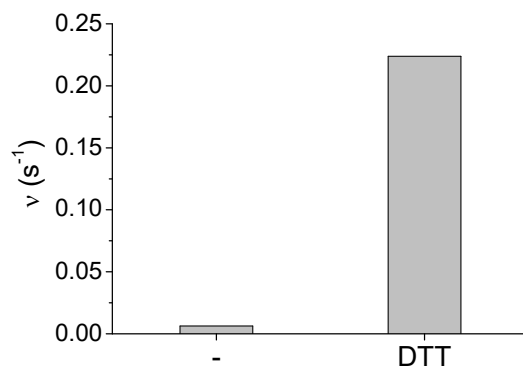


Figure 60 EgtD activity after cleavage of the His-tag by the TEV protease. 50 μ M of His-tag free EgtD were incubated with either no redox active compound (-) or 2 mM DTT for 1 hour on ice and the activity was then determined by spectrophotometric continuous coupled assay under the conditions described in Figure 57.

As we demonstrated that the His-tag is not the cause of the EgtD loss in activity observed in the presence of one equivalent of HOCl, we were interested in determining if the rate of inactivation of EgtD was dependent on the concentration of oxidant. This information would provide a valuable element to understand the mechanism of oxidative inactivation of the MT.

The inactivation rates induced by five different concentrations of HOCl were determined and compared (Figure 61). Thus, we could observe that the rate of HOCl-based inactivation is dependent on the ratio between EgtD and the oxidant. We concluded that the inactivation of the MT seems to be dependent on the concentration of HOCl.

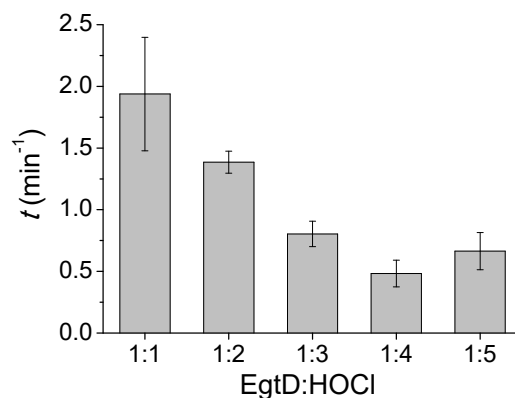


Figure 61 Decay constants of MT activity in presence of five concentrations of HOCl. The rates of inactivation of EgtD were monitored in presence of different concentrations of HOCl (2, 4, 6, 8 and 10 μ M). Reaction conditions: 25 $^{\circ}$ C, 50 mM Tris/HCl pH 8.0, 50 mM NaCl, 200 μ M Mn^{II} , 5 μ M adenine deaminase, 10 μ M SAH nucleosidase, 500 μ M SAM, 500 μ M histidine, the corresponding concentration of HOCl and 2 μ M EgtD WT.

5.2.4 Can EgtB protect EgtD from oxidative damage?

Another experiment aiming at understanding the mechanism of inactivation of EgtD in oxidative environment was to determine if the presence of EgtB (the second enzyme involved in the biosynthesis of ergothioneine) could protect the MT against oxidative damages. EgtB is an oxygen-dependent sulfoxide (see Chapter 1, Figure 11)¹³³ and might then be less sensitive than EgtD to the presence of an oxidant. Moreover, we already discussed in Chapter 3 about EgtD cooperativity and the upstream control of the EgtB substrate. Therefore, we hypothesized that another collaboration mechanism between EgtD and EgtB could be possible.

To test this hypothesis, 50 μM of EgtD were incubated with four different concentrations of HOCl as described in Figure 61, but in presence of 50 μM EgtB. The different rates of histidine methylation were then measured (Figure 62). In the presence of 1 and 4 equivalents of HOCl, EgtD loses 65 and more than 95 % of catalytic activity respectively. The remaining activity in the stoichiometric reaction (1:1) is certainly due to the amount of HOCl that reacts on EgtB instead of EgtD. This interpretation results from the complete inactivation of the MT in the presence of 4 equivalents of HOCl. This experiment shows that EgtB cannot directly protect EgtD from oxidative modification. The presence of the sulfoxide synthase only provides a new site for HOCl to react.

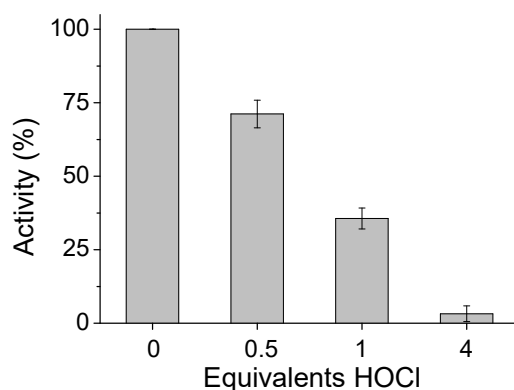


Figure 62 Inactivation of EgtD in presence of EgtB. 50 μM of EgtD and 50 μM of EgtB were incubated with 0, 0.5, 1 and 4 equivalents of HOCl for one hour on ice. The activity was determined by the spectrophotometric coupled assay using the standard conditions described in Figure 57.

5.2.5 Reversibility of the oxidative inactivation

EgtD WT with His tag is inactivated by HOCl, but not by H₂O₂ (only at a high and non-physiological concentration of 10 mM). As we showed that the auto-oxidation of EgtD was a reversible phenomenon (Figures 58 and 60), we were interested to determine if the oxidative induced by HOCl would be reversible as well. This reversibility would indicate that another modification than the oxidation to a sulfinic acid would result from the addition of an oxidant in the solution (conversely to the modification observed on the crystal structure in Figure 55). Indeed, the oxidation of a cysteine residue to its sulfinic acid state cannot be reversed by the sole presence of a reducing agent. The reduction of protein sulfinic acids have already been reported however this reaction is catalyzed by specific enzymes (such as sulfiredoxins).²⁰⁴

EgtD was incubated with four equivalents of HOCl as described in Figure 59. Its inactivation was confirmed by the measurement of the rate of histidine methylation. Following this, 2 mM DTT were added to the solution containing EgtD and HOCl. After five minutes incubation time on ice, the activity of EgtD was tested again (Figure 63). As for the auto-oxidation, the HOCl-induced oxidation is reversible. This strongly supports that the sulfinic acid observed on Cys285 on the crystal structure does not correspond to the modifications occurring upon the addition of HOCl.

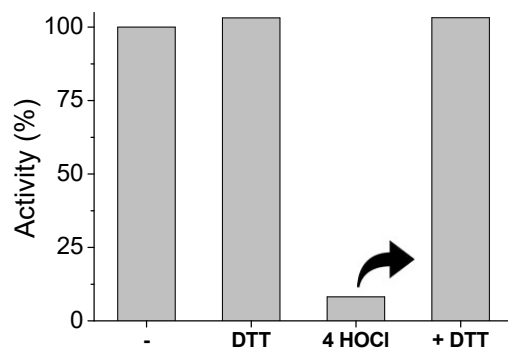


Figure 63 EgtD reactivation after addition of a reducing agent. EgtD was inactivated by incubation with 4 equivalents of HClO as described in Figure 59. Then, the MT could be reactivated by the addition of 2 mM of DTT. The activity was determined by the spectrophotometric coupled assay using the standard conditions described in Figure 57.

EgtD contains two cysteine residues; Cys139 and 285. However as the observations from the crystal structure and the kinetic data were not consistent with respect to the nature of the

oxidative modification, we investigated the oxidative modifications that could occur to each cysteine residue separately. Therefore, we constructed the following variants: C139A, C285A, C285D and C285S, and tested them as for the wild type. These three chosen residues (alanine, aspartate and serine) cannot be oxidized upon the addition of an oxidant but can reveal the functions of Cys139 and Cys285.

5.3 EgtD Cys139 and Cys285

Cysteine is one of the least abundant amino acid incorporated in protein scaffolds. However this residue has essential functions in catalysis and regulation such as redox sensor, catalytic nucleophile, or in the formation of structural disulfide.²⁰⁵ In addition, the oxidation of specific cysteine residues found within redox-sensitive target proteins leads to the regulation of intracellular signaling pathways.^{200,206} The reactive cysteine can be oxidized to a sulfenic form (Cys-SOH) and further to the sulfinic species (Cys-SO₂H). In case of high oxidative stress (excess in peroxide), sulfonic acid (Cys-SO₃H) can be generated.²⁰⁷ We were interested in determining if one of these oxidative modifications could occur on either Cys139 or Cys285 in the presence of HOCl.

Site-directed mutagenesis allows testing the importance of a single residue in an enzyme. If a cysteine residue is engaged in the formation of a disulfide bond in the regulation of its activity, the mutation to an alanine, aspartate or serine residue would drastically alter the enzymatic activity. The mutation to the inert and non-bulky alanine is often used to determine if the cysteine residue contributes in any form, to catalysis. The presence of alanine instead of cysteine suppresses the hydrogen bonding or nucleophilicity of this residue and can therefore lead to inactivation of the enzyme. If Cys285 is engaged in stabilizing hydrogen bonds, the change to a serine would slightly alter EgtD activity. Indeed, cysteine is more hydrophobic and a better nucleophile than serine. However serine can still participate in hydrogen bonding. In our study, the mutation of Cys285 to an aspartate residue aimed to structurally mimic the oxidative modification observed in Figure 55. Therefore, this variant should indicate the consequence of the sulfinic-Cys285 modification on MT activity.

5.3.1 Localization of the two cysteine residues

Under physiological conditions, cysteine is generally considered the most effective nucleophile of all amino acid residues. Subsequently, the thiol side chain can undergo a wide array of oxidative modifications. The formation of intra- and intermolecular disulfide bonds or nitrosothiols, the oxidation to sulfenic/sulfinic/sulfonic acids, are a few of them.²⁰⁸ Theoretically, both cysteine residues in EgtD can be modified by a ROS. The oxidative modification on Cys285 described in Figure 55 maps to the hinge region of the two-lobed structure of EgtD (Figure 64). On the other hand, Cys139 is more surface exposed than Cys285, which suggests that Cys139 could also be available for oxidative modification.

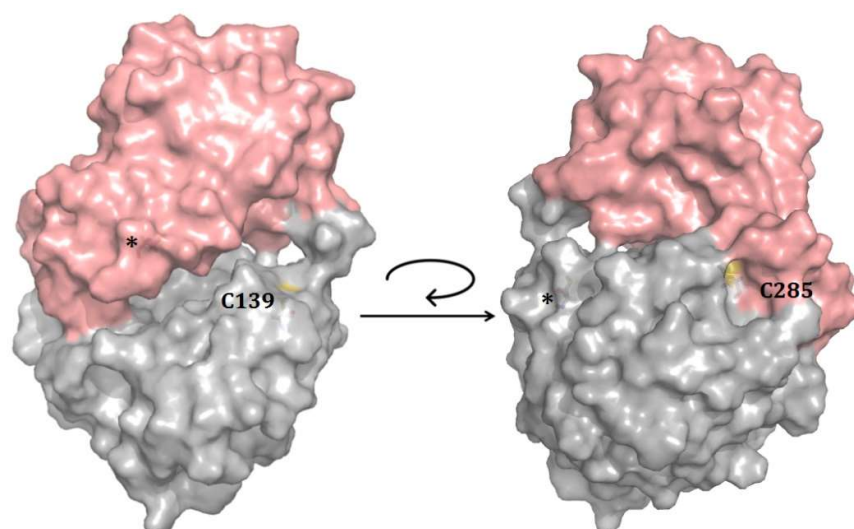


Figure 64 Localization of Cys139 and Cys285 residues (indicated in yellow) in EgtD. The Rossmann-fold and upper domains are represented in grey and salmon respectively. The symbol (*) displays the position of the cysteine residue other than that indicated.

5.3.2 Activity of the variants

5.3.2.1 *Cys285X variants activity is dependent on the presence of a reducing agent*

Prior to the study of the cysteine variants in an oxidative environment, the rate of histidine methylation catalyzed by these mutants was first determined in the presence of 0.5 mM of histidine and SAM to ensure their activity. In the absence of DTT, none of the Cys285 variants showed significant turnover numbers. The addition of 2 mM DTT reactivated these three

mutants which then showed a similar methylation rate than EgtD WT. Only EgtD C139A was active in both in absence or presence of reducing agent (Figure 65). This outcome attests that the auto-oxidation of the Cys285X variants is faster than for the wild type. EgtD C139A shows a similar activity to the wild type in the absence or presence of DTT. This observation indicates that Cys139 is more prone to oxidative modifications than Cys285.

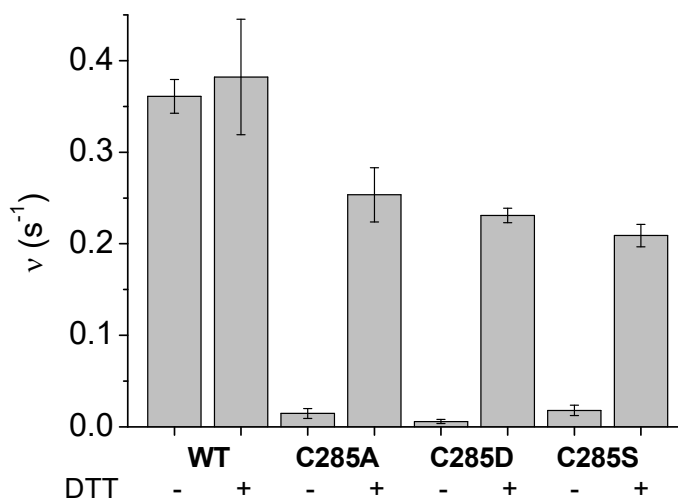


Figure 65 Histidine methyltransferase activity for EgtD WT and 4 variants: C139A and C285A/D/S. Reactions contained 50 mM Tris/HCl pH 8.0, 50 mM NaCl, 200 μ M Mn^{II} , 5 μ M adenine deaminase, 10 μ M SAH nucleosidase, 0.5 mM histidine, 0.5 mM SAM, 2 μ M MT and 0 (-) or 2 mM (+) DTT.

5.3.2.2 Catalytic parameters of the cysteine variants under reducing conditions

The two cysteine residues are not in a close proximity to the substrate binding site. However, to determine if the mutations to an alanine, aspartate or serine residue would affect the MT activity, the catalytic parameters of the four cysteine variants were determined in the presence of 2 mM DTT.

The resulting $k_{cat, His}$ and $K_{M, His}$ values obtained for the EgtD C285A/D/S variants are similar to the WT. (Table 12).*

* Previous measurements showed that the turnover number of EgtD C285D was 10 times lower than the WT (see Section 5.7 Experimental). EgtD C285D is the closest analogue to the cysteine-sulfinic acid observed in the crystal structure in Figure 55. This loss of activity suggested that the sulfinic acid on Cys285 was not a beneficial modification for the activity of EgtD. However, a new batch of EgtD C285D was tested and showed that the mutation of the cysteine 285 to an aspartate residue had similar impact on the MT activity than the alanine or serine mutations.

Table 12 Catalytic parameters of the cysteine variants and EgtD WT^a.

| | k_{cat} (s ⁻¹) | K_M (μM) |
|--------------|------------------------------|------------|
| WT | 0.57 ± 0.03 | 107 ± 12 |
| C139A | 0.30 ± 0.02 | 101 ± 20 |
| C285A | 0.28 ± 0.01 | 114 ± 11 |
| C285D | 0.33 ± 0.02 | 52 ± 12 |
| C285S | 0.32 ± 0.03 | 149 ± 33 |

^aReactions contained 50 mM Tris/HCl pH 8.0, 50 mM NaCl, 200 μM Mn^{II}, 5 μM adenine deaminase, 10 μM SAH nucleosidase, 0.5 mM SAM, 25-750 μM histidine, 2 mM DTT and 2 μM MT.

5.3.2.3 Activity of EgtD C139A in presence of HOCl

Unlike the C285X variants, EgtD C139A does not require the addition of a reducing agent to catalyze methyl transfer (Figure 65). Therefore, among the constructed variants, EgtD C139A was the only mutant which could be tested with HOCl* and compared to the WT. EgtD C139A was incubated on ice with 0, 0.5, 1 and 4 equivalents of HOCl and the catalytic activity was determined as performed with EgtD WT (Figure 66).

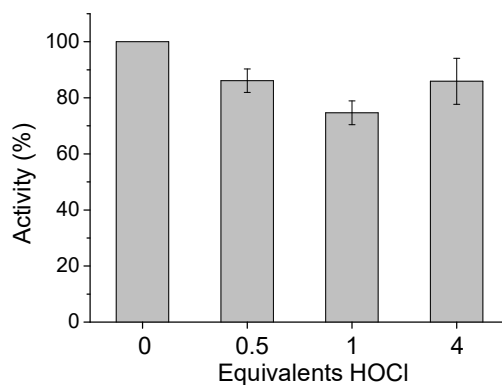


Figure 66 Activity of EgtD C139A in presence of different concentrations of HOCl. 50 μM of the variant were incubated HOCl for 1 hour on ice with 0, 25, 50 or 200 μM of HOCl. The MT activity was then determined by coupled assay using the standard conditions described in Figure 57.

*As for the wild type, the same experiment was performed for the His-tag free C139A variant. The results obtained in both the presence and absence of the His-tag demonstrated that EgtD C139A is not inactivated by HOCl and that the MT activity is not lost during proteolysis.

In the presence of 1 or 4 equivalents of HOCl, EgtD C139A does not lose more than 20 % of its catalytic activity. EgtD C139A appears to be less sensitive to the tested oxidative environment than the WT, which is oxidized and inactivated by HOCl with a 1:1 stoichiometry (Figure 59). This result means that either Cys285 is not modified in presence of HOCl, or that the resulting oxidative modification on this residue does not affect the enzyme activity. In order to determine which of these two hypotheses is correct, the quaternary structures of EgtD wild type and variants were analyzed to detect the possible formation of intermolecular disulfide bonds. Moreover, the molecular weight of the different MTs was measured in order to identify the possible addition of oxygen atoms on the cysteine residues.

5.4 Change in quaternary structure induced by oxidative environment

The quaternary structures of EgtD WT and variants in different redox environments were determined by size-exclusion chromatography. For the WT, both His-tagged and His-tag free enzymes were analyzed, whereas for the Cys285X variants, only the nature of quaternary structures of the His-tagged proteins was studied. In order to correlate the analysis of the molecular weight and the kinetic data of each MT, the activity of the enzymes used to perform the study on the quaternary structure was always measured prior to the analysis by size-exclusion chromatography. For clarity, the traces which correspond to an active enzyme are displayed in black and the ones corresponding to an inactive enzyme are displayed in red.

5.4.1 EgtD wild type

EgtD WT was incubated (A) without any redox active compound, (B) with 2 mM DTT, (C) with 1 mM H₂O₂ and (D) with 1 equivalent of HOCl (Figure 67). After one-hour-long incubation on ice, the four samples were analyzed by size-exclusion chromatography to determine the quaternary structure of EgtD WT in each oxidative environment. The same experiment was performed with the His-tag free enzyme, but only in (A) the absence or (B) the presence of DTT.

The active enzymes for both His-tagged and His tag free EgtD WT are clearly monomers (*, the elution volume is 2.08 mL which corresponds to a species with a molecular weight of 38.2 kDa); whereas inactivated enzyme is present as a mixture of monomer and dimer (**, the elution volume of 1.85 mL corresponds to a molecular weight of 56.8 kDa) according to the established calibration curve (see Experimental part).

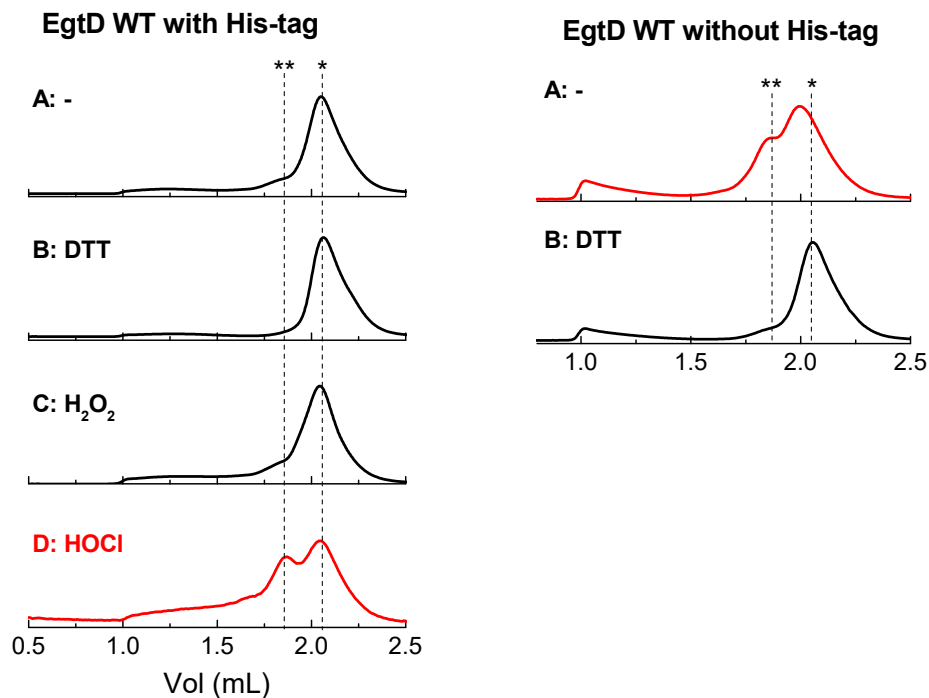


Figure 67 Quaternary structures of EgtD with (**left**) and without (**right**) His-tag in different oxidative environments, A: without any redox compound, B: in presence of 2 mM DTT; C: in presence of 1 mM H₂O₂ and D: in presence of 1 equivalent of HOCl. The black and red traces represent the active and inactivated MT respectively. The symbols (*) and (**) correspond to the monomer and dimer of the MT.

Given that the dimerization is not total but that EgtD is almost completely inactivated after the incubation with 1 equivalent of HOCl (Figure 59), we concluded that dimerization is not the sole cause of the inactivation. The inactivation of EgtD WT rather arises from the oxidation of one or both cysteine residues. Taking into consideration the kinetic results of EgtD C139A and EgtD C285X (Figure 65), we suggested that it is the oxidation of Cys139 which leads to the loss of the MT activity.

5.4.2 EgtD cysteine variants

In order to determine which cysteine residue leads to the observed change in quaternary structure of the WT in oxidizing environment, the same analysis as for the WT was performed for each of the cysteine mutants.

5.4.2.1 *Cys139Ala* variant

As for the WT, EgtD C139A was incubated for one hour on ice (A) without any redox active compound, (B) with 2 mM DTT, (C) with 1 mM H₂O₂ and (D) with 1 equivalent of HOCl. The four samples were then analyzed by size-exclusion chromatography.

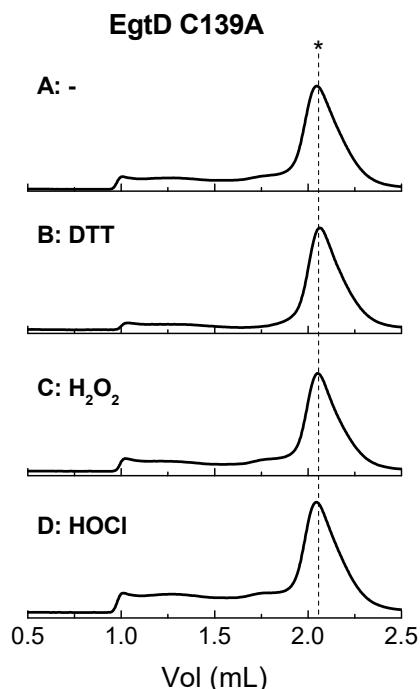


Figure 68 Quaternary structures of EgtD C139A with His-tag in different oxidative environments, A: in the absence of any redox compound, B: in presence of 2 mM DTT; C: in presence of 1 mM H₂O₂ and D: in presence of one equivalent HOCl. In contrast with the WT, EgtD C139A stays as a monomer (*) in the tested conditions (the retention volume of 2.06 mL corresponds to a molecular weight of 39.5 kDa).

The resulting quaternary structures in Figure 68 clearly show that EgtD C139A is present in its monomeric form (*) in oxidative environment, in presence of either 1 equivalent HOCl or 1 mM H₂O₂. This analysis corroborates the results obtained for EgtD WT, which indicated that the active form of the MT is a monomer. The absence of dimerization demonstrates that Cys285 is not engaged in an intermolecular disulfide bond. In addition, on the crystal structure, we observed that Cys285 is oxidized in sulfinic acid. However, the kinetic data indicate that, even if this oxidation occurs, it does not have an impact on the MT activity. In order to determine if in oxidative environment Cys285 is not oxidized at all or if the modification to a sulfinic acid is

present without altering the catalytic activity, the determination of the exact molecular weight of the protein is required (see Section 5.5).

5.4.2.2 Cys285X variants

If Cys285 is mutated to a non-oxidisable residue, the oxidative stress has a negative impact on the MT activity. In order to test if the C285X variants are more prone to oxidative damage and to the formation of disulfide bonds, the quaternary structures of the active and inactive MT were analyzed. EgtD C285A/D/S were incubated for one hour on ice (A) without any redox active compound and (B) with 2 mM DTT (Figure 69).

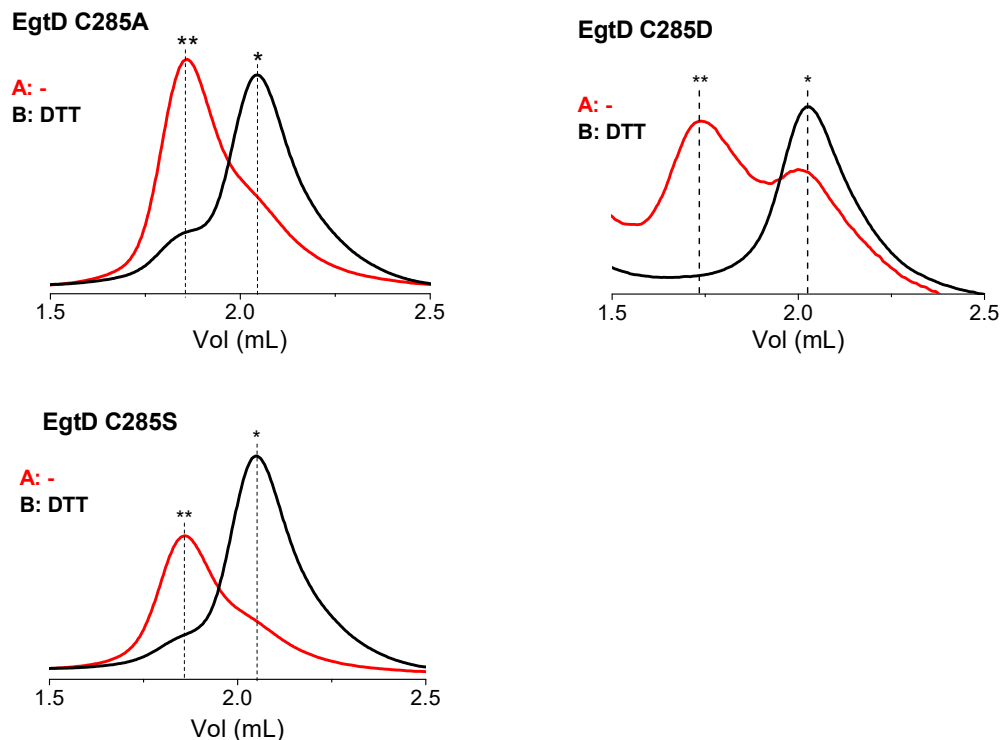


Figure 69 FPLC traces of the three Cys285X variants of EgtD in absence or presence of reducing agent, A: without any redox compound and B: in the presence of 2 mM DTT. 50 μ M of each mutant were incubated on ice with either (A) 0 or (B) 2 mM DTT. The red color indicates an inactive enzyme. The symbols (*) and (**) correspond respectively to the monomer (2.06 mL) and dimer (1.85 mL) of the MTs.

The auto-oxidation/inactivation of the variants is, as for EgtD WT, accompanied with a change in the quaternary structure. The inactive form of the C285A/D/S variants is clearly a dimer (**).

The active form of the Cys285X variants in the presence of DTT is also a monomer (*), like for the WT.

Taking together the results from the four EgtD variants C139A and C285A/D/S, we got strong indication that the oxidative modifications leading to the dimerization of EgtD take place on the Cys139 residue.

5.5 Chemical modifications induced by oxidative environment

5.5.1 EgtD wild type

The crystal structure of EgtD_{ox} indicates the presence of a sulfinic acid moiety on Cys285. As the oxidation to a sulfinic acid is known to be irreversible upon the addition of a reducing agent,²⁰⁴ this oxidative modification is detectable by mass spectrometry with the addition of 32 Da. Moreover, if DTT is added to the oxidized enzyme, this additional mass should remain.

The MS of EgtD WT (with and without) His-tag were recorded in different oxidative environments. EgtD WT was incubated for one hour on ice (A) without any redox active compound, (B) with 2 mM DTT and (C) with 1 equivalent of HOCl (Figure 70).

The inactive form of EgtD WT (red traces) is accompanied with an increase in mass of 32 Da. The addition of 2 mM DTT to the inactivated EgtD (Figure 70 D) leads to the elimination of the signals at M+32 and M+64 Da. Therefore, we concluded that the formation of a sulfinic acid does not occur following the incubation of HOCl.

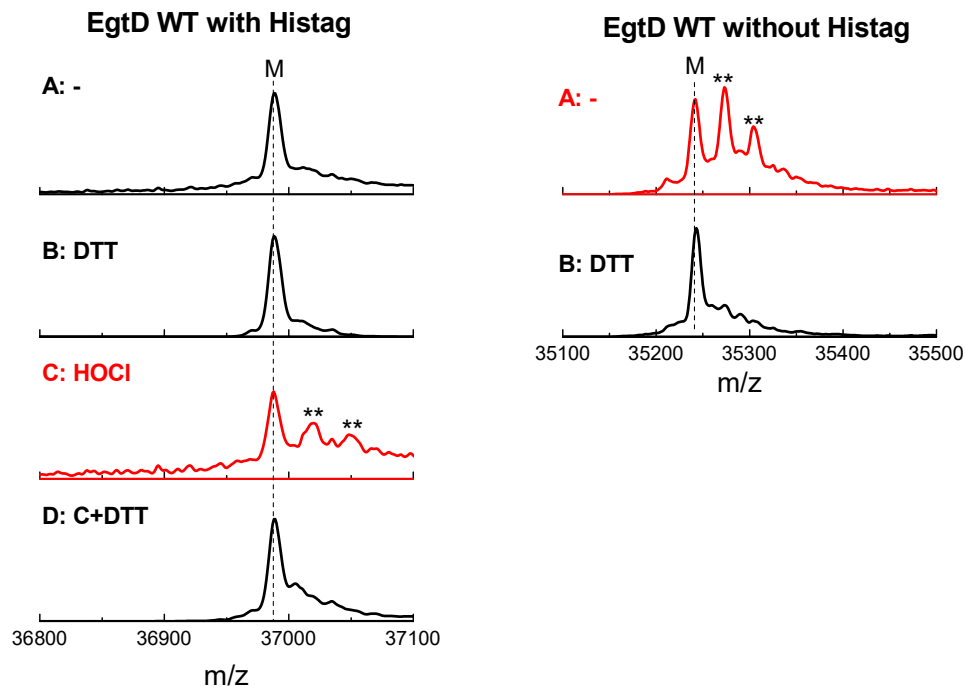


Figure 70 Mass spectra of EgtD WT with (left) and without (right) His-tag. The respective molecular weights of each of the MTs were measured after incubation A: without any reducing or oxidative agent, B: with 2 mM DTT, C: with one equivalent of HOCl and D: C after addition of 2 mM DTT. M represents to the respective molecular weights of EgtD WT with and without Histag (36 989.6 and 35243.7 Da). The symbol (**) corresponds to an addition of 32 Da with respect to the previous peak.

5.5.2 EgtD cysteine variants

The recorded MS for EgtD indicate the additions of 32 and 64 Da to the molecular weight of the MT. From the kinetic data and the analysis of the crystal structure of the cysteine variants, we suspected that these additions would only occur for the C285X variants. To test our assumption, we analyzed the molecular weights of the C139A and C285X variants in their active and inactive form.

5.5.2.1 EgtD C139A

The MS of EgtD C139A were recorded in different redox environments as performed for the WT. EgtD C139A was incubated one hour on ice (A) without any redox active compound, (B) with 2 mM DTT and (C) with 1 equivalent of HOCl (Figure 71).

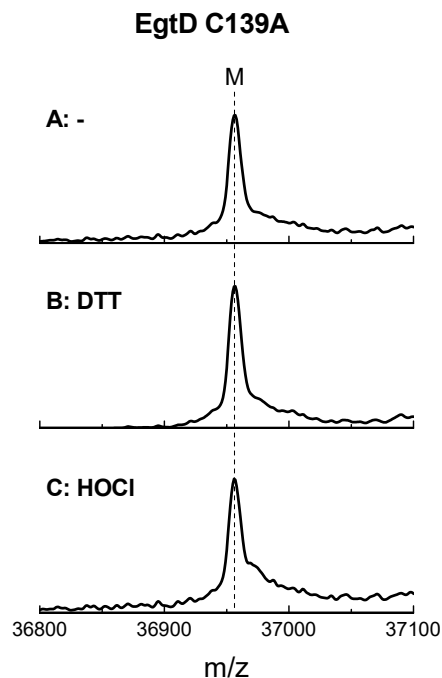


Figure 71 Mass spectra of EgtD C139A. The respective molecular weights of each of the MT were measured after incubation A: without any reducing or oxidative agent, B: with 2 mM DTT and C: with one equivalent of HOCl. M represents to the molecular weight of EgtD C139A (36957.6 Da).

No additional mass was measured on Cys139A variant in the presence of HOCl. Therefore, the oxidative modification on Cys285 observed in Figure 56 does not occur in the tested conditions.

5.5.2.2 *EgtD C285X*

The molecular weights of EgtD C285A/D/S were measured in (A) the presence and (B) the absence of DTT (Figure 72). If the reducing agent is present, only the mass of the monomer (M) is observed, whereas in the absence of DTT, both monomer and dimer (2M) are present. These results are consistent with the quaternary structures determined by size-exclusion chromatography (Figure 72). The dimers of the C285X variants are also found with the addition of 32 and 64 Da. However, the nature of these oxidative modifications could not be identified.

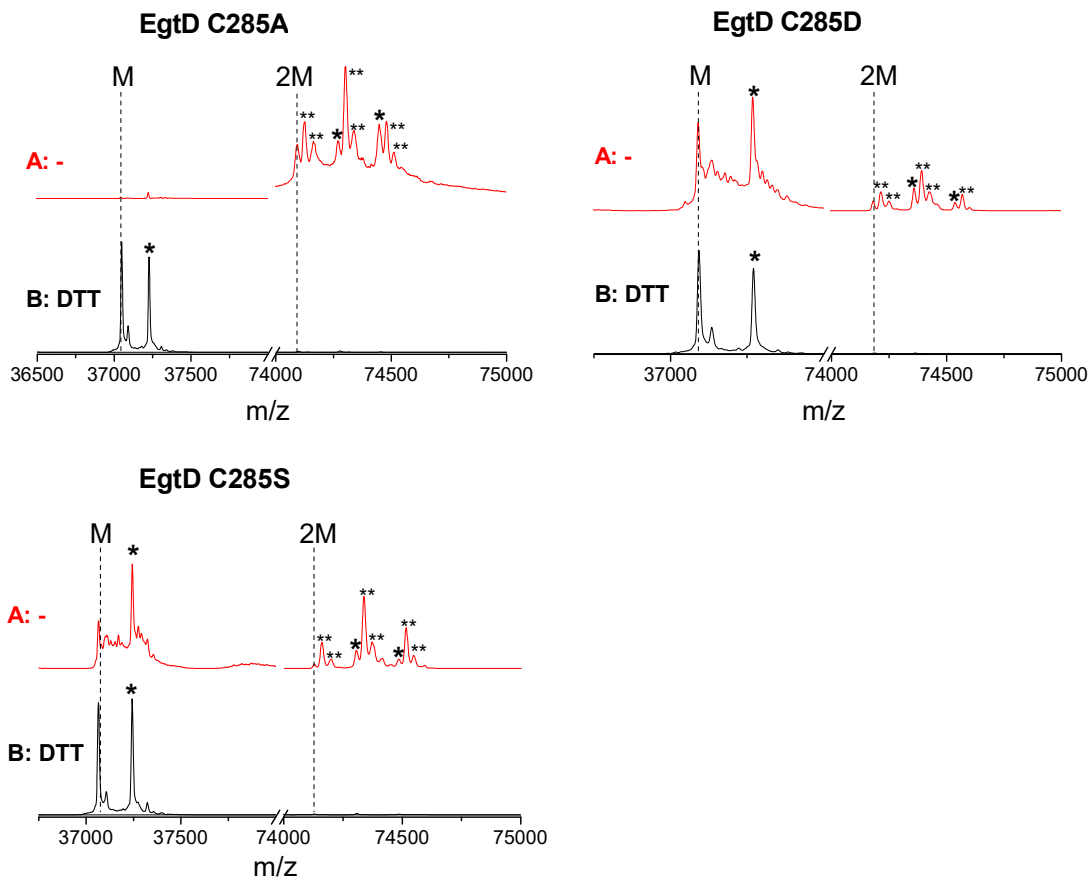


Figure 72 MS spectra of the three EgtD Cys285 variants in presence (B) or absence (A) of 2 mM DTT. The red and black traces indicate the inactive and active enzymes respectively. M corresponds to the molecular weight of each variant (see Appendix). The symbol (*) indicates a glycosylated protein*. The symbol (**) corresponds to an addition of 32 Da with respect to the previous peak

The changes in molecular weight of EgtD WT and the cysteine variants are summarized in the following table. In the absence of an oxidant, the molecular weight of the monomer EgtD is detected. In the presence of one equivalent of HOCl two additional peaks are observed, each with an increase in mass of 32 Da. This could be either the addition of two sulfur atoms or four oxygen atoms. But in each case, the modification would have to be reversible as the enzyme is reduced in presence of DTT.

* The glycosylation of His-tagged protein is a common modification in *E.coli*²⁰⁹ and does not influence the activity of EgtD. The addition of a glucose unit which corresponds to an addition of 178 Da is observed for EgtD WT and C139A, but is not shown in Figures 71 and 72. The cleavage of the His-tag for EgtD wild type suppressed the peak at M+178 Da.

Table 13 Molecular weights of the different MTs without any redox agent (\emptyset), in the presence of 1 equivalents of HOCl and in the presence of 2 mM DTT. M: corresponding molecular weight of each MT (see Appendix). For clarity, the glycosylated proteins are not indicated.

| | \emptyset | HOCl | DTT |
|--------------|-------------|---------|-----|
| WT | M | M+32+32 | M |
| C139A | M | M | M |
| C285A | 2M+32+32 | - | M |
| C285D | M, 2M+32+32 | - | M |
| C285S | M, 2M+32+32 | - | M |

The presence of the dimeric EgtD or the addition of 32 Da (which either correspond to a sulfur atom or two oxygens atoms, but no sulfinic acid) and 64 Da are features of the inactive form of the MT.

5.6 Conclusions and discussion

The active form of EgtD is a monomer. EgtD undergoes auto-inactivation through a slow oxidation by oxygen present in the buffer; however the catalytic activity is not altered by 1 mM H₂O₂. The study of EgtD inactivation was performed under non-physiological concentrations of HOCl. In this respect, we could only conclude that the presence of a strong oxidant might reduce the activity of the MT, but EgtD is certainly not up-regulated in an oxidative environment. The loss of MT activity in the presence of one equivalent of HOCl can be fully recovered upon the addition of DTT. Therefore, different oxidative modifications rather than the irreversible formation of a sulfinic- or sulfonic-cysteine occur. The mass spectra show modifications, through the change in the molecular weight of EgtD when both Cys139 and Cys285 are present and no change when only Cys285 is conserved. The structural analysis shows that Cys285 is oxidized as a sulfinic acid. However, kinetic data and analyses of the quaternary structures suggest instead that the modification on Cys139 affects the activity of EgtD. In addition, as we could not observe the oxidized Cys285 in the presence of 200 μ M HOCl, it seems that the formation of the sulfinic-Cys285 is unlikely to take place due to the only presence of an oxidant.

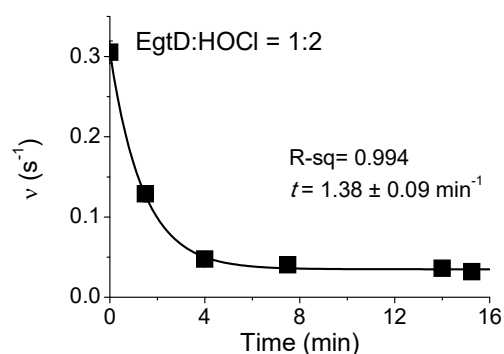
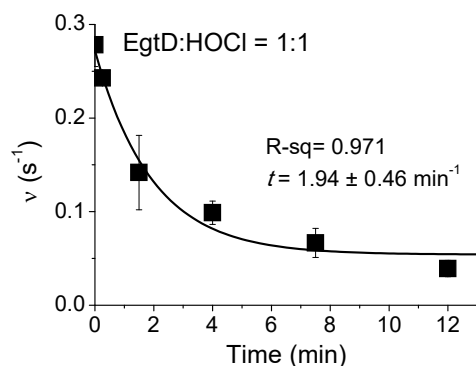
Cys285 does not participate in catalysis (EgtD C285A/D/S have similar turnover numbers than the WT), but it seems that the mutation on Cys285 renders Cys139 more prone to oxidative modification. So far, we did not identify the nature of the additional 32 Da observed by MS. However, analysis of tryptic digested fragments of EgtD might answer this question. EgtD C285D is the closest analogue to the sulfinic-Cys285 observed in the crystal structure. We first observed that this point mutation lowers the MT activity by a factor of 10 (see Experimental section 5.7.1). Taking into account the location of this residue, residing in the hinge of the two domains of EgtD, we suggested that this mutation could also interfere with the binding of SAM and subsequently lead the significant decrease in catalytic activity of the C285D variant. Jeong *et al.* described the inactive “open” conformation of the apo-EgtD and the active “closed” conformation of the MT in the ternary complex [EgtD:His:SAH]¹⁶⁵. Therefore, we proposed that the presence of two additional oxygen atoms in the hinge of the two domains of EgtD could prevent the formation of the closed, namely active, conformation of the MT. Thus, SAM would not be as tightly bound in the catalytic site and the enzyme would then be less active. However, a new batch of EgtD C285D was tested and showed similar activity as EgtD C285A/S variants. Therefore the hypothesis of the inactive open conformation of EgtD due to the point mutation Cys285Asp appeared unlikely.

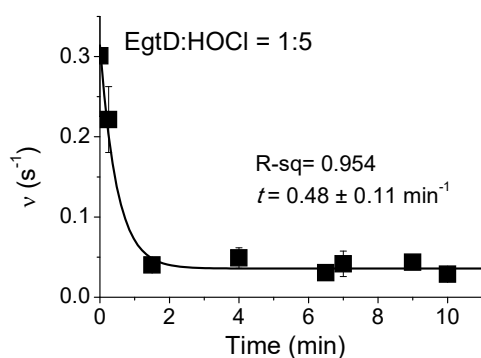
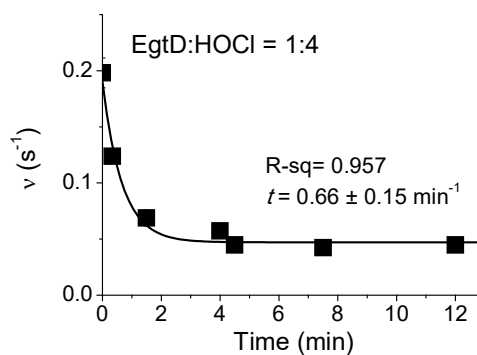
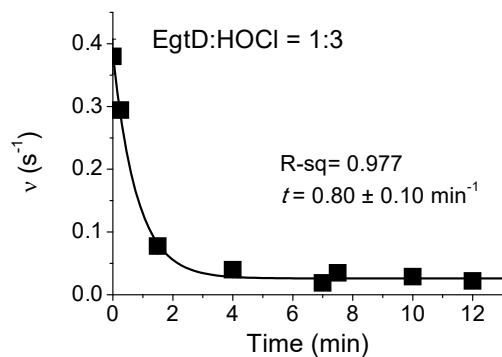
5.7 Experimental

5.7.1 Kinetics

5.7.1.1 Inactivation of EgtD WT

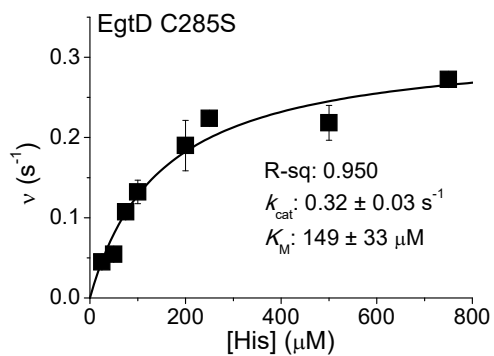
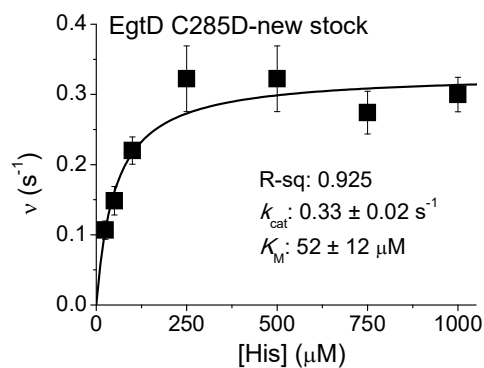
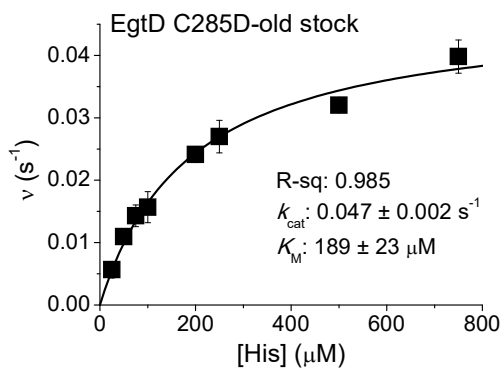
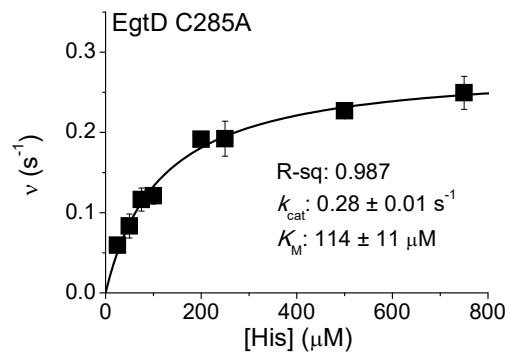
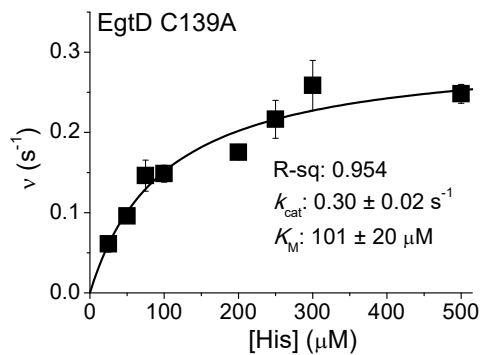
Reactions contained 50 mM Tris/HCl pH 8.0, 50 mM NaCl, 200 μ M Mn^{II}, 5 μ M adenine deaminase, 10 μ M SAH nucleosidase, 0.5 mM SAM, 0.5 mM histidine, 2 mM DTT and 2 μ M EgtD WT.





5.7.1.2 Activity of EgtD variants

Methyltransferase assay. Methyltransferase activity was determined following published protocols.¹⁴⁷ Reactions were monitored in a 2 mm quartz cuvette at 25°C at 265 nm with a Cary 300 spectrophotometer from Agilent. The 200 μL reactions contained 50 mM Tris/HCl pH 8.0, 50 mM NaCl, 200 μM Mn^{II} , 500 μM SAM, 1-1000 μM histidine, 5 μM adenine deaminase, 10 μM SAH nucleosidase, 2 mM DTT and 2 μM methyltransferase. Reactions were started by addition of the methyltransferase. The MT is indicated on each graph. The data were fitted to the function: $v = k_{\text{cat}} \cdot [\text{substrate}] / (K_{\text{M}} + [\text{substrate}])$.



5.7.2 Histag cleavage

TEV protease recognizes the cleavage site: E-N-L-Y-F-Q/-G. The sequence of EgtD in pET19 vector was modified in order to contain this cleavage sequence right after the His-tag at the N-terminal of EgtD.

EgtD was incubated with TEV protease in a dialysis bag in a EgtD:TEV ratio of 14:1. The reaction was dialyzed overnight in 50 mM Tris, 50 mM NaCl at 4 °C. The dialysis buffer was renewed for additional 24 hours (in total, 48 hours are required for the complete cleavage of the His-tag).

The mixture was then applied to Ni-beads and the flow through was collected. To approximate the concentration of the eluted Histag free protein, the measurements of the absorption at 280 nm were performed with a Nanodrop2000 and the molar absorption coefficient $\epsilon_{280}(\text{EgtD}) = 36440 \text{ M}^{-1} \text{ cm}^{-1}$ was used.

→ Sequence of His-tag free EgtD:

*GHHHHHHAENLYFQ*GHMALSLANYLAADSAAEALRRDVRAGLTATQKSLPPKWFYDAVGSDFDQITRLPEYYPT
 RTEAQILRTRSAEIIISAAGADTLVELGSGTSEKTRMLLDAMRDAELLRRFIPFDVDAGVLRSAAGAAIGAEYPGIE
 IDAVCGDFEEHLGKI PHVGRRLVVFLGSTIGNLTPAPRAEFLSTLADTLQPGDSELLGLTDLVKDTGRLVRAAYDDA
 AGVTAAFNRNVLAVVNRELSADFDLDAFEHVAKWNSDEERIEMLRARTAQHVVAALDLEVDFAAGEEMLTEVS
 CKFRPENVVVAELAEAGLRQTHWWTDPAGDFGLSLAVR

m/z (EgtD Histag free): calc.: 35243.7 Da, measured: 35242.5 Da

The sequence in italic and light grey is cleaved by the protease.

5.7.3 FPLC analysis

Quaternary structures were analyzed by FPLC (Åkta FPLC, GE Healthcare) using a Superdex 200 5/150 GL column. 0.1 mg of protein were injected and eluted in an isocratic flow of 0.2 mL/min in a degassed buffer containing 50 mM Tris/HCl pH 8.0 and 200 mM NaCl.

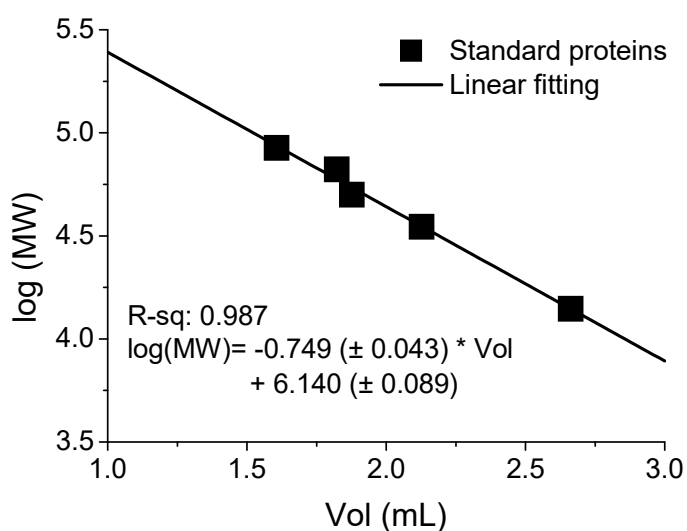


Figure 73 Calibration curve established for the analysis of the quaternary structures of the MTs by size-exclusion chromatography.

6 Appendix

6.1 Cloning and Protein production

EgtD WT and variants. EgtD WT and variants were expressed in *E. coli* BL21 cells grown in LB medium at 37 °C with the appropriate antibiotics (50 mg/L Kanamycin or 100 mg/L Ampicillin and 34 mg/L Chloramphenicol) and induced at $OD_{600} = 0.5$ with 0.1 mM IPTG at 18 °C for at least 16 h. The cells were harvested by centrifugation and frozen until use. The cell pellets were resuspended in lysis buffer (50 mM phosphate buffer pH 8.0 and 300 mM NaCl) and lysed by sonication. The lysates were clarified by centrifugation. The clear lysates were mixed with Ni^{II}-NTA agarose at 4°C for 20 min. The agarose beads were filtered on disposable plastic columns and washed with lysis buffer containing 10 and 20 mM imidazole. The protein was eluted in a lysis buffer containing 250 mM imidazole. The purified proteins were dialyzed against 50 mM Tris/HCl buffer pH 8.0, 50 mM NaCl and stored at -80°C. To approximate the concentration of the prepared proteins, the measurements of the absorption at 280 nm were performed with a Nanodrop2000 and the molar absorption coefficient $\epsilon_{280}(\text{EgtD}) = 36440 \text{ M}^{-1} \text{ cm}^{-1}$ was used.

Adenosylhomocysteine Nucleosidase. SAH nucleosidase was expressed in *E. coli* BL21 cells grown in LB medium at 37 °C with the appropriate antibiotics (50 mg/L Kanamycin and 34 mg/L Chloramphenicol) and induced at $OD_{600} = 0.5$ with 0.1 mM IPTG at 37 °C for 3 h. The cells were harvested by centrifugation and frozen until use. The cell pellets were resuspended in lysis buffer (50 mM phosphate buffer pH 8.0 and 300 mM NaCl) and lysed by sonication. The lysates were clarified by centrifugation. The clear lysate was mixed with Ni^{II}-NTA agarose at 4°C for 20 min. The agarose beads were filtered on disposable plastic columns and washed with lysis buffer containing 10 and 20 mM imidazole. The protein was eluted in a lysis buffer containing 250 mM imidazole. The purified protein was dialyzed against 50 mM Tris/HCl buffer pH 8.0, 50 mM NaCl and stored at -80°C. To approximate the concentration of the prepared protein, the measurements of the absorption at 280 nm were performed with a Nanodrop2000 and the molar absorption coefficient $\epsilon_{280}(\text{AdoNuc}) = 5960 \text{ M}^{-1} \text{ cm}^{-1}$ was used.

Adenine deaminase. Adenine deaminase was expressed in *E. coli* BL21 cells grown in LB medium with 50 mM bipyridine at 37 °C with the appropriate antibiotics (50 mg/L Kanamycin and 34 mg/L Chloramphenicol) and induced at $OD_{600} = 0.5$ with 0.1 mM IPTG and 1 mM MnCl₂ at 37 °C for 3 h. The cells were harvested by centrifugation and frozen until use. The cell pellets were resuspended in lysis buffer (50 mM phosphate buffer pH 8.0, 0.1% Tween 20, 10 %

glycerol and 300 mM NaCl) and lysed by sonication. The lysates were clarified by centrifugation. The clear lysate was mixed with Ni^{II}-NTA agarose at 4°C for 20 min. The agarose beads were filtered on disposable plastic columns and washed with lysis buffer containing 10 and 20 mM imidazole. The protein was eluted in a lysis buffer containing 250 mM imidazole. The purified protein was dialyzed against 50 mM Tris/HCl buffer pH 8.0, 50 mM NaCl, 10 % glycerol and stored at -80°C. To approximate the concentration of the prepared protein, the measurements of the absorption at 280 nm were performed with a Nanodrop2000 and the molar absorption coefficient $\epsilon_{280}(\text{deaminase}) = 41370 \text{ M}^{-1} \text{ cm}^{-1}$ was used.

Cloning and production of SticA. The gene coding for the methyltransferase domain (protein family 10017) of the hypothetical protein AN8594.2 from *Aspergillus nidulans* was purchased from GeneScript with codon adaptations for optimal production in *Escherichia coli*. This fragment was cloned into a pOPIN-expression vector using restriction free protocols. The resulting vector (\rightarrow pOPIN_SticA) encodes SticA as a fusion with an N-terminal hexahistidine tag. SticA was produced in *E. coli* Bl21 cell following the same procedure as described for EgtD.

\rightarrow Sequence of SticA:

AHHHHHHSSGLEVLFGPSQTSSVAQIDIRSDKKDVELRVSLQQSIHSDDAALPDLWWDEQGLRYFEDVITYCPS
 YYLTREEGLLKKYSLQIAEHIQPGSMLVELGSGNLRKTKILLDALEELGRPVDFYFALDVSYPELKRTRLRPVGGV
 YQHVRICYGLLGTYDDGRKWLQHPDLQSRPKTILYLGSTLGNFEKPDAAQFLASFAQPNTSFLGLDGCKNEKQVL
 QAYNDPDPGINHRFVKNGLVVRANHILGHEAFDLKWDVTGAWDEESGAHNQYYITRADVSLDGVDPAGHKLLAVR
 SHKYDADDRKNLCCSAGLKVDFWASESEY

m/z(SticA): calc.: 37217.7 Da, measured: 41641.0 Da

Construction of EgtD variants: Synthetic oligonucleotides were purchased from Microsynth, Switzerland. We used site directed mutagenesis to engineer the variants of interest. The different inserts were obtained by PCR using the following primers:

EgtDs: 5' -ATA TCA TAT GGC GCT CTC ACT GGC CAA-3'
 EgtDa: 5' -ATA TCT CGA GTC ACC GCA CCG CCA GCG ACA-3'
 M252Vs: 5' -ATC GAG GTT TGG TTG CGT GCC CGC A-3'
 M252Va: 5' -CAC GCA ACC AAA CCT CGA TGC GTT CCT-3'
 M252As: 5' -ATC GAG GCT TGG TTG CGT GCC CGC A-3'
 M252Aa: 5' -CAC GCA ACC AAG CCT CGA TGC GTT CCT-3'
 E282As: 5' -GAT GCT CAC CGC AGT GTC CTG CAA GTT-3'
 E282Aa: 5' -TGC AGG ACA CTG CGG TGA GCA TCT CCT-3'
 F47Ws 5' -TGG GAC CAG ATC ACC CGT CTC CCT GAG TAT TA-3'
 F47Wa: 5' -ACG GGT GAT CTG GTC CCA CAG ATC ACT G-3'
 F47W Y56Fs: 5' -TGG GAC CAG ATC ACC CGT CTC CCT GAG TCC TA-3'
 Y56Fs 5' -CTC CCC GAG TTC TAC CCC ACC- 3'
 Y56Fa 5' -GGT GGG GTA GAA CTC GGG GAG- 3'
 N166Da: 5' -GGT GTC AGA TCG CGG ATG GT-3'
 N166Ds: 5' -ACC ATC GGC GAT CTG ACA CC-3'
 C139As: 5' -GGT AGC TGG CGA TTT CGA GGA ACA T-3'
 C139Aa: 5' -TCG AAA TCG CCA GCT ACC GCG TCG ATC T-3'
 C285As: 5' -ACC GAG GTG TCC GCT AAG TTC CGT CCC GAG A-3'

C285Aa: 5'-GAC GGA ACT TAG CGG ACA CCT CGG T-3'
 C285Ds: 5'-GGT GTC CGA TAA GTT CCG TCC CGA GA-3'
 C285Da: 5'-GAC GGA ACT TAT CGG ACA CCT CGG T-3'
 C285Ss: 5'-ACC GAG GTG TCC AGC AAG TCC CGT CCC GAG-3'
 C285Sa: 5'-GAC GGA ACT TGC TGG ACA CCT CGG T-3'
 N217s and N217a: N/A

The gel purified amplified fragments were then digested with NdeI and XhoI restriction enzymes and inserted into a pET19 with modified cleavage site or pET28 expression vectors. The proteins were produced and purified with the same protocol as EgtD WT.

→ Sequence of EgtD WT:

GHHHHHAENLYFQGHMALS LANYLAADSAAEALRRDVRAGLTATQKSLPPKWFYDAVGSDFDQITRLPEYYPT
 RTEAQILRTRSAEII SAAGADTLVELGSGTSEKTRMLLDAMRDAELLRRFIPFDVDAGVLR SAGAAI GAEYPGIE
 IDAVCGDFEEHLGKI PHVGRRLVVFLGSTIGNLTPAPRAEFLSTLADTLQPGD SLLLGTDLVKDTGRLVRAYDDA
 AGVTAAFNRNVLAVVNRELSADFDLDAFEHVAKWNSDEERIE MWLRARTAQHVRVAALDLEVDFAAGEEMLTAVS
 CKFRPENVAELAEAGLRQTHWWTDPAGDFGLSLAVR

m/z (EgtD WT): calc.: 36989.6 Da, measured: 36990.0 Da

→ Sequence of EgtD E282A:

GHHHHHAENLYFQGHMALS LANYLAADSAAEALRRDVRAGLTATQKSLPPKWFYDAVGSDFDQITRLPEYYPT
 RTEAQILRTRSAEII SAAGADTLVELGSGTSEKTRMLLDAMRDAELLRRFIPFDVDAGVLR SAGAAI GAEYPGIE
 IDAVCGDFEEHLGKI PHVGRRLVVFLGSTIGNLTPAPRAEFLSTLADTLQPGD SLLLGTDLVKDTGRLVRAYDDA
 AGVTAAFNRNVLAVVNRELSADFDLDAFEHVAKWNSDEERIE MWLRARTAQHVRVAALDLEVDFAAGEEMLTAVS
 CKFRPENVAELAEAGLRQTHWWTDPAGDFGLSLAVR

m/z (EgtD E282A): calc.: 36931.6 Da, measured: 36931.3 Da

→ Sequence of EgtD E282A M252V:

GHHHHHAENLYFQGHMALS LANYLAADSAAEALRRDVRAGLTATQKSLPPKWFYDAVGSDFDQITRLPEYYPT
 RTEAQILRTRSAEII SAAGADTLVELGSGTSEKTRMLLDAMRDAELLRRFIPFDVDAGVLR SAGAAI GAEYPGIE
 IDAVCGDFEEHLGKI PHVGRRLVVFLGSTIGNLTPAPRAEFLSTLADTLQPGD SLLLGTDLVKDTGRLVRAYDDA
 AGVTAAFNRNVLAVVNRELSADFDLDAFEHVAKWNSDEERIE VWLRARTAQHVRVAALDLEVDFAAGEEMLTAVS
 CKFRPENVAELAEAGLRQTHWWTDPAGDFGLSLAVR

m/z (EgtD M252V E282A): calc.: 36899.5 Da, measured: 36899.1 Da

→ Sequence of EgtD E282A M252A:

GHHHHHAENLYFQGHMALS LANYLAADSAAEALRRDVRAGLTATQKSLPPKWFYDAVGSDFDQITRLPEYYPT
 RTEAQILRTRSAEII SAAGADTLVELGSGTSEKTRMLLDAMRDAELLRRFIPFDVDAGVLR SAGAAI GAEYPGIE
 IDAVCGDFEEHLGKI PHVGRRLVVFLGSTIGNLTPAPRAEFLSTLADTLQPGD SLLLGTDLVKDTGRLVRAYDDA
 AGVTAAFNRNVLAVVNRELSADFDLDAFEHVAKWNSDEERIE AWLRARTAQHVRVAALDLEVDFAAGEEMLTAVS
 CKFRPENVAELAEAGLRQTHWWTDPAGDFGLSLAVR

m/z(EgtD M252A E282A): calc.: 36871.5 Da, measured: 36870.8 Da

→ Sequence of EgtD E282A M252A N217C:

GHHHHHAENLYFQGHMALS LANYLAADSAAEALRRDVRAGLTATQKSLPPKWFYDAVGSDFDQITRLPEYYPT
 RTEAQILRTRSAEII SAAGADTLVELGSGTSEKTRMLLDAMRDAELLRRFIPFDVDAGVLR SAGAAI GAEYPGIE
 IDAVCGDFEEHLGKI PHVGRRLVVFLGSTIGNLTPAPRAEFLSTLADTLQPGD SLLLGTDLVKDTGRLVRAYDDA
 AGVTAAFNRNVLAVVNRELSADFDLDAFEHVAKWNSDEERIE VWLRARTAQHVRVAALDLEVDFAAGEEMLTAVS
 CKFRPENVAELAEAGLRQTHWWTDPAGDFGLSLAVR

m/z (EgtD E282A M252A N217C): calc.: 36888.6 Da, measured: 36888.4 Da

→ Sequence of EgtD F47W:

GHHHHHHAENLYFQGHMALS LANYLAADSAAEALRRDVRAGLTATQKSLPPKWFYDAVGS DL **W**DQ ITRLPEYYPT
RTEAQILRTRSAE I I SAAGADTLVELGSGTSEKTRMLLDAMRDAELLRRFI PFDVDAGV LRSAGAAI GA EYPGIE
IDAVCGDFEEHLGKI PHVGRRLVVFLGSTIGNLTPAPRAEFLSTLADTLQPGD SLL LGTDLVKDTGRLV RAYDDA
AGVTAAFNRNV LAVVNRELSADFDLDAFEHVAKWNSDEERIE MWLRARTA QHVRVAALDLEVDFAAGEEMLTEVS
CKFRPENVAELAEAGLRQTHWWTDPAGDFGLSLAVR

m/z (EgtD F47W): calc.: 37028.6 Da, measured: 37028.0 Da

→ Sequence of EgtD Y56F:

GHHHHHHAENLYFQGHMALS LANYLAADSAAEALRRDVRAGLTATQKSLPPKWFYDAVGS DL **F**DQ ITRLPE **F**YPT
RTEAQILRTRSAE I I SAAGADTLVELGSGTSEKTRMLLDAMRDAELLRRFI PFDVDAGV LRSAGAAI GA EYPGIE
IDAV **C**GD FEEHLGKI PHVGRRLVVFLGSTIGNLTPAPRAEFLSTLADTLQPGD SLL LGTDLVKDTGRLV RAYDDA
AGVTAAFNRNV LAVVNRELSADFDLDAFEHVAKWNSDEERIE MWLRARTA QHVRVAALDLEVDFAAGEEMLTEVS
CKFRPENVAELAEAGLRQTHWWTDPAGDFGLSLAVR

m/z (EgtD Y56F): calc.: 36973.6 Da, measured: 36975.1 Da

→ Sequence of EgtD F47W Y56F:

GHHHHHHAENLYFQGHMALS LANYLAADSAAEALRRDVRAGLTATQKSLPPKWFYDAVGS DL **W**DQ ITRLPE **F**YPT
RTEAQILRTRSAE I I SAAGADTLVELGSGTSEKTRMLLDAMRDAELLRRFI PFDVDAGV LRSAGAAI GA EYPGIE
IDAVCGDFEEHLGKI PHVGRRLVVFLGSTIGNLTPAPRAEFLSTLADTLQPGD SLL LGTDLVKDTGRLV RAYDDA
AGVTAAFNRNV LAVVNRELSADFDLDAFEHVAKWNSDEERIE MWLRARTA QHVRVAALDLEVDFAAGEEMLTEVS
CKFRPENVAELAEAGLRQTHWWTDPAGDFGLSLAVR

m/z (EgtD F47W Y56F): calc.: 37012.6 Da, measured: 37011.7 Da

→ Sequence of EgtD N166D:

GHHHHHHAENLYFQGHMALS LANYLAADSAAEALRRDVRAGLTATQKSLPPKWFYDAVGS DL **F**DQ ITRLPEYYPT
RTEAQILRTRSAE I I SAAGADTLVELGSGTSEKTRMLLDAMRDAELLRRFI PFDVDAGV LRSAGAAI GA EYPGIE
IDAVCGDFEEHLGKI PHVGRRLVVFLGSTIG **D**LTPAPRAEFLSTLADTLQPGD SLL LGTDLVKDTGRLV RAYDDA
AGVTAAFNRNV LAVVNRELSADFDLDAFEHVAKWNSDEERIE MWLRARTA QHVRVAALDLEVDFAAGEEMLTEVS
CKFRPENVAELAEAGLRQTHWWTDPAGDFGLSLAVR

m/z (EgtD N166D): calc.: 36990.6 Da, measured: 36989.4 Da.

→ Sequence of EgtD C139A:

GHHHHHHAENLYFQGHMALS LANYLAADSAAEALRRDVRAGLTATQKSLPPKWFYDAVGS DL **F**DQ ITRLPEYYPT
RTEAQILRTRSAE I I SAAGADTLVELGSGTSEKTRMLLDAMRDAELLRRFI PFDVDAGV LRSAGAAI GA EYPGIE
IDAV **A**GD FEEHLGKI PHVGRRLVVFLGSTIGNLTPAPRAEFLSTLADTLQPGD SLL LGTDLVKDTGRLV RAYDDA
AGVTAAFNRNV LAVVNRELSADFDLDAFEHVAKWNSDEERIE MWLRARTA QHVRVAALDLEVDFAAGEEMLTEVS
CKFRPENVAELAEAGLRQTHWWTDPAGDFGLSLAVR

m/z (EgtD C139A): calc.: 36957.6 Da, measured: 36956.6 Da.

→ Sequence of EgtD C285A:

GSSHHHHHSSGLVPRGSHMALS LANYLAADSAAEALRRDVRAGLTATQKSLPPKWFYDAVGS DL **F**DQ ITRLPEY
YPT **R**TEAQILRTRSAE I I SAAGADTLVELGSGTSEKTRMLLDAMRDAELLRRFI PFDVDAGV LRSAGAAI GA EY
GIE IDAVCGDFEEHLGKI PHVGRRLVVFLGSTIGNLTPAPRAEFLSTLADTLQPGD SLL LGTDLVKDTGRLV RAY
DDAAGVTAAFNRNV LAVVNRELSADFDLDAFEHVAKWNSDEERIE MWLRARTA QHVRVAALDLEVDFAAGEEMLT
EV **S** **A**KFRPENVAELAEAGLRQTHWWTDPAGDFGLSLAVR

m/z (EgtD C285A): calc.: 37049.7 Da, measured: 37048.9 Da.

→ Sequence of EgtD C285D:

GSSHHHHHSSGLVPRGSHMALSLANYLAADSAAEALRRDVRAGLTATQKSLPPKWFYDAVGSDLFDQITRLPEY
YPTRTEAQILRTRS AEIISAAGADTLVELGSGTSEKTRMLLDAMRDAELLRRFIPFDVDAGVLSAGAAIGAEYP
GIEIDAVCGDFEEHLGKIPHVGRRLVVFLGSTIGNLTPAPRAEFLSTLADTLQPGDSLLLGTDLVKDTGRLVRAY
DDAAGVTAAFNRNVLAVVNRELSADFLLDAFEHVAKWNSDEERIEMWLRARTAQHVRVAALDLEVDFAAGEEMLT
EVSDKFRPENNVVAELAEAGLRQTHWWTDPAGDFGLSLAVR

m/z (EgtD C285D): calc.: 37093.6 Da, measured: 37092.7 Da.

→ Sequence of EgtD C285S:

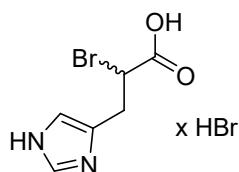
GSSHHHHHSSGLVPRGSHMALSLANYLAADSAAEALRRDVRAGLTATQKSLPPKWFYDAVGSDLFDQITRLPEY
YPTRTEAQILRTRS AEIISAAGADTLVELGSGTSEKTRMLLDAMRDAELLRRFIPFDVDAGVLSAGAAIGAEYP
GIEIDAVCGDFEEHLGKIPHVGRRLVVFLGSTIGNLTPAPRAEFLSTLADTLQPGDSLLLGTDLVKDTGRLVRAY
DDAAGVTAAFNRNVLAVVNRELSADFLLDAFEHVAKWNSDEERIEMWLRARTAQHVRVAALDLEVDFAAGEEMLT
EVSKFRPENNVVAELAEAGLRQTHWWTDPAGDFGLSLAVR

m/z (EgtD C285S): calc.: 37065.7 Da, measured: 37064.7 Da.

6.2 Synthesis of the Inhibitors

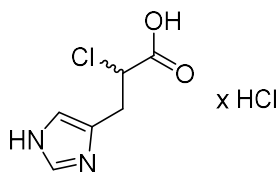
The syntheses of all the inhibitors were performed by Reto Burn. Only 3-(imidazole-4-yl) propionic acid was purchased from Sigma-Aldrich.

General. All reagents used were purchased from commercial sources without further purification. All solvents used in reactions were purchased in HPLC-grade quality and used as such. Dry solvents were purchased in HPLC-grade quality and used as such. Chromatographic purifications (flash) were performed with SiliaFlash P60 from Silicycle (40-63 μm ; (230-400) mesh). NMR spectra were acquired on a Bruker 400 MHz or a Bruker 500 MHz instrument. ^1H and ^{13}C chemical shifts are quoted relative to solvent signals unless for ^{13}C NMRs in D_2O *t*-butanol was added as internal standard. ESI-MS spectra were obtained on a Bruker Esquire3000plus spectrometer by direct injection in positive polarity of the ion trap detector.



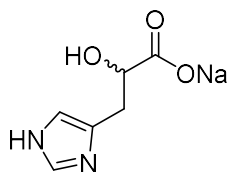
Synthesis of *D,L*- α -bromo histidine (1)²¹⁰. To a stirred solution of *D,L*-Histidine (500 mg, 3.22 mmol, 1 eq.) in concentrated hydrobromic acid (4 ml) was added sodium nitrite (444 mg, 6.4 mmol, 2 eq.) dissolved in water (2 ml) at 0°C. The mixture was stirred for 30 minutes at 0°C and 4 hours at room temperature. Then sodium nitrite (222 mg, 3.2 mmol, 1 eq.) dissolved in water (2 ml) was added at 0 °C. The mixture was stirred over night at room temperature. The solvent was removed *in vacuo* and co-evaporated 3 times with water to remove excess hydrobromic acid. The solid residue was extracted 3 times with acetone. The solvent was removed *in vacuo* to yield the title compound (492 mg, 1.64 mmol, 51%) as brown solid. ^1H NMR (400 MHz, DMSO-d_6 ,

δ /PPM 14.23 (s, 3H), 9.11 (d, J = 1.4 Hz, 1H), 7.57 (d, J = 1.3 Hz, 1H), 4.78 (dd, J = 8.7, 6.1 Hz, 1H), 3.47 (dd, J = 15.7, 6.1 Hz, 1H), 3.26 (dd, J = 15.7, 8.7 Hz, 1H). **^{13}C NMR (101 MHz, DMSO, δ /ppm)** 169.83, 134.05, 129.22, 117.43, 44.26, 29.58. **ESI-MS** m/z calcd. for $\text{C}_6\text{H}_8\text{BrN}_2\text{O}_2$ $[\text{M}+\text{H}]^+$ 218.98 (100.0%), 220.97 (97.3%), found 218.9, 221.0. **HRMS** m/z calcd. for $\text{C}_6\text{H}_7\text{BrN}_2\text{NaO}_2$ $[\text{M}+\text{Na}]^+$ 240.9583, found 240.9582, Δ (ppm) = 0.1.



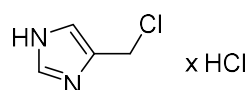
Synthesis of *D,L*- α -chloro histidine (\$2)²¹¹. To a stirred solution of

D,L-histidine (500 mg, 3.22 mmol, 1 eq.) in concentrated HCl (7.5 ml) was added at 0°C a cold solution of sodium nitrite (800 mg, 11.6 mmol, 3.6 eq.) in water (1.5 ml). The reaction was stirred for 2 hours at 0°C and additional 5 hours at room temperature. The precipitate was removed by filtration and washed with conc. HCl. The solvent was removed *in vacuo*. The solid residue was extracted with acetone (3 x 10 ml). The solvent was removed *in vacuo* to yield the title compound (190 mg, 0.90 mmol, 28%) as yellowish solid. **^1H NMR (400 MHz, DMSO- d_6 , δ /ppm)** 14.70 (m, 2H), 9.06 (s, 1H), 7.52 (s, 1H), 4.92 (dd, J = 8.7, 5.3 Hz, 1H), 3.41 (dd, J = 15.5, 5.3 Hz, 1H), 3.22 (dd, J = 15.5, 8.8 Hz, 1H). **^{13}C NMR (101 MHz, DMSO- d_6 , δ /ppm)** 169.36, 133.79, 128.50, 117.41, 55.56, 29.53. **ESI-MS** m/z calcd. for $\text{C}_6\text{H}_8\text{ClN}_2\text{O}_2$ $[\text{M}+\text{H}]^+$ 175.03, found 174.88. **HRMS** m/z calcd. for $\text{C}_6\text{H}_8\text{ClN}_2\text{NaO}_2$ $[\text{M}+\text{H}]^+$ 175.0269, found 175.0268, Δ (ppm) = 0.3;



Synthesis of *D,L*- α -hydroxy histidine (\$3). To a stirred solution of *D,L*-

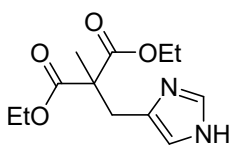
histidine in 4 M sulfuric acid was added sodium nitrite (667 mg, 9.66 mmol, 3.0 eq.) dissolved in water (3.0 ml) at 0°C. The mixture was stirred for 48 hours at room temperature and then sodium nitrite (222 mg, 3.22 mmol, 1 eq.) dissolved in water (2ml) was added at 0°C and the mixture was stirred for further 72 hours at room temperature. The mixture was neutralized with sodium hydrogencarbonate and the solvent was removed *in vacuo*. The solid was extracted with ethanol (20 ml) to yield the title compound as brown solid (124 mg, 0.79 mmol, 25%). **^1H NMR (400 MHz, D_2O , δ /ppm)** 7.65 (d, J = 1.2 Hz, 1H), 6.97 – 6.84 (m, 1H), 4.23 (dd, J = 8.0, 4.1 Hz, 1H), 3.03 (ddd, J = 15.1, 4.1, 0.9 Hz, 1H), 2.87 (ddd, J = 15.1, 8.0, 0.7 Hz, 1H). **^{13}C NMR (101 MHz, MeOD, δ /ppm)** 180.63, 135.60, 133.74, 120.88, 73.28, 33.01. **ESI-MS** m/z calcd. for $\text{C}_6\text{H}_9\text{N}_2\text{O}_3$ $[\text{M}+\text{H}]^+$ 157.06, found 156.9. **HRMS** m/z calcd. for $\text{C}_6\text{H}_9\text{N}_2\text{O}_3$ $[\text{M}+\text{H}]^+$ 157.0608, found 157.0608, Δ (ppm) = -0.2.



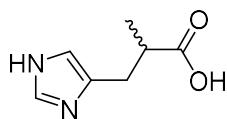
Synthesis of 4-(chloromethyl)-1*H*-imidazole hydrochloride (\$4)²¹².

To 4-(hydroxymethyl)imidazole (613 mg, 6.25 mmol, 1 eq.) was added thionyl chloride (2.2 ml, 31.3 mmol, 5 eq.). The mixture was stirred for 1 day then the solvent was removed at the HV to obtain the title compound (950 mg, 6.2 mmol, 99%) as a beige solid. **^1H NMR (400 MHz, DMSO- d_6 , δ /ppm)** 14.81 (bs, 2H), 9.16-9.10 (m, 1H),

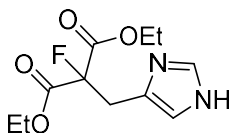
7.88 – 7.64 (m, 1H), 4.88 (s, 2H). ¹³C NMR (400 MHz, DMSO-d₆, δ/ppm) 135.15, 129.42, 118.46, 34.29.



Synthesis of diethyl 2-((1H-imidazol-4-yl)methyl)-2-methylmalonate (\$5)²¹². To a stirred solution of diethyl methylmalonate (0.15 ml, 0.87 mmol, 1 eq.) in DMF (3ml) was added sodium hydride (60% mineral oil dispersion, 60 mg, 1.5 mmol, 2.3 eq.) at 0°C. To this mixture was added \$4 (100 mg, 0.65 mmol, 1.0 eq.) portion wise. The mixture turned yellow. Stirred for 24 h at room temperature. The reaction was diluted with ethylacetate (10 ml), washed with 1 M sodium hydroxide (3x 10 ml) and dried over sodium sulfate. The solvent was removed *in vacuo* and the crude was purified by column chromatography (DCM/MeOH 94:4) to yield the title compound as white solid (67 mg, 0.26 mmol, 40%). ¹H NMR (400 MHz, DMSO-d₆, δ/ppm) 11.80 (s, 1H), 7.49 (d, J = 1.2 Hz, 1H), 6.73 (s, 1H), 4.35 – 3.85 (m, 4H), 3.01 (s, 2H), 1.25 (s, 3H), 1.16 (t, J = 7.1 Hz, 6H). ¹³C NMR (101 MHz, DMSO-d₆, δ/ppm) 171.23, 134.73, 132.39 (HMBC), 117.20 (HMQC), 60.81, 53.69, 32.73, 19.51, 13.86. ESI-MS *m/z* calcd. for C₁₂H₁₉N₂O₄ [M+H]⁺ 255.13, found 255.0.

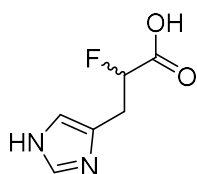


Synthesis of 3-(1H-imidazol-4-yl)-2-methylpropanoic acid (\$6)²¹³. To a stirred solution of \$5 (30 mg, 0.12 mmol, 1 eq.) in water (0.35 ml) was added concentrated HCl (0.35 ml). The mixture was heated to reflux and stirred for 48 hours. The solvent was removed *in vacuo* to yield the title compound as colorless oil (22 mg, 0.12 mmol, 98%). ¹H NMR (400 MHz, D₂O, δ/ppm) 8.59 (d, J = 1.4 Hz, 1H), 7.29 – 7.26 (m, 1H), 3.09 – 2.76 (m, 3H), 1.25-1.15 (m, 3H). ¹³C NMR (400 MHz, D₂O, δ/ppm, *t*-butanol as internal standard) 180.39, 133.59, 131.58, 116.99, 39.79, 28.11, 16.70. ESI-MS *m/z* calcd. for C₇H₁₁N₂O₂ [M+H]⁺ 155.08, found 154.9. HRMS *m/z* calcd. for C₇H₁₁N₂O₂ [M+H]⁺ 155.0815, found 155.0816, Δ (ppm) = -0.5.



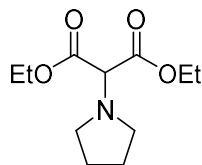
Synthesis of diethyl 2-((1H-imidazol-4-yl)methyl)-2-fluoromalonate (\$7)²¹². To a stirred solution of diethyl fluoromalonate (0.13 ml, 0.825 mmol, 1.26 eq.) in DMF (3 ml) was added sodium hydride (60 % mineral oil dispersion, 60 mg, 1.5 mmol, 2.29 eq.) at 0°C. The ice bath was removed and the reaction was stirred for 15 min at room temperature. The mixture turned slightly yellow. Then the mixture was cooled to 0°C and \$4 (100 mg, 0.653 mmol, 1 eq.) was added. The cooling bath was removed and the mixture was stirred at room temperature for 4 hours. The color turned red. The reaction was diluted with ethyl acetate (10 ml) and washed with water (3 x 10 ml). The organic layer was dried over sodium sulfate and the solvent was removed *in vacuo*. The crude was purified by flash column chromatography (ethylacetate 100%) to yield the title

compound (75 mg, 0.29 mmol, 45%). **¹H NMR (400 MHz, DMSO-d₆, δ/ppm)** 7.51 (d, J = 1.1 Hz, 1H), 6.88 (bs, 1H), 4.22 (qd, J = 7.1, 1.4 Hz, 4H), 3.42-3.28 (m, 1H), 1.19 (t, J = 7.0 Hz, 6H). **¹³C NMR (101 MHz, DMSO, δ/ppm)** 165.33 (d, J = 25.8 Hz), 135.04, 130.18 (HMBC), 117.29, 93.81 (d, J = 197.7 Hz), 62.30, 32.34 (d, J = 22.0 Hz), 13.75. **ESI-MS** *m/z* calcd. for C₁₁H₁₆FN₂O₄ [M+H]⁺ 259.1, found 259.0.



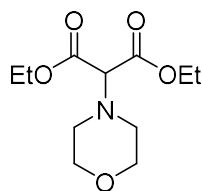
Synthesis of *D,L*-2-fluoro-3-(1*H*-imidazol-4-yl)propanoic acid (\$8)²¹³.

\$7 (75 mg, 0.29 mmol, 1 eq.) was dissolved in concentrated HCl (1.5 ml) and heated to reflux. The mixture was stirred for 34 hours at reflux. The solvent was evaporated *in vacuo* to obtain the title compound as beige solid (45 mg, 0.23 mmol, 80%). **¹H NMR (400 MHz, D₂O, δ/ppm)** 8.65 (d, J = 1.3 Hz, 1H), 7.37 (s, 1H), 5.47 – 5.12 (m, 1H), 3.53 – 3.30 (m, 2H). **¹³C NMR (400 MHz, MeoD, δ/ppm)** 171.15 (d, J = 23.6 Hz), 135.34, 129.53, 118.76, 88.16 (d, J = 184.6 Hz), 28.76 (d, J = 21.8 Hz). **ESI-MS** *m/z* calcd. for C₆H₇FN₂NaO₂ [M+Na]⁺ 181.0, found 180.9. **HRMS** *m/z* calcd. for C₆H₈FN₂O₂ [M+H]⁺ 159.0564, found 159.0565, Δ (ppm) = -0.7.



Synthesis of diethyl 2-(pyrrolidin-1-yl)malonate (\$9)²¹⁴.

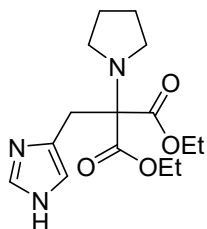
Diethyl bromomalonate (0.5 ml, 2.93 mmol, 1 eq.), pyrrolidine (0.36 ml, 4.4 mmol, 1.5 eq.) and triethylamine (0.82 ml, 5.86, 2 eq.) were dissolved in chloroform (38 ml) and stirred at reflux for 2 hours. The mixture was cooled to room temperature and diluted with NaOH (1M, 40 ml). The phases were separated and the aqueous phase was extracted with ethylacetate (3 x 20 ml). The combined organic layers were washed with water and brine and dried over sodium sulfate. The solvent was removed *in vacuo*. The crude was purified by flash column chromatography (cyclohexane/ethylacetate 7:3) to yield the title compound as yellowish oil (639 mg, 2.79 mmol, 95%). **¹H NMR (400 MHz, DMSO-d₆, δ/ppm)** 4.27 (s, 1H), 4.16 (q, J = 7.1 Hz, 4H), 3.65 – 3.49 (m, 4H), 2.75 – 2.60 (m, 4H), 1.20 (t, J = 7.1 Hz, 6H). **¹³C NMR (400 MHz, DMSO-d₆, δ/ppm)** 167.13, 67.03, 60.72, 49.43, 23.65, 13.98. **ESI-MS** *m/z* calcd. for C₁₁H₂₀NO₄ [M+H]⁺ 230.14, found 230.0.



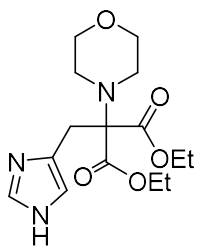
Synthesis of diethyl 2-morpholinomalonate (\$10)²¹⁴.

Diethyl bromomalonate (0.5 ml, 2.93 mmol, 1 eq.), morpholine (0.39 ml, 4.4 mmol, 1.5 eq.) and triethylamine (0.82 ml, 5.86, 2 eq.) were dissolved in chloroform (38 ml) and stirred at reflux for 20 hours. The reaction was cooled to room temperature and diluted with NaOH (1M, 40 ml). The phases were separated and the aqueous phase was extracted with ethylacetate (3 x 20 ml). The combined organic layers were washed with water and brine and dried over sodium sulfate. The solvent was removed *in*

vacuo. The crude was purified by flash column chromatography (cyclohexane/ethylacetate 7:3) to yield the title compound as yellowish oil (635 mg, 2.59 mmol, 88%). **¹H NMR (400 MHz, DMSO-d₆, δ/ppm)** 4.27 (s, 1H), 4.16 (q, J = 7.1 Hz, 4H), 3.65 – 3.49 (m, 4H), 2.75 – 2.60 (m, 4H), 1.20 (t, J = 7.1 Hz, 6H). **¹³C NMR (400 MHz, DMSO-d₆, δ/ppm)** 166.68, 69.46, 66.42, 60.79, 49.75, 14.03. **ESI-MS** *m/z* calcd. for C₁₁H₁₉NNaO₅ [M+Na]⁺ 268.12, found 268.0.

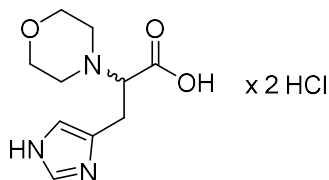


Synthesis of diethyl 2-((1H-imidazol-4-yl)methyl)-2-(pyrrolidin-1-yl)malonate (11**)**²¹². To a stirred solution of **9** (225 mg, 0.98 mmol, 1.5 eq.) in DMF (3 ml) sodium hydride (60% mineral oil dispersion, 65 mg, 1.64 mmol, 2.5 eq.) was added at 0°C. The mixture was stirred for 10 min, then **4** (100 mg, 0.65 mmol, 1 eq.) was added. The mixture was stirred for 36 hours, then the reaction was diluted with ethyl acetate (10 ml) and washed with 1 M NaOH (3 x 10 ml) and brine (5 ml). The organic layer was dried over sodium sulfate. The solvent was removed *in vacuo*. The crude was purified by column chromatography (DCM/MeOH 95:5) to yield the title compound as a yellowish oil (130 mg, 0.42 mmol, 65 %). **¹H NMR (400 MHz, DMSO-d₆, δ/ppm)** 11.66 (s, 1H), 7.58 – 7.34 (m, 1H), 6.74 (s, 1H), 4.20 – 4.05 (m, 4H), 3.20 (s, 2H), 2.84 – 2.78 (m, 4H), 1.68 – 1.54 (m, 4H), 1.14 (t, J = 7.1 Hz, 6H). **¹³C NMR (400 MHz, DMSO, δ/ppm)** 168.28, 134.12, 131.42 (HMBC), 117.77 (HSQC), 73.10, 60.46, 47.20, 32.80, 23.63, 14.02. **ESI-MS** *m/z* calcd. for C₁₅H₂₄N₃O₄ [M+H]⁺ 310.18, found 310.10.

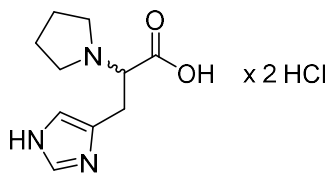


Synthesis of diethyl 2-((1H-imidazol-4-yl)methyl)-2-morpholinomalonate (12**)**²¹². To a stirred solution of **10** (200 mg, 0.815 mmol, 1.5 eq.) in DMF (3 ml) at 0°C sodium hydride (60% mineral oil dispersion, 55 mg, 1.36 mmol, 2.5 eq.) was added. The mixture was stirred 5 min at 0°C then additional 5 min at room temperature. To this mixture **4** (83 mg, 0.54 mmol, 1 eq.) was added at 0°C. The mixture was stirred at room temperature for 48 hours, diluted with ethyl acetate (10 ml), washed with saturated NaHCO₃ (3 x 10 ml) and brine (5 ml). The organic layer was dried over sodium sulfate and the solvent was removed *in vacuo*. The crude was purified by column chromatography (DCM/MeOH 94:6) to yield the title compound as a colorless crystals (55 mg, 0.184 mmol, 31%). The aqueous phase was reextracted with DCM (3x 10 ml). The combined organic layers were washed with brine and dried over sodium sulfate. The solvent was evaporated *in vacuo*. The crude was purified by column chromatography (DCM/MeOH 94:6) to yield the title compound as white crystals (30 mg, 0.092 mmol, 17%). **¹H NMR (400 MHz, DMSO-d₆, δ/ppm)** 11.71 (s, 1H), 7.47 (d, J = 1.2 Hz, 1H), 6.83 – 6.75 (m, 1H), 4.22 – 4.02 (m, 4H), 3.62 – 3.50 (m, 4H), 2.68 – 2.60 (m, 4H), 1.15 (t, J = 7.1 Hz, 6H). **¹³C NMR (400 MHz, DMSO-d₆, δ/ppm)** 167.68, 134.17, 131.47 (HSQC), 117.20

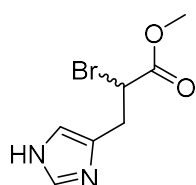
(HMBC), 74.12, 66.70, 60.65, 48.35, 14.01. **ESI-MS** m/z calcd. for $C_{15}H_{24}N_3O_5$ $[M+H]^+$ 326.17, found 326.1.



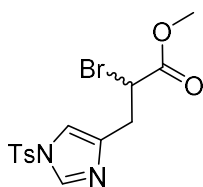
Synthesis of *D,L*- α -morpholino histidine (\$13)²¹³. \$11 (55 mg, 0.17 mmol, 1 eq.) was dissolved in half concentrated HCl (2 ml) and stirred at reflux for 48 hours. The solvent was removed *in vacuo* to obtain the title compound as beige solid (42 mg, 0.16 mmol, 95%). **¹H NMR (400 MHz, D₂O, δ /ppm)** 8.65 (d, J = 1.4 Hz, 1H), 7.38 (s, 1H), 4.09 – 3.84 (m, 5H), 3.65 – 3.40 (m, 5H), 3.30 (dd, J = 14.9, 10.2 Hz, 1H). **¹³C NMR (101 MHz, D₂O, δ /ppm, *t*-butanol as internal standard)** 169.47, 134.43, 126.67, 118.46, 67.91, 64.01, 51.00, 22.61. **ESI-MS** m/z calcd. for $C_{10}H_{16}N_3O_3$ $[M+H]^+$ 226.12, found 226.0. **HRMS** m/z calcd. for $C_{10}H_{16}N_3O_3$ $[M+H]^+$ 226.1186, found 226.1188, Δ (ppm) = -0.7.



Synthesis of *D,L*- α -pyrrolidino histidine (\$14)²¹³. \$12 (74 mg, 0.24 mmol, 1 eq.) was dissolved in half concentrated HCl (2 ml) and stirred at reflux for 48 hours. The solvent was evaporated *in vacuo* to obtain the title compound as beige solid (52 mg, 0.21 mmol, 88 %). **¹H NMR (400 MHz, D₂O, δ /ppm)** 8.56 (d, J = 1.4 Hz, 1H), 7.29 (d, J = 1.2 Hz, 1H), 3.89 (dd, J = 9.6, 4.5 Hz, 1H), 3.81 – 2.90 (m, 6H), 1.98 (br, 4H). **¹³C NMR (101 MHz, D₂O, δ /ppm, *t*-butanol as reference)** 170.22, 134.49, 126.37, 118.54, 66.47, 55.40, 52.80, 24.85, 23.35 (bs). **ESI-MS** m/z calcd. for $C_{10}H_{16}N_3O_2$ $[M+H]^+$ 210.12, found 210.0. **HRMS** m/z calcd. for $C_{10}H_{16}N_3O_2$ $[M+H]^+$ 210.1237, found 226.1239, Δ (ppm) = -1.0.



Synthesis of methyl 2-bromo-3-(1H-imidazol-4-yl) propanoate (\$15). *L*- α -bromo histidine (1 g, approx. 1.83 mmol, 1 eq.) was dissolved in MeOH (5 ml) and cooled to 0°C. There to thionyl chloride (0.2 ml, 2.75 mmol, 1.5 eq.) was added dropwise. The mixture was stirred at 0°C for 30 min, then allowed to reach room temperature. After 1 hour at room temperature, the solvent was removed on the HV and the crude was dissolved in water (approx. 30 ml), basified with sat. sodium carbonate solution, extracted with ethyl acetate (approx. 3 x 30 ml) and dried over sodium sulfate. The solvent was removed *in vacuo* to yield \$15 (324 mg, 1.39 mmol, 76%). No further purification was performed. **¹H NMR (400 MHz, Chloroform-*d*, δ /ppm)** 7.62 (d, J = 1.2 Hz, 1H), 6.92 (d, J = 1.1 Hz, 1H), 4.56 (dd, J = 8.3, 6.6 Hz, 1H), 3.59 – 3.09 (m, 2H). **ESI-MS** m/z calcd. for $C_7H_{10}BrN_2O_2$ $[M+H]^+$ = 233.0, found: $[M+H]^+$ = 233.0.



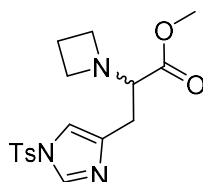
Synthesis of methyl 2-bromo-3-(1-tosyl-1H-imidazol-4-yl)propanoate

(16). **15** (300 mg, 1.29 mmol, 1 eq.) was dissolved in chloroform (6 ml).

TEA (0.18 ml, 1.29 mmol, 1 eq.) was added. The mixture was cooled to 0°C.

Then TsCl (246 mg, 1.29 mmol, 1 eq.) was added. The reaction was stirred

for 10 min at 0°C then allowed to reach room temperature. Stirred overnight. The reaction was diluted with chloroform (10 ml) and then washed with water (3x 5 ml), 0.1 M acetic acid (3x 5 ml) and brine (1x 5 ml). The organic layer was dried over sodium sulfate and then concentrated *in vacuo*. The crude was purified by silica gel column chromatography (cyclohexane/ethyl acetate 7:3) to yield **16** (300 mg, 0.77 mmol, 60%). ¹H NMR (400 MHz, DMSO-d₆, δ/ppm) 8.29 (m, 1H), 7.94 (m, 2H), 7.57 (m, 1H), 7.53 – 7.45 (m, 2H), 4.70 (m, 1H), 3.64 (s, 3H), 3.31 – 3.02 (m, 2H), 2.40 (s, 3H). ESI-MS *m/z* calcd. for C₁₄H₁₆BrN₂O₄S [M+H]⁺ 387.0, found 387.0.

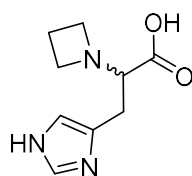


Synthesis of methyl 2-(azetidin-1-yl)-3-(1-tosyl-1H-imidazol-4-yl)propanoate (17).

16 (1000 mg, 2.6 mmol, 1 eq.) was dissolved in DMF (15 ml). Cesium carbonate (1260 mg, 3.9 mmol, 1.5 eq) and azetidine

hydrochloride (266 mg, 2.8 mmol, 1.1 eq.) were added. The reaction was

stirred at 40°C. The mixture was diluted with ethyl acetate (250 ml) after 6 hours. The organic layer was washed with sat. sodium bicarbonate solution (3x 100 ml), brine (100 ml) and dried over sodium sulfate. The solvent was removed *in vacuo*. The crude was purified by silica gel column chromatography (DCM/MeOH 195:5) to yield the product as a slightly brown oil (75 mg, 0.196 mmol 7.6 %). ¹H NMR (400 MHz, Chloroform-d, δ/ppm) 7.89 (m, J = 1.4 Hz, 1H), 7.78 (m, J = 8.4 Hz, 2H), 7.33 (m, J = 8.0, 0.8 Hz, 2H), 7.07 – 6.98 (m, 1H), 3.57 (s, 3H), 3.31 (dd, J = 7.9, 5.6 Hz, 1H), 3.24 (t, J = 7.1 Hz, 4H), 2.86 – 2.68 (m, 2H), 2.42 (s, 3H), 2.11 – 1.97 (m, 2H). ¹³C NMR (400 MHz, Chloroform-d, δ/ppm) 171.81, 146.17, 140.98, 136.29, 135.08, 130.36, 127.30, 114.49, 68.91, 53.47, 51.59, 28.87, 21.70, 17.43.



Synthesis of 2-(azetidin-1-yl)-3-(1H-imidazol-4-yl)propanoic acid

(18). To a stirred solution of **17** (70 mg, 0.19 mmol, 1 eq.) in tetrahydrofuran (1.1 ml) was added 1 M aqueous lithium hydroxide solution

(1.1 ml, 1.1 mmol, 6 eq.). The reaction was stirred for 6 hours then the

solvent was removed *in vacuo*. The crude was purified by ion exchange column chromatography. The sample was dissolved in 1 M HCl (4 ml) and diluted with water (approx. 50 ml) then loaded on Dowex 50 W X 4 (2 ml resin), washed with water (40 ml) and eluted with 0.125 M ammonia solution. The solvent was lyophilized and **18** was obtained as off-white solid (37 mg, 0.19 mmol, 98 %). ¹H NMR (400 MHz, D₂O, δ/ppm) 7.70 (d, J = 1.2 Hz, 1H), 6.98 (d, J = 1.1 Hz, 1H), 4.18 (q, J = 8.9 Hz, 2H), 4.11 – 4.01 (m, 3H), 3.22 – 3.01 (m, 2H), 2.42 (p, J = 8.3 Hz, 2H). ¹³C NMR (400 MHz, D₂O, δ/ppm) 172.31, 136.09, 131.58, 116.49, 69.31, 54.15, 26.02, 15.68. ESI-MS *m/z*

calcd. for $C_9H_{14}N_3O_2$ $[M+H]^+$ 196.10, found 196.0. **HRMS** m/z calcd. for $C_9H_{14}N_3O_2$ $[M+H]^+$ 196.1081, found 196.1081, Δ (ppm) = -0.5.

List of abbreviations

| | |
|-----------|---|
| AHCY | S-adenosylhomocysteine hydrolase |
| ATP | Adenosine triphosphate |
| BHMT | Betaine homocysteine methyltransferase |
| ClHis | α -chlorohistidine |
| DMH | Dimethylhistidine |
| DMW | Dimethyltryptophan |
| DMY | Dimethyltyrosine |
| DNA | Deoxyribonucleic acid |
| DOPA | 3,4-dihydroxyphenylalanine |
| <i>Ds</i> | <i>Dichomitus squalens</i> |
| EC | Enzyme class |
| Egt | Ergothioneine |
| FAD | Flavin adenine dinucleotide |
| Fd | Ferredoxin |
| FPLC | Fast protein liquid chromatography |
| GABA | γ -amino butyric acid |
| GSH | Glutathione |
| HPLC | High performance liquid chromatography |
| HPR | Horseradish peroxidase |
| HRMS | High resolution mass spectroscopy |
| IAA | Indole-3-acetic acid |
| ICT | Isothermal calorimetric titration |
| IE HPLC | Ion-exchange high performance liquid chromatography |
| IL | Ionic liquid |
| LSD | Lysergic acid diethylamide |
| MAT | S-adenosylmethionine synthetase |
| Me | Methyl (group) |
| MetS | Methionine synthase |
| MMH | Methylhistidine |

| | |
|-------------------|--|
| MS | Mass Spectroscopy |
| MT | Methyltransferase |
| OCTN | Organic cation transporter novel |
| OD ₆₀₀ | Optical density measured at 600 nm |
| NAD | Nicotinamide adenine dinucleotide |
| NAFLD | Non-alcoholic fatty liver disease |
| Nu | Nucleophile |
| PDB | Protein data bank |
| pEA | Phosphoethanolamine |
| PfPMT | Phosphoethanolamine methyltransferase |
| PKMT | Protein lysine methyltransferase |
| PQQ | Pyroloquinoline quinone |
| PRMT | Protein arginine methyltransferase |
| ROS | Reactive oxygen species |
| RP HPLC | Reverse-phase high performance liquid chromatography |
| RT | Room temperature |
| SAH | S-adenosylmethionine |
| SAM | S-adenosylhomocysteine |
| <i>Sl</i> | <i>Serpula lacrymans</i> |
| TEA | Tetraethylammonium |
| THF | Tetrahydrofolate |
| TMG | Trimethylglycine |
| TMH | Trimethylhistidine |
| TMW | Trimethyltryptophan |
| TMY | Trimethyltyrosine |
| UV | Ultraviolet |
| WT | Wild type |

References

1. Chen, Z., Nieves-Quinones, Y., Waas, J. R. & Singleton, D. A. Isotope effects, dynamic matching, and solvent dynamics in a Wittig reaction. Betaines as bypassed intermediates. *J. Am. Chem. Soc.* **136**, 13122–13125 (2014).
2. McNeil, S. D., Nuccio, M. L. & Hanson, A. D. Betaines and related osmoprotectants. Targets for metabolic engineering of stress resistance. *Plant Physiol.* **120**, 945–949 (1999).
3. Steiber, A., Kerner, J. & Hoppel, C. L. Carnitine: a nutritional, biosynthetic, and functional perspective. *Mol. Aspects Med.* **25**, 455–473 (2004).
4. Aiello, A. *et al.* Damipipicolin and damituricin, novel bioactive bromopyrrole alkaloids from the Mediterranean sponge *Axinella damicornis*. *Bioorg. Med. Chem.* **15**, 5877–5887 (2007).
5. Bernard, T. & Goas, G. Biosynthèse de la sticticine chez le lichen *Lobaria laetevirens*. *Physiol. Plant.* **53**, 71–75 (1981).
6. Mollica, A., Locatelli, M., Stefanucci, A. & Pinnen, F. Synthesis and bioactivity of secondary metabolites from marine sponges containing dibrominated indolic systems. *Mol. Basel Switz.* **17**, 6083–6099 (2012).
7. Borrelli, F., Campagnuolo, C., Capasso, R., Fattorusso, E. & Taglialatela-Scafati, O. Iodinated indole alkaloids from *Plakortis simplex* – New plakohypaphorines and an evaluation of their antihistamine activity. *Eur. J. Org. Chem.* **2004**, 3227–3232 (2004).
8. Cheah, I. K. & Halliwell, B. Ergothioneine; antioxidant potential, physiological function and role in disease. *Biochim. Biophys. Acta* **1822**, 784–793 (2012).
9. Yamashita, M. *et al.* Selenoneine, a novel selenium-containing compound, mediates detoxification mechanisms against methylmercury accumulation and toxicity in Zebrafish embryo. *Mar. Biotechnol.* **15**, 559–570 (2013).
10. Stanikunaite, R., Radwan, M. M., Trappe, J. M., Fronczek, F. & Ross, S. A. Lanostane-type triterpenes from the mushroom *Astraeus pteridis* with antituberculosis activity. *J. Nat. Prod.* **71**, 2077–2079 (2008).
11. DeBose, J. L., Lema, S. C. & Nevitt, G. A. Dimethylsulfoniopropionate as a foraging cue for reef fishes. *Science* **319**, 1356–1356 (2008).
12. Scheibler, C. Ueber das Betain und seine Constitution. *Berichte Dtsch. Chem. Ges.* **3**, 155–161 (1870).
13. Scheibler, C. Ueber das Betain, eine im Saft der Zuckerrüben (*Beta vulgaris*) vorkommende Pflanzenbase. *Berichte Dtsch. Chem. Ges.* **2**, 292–295 (1869).
14. D Rhodes & Hanson, and A. D. Quaternary ammonium and tertiary sulfonium compounds in higher plants. *Annu. Rev. Plant Physiol. Plant Mol. Biol.* **44**, 357–384 (1993).
15. Lever, M., Sizeland, P. C. B., Bason, L. M., Hayman, C. M. & Chambers, S. T. Glycine betaine and proline betaine in human blood and urine. *Biochim. Biophys. Acta BBA - Gen. Subj.* **1200**, 259–264 (1994).
16. Bougouffa, S., Radovanovic, A., Essack, M. & Bajic, V. B. DEOP: a database on osmoprotectants and associated pathways. *Database J. Biol. Databases Curation* (2014).
17. Venkatesan, S. & Lee, S.-L. Computational investigation on microsolvation of the osmolyte glycine betaine. *J. Mol. Model.* **18**, 5017–5028 (2012).
18. Day, C. R. & Kempson, S. A. Betaine chemistry, roles, and potential use in liver disease. *Biochim. Biophys. Acta* **1860**, 1098–1106 (2016).
19. Tartia, A. P. *et al.* Cell volume regulation is initiated in mouse oocytes after ovulation. *Dev. Camb. Engl.* **136**, 2247–2254 (2009).
20. Burg, M. B. & Ferraris, J. D. Intracellular organic osmolytes: function and regulation. *J. Biol. Chem.* **283**, 7309–7313 (2008).
21. Chen, T. H. H. & Murata, N. Glycinebetaine protects plants against abiotic stress: mechanisms and biotechnological applications. *Plant Cell Environ.* **34**, 1–20 (2011).
22. Chen, T. H. H. & Murata, N. Glycinebetaine: an effective protectant against abiotic stress in plants. *Trends Plant Sci.* **13**, 499–505 (2008).
23. Sizeland, P. C. B., Chambers, S. T., Lever, M., Bason, L. M. & Robson, R. A. Organic osmolytes in human and other mammalian kidneys. *Kidney Int.* **43**, 448–453 (1993).

24. Chambers, S. T. & Kunin, C. M. Isolation of glycine betaine and proline betaine from human urine. Assessment of their role as osmoprotective agents for bacteria and the kidney. *J. Clin. Invest.* **79**, 731–737 (1987).
25. Gallazzini, M. & Burg, M. B. What's new about osmotic regulation of glycerophosphocholine. *Physiology* **24**, 245–249 (2009).
26. Yancey, P. H. Organic osmolytes as compatible, metabolic and counteracting cytoprotectants in high osmolarity and other stresses. *J. Exp. Biol.* **208**, 2819–2830 (2005).
27. Ueland, P. M., Holm, P. I. & Hustad, S. Betaine: a key modulator of one-carbon metabolism and homocysteine status. *Clin. Chem. Lab. Med.* **43**, 1069–1075 (2005).
28. Finkelstein, J. D. Methionine metabolism in mammals. *J. Nutr. Biochem.* **1**, 228–237 (1990).
29. Schwab, U. *et al.* Betaine supplementation decreases plasma homocysteine concentrations but does not affect body weight, body composition, or resting energy expenditure in human subjects. *Am. J. Clin. Nutr.* **76**, 961–967 (2002).
30. Teng, Y.-W., Mehedint, M. G., Garrow, T. A. & Zeisel, S. H. Deletion of betaine-homocysteine S-methyltransferase in mice perturbs choline and 1-carbon metabolism, resulting in fatty liver and hepatocellular carcinomas. *J. Biol. Chem.* **286**, 36258–36267 (2011).
31. Kathuria, H. *et al.* Glycinebetaine-induced water-stress tolerance in codA-expressing transgenic indica rice is associated with up-regulation of several stress responsive genes. *Plant Biotechnol. J.* **7**, 512–526 (2009).
32. Lamb, C. & Dixon, R. A. The oxidative burst in plant disease resistance. *Annu. Rev. Plant Physiol. Plant Mol. Biol.* **48**, 251–275 (1997).
33. Viña, J., Estrela, J. M., Guerri, C. & Romero, F. J. Effect of ethanol on glutathione concentration in isolated hepatocytes. *Biochem. J.* **188**, 549–552 (1980).
34. Kanbak, G., İnal, M. & Bayçu, C. Ethanol-induced hepatotoxicity and protective effect of betaine. *Cell Biochem. Funct.* **19**, 281–285 (2001).
35. Abbott, A. P., Capper, G., Davies, D. L., Rasheed, R. K. & Tambyrajah, V. Novel solvent properties of choline chloride/urea mixtures. *Chem. Commun.* **1**, 70–71 (2003).
36. De Gaetano, Y. *et al.* Ionic liquids derived from esters of glycine betaine: synthesis and characterization. *J. Mol. Liq.* **207**, 60–66 (2015).
37. Yang, B. *et al.* Biodegradable betaine-based aprotic task-specific ionic liquids and their application in efficient SO₂ absorption. *Green Chem.* **17**, 3798–3805 (2015).
38. Choi, Y. H. *et al.* Are natural deep eutectic solvents the missing link in understanding cellular metabolism and physiology? *Plant Physiol.* **156**, 1701–1705 (2011).
39. Strange, K. Cellular volume homeostasis. *Adv. Physiol. Educ.* **28**, 155–159 (2004).
40. Perozo, E. Gating prokaryotic mechanosensitive channels. *Nat. Rev. Mol. Cell Biol.* **7**, 109–119 (2006).
41. Börngen, K. *et al.* The properties and contribution of the *Corynebacterium glutamicum* MscS variant to fine-tuning of osmotic adaptation. *Biochim. Biophys. Acta BBA - Biomembr.* **1798**, 2141–2149 (2010).
42. Landfald, B. & Strøm, A. R. Choline-glycine betaine pathway confers a high level of osmotic tolerance in *Escherichia coli*. *J. Bacteriol.* **165**, 849–855 (1986).
43. Boch, J., Kempf, B., Schmid, R. & Bremer, E. Synthesis of the osmoprotectant glycine betaine in *Bacillus subtilis*: characterization of the gbsAB genes. *J. Bacteriol.* **178**, 5121–5129 (1996).
44. Rathinasabapathi, B. *et al.* Choline monooxygenase, an unusual iron-sulfur enzyme catalyzing the first step of glycine betaine synthesis in plants: prosthetic group characterization and cDNA cloning. *Proc. Natl. Acad. Sci.* **94**, 3454–3458 (1997).
45. Fan & Gadda, G. On the catalytic mechanism of choline oxidase. *J. Am. Chem. Soc.* **127**, 2067–2074 (2005).
46. Nyssola, A., Kerovuo, J., Kaukinen, P., von Weymarn, N. & Reinikainen, T. Extreme halophiles synthesize betaine from glycine by methylation. *J. Biol. Chem.* **275**, 22196–22201 (2000).

47. Chen, T. H. H. & Murata, N. Enhancement of tolerance of abiotic stress by metabolic engineering of betaines and other compatible solutes. *Curr. Opin. Plant Biol.* **5**, 250–257 (2002).
48. Atkinson, D. E. in *Cellular Energy Metabolism and Its Regulation* 72–75 (1977).
49. Niculescu, M. D. & Zeisel, S. H. Diet, methyl donors and DNA methylation: interactions between dietary folate, methionine and choline. *J. Nutr.* **132**, 2333S–2335S (2002).
50. Romburgh, P. van & Barger, G. Preparation of the betaine of tryptophan and its identity with the alkaloid hypaphorine. *J. Chem. Soc. Trans.* **99**, 2068–2071 (1911).
51. Plugge, D. P. C. IV. Ueber die toxische Wirkung von Hypaphorin, dem Alkaloid von *Hypaphorus subumbrans* Hsskl. *Arch. Für Exp. Pathol. Pharmacol.* **32**, 313–320 (1893).
52. Thierry Beguiristain, F. L. Host plant stimulates hypaphorine accumulation in *Pisolithus tinctorius* hyphae during ectomycorrhizal infection while excreted fungal hypaphorine controls root hair development. *New Phytol.* **136**, 525–532 (1997).
53. Béguiristain, T., Cote, R., Rubini, P., Jay-Allemand, C. & Lapeyrie, F. Hypaphorine accumulation in hyphae of the ectomycorrhizal fungus, *Pisolithus tinctorius*. *Phytochemistry* **40**, 1089–1091 (1995).
54. Gilroy, S. & Jones, D. L. Through form to function: root hair development and nutrient uptake. *Trends Plant Sci.* **5**, 56–60 (2000).
55. Peterson, R. L. & Farquhar, M. L. Root hairs: Specialized tubular cells extending root surfaces. *Bot. Rev.* **62**, 1–40 (1996).
56. Ditengou, F. A., Béguiristain, T. & Lapeyrie, F. Root hair elongation is inhibited by hypaphorine, the indole alkaloid from the ectomycorrhizal fungus *Pisolithus tinctorius*, and restored by indole-3-acetic acid. *Planta* **211**, 722–728 (2000).
57. Dauphin, A., Gérard, J., Lapeyrie, F. & Legué, V. Fungal hypaphorine reduces growth and induces cytosolic calcium increase in root hairs of *Eucalyptus globulus*. *Protoplasma* **231**, 83–88 (2007).
58. Dauphin, A., De Ruijter, N. C. A., Emons, A. M. C. & Legué, V. Actin organization during eucalyptus root hair development and its response to fungal hypaphorine. *Plant Biol. Stuttg. Ger.* **8**, 204–211 (2006).
59. Ditengou, F. A., Raudaskoski, M. & Lapeyrie, F. Hypaphorine, an indole-3-acetic acid antagonist delivered by the ectomycorrhizal fungus *Pisolithus tinctorius*, induces reorganisation of actin and the microtubule cytoskeleton in *Eucalyptus globulus* ssp *bicostata* root hairs. *Planta* **218**, 217–225 (2003).
60. Nehls, U., Béguiristain, T., Ditengou, F., Lapeyrie, F. & Martin, F. The expression of a symbiosis-regulated gene in eucalypt roots is regulated by auxins and hypaphorine, the tryptophan betaine of the ectomycorrhizal basidiomycete *Pisolithus tinctorius*. *Planta* **207**, 296–302 (1998).
61. Gong, H., Jiao, Y., Hu, W. & Pua, E. Expression of glutathione-S-transferase and its role in plant growth and development in vivo and shoot morphogenesis in vitro. *Plant Mol. Biol.* **57**, 53–66 (2005).
62. Kawano, T., Kawano, N., Hosoya, H. & Lapeyrie, F. Fungal auxin antagonist hypaphorine competitively inhibits indole-3-acetic acid-dependent superoxide generation by horseradish peroxidase. *Biochem. Biophys. Res. Commun.* **288**, 546–551 (2001).
63. Gazaryan, I. G., Lagrimini, L. M., Ashby, G. A. & Thorneley, R. N. F. Mechanism of indole-3-acetic acid oxidation by plant peroxidases: anaerobic stopped-flow spectrophotometric studies on horseradish and tobacco peroxidases. *Biochem. J.* **313**, 841–847 (1996).
64. Kawano, T. Possible use of indole-3-acetic acid and its antagonist tryptophan betaine in controlled killing of horseradish peroxidase-labeled human cells. *Med. Hypotheses* **60**, 664–666 (2003).
65. Bel-Kassaoui, H. *et al.* Role of hypaphorine in the toxicity of *Astragalus lusitanicus*. *Nat. Prod. Res.* **22**, 453–457 (2008).
66. Janzen, D. H., Lynn, D. G., Fellows, L. E. & Hallwachs, W. The indole alkaloid, hypaphorine and *Pterocarpus* seed protection. *Phytochemistry* **21**, 1035–1037 (1982).

67. Chand, K. *et al.* Major alkaloidal constituent from *Impatiens niamniamensis* seeds as antihyperglycemic agent. *Med. Chem. Res.* **20**, 1505–1508 (2010).
68. Ozawa, M., Honda, K., Nakai, I., Kishida, A. & Ohsaki, A. Hypaphorine, an indole alkaloid from *Erythrina velutina*, induced sleep on normal mice. *Bioorg. Med. Chem. Lett.* **18**, 3992–3994 (2008).
69. Raverty, W. D., Thomson, R. H. & King, T. J. Metabolites from the sponge *Pachymatisma johnstoni*; L-6-bromohypaphorine, a new amino-acid (and its crystal structure). *J. Chem. Soc.* 1204–1211 (1977).
70. Campagnuolo, C., Fattorusso, E. & Tagliatalata-Scafati, O. Plakohypaphorines A–C, iodine-containing alkaloids from the Caribbean sponge *Plakortis simplex*. *Eur. J. Org. Chem.* **2**, 284–287 (2003).
71. Aiello, A. *et al.* Conicamin, a novel histamine antagonist from the mediterranean tunicate *Aplidium conicum*. *Bioorg. Med. Chem. Lett.* **13**, 4481–4483 (2003).
72. Tsopmo, A. & Muir, A. D. Chemical profiling of lentil (*Lens culinaris* Medik.) Cultivars and isolation of compounds. *J. Agric. Food Chem.* **58**, 8715–8721 (2010).
73. Lu, C.-T. *et al.* Indole alkaloids from chickpea seeds (*Cicer arietinum* L.). *Biochem. Syst. Ecol.* **38**, 441–443 (2010).
74. Keller, B. O., Wu, B. T. F., Li, S. S. J., Monga, V. & Innis, S. M. Hypaphorine is present in human milk in association with consumption of legumes. *J. Agric. Food Chem.* **61**, 7654–7660 (2013).
75. Bernard, T., Joucla, M., Goas, G. & Hamelin, J. Caractérisation de la sticticine chez le lichen *Lobaria laetevirens*. *Phytochemistry* **19**, 1967–1969 (1980).
76. Bernard, T., Goas, G., Hamelin, J. & Joucla, M. Characterization of dopa betaine, tyrosine betaine and N-dimethyltyrosine from *Lobaria laetevirens*. *Phytochemistry* **20**, 2325–2326 (1981).
77. Mittermeier, V. K. *et al.* Metabolic profiling of Alpine and Ecuadorian lichens. *Mol. Basel Switz.* **20**, 18047–18065 (2015).
78. Carollo, C. A. *et al.* Fungal tyrosine betaine, a novel secondary metabolite from conidia of entomopathogenic *Metarhizium* spp. fungi. *Fungal Biol.* **114**, 473–480 (2010).
79. Shrestha, T. & Bisset, N. G. Quaternary nitrogen compounds from South American *moraceae*. *Phytochemistry* **30**, 3285–3287 (1991).
80. Eggenberger, F. & Rowell-Rahier, M. Physiological sources of variation in chemical defense of *Oreina gloriosa* (Coleoptera: Chrysomelidae). *J. Chem. Ecol.* **19**, 395–410 (1993).
81. Gründemann, D. *et al.* Discovery of the ergothioneine transporter. *Proc. Natl. Acad. Sci. U. S. A.* **102**, 5256–5261 (2005).
82. Saini, V. *et al.* Ergothioneine maintains redox and bioenergetic homeostasis essential for drug susceptibility and virulence of *Mycobacterium tuberculosis*. *Cell Rep.* **14**, 572–585 (2016).
83. Tanret, C. Sur une base nouvelle retirée du seigle ergote, l'ergothioneine. *Compt Rend* **149**, 222–224 (1909).
84. Genghof, D. S. & Damme, O. V. Biosynthesis of ergothioneine and hercynine by *Mycobacteria*. *J. Bacteriol.* **87**, 852–862 (1964).
85. Genghof, D. S. Biosynthesis of ergothioneine and hercynine by fungi and Actinomycetales. *J. Bacteriol.* **103**, 475–478 (1970).
86. Genghof, D. S., Inamine, E., Kovalenko, V. & Melville, D. B. Ergothioneine in microorganisms. *J. Biol. Chem.* **223**, 9–17 (1956).
87. Tan, C. H. & Audley, B. G. Ergothioneine and hercynine in *Hevea brasiliensis* latex. *Phytochemistry* **7**, 109–118 (1968).
88. Melville, D. B. & Eich, S. The occurrence of ergothioneine in plant material. *J. Biol. Chem.* **218**, 647–651 (1956).
89. Melville, D. B., Horner, W. H. & Lubschez, R. Tissue ergothioneine. *J. Biol. Chem.* **206**, 221–228 (1954).

90. Rae, C. *et al.* Comparison of the ¹H and ³¹P NMR spectra of erythrocytes and plasma from some Australian native animals: bandicoot, echidna, koala, little penguin, tammar wallaby, Tasmanian devil, tree kangaroo and wombat. *Comp. Haematol. Int.* **3**, 71–80 (1993).
91. Shukla, Y., Kulshrestha, O. P. & Khuteta, K. P. Ergothioneine content in normal and senile human cataractous lenses. *Indian J. Med. Res.* **73**, 472–473 (1981).
92. Sotgia, S. *et al.* Clinical and biochemical correlates of serum L-ergothioneine concentrations in community-dwelling middle-aged and older adults. *PLoS ONE* **9**, (2014).
93. Pulte, A., Wagner, S., Kogler, H. & Spiteller, P. Pelianthinarubins A and B, Red pyrroloquinoline alkaloids from the fruiting bodies of the mushroom *Mycena pelianthina*. *J. Nat. Prod.* **79**, 873–878 (2016).
94. Pfeiffer, C., Bauer, T., Surek, B., Schömig, E. & Gründemann, D. Cyanobacteria produce high levels of ergothioneine. *Food Chem.* **129**, 1766–1769 (2011).
95. Fahey, R. C. Glutathione analogs in prokaryotes. *Biochim. Biophys. Acta BBA - Gen. Subj.* **1830**, 3182–3198 (2013).
96. Park, E.-J., Lee, W. Y., Kim, S. T., Ahn, J. K. & Bae, E. K. Ergothioneine accumulation in a medicinal plant *Gastrodia elata*. *J. Med. Plants Res.* **4**, 1141–1147 (2010).
97. Lee, W. Y., Park, E.-J., Ahn, J. K. & Ka, K.-H. Ergothioneine contents in fruiting bodies and their enhancement in mycelial cultures by the addition of methionine. *Mycobiology* **37**, 43–47 (2009).
98. Ey, J., Schömig, E. & Taubert, D. Dietary sources and antioxidant effects of ergothioneine. *J. Agric. Food Chem.* **55**, 6466–6474 (2007).
99. Melville, D. B., Otken, C. C. & Kovalenko, V. On the origin of animal ergothioneine. *J. Biol. Chem.* **216**, 325–331 (1955).
100. Melville, D. B. *Vitamins & Hormones* (ed. Robert S. Harris, G. F. M. and K. V. T.) **17**, 155–204 (Academic Press, 1959).
101. Leone, E. & Mann, T. Ergothioneine in the seminal vesicle secretion. *Nature* **168**, 205–206 (1951).
102. Salt, H. B. The ergothioneine content of the blood in health and disease. *Biochem. J.* **25**, 1712–1719 (1931).
103. Eagles, B. A. & Vars, H. M. The physiology of ergothioneine. *J. Biol. Chem.* **80**, 615–622 (1928).
104. Heath, H., Rimington, C., Searle, C. E. & Lawson, A. Some effects of administering ergothioneine to rats. *Biochem. J.* **50**, 530–533 (1952).
105. Bacher, P. *et al.* Substrate discrimination by ergothioneine transporter SLC22A4 and carnitine transporter SLC22A5: Gain-of-function by interchange of selected amino acids. *Biochim. Biophys. Acta BBA - Biomembr.* **1788**, 2594–2602 (2009).
106. Grigat, S. *et al.* Probing the substrate specificity of the ergothioneine transporter with methimazole, hercynine, and organic cations. *Biochem. Pharmacol.* **74**, 309–316 (2007).
107. Paul, B. & Snyder, S. The unusual amino acid l-ergothioneine is a physiologic cytoprotectant. *Cell Death Differ.* **17**, 1134–1140 (2010).
108. Gründemann, D. The ergothioneine transporter controls and indicates ergothioneine activity--a review. *Prev. Med.* **54 Suppl**, S71-74 (2012).
109. Kato, Y. *et al.* Gene knockout and metabolome analysis of carnitine/organic cation transporter OCTN1. *Pharm. Res.* **27**, 832–840 (2010).
110. Pfeiffer, C. *et al.* Knockout of the ergothioneine transporter ETT in zebrafish results in increased 8-oxoguanine levels. *Free Radic. Biol. Med.* **83**, 178–185 (2015).
111. Meyer, A. J. *et al.* Redox-sensitive GFP in *Arabidopsis thaliana* is a quantitative biosensor for the redox potential of the cellular glutathione redox buffer. *Plant J.* **52**, 973–986 (2007).
112. Bhaskar, A. *et al.* Reengineering redox sensitive GFP to measure mycothiol redox potential of *Mycobacterium tuberculosis* during infection. *PLoS Pathog* **10**, e1003902 (2014).
113. Mehta, M., Rajmani, R. S. & Singh, A. *Mycobacterium tuberculosis* WhiB3 responds to vacuolar pH-induced changes in mycothiol redox potential to modulate phagosomal maturation and virulence. *J. Biol. Chem.* **291**, 2888–2903 (2016).

114. Hartman, P. E. in *Ergothioneine as antioxidant* (ed. Enzymology, B.-M. in) **186**, 310–318 (Academic Press, 1990).
115. Misra, H. P. Generation of superoxide free radical during the autoxidation of thiols. *J. Biol. Chem.* **249**, 2151–2155 (1974).
116. Akanmu, D., Cecchini, R., Aruoma, O. I. & Halliwell, B. The antioxidant action of ergothioneine. *Arch. Biochem. Biophys.* **288**, 10–16 (1991).
117. Zhu, B.-Z. *et al.* Ergothioneine prevents copper-induced oxidative damage to DNA and protein by forming a redox-inactive ergothioneine-copper complex. *Chem. Res. Toxicol.* **24**, 30–34 (2011).
118. Muramatsu, H. *et al.* Characterization of ergothionase from *Burkholderia sp.* HME13 and its application to enzymatic quantification of ergothioneine. *Appl. Microbiol. Biotechnol.* **97**, 5389–5400 (2012).
119. Wolff, J. B. Ergothionase from *Escherichia coli*. *J. Biol. Chem.* **237**, 874–881 (1962).
120. Motohashi, N. & Mori, I. Thiol-induced hydroxyl radical formation and scavenger effect of thiocarbamides on hydroxyl radicals. *J. Inorg. Biochem.* **26**, 205–212 (1986).
121. Whiteman, M. & Halliwell, B. Thiols and disulphides can aggravate peroxynitrite-dependent inactivation of alpha1-antiproteinase. *FEBS Lett.* **414**, 497–500 (1997).
122. Franzoni, F. *et al.* An in vitro study on the free radical scavenging capacity of ergothioneine: comparison with reduced glutathione, uric acid and trolox. *Biomed. Pharmacother.* **60**, 453–457 (2006).
123. Sao Emani, C. *et al.* Ergothioneine is a secreted antioxidant in *Mycobacterium smegmatis*. *Antimicrob. Agents Chemother.* **57**, 3202–3207 (2013).
124. Cheah, I. K. *et al.* Knockout of a putative ergothioneine transporter in *Caenorhabditis elegans* decreases lifespan and increases susceptibility to oxidative damage. *Free Radic. Res.* **47**, 1036–1045 (2013).
125. Yang, N.-C. *et al.* Ergothioneine protects against neuronal injury induced by β -amyloid in mice. *Food Chem. Toxicol.* **50**, 3902–3911 (2012).
126. Song, T.-Y. *et al.* Ergothioneine and melatonin attenuate oxidative stress and protect against learning and memory deficits in C57BL/6J mice treated with D-galactose. *Free Radic. Res.* **48**, 1049–1060 (2014).
127. Bello, M. H., Barrera-Perez, V., Morin, D. & Epstein, L. The *Neurospora crassa* mutant Nc Δ Egt-1 identifies an ergothioneine biosynthetic gene and demonstrates that ergothioneine enhances conidial survival and protects against peroxide toxicity during conidial germination. *Fungal Genet. Biol.* **49**, 160–172 (2012).
128. Peltekova, V. D. *et al.* Functional variants of OCTN cation transporter genes are associated with Crohn disease. *Nat. Genet.* **36**, 471–475 (2004).
129. Leung, E. *et al.* Polymorphisms in the organic cation transporter genes SLC22A4 and SLC22A5 and Crohn's disease in a New Zealand Caucasian cohort. *Immunol. Cell Biol.* **84**, 233–236 (2006).
130. Apostolova, N. & Victor, V. M. Molecular Strategies for targeting antioxidants to mitochondria: therapeutic implications. *Antioxid. Redox Signal.* **22**, 686–729 (2015).
131. Askari, A. & Melville, D. B. The reaction sequence in ergothioneine biosynthesis: hercynine as an intermediate. *J. Biol. Chem.* **237**, 1615–1618 (1962).
132. Genghof, D. S. & Van Damme, O. Biosynthesis of ergothioneine from endogenous hercynine in *Mycobacterium smegmatis*. *J. Bacteriol.* **95**, 340–344 (1968).
133. Seebeck, F. P. *In Vitro* Reconstitution of Mycobacterial Ergothioneine Biosynthesis. *J. Am. Chem. Soc.* **132**, 6632–6633 (2010).
134. Alamgir, K. M., Masuda, S., Fujitani, Y., Fukuda, F. & Tani, A. Production of ergothioneine by *Methylobacterium* species. *Front. Microbiol.* **6**, 1185 (2015).
135. Harth, G., Maslesa-Galić, S., Tullius, M. V. & Horwitz, M. A. All four *Mycobacterium tuberculosis* glnA genes encode glutamine synthetase activities but only GlnA1 is abundantly expressed and essential for bacterial homeostasis. *Mol. Microbiol.* **58**, 1157–1172 (2005).

136. Song, H. *et al.* Mechanistic studies of a novel C-S lyase in ergothioneine biosynthesis: the involvement of a sulfenic acid intermediate. *Sci. Rep.* **5**, 11870 (2015).
137. Hu, W. *et al.* Bioinformatic and biochemical characterizations of C-S bond formation and cleavage enzymes in the fungus *Neurospora crassa* ergothioneine biosynthetic pathway. *Org. Lett.* **16**, 5382–5385 (2014).
138. Raman, S. B. & Rathinasabapathi, B. β -Alanine *N*-methyltransferase of *Limonium latifolium*. cDNA cloning and functional expression of a novel *N*-methyltransferase implicated in the synthesis of the osmoprotectant β -alanine betaine. *Plant Physiol.* **132**, 1642–1651 (2003).
139. Rathinasabapathi, B., Sigua, C., Ho, J. & Gage, D. A. Osmoprotectant β -alanine betaine synthesis in the Plumbaginaceae: *S*-adenosyl-*l*-methionine dependent *N*-methylation of β -alanine to its betaine is via *N*-methyl and *N,N*-dimethyl β -alanines. *Physiol. Plant.* **109**, 225–231 (2000).
140. Richard-Greenblatt, M. *et al.* Regulation of ergothioneine biosynthesis and its effect on *Mycobacterium tuberculosis* growth and infectivity. *J. Biol. Chem.* **290**, 23064–23076 (2015).
141. Cantoni, G. L. Biological methylation: selected aspects. *Annu. Rev. Biochem.* **44**, 435–451 (1975).
142. Siedlecki, P. & Zielenkiewicz, P. Mammalian DNA methyltransferases. *Acta Biochem. Pol.* **53**, 245–256 (2006).
143. Levy, D. *et al.* Lysine methylation of the NF- κ B subunit RelA by SETD6 couples activity of the histone methyltransferase GLP at chromatin to tonic repression of NF- κ B signaling. *Nat. Immunol.* **12**, 29–36 (2011).
144. Cheng, X. & Blumenthal, R. M. *S-Adenosylmethionine-Dependent Methyltransferases: Structures And Functions*. (World Scientific, 1999).
145. Schubert, H. L., Blumenthal, R. M. & Cheng, X. Many paths to methyltransfer: a chronicle of convergence. *Trends Biochem. Sci.* **28**, 329–335 (2003).
146. Vit, A., Misson, L., Blankenfeldt, W. & Seebeck, F. P. Ergothioneine biosynthetic methyltransferase EgtD reveals the structural basis of aromatic amino acid betaine biosynthesis. *Chembiochem Eur. J. Chem. Biol.* **16**, 119–125 (2015).
147. Dorgan, K. M. *et al.* An enzyme-coupled continuous spectrophotometric assay for *S*-adenosylmethionine-dependent methyltransferases. *Anal. Biochem.* **350**, 249–255 (2006).
148. Lee, S. G., Kim, Y., Alpert, T. D., Nagata, A. & Jez, J. M. Structure and reaction mechanism of phosphoethanolamine methyltransferase from the malaria parasite *Plasmodium falciparum*: an antiparasitic drug target. *J. Biol. Chem.* **287**, 1426–1434 (2012).
149. Duchin, S., Vershinin, Z., Levy, D. & Aharoni, A. A continuous kinetic assay for protein and DNA methyltransferase enzymatic activities. *Epigenetics Chromatin* **8**, 56 (2015).
150. Gana, R., Rao, S., Huang, H., Wu, C. & Vasudevan, S. Structural and functional studies of *S*-adenosyl-*L*-methionine binding proteins: a ligand-centric approach. *BMC Struct. Biol.* **13**, 6 (2013).
151. Vit, A., Misson, L., Blankenfeldt, W. & Seebeck, F. P. Crystallization and preliminary X-ray analysis of the ergothioneine-biosynthetic methyltransferase EgtD. *Acta Crystallogr. Sect. F Struct. Biol. Commun.* **70**, 676–680 (2014).
152. Horowitz, S. & Trievel, R. C. Carbon-oxygen hydrogen bonding in biological structure and function. *J. Biol. Chem.* **287**, 41576–41582 (2012).
153. Horowitz, S., Yesselman, J. D., Al-Hashimi, H. M. & Trievel, R. C. Direct evidence for methyl group coordination by carbon-oxygen hydrogen bonds in the lysine methyltransferase SET7/9. *J. Biol. Chem.* **286**, 18658–18663 (2011).
154. Horowitz, S. *et al.* Conservation and functional importance of carbon-oxygen hydrogen bonding in AdoMet-dependent methyltransferases. *J. Am. Chem. Soc.* **135**, 15536–15548 (2013).
155. Rizzo, P. A. D. *et al.* SET7/9 Catalytic mutants reveal the role of active site water molecules in lysine multiple methylation. *J. Biol. Chem.* **285**, 31849–31858 (2010).
156. Berg, J. M., Tymoczko, J. L. & Stryer, L. *Biochemistry, Fifth Edition: International Version*: (W.H. Freeman, 2002).

157. Wyman, C. & Botchan, M. DNA Replication: A familiar ring to DNA polymerase processivity. *Curr. Biol.* **5**, 334–337 (1995).
158. Abeliovich, H. An empirical extremum principle for the hill coefficient in ligand-protein interactions showing negative cooperativity. *Biophys. J.* **89**, 76–79 (2005).
159. Lorenz, N., Olšovská, J., Sulc, M. & Tudzynski, P. Alkaloid cluster gene *ccsA* of the ergot fungus *Claviceps purpurea* encodes chanoclavine I synthase, a flavin adenine dinucleotide-containing oxidoreductase mediating the transformation of *N*-methyl-dimethylallyltryptophan to chanoclavine I. *Appl. Environ. Microbiol.* **76**, 1822–1830 (2010).
160. Xu, J., Song, Y. C., Guo, Y., Mei, Y. N. & Tan, R. X. Fumigaclavines D-H, new ergot alkaloids from endophytic *Aspergillus fumigatus*. *Planta Med.* **80**, 1131–1137 (2014).
161. Ryadnov, M. & Hudecz, F. *Amino acids, peptides and proteins Volume 40*. (Royal Society of Chemistry, 2015).
162. Chen, M. *et al.* Strategies to reduce end-product inhibition in family 48 glycoside hydrolases. *Proteins Struct. Funct. Bioinforma.* **84**, 295–304 (2016).
163. Probst, M. *et al.* End-product inhibition and acidification limit biowaste fermentation efficiency. *Bioresour. Technol.* **198**, 540–549 (2015).
164. Gerhart, J. C. & Pardee, A. B. The enzymology of control by feedback inhibition. *J. Biol. Chem.* **237**, 891–896 (1962).
165. Jeong, J.-H., Cha, H. J., Ha, S.-C., Rojviriyaya, C. & Kim, Y.-G. Structural insights into the histidine trimethylation activity of EgtD from *Mycobacterium smegmatis*. *Biochem. Biophys. Res. Commun.* **452**, 1098–1103 (2014).
166. Vallance P. *Homocysteine in Health and Disease*. (Cambridge University Press, 2002).
167. Aktas, M. & Narberhaus, F. *In vitro* characterization of the enzyme properties of the phospholipid *N*-methyltransferase PmtA from *Agrobacterium tumefaciens*. *J. Bacteriol.* **191**, 2033–2041 (2009).
168. Tongsook, C. *et al.* Structural and kinetic studies on RosaA, the enzyme catalysing the methylation of 8-demethyl-8-amino-d-riboflavin to the antibiotic roseoflavin. *FEBS J.* **283**(8):1531–49 (2016).
169. Fersht, A. *Structure and Mechanism in Protein Science* 102–131 (W.H. Freeman and Company, 1999).
170. Goncharenko, K. V., Vit, A., Blankenfeldt, W. & Seebeck, F. P. Structure of the sulfoxide synthase EgtB from the ergothioneine biosynthetic pathway. *Angew. Chem. Int. Ed.* **54**, 2821–2824 (2015).
171. Howard, E. i. *et al.* Ultrahigh resolution drug design I: Details of interactions in human aldose reductase–inhibitor complex at 0.66 Å. *Proteins Struct. Funct. Bioinforma.* **55**, 792–804 (2004).
172. Auffinger, P., Hays, F. A., Westhof, E. & Ho, P. S. Halogen bonds in biological molecules. *Proc. Natl. Acad. Sci. U. S. A.* **101**, 16789–16794 (2004).
173. Wolfenden, R. Conformational aspects of inhibitor design: enzyme-substrate interactions in the transition state. *Bioorg. Med. Chem.* **7**, 647–652 (1999).
174. Purich, D. L. in *Enzyme Kinetics: Catalysis & Control* 335–378 (Elsevier, 2010).
175. Cook, P. F. & Cleland, W. W. *Enzyme Kinetics and Mechanism* 68–74 (Garland Science, 2007).
176. Wu, Q. & McLeish, M. J. Kinetic and pH studies on human phenylethanolamine *N*-methyltransferase. *Arch. Biochem. Biophys.* **539**, 1–8 (2013).
177. Fu, Z. *et al.* Crystal structure of glycine *N*-methyltransferase from rat liver. *Biochemistry (Mosc.)* **35**, 11985–11993 (1996).
178. Francis, D. M., Thompson, M. F. & Greaves, M. W. The kinetic properties and reaction mechanism of histamine methyltransferase from human skin. *Biochem. J.* **187**, 819–828 (1980).
179. Lotta, T. *et al.* Kinetics of human soluble and membrane-bound catechol *O*-methyltransferase: a revised mechanism and description of the thermolabile variant of the enzyme. *Biochemistry (Mosc.)* **34**, 4202–4210 (1995).
180. Shavit, N., Wolfe, R. G. & Alberty, R. A. The electrophoresis and titration of fumarase. *J. Biol. Chem.* **233**, 1382–1386 (1958).

181. Fromm, H. J. & Nelson, D. R. Ribitol dehydrogenase. III. Kinetic studies with product inhibition. *J. Biol. Chem.* **237**, 215–220 (1962).
182. Kirmse, W. Nitrogen as leaving group: aliphatic diazonium ions. *Angew. Chem. Int. Ed. Engl.* **15**, (1976).
183. Glavas, S. & Tanner, M. E. Active Site Residues of Glutamate Racemase. *Biochemistry (Mosc.)* **40**, 6199–6204 (2001).
184. Mentel, M., Blankenfeldt, W. & Breinbauer, R. The active site of an enzyme can host both enantiomers of a racemic ligand simultaneously. *Angew. Chem. Int. Ed.* **48**, 9084–9087 (2009).
185. Zhang, J. & Zheng, Y. G. SAM/SAH analogs as versatile tools for SAM-dependent methyltransferases. *ACS Chem. Biol.* **11**, 583–597 (2016).
186. Scavetta, R. D. *et al.* Structure of RsrI methyltransferase, a member of the N⁶-adenine β class of DNA methyltransferases. *Nucleic Acids Res.* **28**, 3950–3961 (2000).
187. Struck, A.-W., Thompson, M. L., Wong, L. S. & Micklefield, J. S-adenosyl-methionine-dependent methyltransferases: highly versatile enzymes in biocatalysis, biosynthesis and other biotechnological applications. *ChemBioChem* **13**, 2642–2655 (2012).
188. Woodard, R. W., Tsai, M. D., Floss, H. G., Crooks, P. A. & Coward, J. K. Stereochemical course of the transmethylation catalyzed by catechol O-methyltransferase. *J. Biol. Chem.* **255**, 9124–9127 (1980).
189. Saen-oon, S., Lee, S. G., Jez, J. M. & Guallar, V. An alternative mechanism for the methylation of phosphoethanolamine catalyzed by *Plasmodium falciparum* phosphoethanolamine methyltransferase. *J. Biol. Chem.* **289**, 33815–33825 (2014).
190. Taverna, S. D., Li, H., Ruthenburg, A. J., Allis, C. D. & Patel, D. J. How chromatin-binding modules interpret histone modifications: lessons from professional pocket pickers. *Nat. Struct. Mol. Biol.* **14**, 1025–1040 (2007).
191. Wei, H., Mundade, R., Lange, K. C. & Lu, T. Protein arginine methylation of non-histone proteins and its role in diseases. *Cell Cycle* **13**, 32–41 (2014).
192. Collins, R. E. *et al.* *In vitro* and *in vivo* Analyses of a Phe/Tyr switch controlling product specificity of histone lysine methyltransferases. *J. Biol. Chem.* **280**, 5563–5570 (2005).
193. Boriack-Sjodin, P. A. & Swinger, K. K. Protein methyltransferases: a distinct, diverse, and dynamic family of enzymes. *Biochemistry (Mosc.)* **55**, 1557–1569 (2016).
194. Zhang, X., Zhou, L. & Cheng, X. Crystal structure of the conserved core of protein arginine methyltransferase PRMT3. *EMBO J.* **19**, 3509–3519 (2000).
195. Rust, H. L., Zurita-Lopez, C. I., Clarke, S. & Thompson, P. R. Mechanistic studies on transcriptional coactivator protein arginine methyltransferase 1. *Biochemistry (Mosc.)* **50**, 3332–3345 (2011).
196. Newby, Z. E. R., Lau, E. Y. & Bruice, T. C. A theoretical examination of the factors controlling the catalytic efficiency of the DNA-(adenine-N⁶)-methyltransferase from *Thermus aquaticus*. *Proc. Natl. Acad. Sci.* **99**, 7922–7927 (2002).
197. Bartlett, G. J., Porter, C. T., Borkakoti, N. & Thornton, J. M. Analysis of catalytic residues in enzyme active sites. *J. Mol. Biol.* **324**, 105–121 (2002).
198. Chance, B., Sies, H. & Boveris, A. Hydroperoxide metabolism in mammalian organs. *Physiol. Rev.* **59**, 527–605 (1979).
199. McRipley, R. J. & Sbarra, A. J. Role of the phagocyte in host-parasite interactions XI. Relationship between stimulated oxidative metabolism and hydrogen peroxide formation, and intracellular killing. *J. Bacteriol.* **94**, 1417–1424 (1967).
200. Marinho, H. S., Real, C., Cyrne, L., Soares, H. & Antunes, F. Hydrogen peroxide sensing, signaling and regulation of transcription factors. *Redox Biol.* **2**, 535–562 (2014).
201. Halliwell, B., Clement, M. V. & Long, L. H. Hydrogen peroxide in the human body. *FEBS Lett.* **486**, 10–13 (2000).
202. Huang, Y. *et al.* Ratiometric detection and imaging of endogenous hypochlorite in live cells and *in vivo* achieved by using an aggregation induced emission (AIE)-based nanoprobe. *Chem. Commun.* (2016). doi:10.1039/C6CC03415B

203. Dickson, J. M. J., Lee, W.-J., Shepherd, P. R. & Buchanan, C. M. Enzyme activity effects of *N*-terminal His-tag attached to catalytic sub-unit of phosphoinositide-3-kinase. *Biosci. Rep.* **33**, (2013).
204. Woo, H. A. *et al.* Reversing the inactivation of peroxiredoxins caused by cysteine sulfinic acid formation. *Science* **300**, 653–656 (2003).
205. Pace, N. J. & Weerapana, E. Diverse functional roles of reactive cysteines. *ACS Chem. Biol.* **8**, 283–296 (2013).
206. Finkel, T. Signal transduction by reactive oxygen species. *J. Cell Biol.* **194**, 7–15 (2011).
207. Chang, Y.-C., Huang, C.-N., Lin, C.-H., Chang, H.-C. & Wu, C.-C. Mapping protein cysteine sulfonic acid modifications with specific enrichment and mass spectrometry: An integrated approach to explore the cysteine oxidation. *Proteomics* **10**, 2961–2971 (2010).
208. Murray, C. I. & Van Eyk, J. E. Chasing cysteine oxidative modifications: proteomic tools for characterizing cysteine redox-status. *Circ. Cardiovasc. Genet.* **5**, 591 (2012).
209. Geoghegan, K. F. *et al.* Spontaneous alpha-*N*⁶-phosphogluconoylation of a 'His-tag' in *Escherichia coli*: the cause of extra mass of 258 or 178 Da in fusion proteins. *Anal. Biochem.* **267**, 169–184 (1999).
210. Maat, L., Beyerman, H. C. & Noodrdam, A. Synthesis of 2-bromo-3-(5-imidazolyl)propanol, its *nπ*-methyl analogue and related 2-bromohistidine derivatives. *Tetrahedron* **35**, 273–275 (1979).
211. Allerton *et al.* US2002/147229. A1 (2002).
212. Matziari, M., Bauer, K., Dive, V. & Yiotakis, A. Synthesis of the phosphinic analogue of thyrotropin releasing hormone. *J. Org. Chem.* **73**, 8591–8593 (2008).
213. Madsen, C. *et al.* 5-Substituted imidazole-4-acetic acid analogues: synthesis, modeling, and pharmacological characterization of a series of novel gamma-aminobutyric acid (C) receptor agonists. *J. Med. Chem.* **50**, 4147–4161 (2007).
214. Hess, W. & Burton, J. W. Palladium-catalysed cyclisation of *N*-alkynyl aminomalonates. *Chem. Weinh. Bergstr. Ger.* **16**, 12303–12306 (2010).

Acknowledgments

I would like to express my deepest gratitude to Prof. Dr. Florian Seebeck for believing in me and choosing me as the first PhD student in his group in Basel. It was quite a challenge for me to start a PhD in a new field and if I was able to face this challenge, it was through all the knowledge and skills he passed on me. I am sincerely grateful for his patience and trust.

I would like to thank Prof. Dr. Wulf Blankenfeldt, first for accepting the co-examination of my PhD thesis, but also for our successful collaboration.

Furthermore, I would like to thank Prof. Dr. Dennis Gillingham for contributing to the nice atmosphere of the third floor and chairing my PhD defense.

To my dear lab mates: Doctor Gao, Matthias, Roxana, Kristina, Gabriel, Sébastien, Ali, Pascal, Alma, Lukas, Thanh, Sebastian, Liao, Marcel, Reto, Anja and Alice, working with you guys was a great time, I really enjoyed our nice international atmosphere and I learnt a lot from all your different cultures. I sincerely hope that I would have the chance to work with such awesome colleagues in the future. Many thanks go to Matthias who taught me the basics in enzymology and was a great help at the beginning of my PhD. I am also obliged to my sharp-minded proof-readers, Bananja and Kris, for their help and constructive criticism. I would like to thank my Master student Alma; it was really pleasant to share knowledge with her and to supervise such an interested and motivated student.

I would also like to thank Livia who was a great support at the really beginning of my PhD and helped me a lot to set up my experiments.

I would like to thank Dr. Heinz Nadig for his technical support and our instructive discussions about mass spectroscopy.

I would like to thank all the third-floor neighbors for the cool time we spent together from our barbecues to hikes, Glühwy, concerts and festivals.

I do think that my PhD studies would not have been possible without all the friends I made in Basel, who supported me during these four years and the good moments we enjoyed together. I think particularly about Yvonne, who was one of the kindest people I have ever met and the first one who helped me to move in in Basel. Sadly, life can be very unfair.

I am also thankful to my parents who have made me the strong person I am today. To my dad, who always tells me that I am capable to achieve whatever I want and to my mum, who showed me that giving up is the worst thing one could do. I also thank all my family for their support,

especially my little sisters Cynthia and Flavia who are always able to make me smile and my two grandmas for their incommensurable kindness and love. I am also grateful to Marcella, who I consider as a role model, for all she has done and continues to do for the family.

I would also like to thank my friends in France, Céline, Loïc, Marion, Cyril, Joannie and especially my best friend Pauline, the best mix of craziness and generosity you can find in a person, who was always there to support me despite the distance.

To finish, to all my chocolate dealers, thank you so much. You were a crucial support during the writing of my dissertation.